Universidad de Valladolid

Thesis Dissertation

Synthesis and Evaluation of Novel Materials for Gas Separation Membranes Through Thermal Rearrangement Processes of *ortho*-Funtionalized Polyimides

Bibiana Comesaña Gándara

Dissertation submitted to the University of Valladolid, in Fulfilment of the Requirements for the Award of the Degree of **Doctor of Philosophy**

University of Valladolid

October, 2015

Advisors:

Prof. Javier de Abajo

Dr. Angel E. Lozano

Prof. Young Moo Lee

Ph.D. Advisors and Tutors:

Prof. Dr. Javier de Abajo González (Ph D Advisor)

Research Professor of Institute of Polymer Science and Technology, CSIC, Madrid, Spain

Dr. Angel E Lozano (Ph D Advisor)

Senior Researcher of Institute of Polymer Science and Technology, CSIC, Madrid, Spain
Researcher of SMAP, University of Valladolid-CSIC research unit, Valladolid, Spain

Prof. Dr. Young Moo Lee (Ph D Advisor)

Professor of Energy Engineering, Hanyang University, Seoul, Republic of Korea

Prof. Dr. Camino Bartolomé Albistegui (Ph D Tutor)

Professor of Inorganic Chemistry, IU Cinquima, University of Valladolid, Valladolid, Spain

Universidad de Valladolid

AUTORIZACIÓN DE LOS DIRECTORES DE LA TESIS

(Art. 2.1. c de la Normativa para la presentación y defensa de la Tesis Doctoral en la UVA)

Dr. Javier de Abajo González, con DNI. nº 12157893R y **Dr. Angel E. Lozano López**, con DNI. nº 12243527Y, Investigadores del Departamento de Química Macromolecular del Instituto de Ciencia y Tecnología de Polímeros del CSIC, **Prof. Dr. Young Moo Lee**, con Pasaporte de la República de Corea nº M29710734, Profesor del Departamento de Hanyang University, Seúl, Corea del Sur (Ph.D. advisors) y **Dra. Camino Bartolomé Albistegui** con DNI. nº 09324689Y, Profesora del Departamento de Química Física y Química Inorgánica de la Universidad de Valladolid (Ph.D. tutor), como Directores y Tutora de la Tesis Doctoral titulada: ***Synthesis and Evaluation of Novel Materials for Gas Separation Membranes Through Thermal Rearrangement Processes of ortho-funtionalized polyimides***, presentada por Dª. Bibiana Comesaña Gándara, alumna del programa "*Doctorado en Química: Química de Síntesis, Métodos de Separación, Catálisis y Materiales Avanzados*" impartido por el Instituto CINQUIMA, autorizan la presentación de la misma considerando que la doctoranda ha desarrollado un trabajo experimental original, ha cumplido las diferentes etapas de formación y ha conseguido los objetivos propuestos.

En Valladolid, a 5 de Octubre de 2015

Los Directores y Tutores de la Tesis,

Fdo.: Javier de Abajo González   *Fdo.: Young Moo Lee*

Fdo. Angel E Lozano López   *Fdo. Camino Bartolomé Ibastegui*

TABLE OF CONTENTS

CHAPTER III: Thermally Rearranged Polybenzoxazoles and Poly(benzoxazole-co-imide)s from ortho-Hydroxyamine Monomers: Influence of OH Amount

CHAPTER IV: Thermally Rearranged Polybenzoxazole Membranes with Biphenyl Moieties: Monomer Isomeric Effect

CHAPTER V: Gas Separation Membranes Made Through Thermal Rearrangement: Influence of the ortho-Substituent

CHAPTER VI: Conclusions

Appendix 1

Appendix 2

Summary

RESUMEN

Los objetivos del trabajo presentado en esta Memoria se enmarcan dentro del esfuerzo de I+D que se está realizando en numerosos laboratorios de todo el mundo para paliar los efectos de la emisión de dióxido de carbono a la atmósfera, para separar el CO_2 de mezclas gaseosas en las que es un componente no deseado o para almacenarlo como agente químico y utilizarlo en una variedad de procesos químicos.

Hay una evidencia, admitida ya universalmente, de que el CO_2 en el aire es uno de los responsables directos y más importantes del efecto invernadero y del calentamiento de la Tierra. La actividad industrial, fundamentalmente la utilización de combustibles fósiles como gasolinas, gas o carbón, es la principal responsable del incremento del contenido de CO_2 en el aire desde 280 ppm hasta 400 ppm en los últimos 150 años, dando origen a una subida de la temperatura media del globo de aproximadamente 0.85 ºC respecto a los niveles de la era preindustrial, y las previsiones anuncian un incremento del 40% de la demanda energética entre 2007 y 2030. Para mitigar la grave amenaza para la vida en la tierra de un incremento tan notable del efecto invernadero, se han programado varias soluciones tecnológicas entre la que destacan el desarrollo de las energías renovables y la captura y almacenamiento de gases de efecto invernadero como el CO_2.

Para la captura y almacenamiento/utilización de CO_2, se han identificado cuatro estrategias fundamentales hasta ahora: captura del CO_2 de las emisiones de procesos industriales; captura de CO_2 de los gases originados en la combustión, captura de CO_2 de gases antes de la combustión, y captura de CO_2 de gases de oxi-combustión. En la **Figura 1** se esquematizan estas cuatro líneas de actuación.
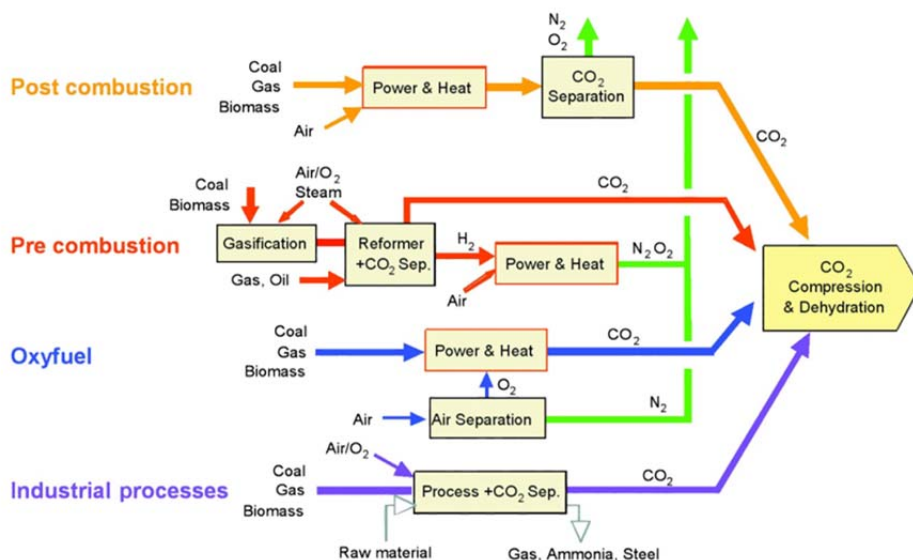
Figura 1. Esquema de los procesos de captura de CO_2

El mayor esfuerzo hasta ahora se está haciendo en la separación de CO_2 de la mezcla de gases de combustión, que se emiten a la atmósfera desde millones de chimeneas en todo el mundo, y en la separación de CO_2 de gas natural, donde se puede encontrar CO_2 en cantidades variables de hasta el 20%.

La utilización de membranas en procesos de separación de gases es una tecnología que ha experimentado un crecimiento sostenido desde que se comercializaron los primeros módulos para esta aplicación hace más de treinta años. La primera aplicación a nivel industrial de estas membranas fue la recuperación de hidrógeno de las purgas en la fabricación de amoniaco, y desde entonces su utilización se ha extendido a un gran número de aplicaciones, como son: la obtención de nitrógeno a partir del aire, la obtención de aire enriquecido en oxígeno, la recuperación de hidrocarburos volátiles en grandes depósitos de combustible, la dehumidificación del aire, la separación de CO y CO_2 del gas de síntesis, la recuperación de monómeros volátiles tóxicos como el cloruro de vinilo, la eliminación de CO_2 del gas natural, y la eliminación de CO_2 y otros gases nocivos de las mezclas gaseosas originadas en la combustión de gas, carbón y combustibles líquidos. La tecnología de membranas para separación de gases ha experimentado un gran desarrollo gracias al descubrimiento de nuevos

materiales y al perfeccionamiento de la ingeniería implicada en estas operaciones, de tal forma que hoy se puede afirmar que las membranas de separación de gases ofrecen una alternativa energéticamente más favorable, menos contaminante, y unas instalaciones más simples y modulables que los procedimientos clásicos, como pueden ser la destilación criogénica o la utilización de grandes columnas de adsorción/absorción.

En lugar destacado de este esfuerzo innovador está la búsqueda de nuevos materiales para la fabricación de membranas, fundamentalmente la preparación y evaluación de nuevos polímeros con capacidades mejoradas de permeación y separación. Las membranas poliméricas, tanto las comerciales como las experimentales, son membranas que funcionan convenientemente gracias al principio de disolución-difusión ya que el transporte de las moléculas de gas se verifica merced a un mecanismo que implica la disolución primero del gas en la matriz polimérica y su posterior difusión a través del material. Este mecanismo se fundamenta en las interacciones específicas entre el polímero y las moléculas de cada gas de una mezcla, que se pueden definir mediante unos coeficientes específicos de disolución y de transporte. La expresión que relaciona estos parámetros que gobiernan el paso de un gas a través de un polímero es la siguiente:

$$P = D \cdot S$$

S es el coeficiente de solubilidad; es el factor termodinámico y depende fundamentalmente de las interacciones polímero-gas y de la temperatura crítica del gas. El coeficiente de difusión, D, es de naturaleza cinética y depende fundamentalmente del tamaño de las moléculas del gas y del volumen libre del polímero. En la **Figura 2** se puede observar cómo de importante es la composición química del polímero en relación a sus propiedades de permeación.

Oxygen permeability

RT

10.000 ——————— PTMPS (Polyacetylenes)

100 ——————— PDMS

Barrers

1 ——————— Polysulfones, polycarbonates
MATRIMID

ULTEM

0,1 ——————— PET PMMA
KAPTON
Poly(amide-imide)

0,01 ——————— PVC, Nylon-6, Nomex

0,001 ——————— Kevlar (crystalline aromatic polyamides)

0,0001 ——————— PAN
Liquid crystal polymer (LCP)
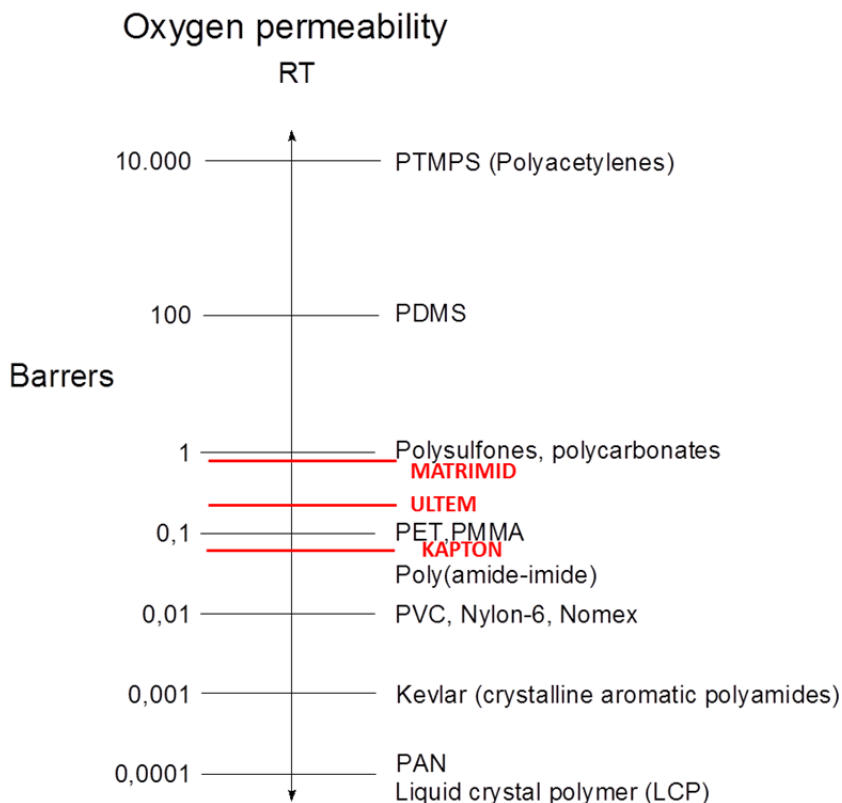
Figure 2. Permeabilidad al oxígeno de distintos polímeros (1 Barrer: 10^{-10} cm^3(STP)·cm/cm² ·s ·cmHg)

Como se ve en la **Figura 2**, diez órdenes de magnitud separan a los polímeros más permeables al oxígeno de los menos permeables. En principio los muy permeables serían los más apropiados para separación de gases, sin embargo, a la hora de evaluar un polímero como formador de membranas para gases se han de tener en cuenta otras consideraciones. Una membrana con posibilidades de ser valorada para separar gases debe tener al mismo tiempo alta permeabilidad y alta selectividad. Se ha demostrado que existe una relación inversa entre permeabilidad y selectividad, de tal forma que siempre hay un compromiso entre estas dos magnitudes, y cuanto más productiva es una membrana respecto a una pareja de gases menor es su selectividad. En 1991, L.M. Robeson confeccionó una serie de diagramas permeabilidad/selectividad

para las parejas de gases técnicos más importantes, en las que se representaron los valores de un gran número de membranas poliméricas, y gracias a ellas se definió un límite empírico, el denominado "límite de Robeson" (*upper bound*). Estas representaciones han sido de gran utilidad desde entonces y han sido una referencia indiscutible en cuantos avances se han venido produciendo en la búsqueda de nuevos materiales y nuevas membranas.
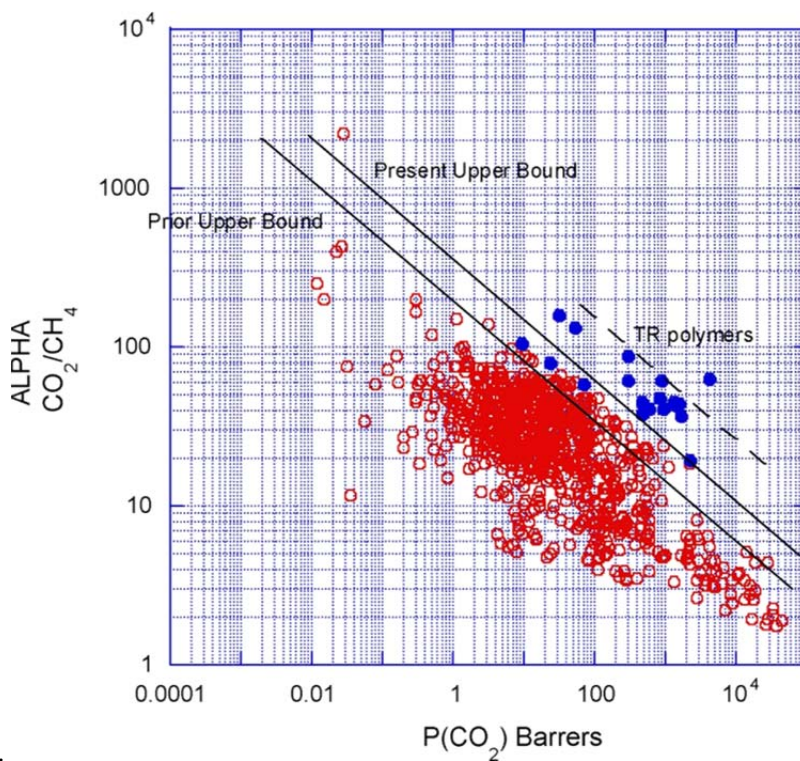
Figura 3. Diagrama de Robeson para CO_2/CH_4

En la **Figura 3** se muestra el diagrama de Robeson para la pareja CO_2/CH_4. Los diagramas se revisaron en 2008, y la incorporación de datos de polímeros desarrollados y probados en ese intervalo permitió el desplazamiento del *upper bound* a valores muy superiores, gracias a las propiedades mejoradas de las membranas descubiertas en ese tiempo.

De entre el gran número de polímeros ensayados, las poliimidas han resultados especialmente interesantes por sus propiedades de permeación (productividad y selectividad), y además porque tienen unas propiedades físicas especialmente adecuadas para la fabricación de membranas. Hoy se pueden diseñar poliimidas solubles que tengan una T_g muy alta, por encima de 250 ^{o}C, y una temperatura límite de servicio por encima de 200 ^{o}C, junto con una resistencia mecánica superior a la de la mayoría de los termoplásticos para ingeniería. Adicionalmente, la mayoría de las nuevas poliimidas son amorfas, lo cual favorece sus propiedades de permeación. De las poliimidas comerciales solo Ultem® y Matrimid® se utilizan en la fabricación de membranas para separación de gases. Las razones de su utilización son puramente económicas, pues son escasamente permeables a gases (2 Barrers y 8-9 Barrers al CO_2 para Ultem y Matrimid respectivamente), mientras que hay docenas de poliimidas experimentales que muestran productividades al CO_2 un orden de magnitud superiores, con selectividades CO_2/CH_4 y CO_2/N_2 comparables a las de poliimidas comerciales, y que sin duda alcanzarán un nivel de aceptación competitivo en el momento en que se escale su producción.

Como consecuencia de la investigación continuada en busca de polímeros con propiedades de permeación mejorada, se han definido dos familias de polímeros sintéticos que despiertan en la actualidad el mayor interés desde el punto de vista científico y práctico. Son los denominados PIM, polímeros de microporosidad intrínseca, y los polímeros TR que son polímeros obtenidos mediante trasposición térmica a partir de precursores poliméricos, en particular poliimidas funcionalizadas. En los polímeros PIM se suceden unidades de espiro-bis-indano en la cadena principal, lo cual dota al sistema de un volumen libre extraordinariamente grande merced a la dislocación y no linealidad del grupo bis-indano, lo que se traduce en valores de permeabilidad por encima de 1000 Barrers en algunos casos. En los polímeros TR, la trasposición térmica origina cambios conformacionales y de composición química que favorecen también una modificación importante del volumen libre y de la distribución de los elementos de volumen libre, que se traduce en permeabilidades próximas o superiores a 1000 Barrers según los casos.

Los objetivos concretos de esta tesis son precisamente profundizar en el conocimiento de estos nuevos materiales y contribuir a su expansión como formadores de membranas para separación de gases. En este trabajo, se ha incidido fundamentalmente en los aspectos de preparación y evaluación de nuevos polímeros TR, y en el estudio pormenorizado de los mecanismos que gobiernan la trasposición y conducen a los materiales finales mediante un tratamiento térmico extremo. Como se muestra en la **Figura 4**, los polímeros TR se preparan tradicionalmente a partir de poliimidas *orto*-hidroxiladas, que se obtienen por métodos clásicos de policondensación a partir de dianhidridos y *orto*-hidroxidiaminas.
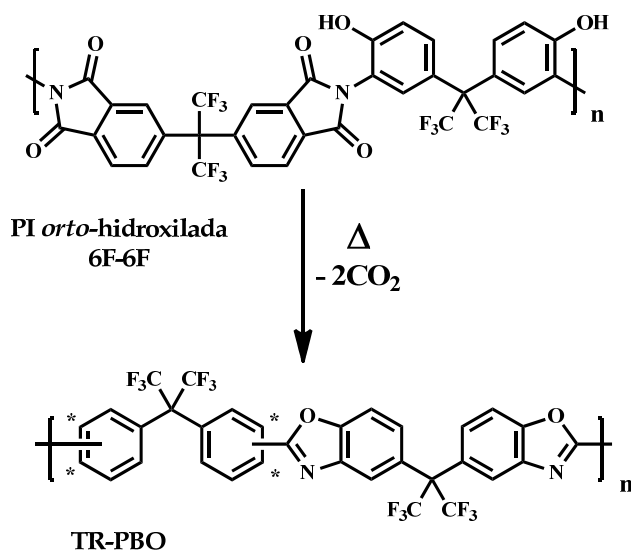
Figura 4. Preparación de TR-PBO mediante trasposición térmica de la polihidroxi-imida 6F-6F

Los aspectos innovadores más sobrealientes de esta tesis se pueden resumir en los siguientes apartados:

- Síntesis y evaluación de polímeros TR a partir de monómeros comerciales no utilizados anteriormente, como son el 2,4-diaminofenol y la 4,6-diaminoresorcina.
- Síntesis y evaluación de polímeros TR a partir de un monómero original, 3,3'-diamino-4,4'-dihidroxibifenilo, isómero de la 3,3'-dihidroxibencidina, que se ha utilizado repetidamente como monómero de partida para TR-PBOs.
- Síntesis y evaluación de polímeros TR a partir de diaminas con sustituyentes en *orto* distintos del grupo hydroxilo, en particular a partir de *orto*-metoxidiaminas.

En el primer apartado se ha hecho un destacable esfuerzo en la preparación de monómeros suficientemente puros y reactivos a partir de los productos comerciales que, por su gran inestabilidad, no se pueden obtener suficientemente puros para policondensación. Para solucionar este problema se prepararon los derivados dihidroclorados de las diaminas 2,4-diaminofenol y 4,6-diaminoresorcina, y se pudieron obtener poliimidas *orto*-hidroxiladas de alto peso molecular al reaccionar con el dianhidrido 2,2'-bis-(3,4-dicarboxifenil) hexafluoropropano, que es el dianhidrido universalmente elegido para la síntesis de estos polímeros porque se purifica fácilmente, tiene gran reactividad como electrofílico y asegura la solubilidad de las poliimidas finales.

La reacción de policondensación para la obtención de *orto*-hidroxipoliimidas (**Figura 5**) se hace mediante un procedimiento de síntesis optimizado, que incluye la utilización de cloro-trimetilsilano, piridina y dimetil-aminopiridina como catalizadores y promotores de condensación. Mediante este procedimiento se alcanzan pesos moleculares generalmente muy altos, que en cualquier caso dotan al polímero de las propiedades mecánicas y térmicas suficientes para poder utilizarlo en la fabricación de filmes (membranas densas) que se someten al tratamiento térmico de trasposición a temperaturas de hasta 450 ºC.
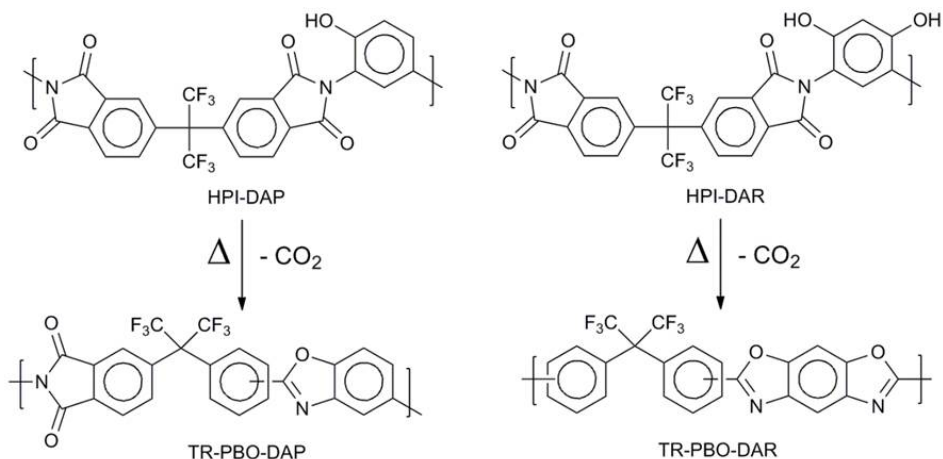
Figura 5. Preparación de TR-PBOs a partir de 2,4-diaminofenol y 4,6-diaminoresorcina

La valoración de las propiedades de permeación de los TR-PBOs obtenidos en esta parte del trabajo ha permitido concluir que los polímeros obtenidos son comparables a los TR-PBO clásicos obtenidos con monómeros convencionales, muestran propiedades de permeación excepcionales, con permeabilidades al CO_2 superiores a 350 Barrers y próximas a 80 Barrers al O_2 para TR-PBO-DAR (**Figura 6** y **Figura 7**). Para el caso del polímero TR-PBO-DAP no se alcanzaron valores tan altos de permeación, y ello es debido a que su precursor HPI-DAP tiene solo un grupo hidroxilo y, tras el tratamiento térmico resulta un polímero que es realmente un copolímero con unidades de poliimida y polibenzoxazol que no ha experimentado los cambios químicos y conformacionales que conducen a la gran ganancia de volumen libre que se alcanza en el TR-PBO-DAR.
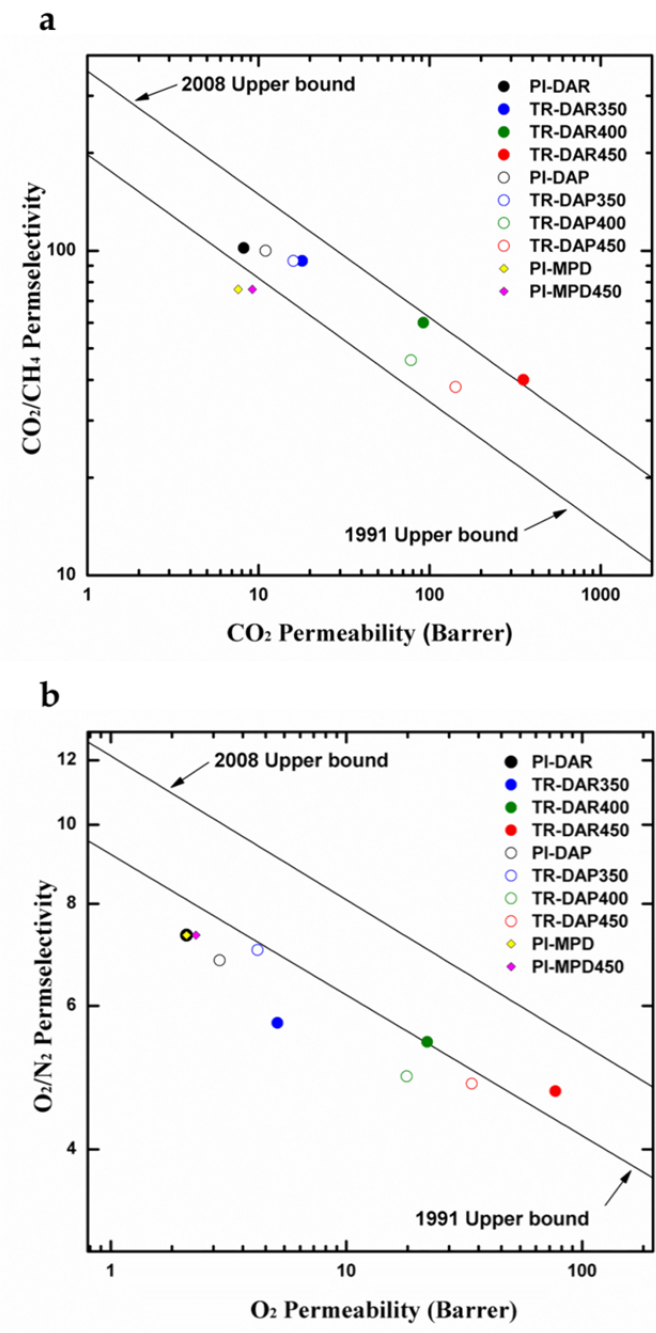
Figura 6. Propiedades de separación de gases de polímeros TR. Relación entre permeabilidad y selectividad para los pares CO_2/CH_4 (a) y O_2/N_2 (b)
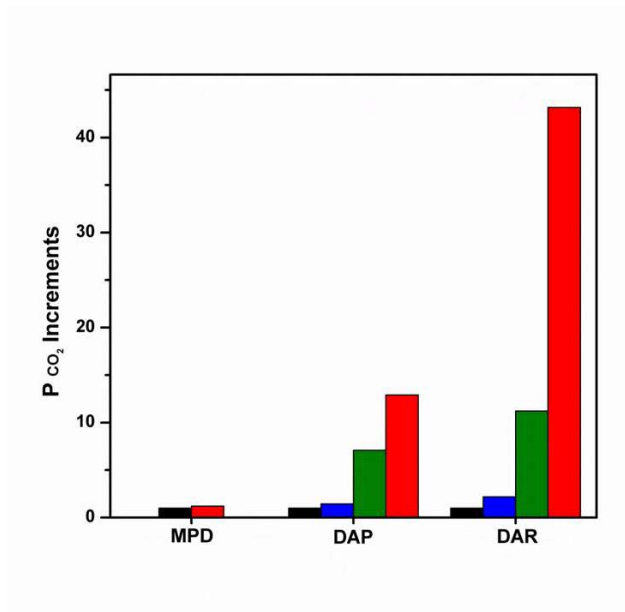
Figura 7. Incremento de permeabilidad al CO_2 por efecto de la temperatura. PI-MPD se refiere a una poliimida no hidroxilada, de composición semejante a HPI-DAR y HPI-DAP

En la siguiente etapa de este trabajo se ha estudiado el efecto de isomería en el monómero hidroxi-amina sobre las reacciones de polimerización, el proceso de trasposición y las propiedades generales de los precursores y los polímeros TR finales. En el proceso de trasposición se pierde una molécula de CO_2 por cada grupo imida que pasa a benzoxazol, según el siguiente esquema:
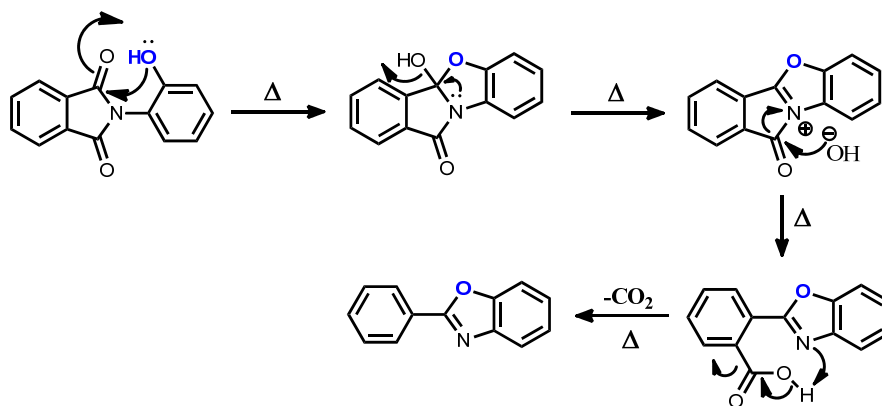
Como se ve, se admiten dos pasos intermedios y la formación de un ácido-benzoxazol que se descarboxila a muy alta temperatura con formación de benzoxazol y pérdida de CO_2. En monómeros derivados del bifenilo, es interesante conocer la influencia de la posición de la imida respecto al enlace puente entre los dos restos de fenileno puesto que la trasposición implica intercambio de átomos que solo se pueden dar si se producen movimientos de todo el anillo de benceno. Por ello, en este apartado se han preparado *orto*-hidroxipoliimidas a partir del monómero 3,3'-diamino-4,4'-dihidroxibifenilo (*m*HAB), y se han estudiado sus propiedades y sus capacidades para dar polímeros TR, en comparación con su *orto*-hidroxipoliimida homóloga preparada a partir de 3,3'-dihidroxibencidina (HAB), que se ha utilizado con éxito anteriormente en repetidas ocasiones como monómero de partida para TR-PBOs.

La optimización de una ruta de síntesis para el nuevo monómero y la mejora de los protocolos de purificación fueron objetivos de la primera etapa, que se cubrió con éxito y ello permitio la obtención de *orto*-hidroxipoliimidas de alto peso molecular a partir de ambos isómeros dihidroxi-diamina y el dianhidrido 6F. En la **Figura 8** se muestra la reacción de policondensación a partir de ambos monómeros isoméricos. La ciclación de ácido poliámico a poliimida se efectuó en los dos casos mediante deshidratación azeotrópica para evitar la esterificación del grupo OH con anhidrido acético, que es el agente deshidratante tradicional en la formación de imidas cíclicas.
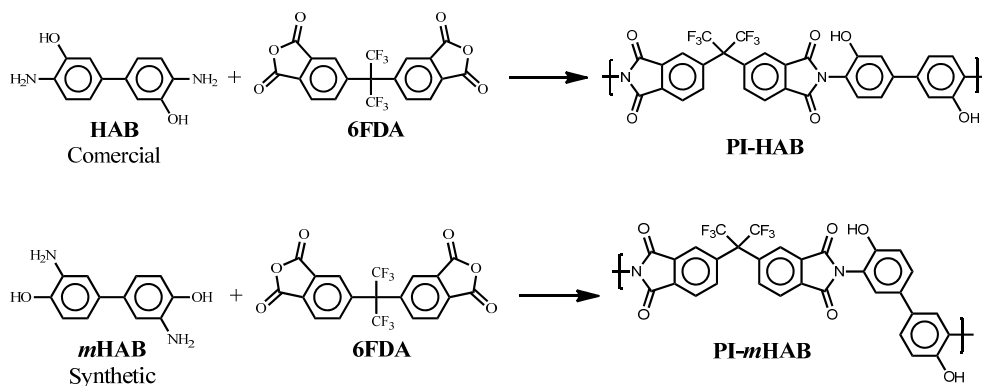
Figura 8. Síntesis de precursores *orto*-hidroxipoliimida a partir de HAB y *m*HAB

Las propiedades físicas de ambas poliimidas no difieren prácticamente, excepto en la T_g, que es más alta para *PI-HAB* (356 ºC) que para *PI-mHAB* (330 ºC), como cabe esperar puesto que la primera puede adoptar una conformación "todo lineal", que le permite alcanzar un mejor empaquetamiento molecular que PI-*m*HAB y por tanto una temperatura de transición vítrea más alta. La conversión de estas especies precursoras a TR-PBOs se pudo llevar a cabo satisfactoriamente en el estado sólido sobre filmes de buenas propiedades mecánicas. La **Figura 9** ilustra el proceso de trasposición química de ambas *orto*-hidroxipoliimidas a alta temperatura.
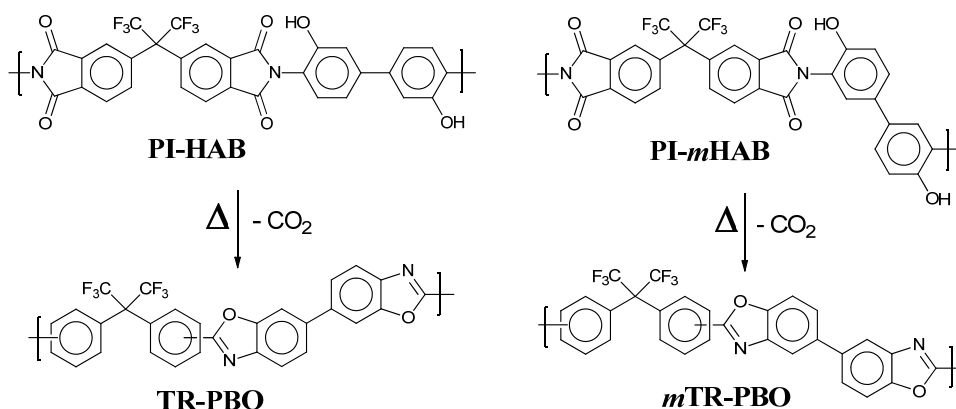
Figura 9. Conversión *orto*-hidroxipoliimida a bezoxazol mediante trasposición química a alta temperatura de *PI-HAB* y *PI-mHAB*

El seguimiento del proceso de conversión mediante diversas técnicas, y en especial mediante análisis termogravimétrico, TGA, y medidas de densidad, puso de manifiesto un claro comportamiento diferencial que solo puede ser atribuido a la distinta orientación del grupo imida y el fenileno vecino en los dos precursores isómeros. Además, la menor T_g del polímero *PI-mHAB* facilita que la trasposición se produzca a menor temperatura que en *PI-HAB*, aunque en este último se alcanzó un grado mayor de conversión a alta temperatura y largos tiempos de residencia. No obstante, el polímero *PI-mHAB* dio lugar a un TR-PBO con mayor fracción de volumen libre (*FFV*) y mejores propiedades de permeación; de hecho, mientras que el tratamiento térmico entre 350 ºC y 450 ºC

produjo notables incrementos sucesivos de *FFV* para *PI-mHAB*, la ganancia en *FFV* para *PI-HAB* no fue tan alta, ni siquiera a 450 ºC. Consecuentemente, al ir ganando en contenido de PBO, el precursor orientado en *meta* fue produciendo membranas que se localizan bien por encima del límite de Robeson de 1991, y próximas al límite de 2008 a medida que la temperatura del tratamiento se acercaba a 450 ºC, llegando a permeabilidades al CO_2 por encima de 700 Barrers y más de 120 Barrers para el oxígeno. Por el contrario, las membranas obtenidas a partir de *PI-HAB* en ningún momento superaron el límite de Robeson de 1991, como se puede observar en la **Figura 10**.

Todo lo cual viene a confirmar que la utilización de monómeros isómeros de los comerciales, es una alternativa muy favorable en términos de simplificación del proceso, por poder efectuar la trasposición a menor temperatura, y en términos de eficiencia puesto que se obtienen polímeros TR con mejores propiedades de permeación.
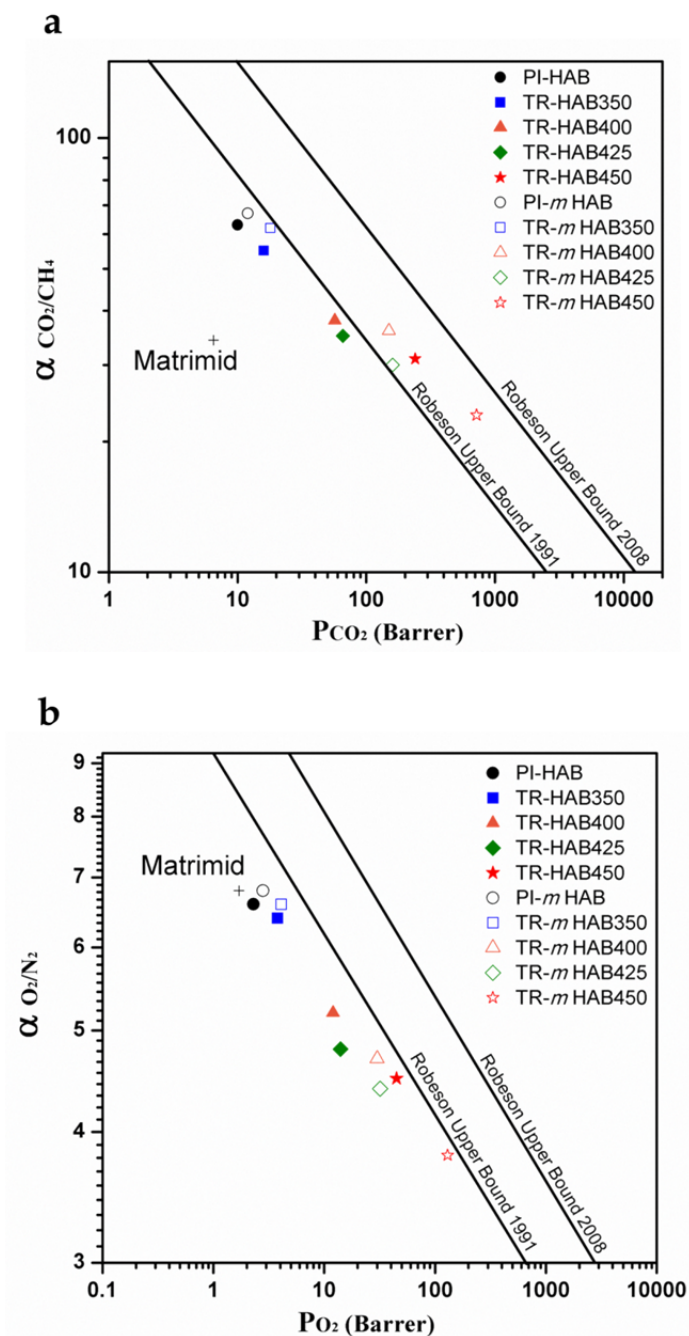
Figura 10. Diagramas permeabilidad/selectividad para CO_2/CH_4 (a) y O_2/N_2 (b) de TR-PBOs a partir de *PI-HAB* y *PI-mHAB*

La tercera parte del proyecto completado en esta tesis significa un paso más en el estudio de los mecanismos que conducen a polímeros TR por vía térmica a partir depoliimidas *orto*-funcionalizadas. En la última parte del trabajo se ha llevado a cabo un estudio comparativo del comportamiento de poliimidas *orto*-funcionalizadas con distintos sustituyentes: metoxilo, hidroxilo y acetiloxi.

En el anterior apartado ya se sintetizó y se estudió exhaustivamente la poliimida *orto*-hidroxilada derivada de 3,3'-dihidroxibencidina (HAB) y el dianhidrido 6F, que se ha denominado *PI-HAB*. Ahora se estudian sus propiedades en comparación con dos poliimidas homólogas que tienen acetilo y metoxi como sustituyentes en *orto* al grupo imida y que denominaremos *PI-AcAB* y *PI-MeAB*.   En la **Figura 11** se presenta el esquema de síntesis de estas polimidas. Como se puede observar, las poliimidas *PI-HAB* y *PI-AcAB* se obtienen a partir de los mismos monómeros, pero esta última se obtiene mediante imidación química del intermedio ácido poliámico, empleando el sistema Ac_2O/piridina como agente deshidratante, lo que conduce a la acetilación prácticamente completa de los grupos hidroxilo. En cambio, la ciclación azeotrópica conduce a la poliimida hidroxilada pura.
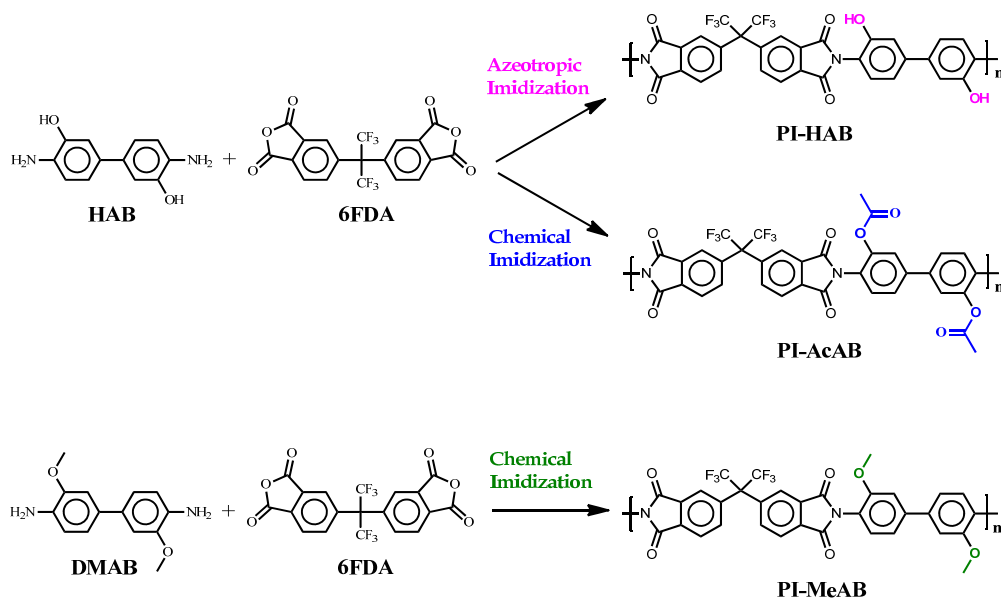
Figura 11. Esquema de síntesis de *PI-HAB*, *PI-AcAB* y *PI-MeAB*

Para la preparación de la poliimida metoxilada se utilizó 3,3'-dimetoxi-bencidina (DMAB) como monómero hidrofílico frente al dianhidrido 6F. Esta diamina es un reactivo químico muy antiguo, relativamente barato y de fácil purificación, que no ha sido utilizado hasta ahora en la preparación de membranas de separación de gases previa conversión térmica en el correspondiente polímero TR. Este monómero reacciona muy bien con dianhidrido 6F y se obtuvo un polímero de muy buenas propiedades, soluble y con una T_g de 311 °C, que es intermedia entre la T_g de *PI-HAB* y *PI-AcAB*. Como los demás intermedios estudiados a lo largo de este trabajo, la poliimida *orto*-metoxilada muestra excelentes capacidades para formar filmes y tiene unas propiedades térmicas y mecánicas que permiten aplicar el tratamiento térmico necesario para forzar la trasposición y formación de polímero TR, y lo mismo se puede decir para el polímero *PI-AcAB*.

Sin embargo, al aplicar las condiciones extremas de calentamiento que son necesarias para la trasposición química, se pudo observar que las propiedades, y la composición química de los polímeros TR finales, son muy distintas dependiendo de la naturaleza del sustituyente en posición *orto* de cada precursor. Mientras que la composición química del material obtenido tras tratamiento térmico del precursor *PI-HAB* es la esperada, es decir, fundamentalmente TR-PBO, en los otros dos casos evidencias espectroscópicas han demostrado que ni el mecanismo ni la composición final son las mismas, y que si bien hay que admitir la formación de TR-PBO en cierta extensión, la presencia de grupos benzoxazol es pequeña en el caso de *PI-AcAB* y prácticamente indetectable en el caso *PI-MeAB*. Basados en recientes antecedentes, y en los propios datos analíticos obtenidos en este trabajo, se ha podido postular un mecanismo de trasposición química a alta temperatura que se basa en la formación de intermedios lactona/lactama y la conservación en proporción muy considerable del esqueleto poliimida del precursor original, de tal forma que, en lugar de TR-PBOs netos, lo que se obtiene por trasposición química en el caso de precursores con *orto*-sustituyentes distintos de OH son polímeros TR de composición no bien definida en la que se encuentran ciclos imida y lactama, y en cantidad variable pero minoritaria, ciclos de benzoxazol, y se postula que la proporción final de estos ciclos depende no solo de la composición química inicial sino también, y en gran medida, de la temperatura

final del tratamiento y el programa térmico aplicado. Sin embargo, aún queda una laguna de conocimiento puesto que los métodos espectroscópicos utilizados no dan información precisa de los porcentajes de cada ciclo en el TR final, y por ello se ha propuesto un mecanismo que viene a explicar la formación de las distintas unidades por recombinación y trasposición. En este mecanismo se da especial importancia a la existencia de hidrógenos móviles cuya acción juega un papel fundamental en la formación de los distintos ciclos.

En cuanto a las propiedades de permeación, se comprobó que, tanto la poliimida *PI-AcAB* como la *PI-MeAB* dieron lugar a polímeros TR con mejores propiedades que la poliimida *PI-HAB*. Por ejemplo, la permeabilidad al CO_2 del *TR-AcAB* es de 632 Barrers y la del *TR-MeAB* es 540 Barrers, mientras que el *TR-HAB* presenta una permeabilidad al CO_2 de solo 240 Barrers. Estos resultados no han de explicarse solamente por el mayor tamaño molecular de las moléculas que se desprenden en los primeros estadios del tratamiento térmico: además del CO_2 común en todos los casos, se desprende CH_3 en *PI-MeAB* y cetena en *PI-AcAB*. Aunque cabría pensar que el orden en los valores de permeabilidad coincide con el tamaño creciente de los productos secundarios que se desprenden, y solo ese efecto podría explicar los resultados de permeabilidad encontrados, es en la distinta composición química de los TR finales en la que se ha de buscar la justificación definitiva de las propiedades de permeación de las membranas obtenidas a partir de los tres polímeros distintos.
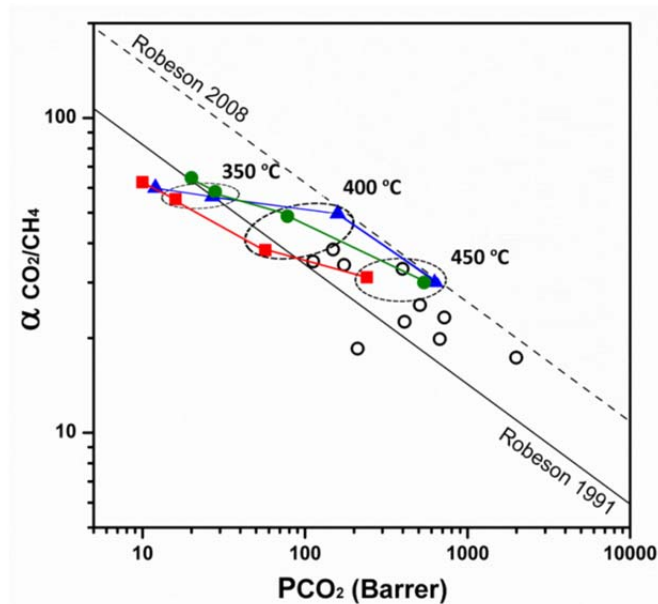
Figura 12. Diagrama de Robeson para las tres series de poliimidas: ■*TR-HAB*, ▲ *TR-AcAB*, ●*TR-MeAB*, ○ Datos de polímeros TR previamente descritos en la literatura. En la gráfica se muestran las diferentes temperaturas de conversión térmica

Se puede concluir que en este trabajo de tesis doctoral se ha podido establecer que a partir de *orto*-hidroxipoliimidas sintetizadas con monómeros originales, se pueden obtener polímeros TR-PBO y TR-PI-PBO con excelentes propiedades de permeación a gases, y en particular con un alto potencial para la separación de CO_2 de mezclas gaseosas, mediante un proceso de calentamiento controlado a altas temperaturas. También se ha podido probar que se obtienen polímeros TR con una proporción variable de ciclos imida, lactona/lactama y benzoxazol a partir de *orto*-acetilpoliimidas y *orto*-metoxipoliimidas mediante tratamiento térmico en las condiciones de síntesis de polímeros TR. Las propiedades de permeación de estos nuevos polímeros como membranas para gases, son comparables, y en algunos casos claramente mejores, que las propiedades de TR-PBOs descritos hasta ahora y evaluados para estas aplicaciones.

Chapter I

General Introduction

1.1. GLOBAL WARMING

Global warming is the term for the observed century-scale rise in the average temperature of the Earth's climate system and its related effects [1-12].

Already in its Fourth Assessment Report (AR4) [13,14], the Intergovernmental Panel on Climate Change (IPCC), a group of 1,300 independent scientific experts under the auspices of the United Nations, concluded that there is a better than 95 percent probability that greenhouse gases (GHG) emitted through human activities such as carbon dioxide (CO_2), methane (CH_4) and nitrous oxide (N_2O) have caused much of the observed increase in the average Earth's temperature over the past 50 years. Later, the Fifth Assessment Report (AR5) determined in a more accurate way the effect and projections of global warming for mankind [15-18].

The industrial activities have raised the combustion of fossil fuels like coal, oil and natural gas. Accordingly, they have caused an increment in atmospheric CO_2 levels from 280 parts per million to almost 400 parts per million in the last 150 years, producing an increase in the average temperature of the Earth's surface of 0.85 °C respect of pre-industrial level [3,19,20]. Unavoidably, world primary energy demand continues to rise, mainly driven by the growing energy needs of developing countries. Latest projections forecast energy growth to rise 40 % between 2007 and 2030 [20-23]. China and India alone will account for over 50 % of the total increase. Coal use is forecast to rise by over 60 % over this same period, with developing countries responsible for 97 % of this increase, primarily to meet increased rates of electrification.

The challenge is to reduce emissions at the actual level required to keep average global temperatures rising no more than 2 ºC above their pre-industrial level, above which there is a much higher risk of very serious climate impacts.

Nations are working toward a new global climate change agreement, *"Durban Platform for Enhanced Action"* [24-27], which will be formalized at the 21st Conference of the Parties in Paris, next December 2015. This international agreement offers governments a critical opportunity to craft a broad, balanced and durable agreement strengthening the international climate efforts.

The negotiations are aiming for an agreement to reduce greenhouse emissions that has "legal force" and is "applicable to all". This agreement, which will take effect from 2020, will bind major developing economies such as China, India and Brazil to emissions reduction commitments for the first time.

In order to mitigate the climate change, current worldwide energy policies are focused on the necessity to introduce novel strategies to reduce the emission of GHG into the atmosphere. Several characteristics in these energy policies are to increase the energy conservation and energy efficiency and invest in "clean energy". Numerous technology solutions offer substantial CO_2-reductions potential, including renewable energies, fossil-fuel use with CO_2 capture and storage, nuclear fission, fusion energy, hydrogen, biofuels, fuel cells and efficient energy end use. However, no single technology can meet this challenge by itself.

1.2. CARBON CAPTURE, UTILIZATION AND STORAGE

In this regard, one of the most promising alternatives for recovery of CO_2 is the Carbon Capture, Utilization and Storage (CCUS) [28-34], which become an important strategic option in reducing CO_2 emissions and allowing the continued use of fossil fuels and, consequently, the progressive economic development at the same time.

CCUS is considered as a "key technology" to palliate the climate change while meeting increasing global energy demand, being the only currently available technology that allows very deep cuts to be made in CO_2 emissions to atmosphere from fossil fuels at the scale needed.

This still not mature process encloses methods and technologies to remove CO_2 from the flue gas and from the atmosphere, followed by recycling the CO_2 for utilization and determining safe and permanent storage options. A general scheme of the CCUS process can be observed in **Figure 1.1**.

The first step in CCUS is separating CO_2 from other gases in the exhaust streams and capturing the CO_2, which can be applied to a variety of stationary sources of CO_2, using a diversity of CO_2 capture technologies.

There are four basic systems for capturing CO_2 from fossil fuels and/or biomass, known as capture from industrial process streams, post-combustion capture, pre-combustion capture and oxy-fuel combustion capture. These systems are shown in simplified form in **Figure 1.2**.
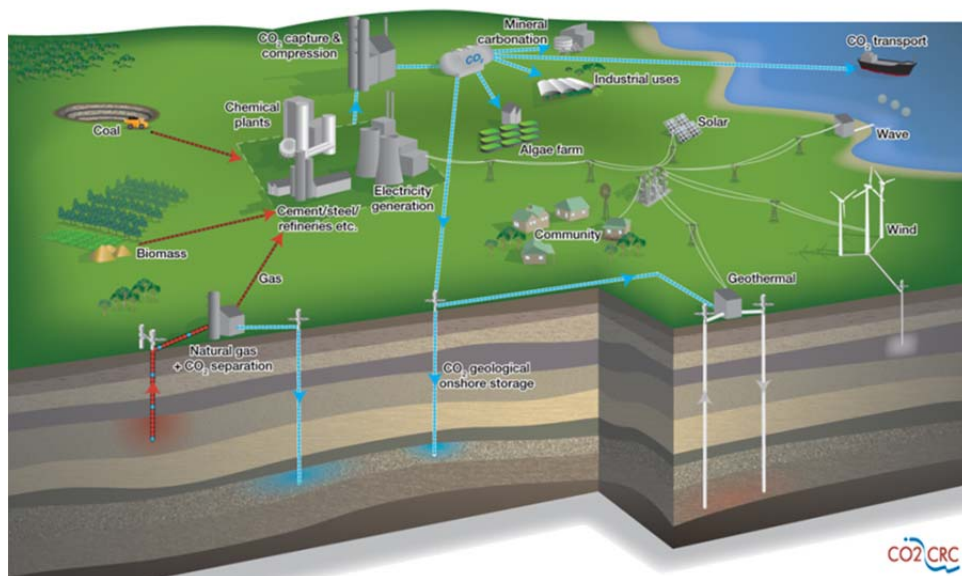
Figure 1.1. General scheme of CCUS process [35] (reproduced with permission of the copyright owner). Copyright © CO2CRC
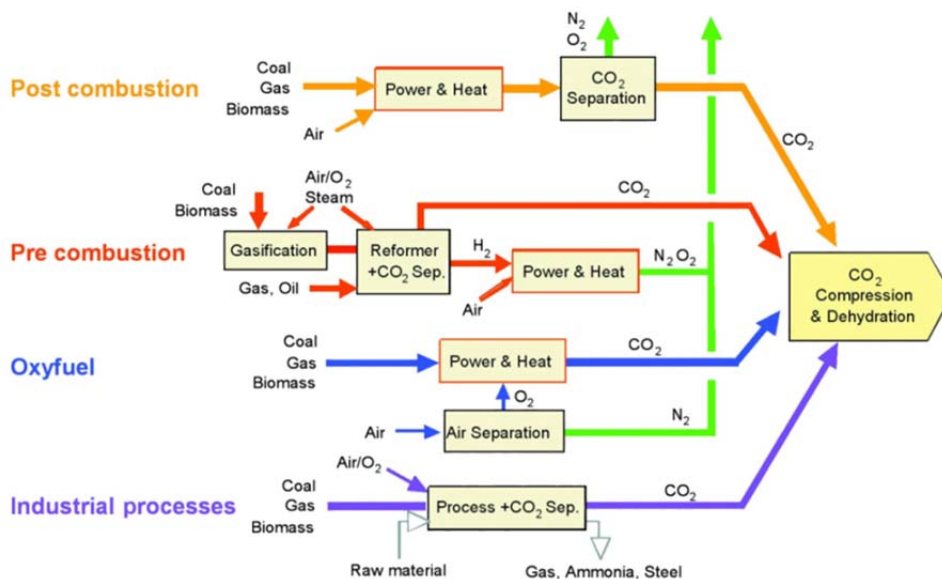
Figure 1.2. Overviews of CO_2 capture processes and systems. Source: Intergovernmental Panel on Climate Change (IPCC) [15]

Post-combustion systems separate CO_2 from the flue gases produced by the combustion in air (mainly N_2 and CO_2) [36-40]. Instead of being discharged directly to the atmosphere, flue gas is passed through equipment which separates most of CO_2. The CO_2 is fed to a storage reservoir and the remaining flue gas is discharged to the atmosphere.

Pre-combustion capture involves reacting a fuel with oxygen or air and/or steam to produce a mixture consisting mainly of carbon monoxide and hydrogen ("synthesis gas"). The carbon monoxide is reacted with steam in a catalytic reactor, called a shift converter, to give CO_2 and more hydrogen. The resulting mixture of hydrogen and CO_2 can then be separated into a CO_2 gas stream, and a hydrogen-rich fuel which is carbon-free that can be used to generate power or heat [41-46].

Oxy-fuel combustion systems use oxygen instead of air for combustion of the primary fuel to produce a flue gas that is mainly water vapor and CO_2 (no N_2). The resulting gas from this system is therefore highly concentrated in CO_2 (greater than 80 % by volume). After removal of water vapor by cooling and compressing the gas stream, the CO_2 is ready for subsequent transport and storage [47-50].

Current examples of CO_2 capture from industrial process streams are purification of natural gas and production of hydrogen-containing synthesis gas for the manufacture of ammonia, alcohols and synthetic liquid fuels. Most of the techniques employed for CO_2 capture in the mentioned examples are also similar to those used in pre-combustion capture. Other industrial process streams which are a source of CO_2 that should be captured include cement and steel production, and fermentation processes for food and drink production. CO_2 could be captured from these streams using techniques that are common to post-combustion capture, oxy-fuel combustion capture and pre-combustion capture.

1.3. NATURAL GAS SWEETENING

This thesis focuses on the development of new polymeric membranes for CO_2 removal, not only from flue gases but also from natural gas. CO_2 capture from this second source will not be the complete answer to the needs of climate change, since the volumes of combustion-generated CO_2 are much higher, but it may well be the first place where the capture and storage occurs.

Raw natural gas is often the only fuel in remote locations and on offshore platforms. Although natural gas is mostly considered as a "clean" fuel as compared to other fossil fuels, the natural gas found in reservoirs deposit is not necessarily "clean" and free of impurities. Natural gas consists primarily of methane but it also contains considerable amounts of light and heavier hydrocarbons as well as contaminating compounds such as CO_2, N_2 and H_2S, depending on the rock formation where it comes from.

As one of the major contaminants in natural gas feed, CO_2 reduces the heating value of natural gas in power plants and its presence can lead to corrosion in equipment and pipelines due to its acidic character [51-53]. Hence, the presence of CO_2 in natural gas remains one of the challenging gas separation problems in process engineering for CO_2/CH_4 systems [36,45,54-57].

Acid gas removal processes, also commonly known as gas sweetening processes, are used to purify the natural gas from acid gases such as CO_2 and H_2S. The technologies that are widely used to treat the natural gas include absorption processes, adsorption processes, cryogenic condensation and membranes. Although solvent absorption with amine or carbonate compounds is still the main separation technology applied for large productive plants, this traditional method implies the setting up of large absorption columns, the frequent regeneration of the absorbent and eventually its replacement. The global operation involves a serious investment in materials and energy consumption and, additionally, the continuous elimination of by-products is becoming a major concern in terms of ambient pollution and economical misbalance.

However, this acid gas removal is a growing area for membrane technology due to their numerous advantages such as high energy efficiency, environmentally friendly, non-requirement of a phase change, ease to operate, small foot-print, and ability to economically treat high concentration of CO_2 gas streams. Thus, membrane modules compete strongly with amine absorption in a wide range of operative conditions and are preferred to satisfy logistic constrains, i.e. offshore installations, or when reduced size is required. As showed in **Figure 1.3**, membranes are preferable in case of high CO_2 concentration, able to ensure a sufficient driving force, and for rather low flow rate, in order to limit the surface area required to meet the separation goal, hence maintaining the economical convenience of the process.
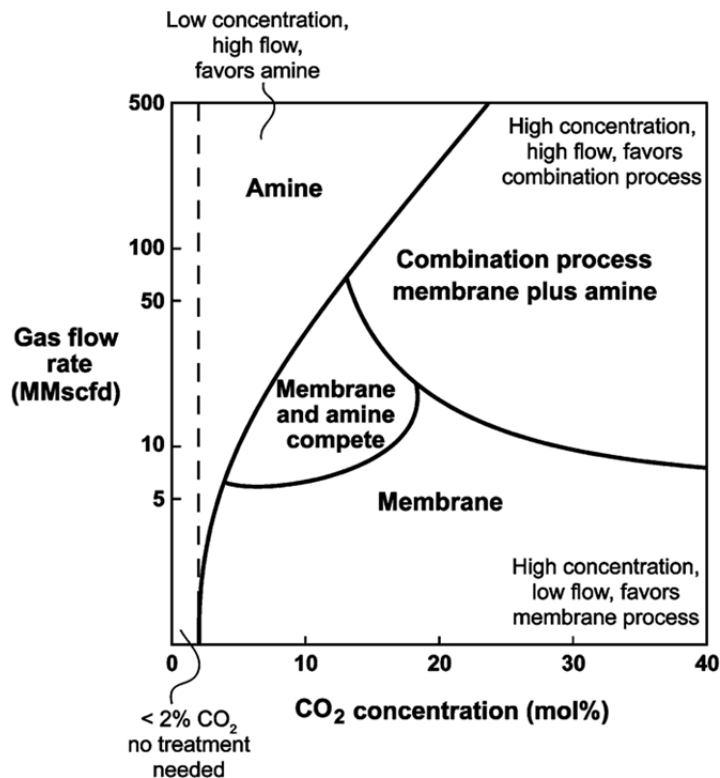
Figure 1.3. Comparison between membrane and amino absorption processes for CO_2 removal as a function of the CO_2 concentration and the gas flow rate [58] (reproduced with permission of the copyright owner). Copyright © 2008 American Chemical Society

1.4. MEMBRANES FOR GAS SEPARATION

1.4.1. HISTORY

Even though since more than one century ago gas diffusion and mass transport principles through polymer membranes are known, only in the last 40 years membranes have been applied on industrial scale in gas separation (GS). A strong push to the technology to produce economically high-performance membranes was given by the development of the innovative concept of high-flux asymmetric membranes (Loeb and Sourirajan, 1962) initially for reverse osmosis and later adapted to gas separation. Thus, several companies investigated a limited number of polymers for specific separations. Membrane-based GS has become a competitive separation technology since the first large industrial application of Prism® membranes by Permea (Monsanto) for hydrogen separation from the purge gas stream of ammonia plants. Within a few years, Permea systems were installed in many plants, encouraging other companies to advance their own technologies. By the mid-1980s Cyanara, Separex and Grace Membrane Systems were producing membrane plants to remove CO_2 from CH_4 in natural gas [53]. At about the same time, Dow launched Generon®, the first separation system to separate nitrogen from air. By 1990, Dow, Ube and DuPont developed materials with improved selectivity that made membrane separation much more competitive. **Figure 1.4** shows a timeline with the most relevant milestones in the history of membrane-based separation technology.
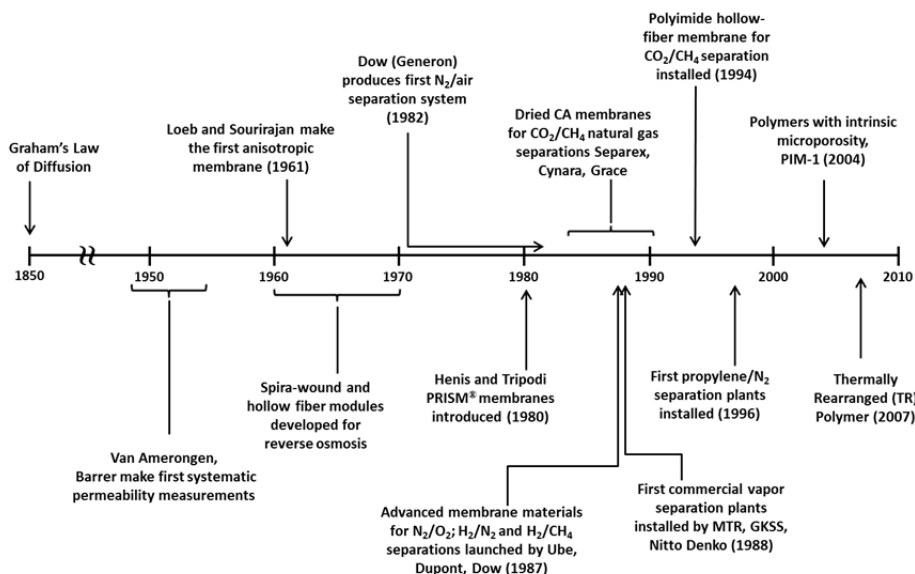
Figure 1.4. Milestones in the development of membrane gas separations [59] (adapted with permission of the copyright owner). Copyright © 2002 American Chemical Society

The use of membranes in separation processes has grown significantly and a continued growth is expected in the coming years as technology improves and application expands. Baker in 2002 estimated the market scale of membrane GS technology in year 2020 to be five times that of year 2000 [36,59,60]. However, membrane market is increasing more than it was expected to a large extent by the development of new materials with promising properties and characteristics, which play an increasingly important role in reducing the environmental impact and cost of industrial processes such as pre- and post-combustion processes. Currently, much of the research work is being addressed to the design of new materials for future generations of membranes and to the improvement of existing membranes. The main objective is to develop new membranes that exhibit both higher selectivity and permeability to specific gases. The proliferation of papers published in this area indicates that, presumably, the use of membranes in gas separation processes will become a common and widely accepted practice in all countries.

1.4.2. TRANSPORT IN GAS SEPARATION MEMBRANES

"A membrane is a physical device able to separate selectively one or more components in a mixture while rejecting others."

A molecule or a particle is transported across a membrane from one phase to another because a force acts on that molecule or particle. The driving force for the gas to permeate the membrane is a pressure gradient. The principle of gas separation is illustrated in **Figure 1.5.**

Porous or dense membranes can be used as selective gas separation barriers. Consequently, gas transport on these membranes is based on different mechanisms depending on the membrane porosity as shown in **Figure 1.6**.

Regarding porous membranes, three types can be distinguished depending on the pore size. If the pores are relatively large (from 0.1 to 10 µm) gases permeate through the membrane by convective flow, and no separation occurs. If the pores are smaller than 0.1 µm, then the pore diameter is smaller than the mean free path length (defined as the average distance a gas molecule travels before it will collide with another gas molecule) of the diffusing gas molecules. Diffusion through such pores is ruled by Knudsen diffusion, and the transport rate of gas is inversely proportional to the square root of its molecular weight (Graham's law of diffusion). Finally, if the membrane pores are extremely small (5-20 Å), gases are separated thanks to molecular sieving effect (**Figure 1.6**). Gas transport of this type of membranes is based primarily on the much higher diffusion rates of the smallest molecule, but sorption level differences may be important factors for similarly sized. In other words, this complex mechanism involves diffusion in the gas phase and diffusion of adsorbed species on the surface of the pores.
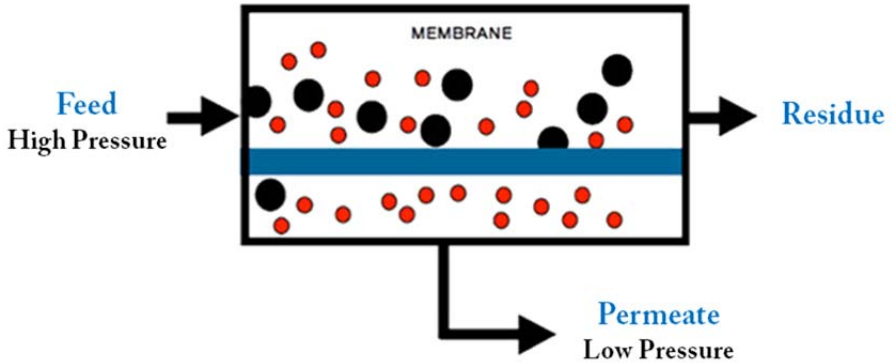
Figure 1.5. Schematic membrane-based gas separation process
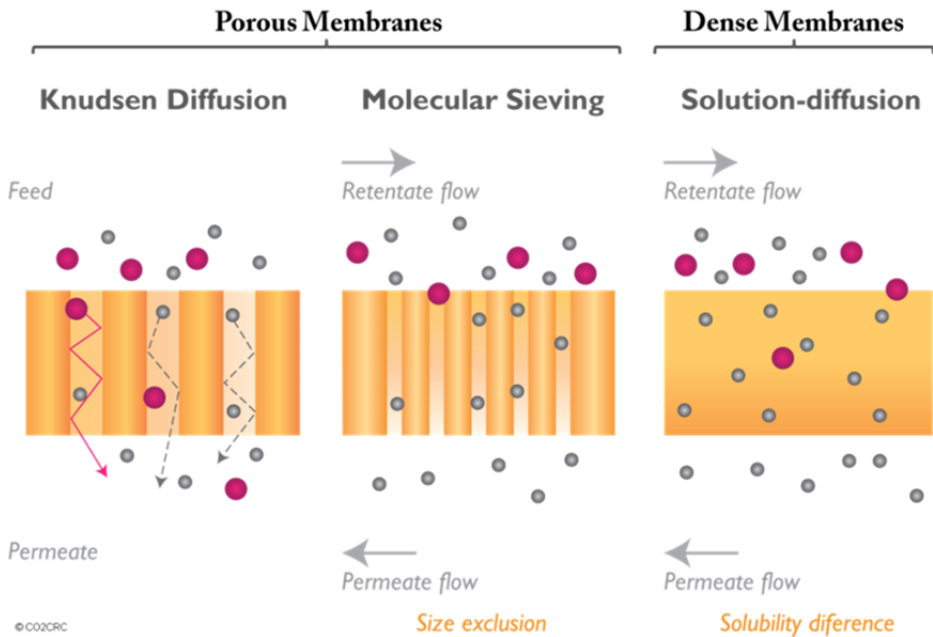
Figure 1.6. Mechanism for permeation of gases through porous and dense membranes [61] (adapted with permission of the copyright owner). Copyright © CO2CRC

Though microporous membranes are topics of research interest, yet almost all current commercial gas separations are based on dense polymeric membranes that are the main target of this thesis. Thus, the current work is focused on the solution-diffusion mechanism, which is understood to govern gas transport in all nonporous polymeric gas separation membranes [62-64] (**Figure 1.6**).

Early in the 19th century, works by J. K. Mitchell, A. Fick, and T. Graham [65-67] provided the fundamental mathematical basis for mass transfer through nonporous membranes. By measuring the permeation rates of different gases across polymeric membranes, T. Graham observed that there was no direct relation between known gas diffusion coefficients and the permeation rates. These observations led to the basic principles supporting the solution-diffusion model of transport through polymeric membranes [68].

The mass transport in a so-called solution-diffusion membrane is illustrated in **Figure 1.7** and consists of three relevant steps [69]: *sorption* of the various components from a feed mixture according to their partition coefficient between the gas and polymer phase, *diffusion* of the individual component within the membrane phase according to their activity gradients, and *desorption* of the components from the membrane in the permeate gas phase. Gas permeation is controlled by the diffusion of the penetrant gas molecules in the membrane matrix, while sorption/desorption equilibrium is assumed to be established at two interfaces between the gas and the membrane. A gas mixture is separated because of the differences in the solubility and mobility of the gas components in the membrane matrix.
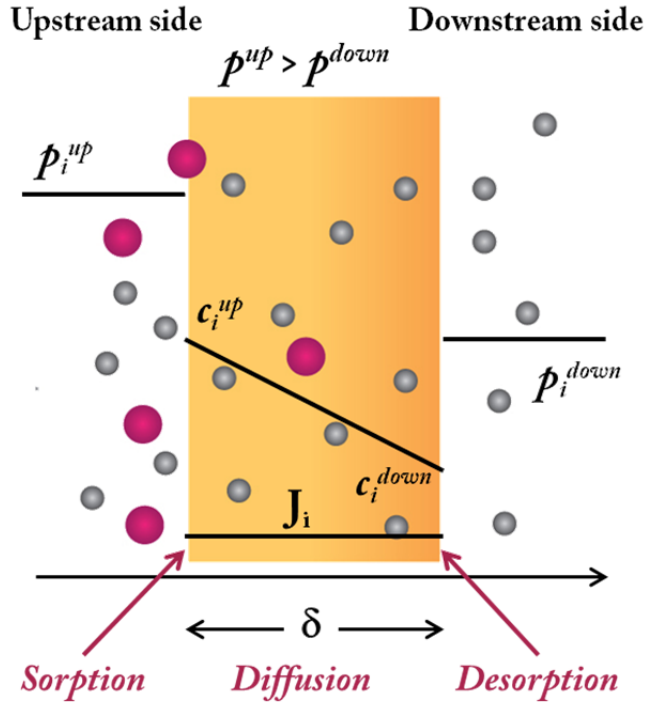
Figure 1.7. Membrane profiles through a gas permeation membrane, according to the solution-diffusion model, as the high-pressure feed and low-pressure permeate pressure change

The fundamental parameter to evaluate the transport properties in a gas separation membrane is the Permeability coefficient (P), theoretically defined as the amount of gas permeating across the layer per unit time and unit area scaled on the pressure drop and the membrane thickness:

$$P_i = \frac{J_i \cdot \delta}{p_i^{up} - p_i^{down}} \qquad \text{(Eq. 1.1)}$$

where J_i is the gas flux per unit area of the i species, δ is the membrane thickness and p_i^{up}, p_i^{down} are the partial pressure of component i on the upstream and downstream side of the selective layer, respectively.

Among several units used to express permeability, the most common one for non-porous membranes is the Barrer [70], defined as:

$$1 \ Barrer = 10^{-10} \frac{cm^3 (STP) \cdot cm}{cm^2 \cdot cmHg \cdot s} \qquad \text{(Eq. 1.2)}$$

Taking into account the sorption and desorption step at the equilibrium and describing the diffusion coefficient with Fick's law, the penetrant flux, J_i, can be expressed as a product of the diffusion coefficient, D_i, and the concentration gradient calculated on the thickness direction (∂x) (**Figure 1.7**):

$$J_i = -D_i \cdot \frac{\partial c_i}{\partial x} \qquad \text{(Eq. 1.3)}$$

Under the assumption of no external mass transfer resistance and conditions of equilibrium at gas–membrane interfaces, the solubility coefficient of a gas, S_i, in a membrane can be expressed by Henry's law, which indicates that a linear relationship exists between the external pressure p_i and the concentration c_i inside the membrane:

$$c_i = S_i \cdot p_i \qquad \text{(Eq. 1.4)}$$

Accepting a system with homogeneous properties, D_i can be considered independent from the space variable or membrane thickness (δ). Substitution of Equation 1.4 in Equation 1.3 and integrating across the membrane leads to:

$$J_i = D_i \cdot S_i \frac{p_i^{up} - p_i^{down}}{\delta} = D_i \cdot S_i \cdot \frac{\Delta p_i}{\delta} \qquad \text{(Eq. 1.5)}$$

Thus, the permeability can also be written as follows:

$$P_i = D_i \cdot S_i \qquad \text{(Eq. 1.6)}$$

The diffusion coefficient, D_i, is a kinetic term governed by 1) the amount of energy necessary for a particular penetrant to execute a diffusive jump through the polymer and 2) the intrinsic degree of segmental packing in the polymer matrix. The solubility coefficient, S_i, is a thermodynamic term that depends on factors such as the condensability of the penetrant, interactions between the polymer and penetrant, and the amount of penetrant-scale non-equilibrium excess volume in glassy polymers [71].

Several theoretical formalisms have been proposed to describe the diffusion of small molecules through a dense polymeric layer, and likely the most accurate one is the Free Volume Theory (FVT) [72]. Accordingly with FVT, gas molecules motion through the membrane can be described as a jumping mechanism and depends on the fractional free volume (FFV) of the polymer [68] (defining FFV as the fraction of volume in a polymer that is available to assist in molecular transport), as well as on the available energy, necessary to overcome the polymer-polymer interaction forces. Hence, the permeation of low molecular weight penetrants can be viewed as a temperature activated process, involving local motions of chains segments, schematically described in **Figure 1.8**, which temporarily permits the opening of narrow constrictions separating volume elements.

Based on the previous consideration, the permeability coefficient tends to increase along with the fractional free volume because diffusivity is a strong function of free volume, and the relationship is given by Fujita [73] expression:

$$D_i = A_i \cdot e^{\left(\frac{-B_i}{FFV}\right)} \qquad \text{(Eq. 1.7)}$$

where A_i and B_i are constant parameters characteristic for the polymer-penetrant pair.

Polymer chain

Dissolved penetrant

Opening of transient penetrant-sized gap in polymer matrix due to cooperative segmental motion

Gap closes behind penetrant, which has executed a diffusion step to a new region of polymer matrix
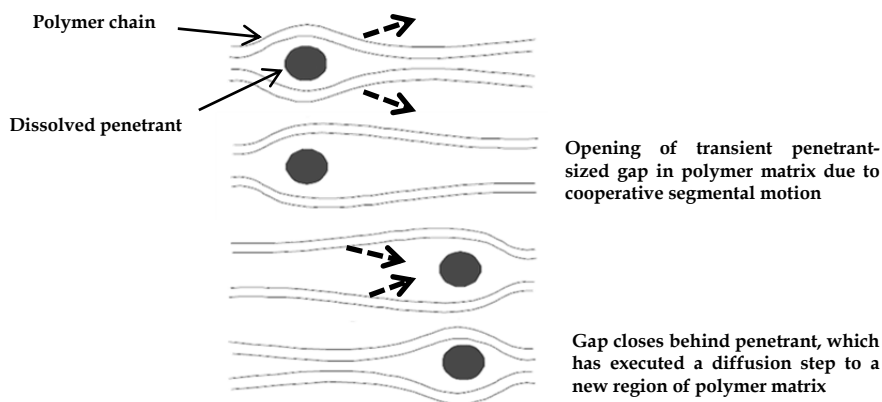
Figure 1.8. Schematic representation of small molecules motion across a dense membrane

Separation of a binary gas mixture is achieved by using a membrane material that permits different permeation rates for two components, *i* and *j*. The efficiency of a membrane in enriching a component over the other in the permeate stream can be expressed as a quantity called the separation factor, $\alpha_{(i/j)}$, which can be written as the ratio of permeabilities of the two gas penetrants:

$$\alpha_{i/j} = \frac{P_i}{P_j} \qquad \text{(Eq. 1.8)}$$

Based on solution diffusion model, also the selectivity can be decoupled in diffusivity and solubility terms:

$$\alpha_{i/j} = \frac{D_i \times S_i}{D_j \times S_j} \qquad \text{(Eq. 1.9)}$$

where D_i/D_j is the ratio of the diffusion coefficients of penetrants *i* and *j* and is called the "diffusivity selectivity" and S_i/S_j is the ratio of solubility coefficients of penetrants and is referred as "solubility selectivity".

An optimal membrane for gas separation processes must show high values of permeability (flow) and high selectivity (separation capacity) at the same time. It has been shown, empirical and theoretically, that there is an inverse relationship between permeability to different gases and its ability to separate these gases [74,75]. By comparison of permeability and selectivity values for numerous rubbery and glassy polymers, L. M. Robeson obtained the well-known Robeson plots for different couples of gases where the Robeson upper bounds are depicted. These upper bounds, which were set up in 1991 and reviewed in 2008 in order to update with new polymer data, represents one of the most useful device for evaluating membrane performance and are considered the benchmark in gas separation membrane development. Upper bounds move towards the upper right corner of the plot as new materials with enhanced gas properties are developed. **Figure 1.9** shows, as an example, the Robeson plot for CO_2/CH_4 separation where the black solid lines represent the 1991 and 2008 upper bounds. Due to this trade-off, polymeric membranes show a balanced behavior, in such a way that an increase in permeability usually corresponds to a decrease in selectivity and *vice versa*.

Considerations performed by Robeson allowed to describe the requirements for being a good candidate in gas separation, and described the following empirical correlation to define the upper bound for a pair of gases *i* and *j*:

$$P_i = K\alpha_{ij}^n \qquad \text{(Eq. 1.10)}$$

where P_i is the permeability of the more permeable gas, *n* is the slope of the upper bound line, and *K* is a constant for one specific gas pair termed the front factor. Thus, it can be concluded that the closer to the line that marks the limit, or even better if it is surpassed, the better the gas separation properties of the membrane for a determined pair of gases.
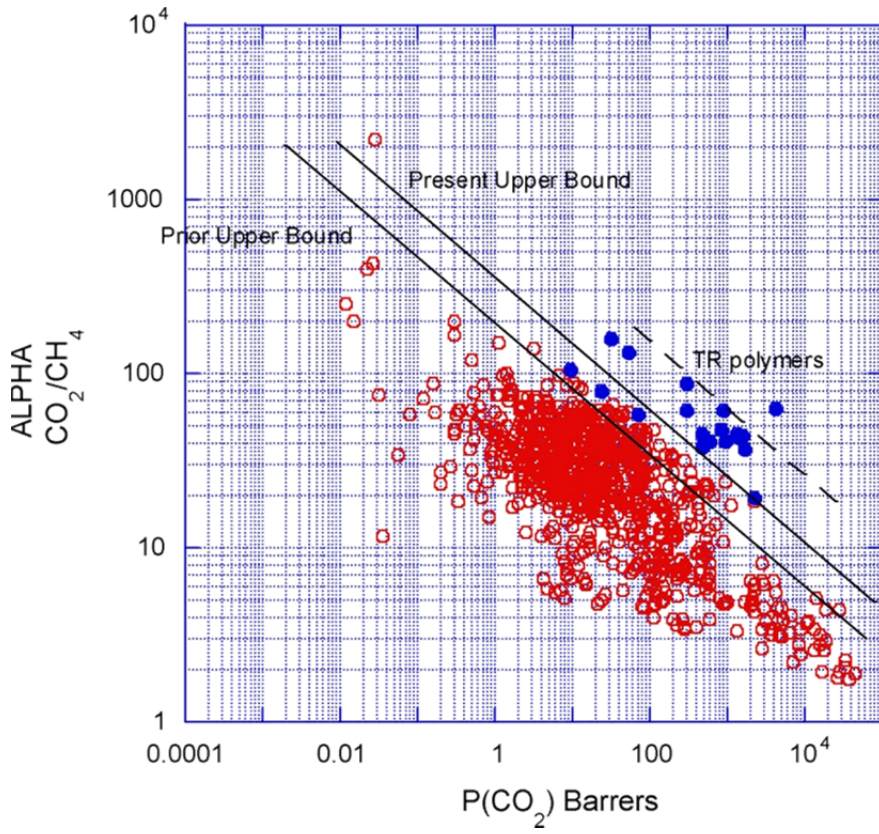
Figure 1.9. Robeson Plot for CO_2/CH_4 separation [75]

1.5. CHALLENGES IN MEMBRANE-BASED GAS SEPARATIONS

To be a potential candidate for gas separation, a polymer membrane must show good permeability and selectivity balance, and also high productivity and high stability. Membrane productivity is concerned with the permeation rate, determined by the intrinsic permeability of the polymer, the effective membrane thickness, and the membrane packing density (i.e. the amount of membrane area per unit module volume). Membrane stability is the ability to maintain membrane performance for a long period of time, in other words, membrane should show low physical aging and high resistance to plasticization. In addition, other requirements are desirable in a membrane such as high chemical and thermal stability, good mechanical properties and suitable processability. Thus, it can be considered that to attain a material with low physical aging and high resistance to plasticization, which overpasses the 2008 Robeson upper bound, is the "key" challenge in polymeric membranes for gas separation.

1.5.1. BALANCE OF GAS PERMEABILITY AND SELECTIVITY

The ability to achieve higher permeability without compromising selectivity has been recognized as one of the routes to expand the market for gas membrane materials. As a consequence, structure-property studies related to membranes separation have been a significant area of research due to the polymer used to make a membrane is crucial to separation performance.

A modern study of the Robeson's Upper Bound made by Freeman in 1999 [76] suggested that, to surpass the upper bound, emphasis should be placed on increasing the selectivity by controlling inter-chain spacing and chain stiffness, up to a limit from which diffusion is not governed by the segmental motion of polymer. At this maximum point, gas separation enhancements are feasible if the selectivity increases by solubility through the incorporation of groups that interact specifically with a particular gas. This approach is universal and is one of the fundamentals that exist today to rationally design polymer molecular structures for gas separation membranes capable of surpassing the trade-off.

Currently, while many polymeric materials have surpassed the 1991 bound, the 2008 upper bond has been surpassed by only very few polymers. In particular, polymers which offer the best balances of permeability and permselectivity are generally glassy polymers having high fractional free volume (poor packing density) and rigid structures. For instance, some of these high performance polymers include cross-linkable 6FDA-durene/DABA co-polyimides grafted with α, β and γ cyclodextrin [77]; microporous polybenzimidazoles [78]; polymers of intrinsic microporosity (PIM) [79-81]; poly(benzoxazole-co-pyrrolone) [82]; and thermally rearranged aromatic polyimides (TR) [83-85]. However, even though surpassing the Robeson upper bound always involves an enhancement in the transport properties of fabricated membranes, the utmost concerns of material scientists in gas separation membranes are penetrant-induced plasticization and physical aging.

1.5.2. PHYSICAL AGING AND PLASTICIZATION

Currently, a considerable amount of glassy polymers present an excellent productivity to separate gases at high pressure. However, these materials have some drawbacks such as its physical aging (decrease of the free volume over time) and a tendency to plasticize with certain penetrants that affect significantly the permeability and the industrial viability of a membrane.

Glassy polymers exhibit a non-equilibrium structure and, specifically, they are characterized by an excess of the thermodynamic quantities (i.e. enthalpy, entropy, specific volume) compared to the equilibrium state [86,87]. The distance from equilibrium generates a driving force responsible of the natural evolution of the polymer structure towards a state closer to the fully relaxed thermodynamic conformation. Physical aging is manifested through volume relaxations [88] of the specimen, which are responsible of the densification of the polymer structure and, consequently, of the decline in the available free volume elements for penetrants to diffuse through the membrane over time [89,90]. Thus, physical aging reduces gas permeability and modifies other physical properties of polymers such as specific volume, enthalpy and entropy [91-97]. Facing the negative effect on the gas permeability, physical aging produces usually an increase of the separation factor [97,98]. The reduction of void's dimensions distribution affects more significantly the penetrant with the larger kinetic

diameter, enhancing the membrane selectivity, in agreement with Robeson trade-off [75].

In addition, recent studies showed that physical aging is also closely related to the membrane thickness, especially when membranes exhibit thickness less than 1 μm. This dependence has important implications for gas separation membranes, since at the industry level is frequent using membranes with low thicknesses in order to increase their productivity [91,97,99,100]. As an example, **Figure 1.10** illustrates the values of permeability to oxygen (Barrer) *vs* time of physical aging for a Matrimid® coated with PDMS membrane. It is evident that as the time of aging gets longer, the permeability to oxygen decreases, and it can be also observed that the rates of physical aging at short aging times are higher when the membrane thickness are lower. Therefore, the membrane thickness is an important factor to consider in the manufacture of commercial membranes, since an uncontrolled physical aging can lead to a substantial loss in transport properties.

Definitively, it is expected that productivity of commercial polymer membrane modules will decline significantly over their life of several years due to physical aging. This in turns affects the membrane performance and hinders commercialization of membranes for industrial separation [101].

The increment in gas concentration within a polymer matrix produces an increase in the free volume and chain motion that, in turn, increases gas diffusion coefficients and decreases diffusion selectivity. This phenomenon, known as plasticization, can be induced by condensable gases which include CO_2, hydrocarbons and other organic vapors. Plasticization induced by CO_2 remains a problem commonly encountered in gas separation involving aggressive feed streams, such as in natural gas stream [102,103]. At low pressure, an increment in the pressure generally produces a decrease in permeability due to volume relaxation and gradual saturation of microvoids in the membrane [101,104,105]. Plasticization occurs at high partial pressure (concentration) of CO_2, and when this phenomenon occurs, CO_2 increases the mobility of polymer chain segments, thereby increasing the diffusion coefficients of all penetrants in the membrane [104]. Consequently, plasticization produces an increase in permeability and a decrease in selectivity as the partial pressure of plasticizing penetrant rises over a critical level. The pressure at which the permeability shows a minimum

value is the plasticization pressure, beyond which permeability begins to increase with increasing pressure [101,106] and, consequently, membrane performance starts to decline. This fact negatively impacts on process economics and reliability.
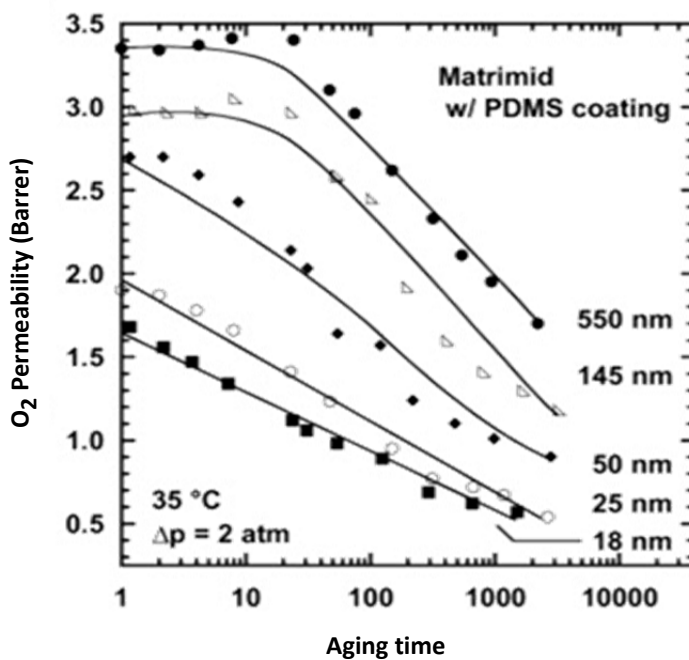

Figure 1.10. The effect of film thickness on Matrimid® with PDMS coating O_2 permeability in ultrathin films [91] (reproduced with permission of the copyright owner). Copyright © Elsevier

1.6. HIGH PERFORMANCE POLYMERS FOR GAS SEPARATIONS

In recent years, membrane technology has undergone outstanding development thanks to the use of new polymer materials which have improved the existing families of gas separation membranes. Some of these polymers include high free-volume glassy polymers, which offer a suitable approach for making efficient gas separation membranes due to their free volume elements are essentially interconnected. In other words, these polymers, known as microporous polymers, contain micropores (pores with dimensions < 2nm as defined by IUPAC in the context of adsorption studies [107]) and may exhibit adsorption behavior like that of a molecular sieve [108].

Some examples include polymers such as substituted polyacetylenes [109-111] like poly(1-trimethylsilyl-1-propyne (PTMSP), perfluoropolymers like Teflon AF2400, and aromatic polyimides (PIs).

PTMSP has the highest gas permeability among polymeric membranes. However, it does not exhibit efficient separation properties for small molecules [111,112] because the polymer main chain structure is not rigid enough. In addition, as a consequence of its non-rigid structure, large aging effects have been observed with permeability decreasing over time [113]. Commercially available Teflon AF2400 and AF1600 are perfluoropolymers with high gas permeabilities. They have very low densities, reflecting their high free volume. The strategic molecular peculiarity of Teflon AF is the bulky dioxole moeity, which disrupts chain packing leading to high permeability. However, their relatively flexible polymer backbone prevents competent gas separation performance. Both polymer families, substituted polyacetylenes and perfluoropolymers, have demonstrated higher permeability than other conventional polymers; however, due to the trade-off relationship, they exhibit a low selectivity [51].

Aromatic polyimides (PIs) have shown to be interesting materials for gas separation applications, since they reveal notable separation performance with good mechanical and thermal stability. The selectivity of these polymers is associated to their rigid molecular chains, generated from strong intermolecular bonds, which impose major constraints to rotation and mobility of the chain elements. Furthermore, the very high thermal stability (T_g usually higher than 250°C, and thermal degradation onset above 450 °C) makes polyimides suitable for a wide variety of gas separation processes. During the last decades, many research groups have studied the properties of the PIs as gas separation membranes for advanced industrial processes [114,115]. Most of these studies focused on the synthesis and development of new well-designed PIs having improved properties in terms of solubility-processability and, in addition, showing good values of productivity in gas separation processes [116]. The most used strategy to obtain materials with higher permeabilities is the incorporation of bulky groups [117-122] such as CF_3 in the polymer main chain, making difficult the chain packing and, consequently, increasing the fractional free volume and the polymer solubility. In addition, the optimum would be that these groups also restrict the mobility of the chain, which would provide a high structural rigidity, and consequently a high selectivity [117].

Recently, the search of new rigid porous materials to improve the separation ability and durability of membranes led to the emergence of a new class of microporous polymers with adequate rigidity, such as polymers of intrinsic microporosity (PIMs) and thermally rearranged polymers (TRs), which show high selectivity, as well as extraordinary permeability compared with other membrane materials. The membranes derived from these polymers surpassed the Robeson upper bound [83,123], providing the potential for more efficient membranes for gas separation processes in many industrial applications.

1.6.1. POLYMERS OF INTRINSIC MICROPOROSITY (PIMs)

Polymers of intrinsic microporosity (PIMs) were introduced by Budd and McKeown as polymers with a continuous network of interconnected intermolecular microcavities, which is formed as a consequence of the shape and rigidity of the polymer structure [79,81,123,124]. Thus, a rigid ladder-like backbone and contorted structure prevent efficient packing of the macromolecules in the solid state, providing an intrinsic microporous structure with high free volume elements and high surface areas, so that they behave like molecular sieves. **Figure 1.11** shows the PIM-1 and PIM-7 structures, as well as a molecular model of fragment of PIM-1, which shows its irregular and kinked shape.

PIMs show two key structural characteristics. Firstly, the highly restricted backbone rotational movements due to their structure with no single bonds about which free rotation can occur. On the other hand, they incorporate sites of contortion (spiro centers or other rigid non-planar structural units)) giving the backbone an irregular and kinked shape. Solution-processability of PIMs depends on the choice of monomers. In **Figure 1.12** some examples of monomers used for the synthesis of PIMs are illustrated. The use of bifunctional monomers allows obtaining linear soluble polymers such as PIM-1 and PIM-7, prepared from monomers A1 and B4 and monomers A1 and B8, respectively.
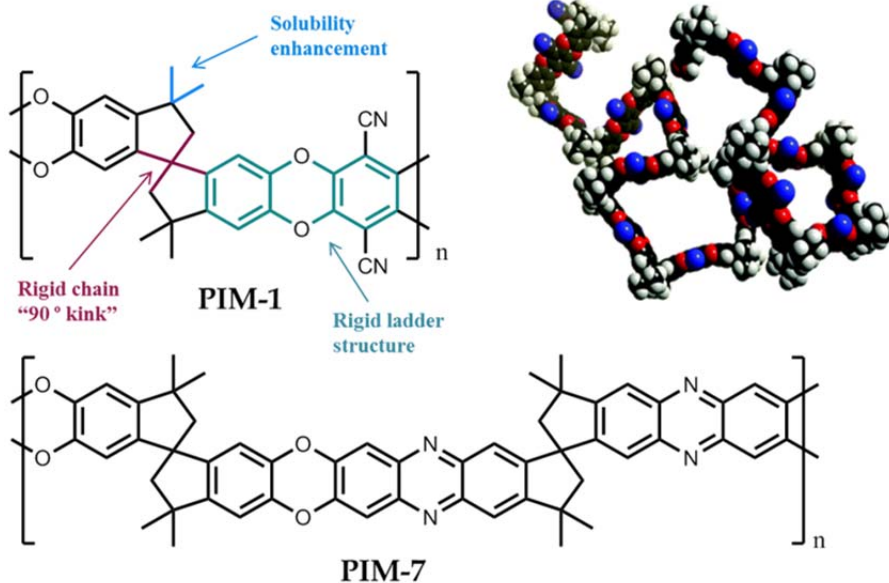
Figure 1.11. PIM-1 and PIM-7 structures and a molecular model fragment of PIM-1 [123] (adapted with permission of the copyright owner). Copyright © The Royal Society of Chemistry
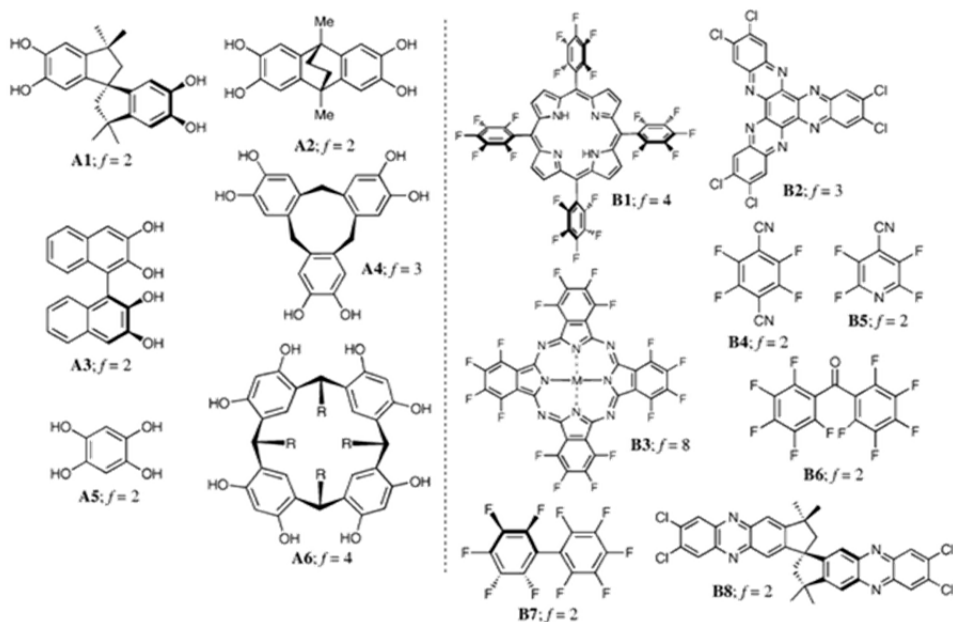

Figure 1.12. Some examples of monomers A and B for synthesis of PIMs [123] (reproduced with permission of the copyright owner). Copyright © The Royal Society of Chemistry

PIMs show excellent thermal and chemical stability and provide anti-plasticization properties and robust mechanical strength. In particular, PIM-1 exhibited no glass transition or melting temperature and also showed great stability in acidic, basic and oxidant conditions [124]. In addition, soluble PIMs such as PIM-1 and PIM-7 showed substantially adequate selectivity with an outstanding permeability, which implies advancement across the upper bound for O_2/N_2 separation. Reported O_2 permeability of PIM-1 ranged from 370 to 2270 Barrers, while the CO_2 permeability ranged from 2300 to 13600 Barrers, as summarized by Kim *et al*. [125]. Gas performance of PIMs membranes depends on polymer synthesis parameters, such as monomer purities, solvent used, and non-solvent post-treatment (methanol, for instance). Specifically, membranes treated with methanol before gas permeability measurements improved gas permeability nearly three-fold compared with non-treated membranes [80,126]. However, PIMs treated with methanol suffer intensive physical aging, showing a decrease in permeability of 23 % and 40 % for O_2 and N_2, respectively, after 45 days [80].

Several approaches have been carried out in order to improve PIMs performance. For instance, cross-linking methods have been introduced in PIM membranes to improve the gas separation properties using thermal energy and UV radiation [126-128]; since cross-linking stabilizes the polymer structures by forming a polymer network, reduces plasticization and improves membrane selectivity. Recent studies have been conducted to improve PIMs rigidity by introducing more non-flexible units such as Tröger's base and ethanoanthracene [129,130] or by modification of PIMs structure using click chemistry [131-134]. Polyimides having moieties with the observed ladder-like and contorted structure in PIMs, known as PI-PIMs, have been also developed to improve the physical properties of PIMs, attaining both the microporosity of PIMs and the advanced physical properties of PIs [135-139].

1.6.2. THERMALLY REARRANGED POLYMERS (TR POLYMERS)

As mentioned above, conventional polymeric membranes have been applied for many separation processes due to their numerous advantages [59]. On the other hand, aromatic glassy polymers having heterocyclic rings such as polybenzoxazoles (PBO), polybenzothiazoles (PBT), and polybenzimidazoles (PBI) have a rigid-rod structure with high-torsional energy barriers and excellent thermal stability [140]. Nevertheless, the stiff, rigid ring units in such topologies pack efficiently, leaving few penetrant-accessible free-volume elements and making these materials not much attractive for gas separation membranes due to its intrinsic low permeability. In addition, these rigid-rod polymers have such a high chemical resistance that they cannot be dissolved in common solvents for membrane preparation and can only be dissolved in strong acids [141]. Therefore, new synthetic routes of these rigid-rod polymers have focused mainly on increasing solubility and processability. Regarding gas separation membranes, the search of polyheterocycles having high FFV could be very interesting for applying these polymers in high values of gas productivity.

In 2007, Park *et al.* [83] accomplished a milestone in the preparation of gas separation membranes based on poly(1,3-benzoazole)s by making an *in situ* thermal rearrangement in solid state of aromatic polyimides containing *ortho*-positioned functional groups (i.e., –OH, -SH and –NH$_2$) to afford PBO, PBT and PBI membranes, as shown in **Figure 1.13**. This thermal rearrangement process, which involves a step of decarboxylation produced at high temperature, rendered materials with very high FFV. Park *et al.* based their work on previous studies carried out by Tullos *et al.* [142,143], where thermal rearrangement mechanism of polyimides having *ortho*-positioned functional groups was proposed. Subsequently, as an extension of the Park *et al.* work, the thermal conversion of diverse polymer precursors for membrane materials was also studied [78,82,144-150]. Thermally rearranged polymers, so-called TR polymers, cannot be processed due to the rigid polymer backbone of their aromatic structures and also to the presence of crosslinking due to the high temperature employed during their conversion; however, their precursor aromatic polymers are easily dissolved in common organic solvents, allowing TR membranes to be prepared in form of flat films or hollow fibers.

The precursors of TR polymers can be *ortho*-funtionalized polyimides or polyamides. Thus, two different types of TR polymers could be discerned; *i.* TR polymers obtained from *ortho*-funtionalized polyimides, so-called α-TR polymers, and *ii.* TR polymers obtained from *ortho*-funtionalized polyamides, so-called β-TR polymers. The most widely studied TR polymers are those TR-PBOs achieved by thermal rearrangement of *ortho*-hydroxyl polyimides (HPIs), and its thermal rearrangement mechanism is shown in **Figure 1.14**. Thermal conversion in the solid state of hydroxyl-containing polyamide precursors (HPAs) into TR-PBO has been also investigated [151,152] and is shown in **Figure 1.14** as well. Although the final TR-PBO structure is identical in both cases, yet α-TR membranes exhibit different properties compared with β-TR membranes, especially on considering gas transport properties.
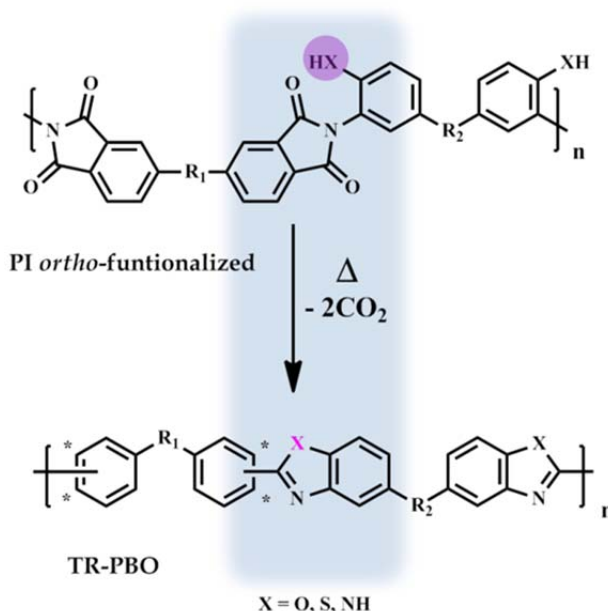

Figure 1.13. Thermal rearrangement scheme of aromatic *ortho*-funtionalized polyimides. * represents the possible substitution position of the aromatic rings
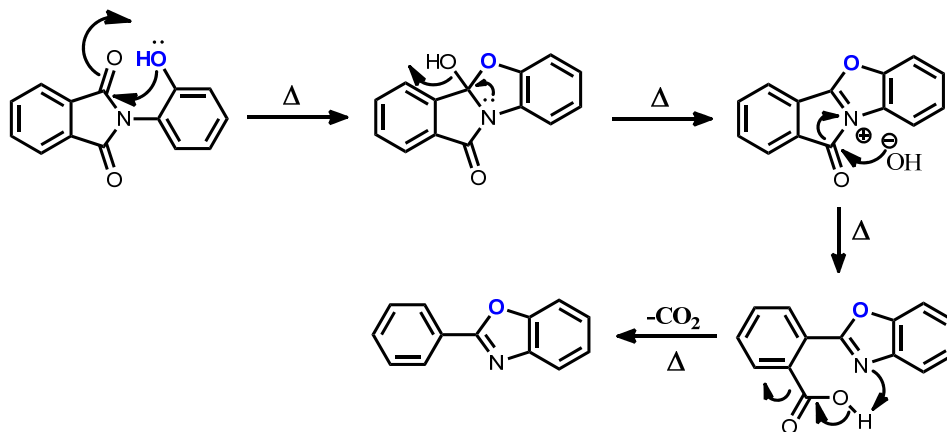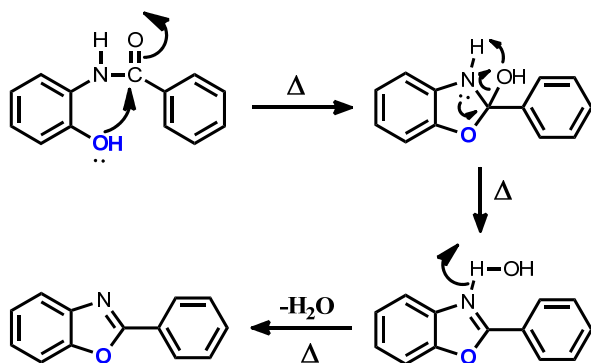
α-TR-PBO Mechanism

β-TR-PBO Mechanism

Figure 1.14. General thermal rearrangement mechanism from HPIs to TR-PBOs (α-TR-PBO) and general thermal rearrangement mechanism from HPAs to TR-PBOs (β-TR-PBO)

This thesis has been mainly focused on the thermal rearrangement of *ortho*-hydroxyl polyimides into TR-PBOs. Therefore, it will proceed with further detailed description of properties and characteristics of this α-TR-PBO.

The TR-PBO precursors are prepared by polycondensation reaction, in common aprotic solvents, of dianhydrides with diamines having –OH groups at the *ortho*-position. Obviously, different monomer structures lead to different polyimide structures and, therefore, to different TR-PBO structures after thermal treatment. Precursor polyimides exhibit different physical and transport properties depending on the imidization route used to prepare them [147]. As a consequence, the final TR-PBO properties are also dependent on the cyclization method. This effect of the imidization method used on the physical properties and gas performance will be discussed in the following chapters.

As described by Park *et al.*[83], an individual TR polymer chain would have a random-sequenced chain conformation that is arbitrarily formed with three different types of isomer PBO (assuming that the CO_2 loss can come from the breakdown of any CO moiety of the imide group): *meta-meta*, *para-para*, and *meta-para* (=*para-meta)*, as can be seen in **Figure 1.13**. These different polymer chain configurations result in the evolution of well-interconnected microcavities with a narrow cavity size distribution, which result in extraordinarily high gas permeability for small gas molecules, in particular, for CO_2 molecules [147]. In contrast with conventional polymeric membranes, which show cavity sizes with unimodal broad distribution that disturbs efficient gas separation, TR polymers exhibit bimodal cavity distributions (see **Figure 1.15**). Pores exhibit a hourglass-shape that provides the polymer membranes superior selectivity and permeability, in particular for CO_2/CH_4 separations. As shown in **Figure 1.15**, large cavities, which contribute efficiently for fast gas transport, are about 8 – 10 Å, while small cavities, which are appropriate for CO_2 separation by size difference in gas molecules, are about 3 – 4 Å. This bimodal cavity distribution can be tuned by the choice of the precursor structure and thermal treatment protocol applied to convert it into TR-PBO.
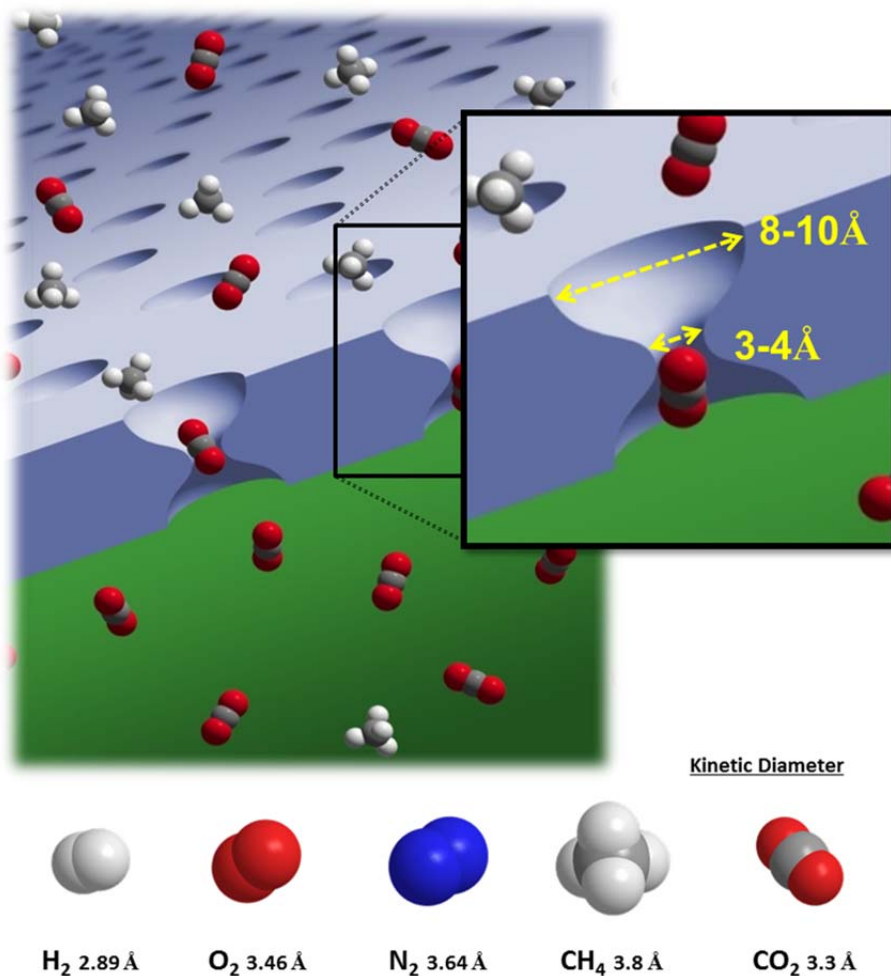
Figure 1.15. Scheme of hourglass-shaped pores [153] (adapted with permission of the copyright owner). Copyright © CSIRO

The relationships between the polymer structure and the cavity size have been studied by computer simulation approach. According to molecular modeling studies [154–157], thermal rearrangement produces property changes in terms of free volume (**Figure 1.16**) and angle distribution. Thus, TR polymers contain enlarged free volume elements and narrowed cavity sizes with respect to their precursor polyimides, increasing gas diffusion and solubility [148,149]. However, diffusivity term provides a much larger contribution than solubility term for the gas permeability increase. Hence, the rigid-rod structure of the resulting TR-PBO and the large increase in fractional free volume after thermal rearrangement are most likely responsible of the large increases in permeability, which reach more than one order of magnitude over those values of permeability of polyimide precursors. Additionally, the values of permeability of TR materials are much higher than those of typical glassy polymers.
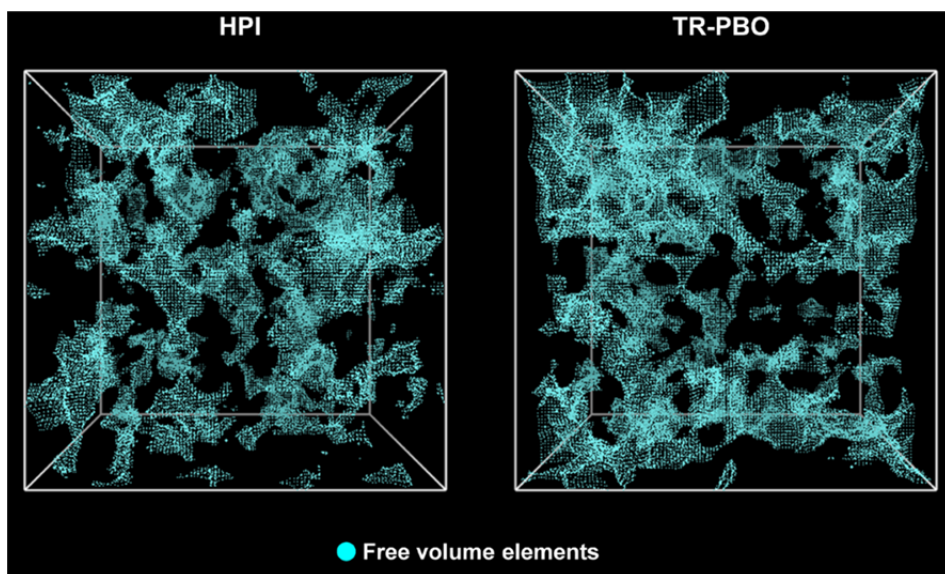
Figure 1.16. Simulated free volume distribution of HPI and TR-PBO [154,155] (reproduced with permission of the copyright owner). Copyright © American Chemical Society

Gas transport properties of TR polymer membranes are also dependent on the degree of thermal rearrangement, which can be modified by control of the thermal process temperature, time and other conditions [84]. Subsequently, the study of thermal rearrangement conditions is fundamental in order to find out the relationship between chain mobility, glass transition temperature, T_g, and thermal rearrangement [144,158]. Thermal rearrangement temperature, T_{TR}, is related to the glass transition temperature of precursor polyimide, which is strongly affected by polyimide structure.

Hence, precursor polyimides with high chain mobility (low T_g) exhibit a lower T_{TR} than that of highly stiff polyimides. Accordingly, it can be concluded that chemical structure and rigidity of polyimide precursor play a major role in the conversion from HPI to TR-PBO [144,158]. Moreover, there is no linear relationship between thermal conversion ratio and T_{TR}, even if thermal rearrangement is accelerated at high temperature. It has been also demonstrated that thermal rearrangement produces intermolecular and intramolecular side reactions, which form insoluble and cross-linked networks [158]. Thus, it can be confirmed that thermal rearrangement increases the gel fraction of TR polymers (insoluble portion), reaching 100 % when the conversion is completed. However, thermal rearrangement process requires high temperature treatments (generally > 400 ºC) to afford TR-PBO with good separation properties, and the use of these so-high temperatures (and also the enlargement of residence time at these temperatures) may determine that the thermal degradation process will overlap with the TR process resulting in reduced mechanical properties of the TR membranes [148].

Efforts have been made to enhance TR membrane properties for gas separation processes; thus, several approaches have been carried out to attain these targets. For instance, the use of copolymers such as TR poly(benzoxazole-co-imide) and TR poly(benzoxazole-co-pyrrolone) has been investigated to achieve synergistic effects of various TR polymers and glassy polymers [82,146,159,160]. Also, α,β-TR copolymers have been studied due to the synergy effects of α-TR-PBO membranes, which show high permeability, and β-TR-PBO membranes, which exhibit high selectivity [161]. In addition, TR-PIM copolymers have been accomplished, in such a way that high gas permeability coupled with robust mechanical properties were obtained [162]. Another interesting approach is

the crosslinking of TR polymers which has been proved to increase the free volume, and consequently, to enhance the permeability-selectivity balance [163].

In summary, it can be concluded that TR polymers are a strategic investment for high performance membrane materials for gas separation processes due to their numerous benefits, such as high gas separation performance, resistance to plasticization, low physical aging, high chemical resistance and the possibility of preparation in form of hollow fibers by conventional spinning processing. However, the development of TR membranes for functional applications seems to be hindered by several drawbacks such as the high temperature required to attain the conversion, the high-cost of precursors and the poor mechanical properties exhibited by these materials. In this regard, research efforts are required to overcome these limitations in such a way that TR membranes could be an affordable approach for energy-efficient gas separation technology.

1.7. AIM AND OUTLINE OF THIS THESIS

As mentioned above, T_{TR} is closely-related to the precursor structure, since it mainly depends on the T_g that, in turn, it depends on the polymer chain mobility. Hence, this thesis work is focused on the study of the structure-property relationship in order to optimize the separation processes and thus, overcome some TR polymer drawbacks. We have tried to carry out a rigorous research always considering the close relationship between scientific and practical terms.

Monomers have been chosen in pursuit of several preliminary conditions such as low cost and ability of imparting high stiffness into the macromolecular chain, which should increase the efficiency of cavity formation and inhibit the rapid collapse of the formed cavities. Hence, the search of more competitive formulations is one of the goals of this thesis.

This manuscript has been structured in three different works in order to facilitate its reading as much as possible, since three different structure aspects have been studied. Therefore, it has been considered appropriate to carry out a full separate study in each work, always focusing on the main features that affect the transport properties, and thus assembling all the requirements for each family, from its synthesis and characterization to its evaluation as gas separation membranes, in order to establish a link between structure and properties for each family, which is the major aim of this research (Chapters 3, 4 and 5).

Previously, general aspects of methodology and concepts, materials and reagents that have been employed, details of the processes carried out, and techniques used for the characterization and evaluation of materials, have been compiled in Chapter 2.

Finally, Chapter 6 collects the main conclusions to get an overview of the work done in this research.

1.8. REFERENCES

1.   Weber, E. U. 'Experience-Based And Description-Based Perceptions Of Long-Term Risk: Why Global Warming Does Not Scare Us (Yet).' *Climatic Change* **77,** 103–120 (2006).

2.   Kessel, D. G. 'Global Warming — Facts, Assessment, Countermeasures.' *Journal of Petroleum Science and Engineering* **26,** 157–168 (2000).

3.   Zecca, A. & Chiari, L. 'Fossil-fuel Constraints On Global Warming.' *Energy Policy* **38,** 1–3 (2010).

4.   Paterson, N. R. 'Global Warming: A Critique Of The Anthropogenic Model And Its Consequences.' *Geoscience Canada* **38,** 41–48 (2011).

5.   Hansen, J. 'Defusing The Global Warming TIME BOMB.' *Scientific American* **290,** 68–77 (2004).

6.   Krosnick, J. A., Holbrook, A. L., Lowe, L. & Visser, P. S. 'The Origins And Consequences Of Democratic Citizens' Policy Agendas: A Study Of Popular Concern About Global Warming.' *Climatic Change* **77,** 7–43 (2006).

7.   Rosenzweig, C. & Hillel, D. 'Global Warming And Agriculture.' in *Perspectives in World Food and Agriculture, Volume 2* 181–210 (2008). Blackwell Publishing

8.   Nordhaus, W. D. 'CLIMATE CHANGE: Global Warming Economics.' *Science* **294,** 1283–1284 (2001).

9.   Nordell, B. 'Thermal Pollution Causes Global Warming.' *Global and Planetary Change* **38,** 305–312 (2003).

10.   Young, C. ':The Discovery Of Global Warming.' *Isis* **97,** 804–806 (2006).

11.   Houghton, J. 'Global Warming.' *Reports on Progress in Physics* **68,** 1343–1403 (2005).

12.   BOTKIN, D. B. *et al.* 'Forecasting The Effects Of Global Warming On Biodiversity.' *BioScience* **57,** 227 (2007).

13.   Intergovernmental Panel on Climate Change. 'CLIMATE CHANGE 2007.' *synthesis report. Geneva: IPCC* (2007). Cambridge University Press

14.   IPCC. 'IPCC Fourth Assessment Report (AR4).' *IPCC* **1,** 976 (2007).

15.   IPCC. 'IPCC AR5 Technical Summary.' *IPCC* (2013).

16.   IPCC. 'IPCC Fifth Assessment Report (AR5) - The Physical Science Basis.' *IPCC* (2013).

17.   Stocker, T., Dahe, Q., Plattner, G.-K., Tignor, M. & Midgley, P. 'IPCC EXPERT MEETING ON ASSESSING AND COMBINING MULTI MODEL CLIMATE PROJECTIONS - MEETING REPORT.' *National Center for …* (2010).

18.   IPCC. 'Climate Change 2014 Synthesis Report Summary Chapter For Policymakers.' *Ipcc* (2014).

19. Aaron, D. & Tsouris, C. 'Separation Of CO 2 From Flue Gas: A Review.' *Separation Science and Technology* **40,** 321–348 (2005).

20. Cao, L. & Caldeira, K. 'Atmospheric Carbon Dioxide Removal: Long-term Consequences And Commitment.' *Environmental Research Letters* **5,** 024011 (2010).

21. Hoffert, M. I. *et al.* 'Energy Implications Of Future Stabilization Of Atmospheric CO2 Content.' *Nature* **395,** 881–884 (1998).

22. Sage, R. F. & Coleman, J. R. 'Effects Of Low Atmospheric CO2 On Plants: More Than A Thing Of The Past.' *Trends in Plant Science* **6,** 18–24 (2001).

23. Lacis, A. A., Schmidt, G. A., Rind, D. & Ruedy, R. A. 'Atmospheric CO2: Principal Control Knob Governing Earth's Temperature.' *Science* **330,** 356–359 (2010).

24. Banerjee, S. B. 'A Climate For Change? Critical Reflections On The Durban United Nations Climate Change Conference.' *Organization Studies* **33,** 1761–1786 (2012).

25. Chagas, T., Streck, C., O'Sullivan, R. & von Unger, M. 'The Durban Climate Conference Between Success And Frustration.' *Journal for European Environmental & Planning Law* **9,** 201–221 (2012).

26. Bodansky, D. 'The Durban Platform Negotiations: Goals And Options.' *Harvard Project on Climate Agreements* 12 (2012).

27. Govind, P. 'The Durban Platform For Enhanced Action – Prospects For Delivering Distributive Justice Through The Operation Of The Green Climate Fund.' *Ethics, Policy & Environment* **15,** 293–297 (2012).

28. Fu, C. & Gundersen, T. 'Carbon Capture And Storage In The Power Industry: Challenges And Opportunities.' *Energy Procedia* **16,** 1806–1812 (2012).

29. Spigarelli, B. P. & Kawatra, S. K. 'Opportunities And Challenges In Carbon Dioxide Capture.' *Journal of CO2 Utilization* **1,** 69–87 (2013).

30. Kentish, S., Scholes, C. & Stevens, G. 'Carbon Dioxide Separation Through Polymeric Membrane Systems For Flue Gas Applications.' *Recent Patents on Chemical Engineeringe* **1,** 52–66 (2008).

31. Pires, J. C. M., Martins, F. G., Alvim-Ferraz, M. C. M. & Simões, M. 'Recent Developments On Carbon Capture And Storage: An Overview.' *Chemical Engineering Research and Design* **89,** 1446–1460 (2011).

32. Anderson, S. & Newell, R. 'PROSPECTS FOR CARBON CAPTURE AND STORAGE TECHNOLOGIES.' *Annual Review of Environment and Resources* **29,** 109–142 (2004).

33. Boot-Handford, M. E. *et al.* 'Carbon Capture And Storage Update.' *Energy & Environmental Science* **7,** 130 (2014).

34. Haszeldine, R. S. 'Carbon Capture And Storage: How Green Can Black Be?' *Science* **325,** 1647–1652 (2009).

35. Cooperative Research Centre for Greenhouse Gas Technologies. 'CLEAN ENERGY FACILITIES.' at <http://www.co2crc.com.au/>

36. Baker, R. W. & Low, B. T. 'Gas Separation Membrane Materials: A Perspective.' *Macromolecules* **47,** 6999–7013 (2014).

37. Tena, A. *et al.* 'Gas Separation Properties Of Systems With Different Amounts Of Long Poly(ethylene Oxide) Segments For Mixtures Including Carbon Dioxide.' *International Journal of Greenhouse Gas Control* **12,** 146–154 (2013).

38. Drage, T. C., Arenillas, A., Smith, K. & Snape, C. E. 'Comparison Of Pre And Postcombustion CO2 Adsorbent Technologies.' *8th International Conference on Greenhouse Gas Control Technologies* 19–22 (2006).

39. Favre, E. 'Membrane Processes And Postcombustion Carbon Dioxide Capture: Challenges And Prospects.' *Chemical Engineering Journal* **171,** 782–793 (2011).

40. Puxty, G. *et al.* 'Carbon Dioxide Postcombustion Capture: A Novel Screening Study Of The Carbon Dioxide Absorption Performance Of 76 Amines.' *Environmental Science & Technology* **43,** 6427–6433 (2009).

41. Hoffmann, S., Bartlett, M., Finkenrath, M., Evulet, A. & Ursin, T. P. 'Performance And Cost Analysis Of Advanced Gas Turbine Cycles With Precombustion CO[sub 2] Capture.' *Journal of Engineering for Gas Turbines and Power* **131,** 021701 (2009).

42. Mori, Y., Masutani, S. M., Nihous, G. C., Vega, L. A. & Kinoshita, C. M. 'Pre-Combustion Removal Of Carbon Dioxide From Natural Gas Power Plants And The Transition To Hydrogen Energy Systems.' *Journal of Energy Resources Technology* **114,** 221 (1992).

43. Lee, S. H. *et al.* 'Development Of Water Gas Shift/membrane Hybrid System For Precombustion CO2 Capture In A Coal Gasification Process.' *Energy Procedia* **4,** 1139–1146 (2011).

44. Elwell, L. C. & Grant, W. S. 'Technology Options For Capturing CO2.' *Power* **150,** 0–60 (2006).

45. D'Alessandro, D. M., Smit, B. & Long, J. R. 'Carbon Dioxide Capture: Prospects For New Materials.' *Angewandte Chemie International Edition* **49,** 6058–6082 (2010).

46. Singh, R. *et al.* 'High Temperature Materials For CO2 Capture.' *Energy Procedia* **1,** 623–630 (2009).

47. Liszka, M. & Ziębik, A. 'Coal-fired Oxy-fuel Power Unit – Process And System Analysis.' *Energy* **35,** 943–951 (2010).

48. Al-Makhadmeh, L., Maier, J., Al-Harahsheh, M. & Scheffknecht, G. 'Oxy-fuel Technology: An Experimental Investigations Into Oil Shale Combustion Under Oxy-fuel Conditions.' *Fuel* **103,** 421–429 (2013).

49. Scheffknecht, G., Al-Makhadmeh, L., Schnell, U. & Maier, J. 'Oxy-fuel Coal Combustion—A Review Of The Current State-of-the-art.' *International Journal of Greenhouse Gas Control* **5,** S16–S35 (2011).

50. Chen, W., Chen, C., Bouwmeester, H. J. M., Nijmeijer, A. & Winnubst, L. 'Oxygen-selective Membranes Integrated With Oxy-fuel Combustion.' *Journal of Membrane Science* **463,** 166–172 (2014).

51. Bernardo, P., Drioli, E. & Golemme, G. 'Membrane Gas Separation: 1 Review Of State Of The Art.' *Industrial Chemical Engineering* **48,** 4638–63 (2009).

52. Ku, A. Y., Kulkarni, P., Shisler, R. & Wei, W. 'Membrane Performance Requirements For Carbon Dioxide Capture Using Hydrogen-selective Membranes In Integrated Gasification Combined Cycle (IGCC) Power Plants.' *Journal of Membrane Science* **367,** 233–239 (2011).

53. Spillman, R. W. 'Economics Of Gas Separation Membranes.' *Chemical Engineering Progress* **85,** 41–62 (1989).

54. Washim Uddin, M. & Hägg, M.-B. 'Natural Gas Sweetening—the Effect On CO2–CH4 Separation After Exposing A Facilitated Transport Membrane To Hydrogen Sulfide And Higher Hydrocarbons.' *Journal of Membrane Science* **423-424,** 143–149 (2012).

55. Peters, L., Hussain, A., Follmann, M., Melin, T. & Hägg, M.-B. 'CO2 Removal From Natural Gas By Employing Amine Absorption And Membrane Technology—A Technical And Economical Analysis.' *Chemical Engineering Journal* **172,** 952–960 (2011).

56. Swaidan, R., Ma, X., Litwiller, E. & Pinnau, I. 'High Pressure Pure- And Mixed-gas Separation Of CO2/CH4 By Thermally-rearranged And Carbon Molecular Sieve Membranes Derived From A Polyimide Of Intrinsic Microporosity.' *Journal of Membrane Science* **447,** 387–394 (2013).

57. Yampolskii, Y. 'Polymeric Gas Separation Membranes.' *Macromolecules* **45,** 3298–3311 (2012).

58. Baker, R. W. & and Kaaeid Lokhandwala*. 'Natural Gas Processing With Membranes: An Overview.' *Industrial & Engineering Chemistry Research* **47,** 2109–2121 (2008).

59. Baker, R. W. 'Future Directions Of Membrane Gas Separation Technology.' *Industrial & Engineering Chemistry Research* **41,** 1393–1411 (2002).

60. Lokhandwala, K. a. *et al.* 'Membrane Separation Of Nitrogen From Natural Gas: A Case Study From Membrane Synthesis To Commercial Deployment.' *Journal of Membrane Science* **346,** 270–279 (2010).

61. Cooperative Research Centre for Greenhouse Gas Technologies. 'MEMBRANE GAS SEPARATION.' at <http://www.co2crc.com.au/>

62. Pandey, P. & Chauhan, R. S. 'Membranes For Gas Separation.' *Progress in Polymer Science* **26,** 853–893 (2001).

63. George, S. 'Transport Phenomena Through Polymeric Systems.' *Progress in Polymer Science* **26,** 985–1017 (2001).

64. Wijmans, J. G. & Baker, R. W. 'The Solution-diffusion Model: A Review.' *Journal of Membrane Science* **107,** 1–21 (1995).

65. Mitchell, J. K. 'On The Penetrativeness Of Fluids.' *Journal of Membrane Science* **100,** 11–16 (1995).

66. Fick, A. 'On Liquid Diffusion.' *Journal of Membrane Science* **100,** 33–38 (1995).

67. Graham, T. 'On The Absorption And Dialytic Separation Of Gases By Colloid Septa Part I.—Action Of A Septum Of Caoutchouc.' *Journal of Membrane Science* **100,** 27–31 (1995).

68. Baker, R. W. 'Membrane technology and applications.' (2012). John Wiley & Sons, Ltd

69. Koros, W. J. & Fleming, G. K. 'Membrane-based Gas Separation.' *Journal of Membrane Science* **83,** 1–80 (1993).

70. Stern, S. A. 'The "barrer" Permeability Unit'. *Journal of Polymer Science Part A-2: Polymer Physics* **6,** 1933–1934 (1968).

71. Ghosal, K. & Freeman, B. 'Gas Separation Using Polymer Membranes: An Overview.' *Polymers for Advanced Technology* **5,** 673–697 (1994).

72. Vrentas, J. S. & Vrentas, C. M. 'Solvent Self-Diffusion In Glassy Polymer-Solvent Systems.' *Macromolecules* **27,** 5570–5576 (1994).

73. Fujita, H. 'Diffusion In Polymer-diluent Systems.' in *Fortschritte Der Hochpolymeren-Forschung* 1–47 (2006). Springer-Verlag

74. Robeson, L. M. 'Correlation Of Separation Factor Versus Permeability For Polymeric Membranes.' *Journal of Membrane Science* **62,** 165–185 (1991).

75. Robeson, L. M. 'The Upper Bound Revisited.' *Journal of Membrane Science* **320,** 390–400 (2008).

76. Freeman, B. D. 'Basis Of Permeability/Selectivity Tradeoff Relations In Polymeric Gas Separation Membranes.' *Macromolecules* **32,** 375–380 (1999).

77. Askari, M., Xiao, Y., Li, P. & Chung, T. S. 'Natural Gas Purification And Olefin/paraffin Separation Using Cross-linkable 6FDA-Durene/DABA Co-polyimides Grafted With A, B, And Γ-cyclodextrin.' *Journal of Membrane Science* **390-391,** 141–151 (2012).

78. Han, S. H., Lee, J. E., Lee, K.-J., Park, H. B. & Lee, Y. M. 'Highly Gas Permeable And Microporous Polybenzimidazole Membrane By Thermal Rearrangement.' *Journal of Membrane Science* **357,** 143–151 (2010).

79. Budd, P. M. *et al.* 'Gas Separation Membranes From Polymers Of Intrinsic Microporosity.' *Journal of Membrane Science* **251,** 263–269 (2005).

80. Budd, P. M. *et al.* 'Gas Permeation Parameters And Other Physicochemical Properties Of A Polymer Of Intrinsic Microporosity: Polybenzodioxane PIM-1.' *Journal of Membrane Science* **325,** 851–860 (2008).

81. Budd, P. M. *et al.* 'Polymers Of Intrinsic Microporosity (PIMs): Robust, Solution-processable, Organic Nanoporous Materials.' *Chemical Communications* 230–231 (2004).

82. Choi, J. I., Jung, C. H., Han, S. H., Park, H. B. & Lee, Y. M. 'Thermally Rearranged (TR) Poly(benzoxazole-co-pyrrolone) Membranes Tuned For High Gas Permeability And Selectivity.' *Journal of Membrane Science* **349,** 358–368 (2010).

83. Park, H. B. *et al.* 'Polymers With Cavities Tuned For Fast Selective Transport Of Small Molecules And Ions.' *Science* **318,** 254–258 (2007).

84. Park, H. B., Han, S. H., Jung, C. H., Lee, Y. M. & Hill, A. J. 'Thermally Rearranged (TR) Polymer Membranes For CO2 Separation.' *Journal of Membrane Science* **359,** 11–24 (2010).

85. Kim, S., Han, S. H. & Lee, Y. M. 'Thermally Rearranged (TR) Polybenzoxazole Hollow Fiber Membranes For CO2 Capture.' *Journal of Membrane Science* **403-404,** 169–178 (2012).

86. Strum, L. C. E. 'Physical Aging In Plastics And Other Glassy Materials.' *Polymer Engineering and Science* **17,** 165–173 (1977).

87. Hutchinson, J. M. 'Physical Aging Of Polymers.' *Progress in Polymer Science* **20,** 703–760 (1995).

88. Struik, L. C. E. 'Volume Relaxation And Secondary Transitions In Amorphous Polymers.' *Polymer* **28,** 1869–1875 (1987).

89. Consolati, G., Genco, I., Pegoraro, M. & Zanderighi, L. 'Positron Annihilation Lifetime (PAL) In Poly[1-(trimethyl-silyl)propine] (PTMSP): Free Volume Determination And Time Dependence Of Permeability.' *Journal of Polymer Science Part B: Polymer Physics* **34,** 357–367 (1996).

90. Duthie, X. *et al.* 'Thermal Treatment Of Dense Polyimide Membranes.' *Journal of Polymer Science Part B: Polymer Physics* **46,** 1879–1890 (2008).

91. Rowe, B. W., Freeman, B. D. & Paul, D. R. 'Physical Aging Of Ultrathin Glassy Polymer Films Tracked By Gas Permeability.' *Polymer* **50,** 5565–5575 (2009).

92. Rowe, B. W. *et al.* 'A Variable Energy Positron Annihilation Lifetime Spectroscopy Study Of Physical Aging In Thin Glassy Polymer Films.' *Polymer* **50,** 6149–6156 (2009).

93. Rowe, B. W., Freeman, B. D. & Paul, D. R. 'Influence Of Previous History On Physical Aging In Thin Glassy Polymer Films As Gas Separation Membranes.' *Polymer* **51,** 3784–3792 (2010).

94. Murphy, T. M. *et al.* 'Physical Aging Of Layered Glassy Polymer Films Via Gas Permeability Tracking.' *Polymer* **52,** 6117–6125 (2011).

95. Cui, L., Qiu, W., Paul, D. R. & Koros, W. J. 'Physical Aging Of 6FDA-based Polyimide Membranes Monitored By Gas Permeability.' *Polymer* **52,** 3374–3380 (2011).

96. Murphy, T. M., Freeman, B. D. & Paul, D. R. 'Physical Aging Of Polystyrene Films Tracked By Gas Permeability.' *Polymer* **54,** 873–880 (2013).

97. Wang, H., Chung, T.-S. & Paul, D. R. 'Physical Aging And Plasticization Of Thick And Thin Films Of The Thermally Rearranged Ortho-functional Polyimide 6FDA–HAB.' *Journal of Membrane Science* **458,** 27–35 (2014).

98. Kim, J. H., Koros, W. J. & Paul, D. R. 'Physical Aging Of Thin 6FDA-based Polyimide Membranes Containing Carboxyl Acid Groups. Part II. Optical Properties.' *Polymer* **47,** 3104–3111 (2006).

99. Huang, Y. & Paul, D. R. 'Physical Aging Of Thin Glassy Polymer Films Monitored By Gas Permeability.' *Polymer* **45,** 8377–8393 (2004).

100.   Huang, Y., Wang, X. & Paul, D. R. 'Physical Aging Of Thin Glassy Polymer Films: Free Volume Interpretation.' *Journal of Membrane Science* **277,** 219–229 (2006).

101.   Xiao, Y., Low, B. T., Hosseini, S. S., Chung, T. S. & Paul, D. R. 'The Strategies Of Molecular Architecture And Modification Of Polyimide-based Membranes For CO2 Removal From Natural Gas—A Review.' *Progress in Polymer Science* **34,** 561–580 (2009).

102.   Qiu, W. *et al.* 'Sub- T G Cross-linking Of A Polyimide Membrane For Enhanced CO2 Plasticization Resistance For Natural Gas Separation.' *Macromolecules* **44,** 6046–6056 (2011).

103.   Wind, J. D., Paul, D. R. & Koros, W. J. 'Natural Gas Permeation In Polyimide Membranes.' *Journal of Membrane Science* **228,** 227–236 (2004).

104.   Murphy, T. M., Offord, G. T. & Paul, D. R. 'Fundamentals Of Membrane Gas Separation.' in *Membrane Operations* 63–82 (2009). Wiley-VCH Verlag GmbH & Co. KGaA

105.   Reijerkerk, S. R., Jordana, R., Nijmeijer, K. & Wessling, M. 'Highly Hydrophilic, Rubbery Membranes For CO2 Capture And Dehydration Of Flue Gas.' *International Journal of Greenhouse Gas Control* **5,** 26–36 (2011).

106.   Scholes, C. A., Chen, G. Q., Stevens, G. W. & Kentish, S. E. 'Plasticization Of Ultra-thin Polysulfone Membranes By Carbon Dioxide.' *Journal of Membrane Science* **346,** 208–214 (2010).

107.   Everett, D. H. 'Manual Of Symbols And Terminology For Physicochemical Quantities And Units, Appendix II: Definitions, Terminology And Symbols In Colloid And Surface Chemistry.' *Pure and Applied Chemistry* **31,** (1972).

108.   Budd, P. M., McKeown, N. B. & Fritsch, D. 'Free Volume And Intrinsic Microporosity In Polymers.' *Journal of Materials Chemistry* **15,** 1977 (2005).

109.   Masuda, T. 'Substituted Polyacetylenes.' *Journal of Polymer Science, Part A: Polymer Chemistry* **45,** 165–180 (2007).

110.   Morisato, A. & Pinnau, I. 'Synthesis And Gas Permeation Properties Of Poly(4-methyl-2-pentyne).' *Journal of Membrane Science* **121,** 243–250 (1996).

111.   Nagai, K., Masuda, T., Nakagawa, T., Freeman, B. D. & Pinnau, I. 'Poly[1-(trimethylsilyl)-1-propyne] And Related Polymers: Synthesis, Properties And Functions.' *Progress in Polymer Science* **26,** 721–798 (2001).

112.   Masuda, T., Isobe, E. & Higashimura, T. 'Poly[l-(trimethylsily1)-1-propyne]: A New High Polymer Synthesized With Transition-Metal Catalysts And Characterized By Extremely High Gas Permeability.' *Journal of the American Chemical Society* **105,** 7473–7474 (1983).

113.   Morlière, N., Vallières, C., Perrin, L. & Roizard, D. 'Impact Of Thermal Ageing On Sorption And Diffusion Properties Of PTMSP.' *Journal of Membrane Science* **270,** 123–131 (2006).

114.   Freeman, B. D. & Pinnau, I. 'Polymeric Materials For Gas Separations.' *Polymer Membranes for Gas and Vapor Separation* **733,** 1–27 (1999).

115. Yampolskii, Y., Pinnau, I. & Freeman, B. D. 'MATERIALS SCIENCE OF MEMBRANES FOR GAS AND VAPOR SEPARATION.' *Materials Science of Membranes for Gas and Vapor Separation* (2006). John Wiley & Sons, Ltd

116. Wang, Y. C. *et al.* 'Sorption And Transport Properties Of Gases In Aromatic Polyimide Membranes.' *Journal of Membrane Science* **248,** 15–25 (2005).

117. Maya, E. M., García-Yoldi, I., Lozano, A. E., de la Campa, J. G. & de Abajo, J. 'Synthesis, Characterization, And Gas Separation Properties Of Novel Copolyimides Containing Adamantyl Ester Pendant Groups.' *Macromolecules* **44,** 2780–2790 (2011).

118. De Abajo, J., de la Campa, J. G. & Lozano, A. E. 'Designing Aromatic Polyamides And Polyimides For Gas Separation Membranes.' *Macromolecular Symposia* **199,** 293–306 (2003).

119. Calle, M., Lozano, A. E., de La Campa, J. G. & de Abajo, J. 'Novel Aromatic Polyimides Derived From 5'- T -Butyl-2'-pivaloylimino-3,4,3″,4″- M -terphenyltetracarboxylic Dianhydride With Potential Application On Gas Separation Processes.' *Macromolecules* **43,** 2268–2275 (2010).

120. Coleman, M. R. & Koros, W. J. 'Transport Properties Of Polyimide Isomers Containing Hexafluoroisopropylidene In The Diamine Residue.' *Journal of Polymer Science, Part B: Polymer Physics* **32,** 1915–1926 (1994).

121. Liu, Y., Zhang, Y., Guan, S., Li, L. & Jiang, Z. 'Synthesis And Properties Of Soluble Fluorinated Poly(ether Imide)s With Different Pendant Groups.' *Polymer* **49,** 5439–5445 (2008).

122. Dhara, M. G. & Banerjee, S. 'Fluorinated High-performance Polymers: Poly(arylene Ether)s And Aromatic Polyimides Containing Trifluoromethyl Groups.' *Progress in Polymer Science (Oxford)* **35,** 1022–1077 (2010).

123. McKeown, N. B. & Budd, P. M. 'Polymers Of Intrinsic Microporosity (PIMs): Organic Materials For Membrane Separations, Heterogeneous Catalysis And Hydrogen Storage.' *Chemical Society Reviews* **35,** 675 (2006).

124. McKeown, N. B. & Budd, P. M. 'Polymers With Inherent Microporosity.' in *Porous Polymers* 1–29 (2011). John Wiley & Sons, Inc.

125. Kim, S. & Lee, Y. M. 'Rigid And Microporous Polymers For Gas Separation Membranes.' *Progress in Polymer Science* **43,** 1–32 (2015).

126. Li, F. Y., Xiao, Y., Chung, T.-S. & Kawi, S. 'High-Performance Thermally Self-Cross-Linked Polymer Of Intrinsic Microporosity (PIM-1) Membranes For Energy Development.' *Macromolecules* **45,** 1427–1437 (2012).

127. Li, F. Y., Xiao, Y., Ong, Y. K. & Chung, T.-S. 'UV-Rearranged PIM-1 Polymeric Membranes For Advanced Hydrogen Purification And Production.' *Advanced Energy Materials* **2,** 1456–1466 (2012).

128. Du, N., Dal-Cin, M. M., Robertson, G. P. & Guiver, M. D. 'Decarboxylation-Induced Cross-Linking Of Polymers Of Intrinsic Microporosity (PIMs) For Membrane Gas Separation†.' *Macromolecules* **45,** 5134–5139 (2012).

129. Guiver, M. D. & Lee, Y. M. 'Polymer Rigidity Improves Microporous Membranes.' *Science* **339,** 284–285 (2013).

130. Carta, M. *et al.* 'An Efficient Polymer Molecular Sieve For Membrane Gas Separations.' *Science* **339,** 303–307 (2013).

131. Du, N. *et al.* 'Polymer Nanosieve Membranes For CO2-capture Applications.' *Nature materials* **10,** 372–375 (2011).

132. Du, N. *et al.* 'Polymers Of Intrinsic Microporosity Containing Trifluoromethyl And Phenylsulfone Groups As Materials For Membrane Gas Separation.' *Macromolecules* **41,** 9656–9662 (2008).

133. Du, N., Robertson, G. P., Song, J., Pinnau, I. & Guiver, M. D. 'High-Performance Carboxylated Polymers Of Intrinsic Microporosity (PIMs) With Tunable Gas Transport Properties †.' *Macromolecules* **42,** 6038–6043 (2009).

134. Du, N., Robertson, G. P., Dal-Cin, M. M., Scoles, L. & Guiver, M. D. 'Polymers Of Intrinsic Microporosity (PIMs) Substituted With Methyl Tetrazole.' *Polymer* **53,** 4367–4372 (2012).

135. Ghanem, B. S. *et al.* 'Synthesis, Characterization, And Gas Permeation Properties Of A Novel Group Of Polymers With Intrinsic Microporosity: PIM-Polyimides.' *Macromolecules* **42,** 7881–7888 (2009).

136. Ghanem, B. S., McKeown, N. B., Budd, P. M., Selbie, J. D. & Fritsch, D. 'High-performance Membranes From Polyimides With Intrinsic Microporosity.' *Advanced Materials* **20,** 2766–2771 (2008).

137. Ma, X. *et al.* 'Synthesis And Gas Transport Properties Of Hydroxyl-Functionalized Polyimides With Intrinsic Microporosity.' *Macromolecules* **45,** 3841–3849 (2012).

138. Rogan, Y. *et al.* 'Synthesis And Gas Permeation Properties Of Novel Spirobisindane-based Polyimides Of Intrinsic Microporosity.' *Polymer Chemistry* **4,** 3813 (2013).

139. Zhuang, Y. *et al.* 'Intrinsically Microporous Soluble Polyimides Incorporating Tröger's Base For Membrane Gas Separation.' *Macromolecules* **47,** 3254–3262 (2014).

140. Hu, X.-D., Jenkins, S. E., Min, B. G., Polk, M. B. & Kumar, S. 'Rigid-Rod Polymers: Synthesis, Processing, Simulation, Structure, And Properties.' *Macromolecular Materials and Engineering* **288,** 823–843 (2003).

141. Imai, Y., Taoka, I., Uno, K. & Iwakura, Y. 'Polybenzoxazoles And Polybenzothiazoles.' *Die Makromolekulare Chemie* **83,** 167–178 (1965).

142. Tullos, G. & Mathias, L. 'Unexpected Thermal Conversion Of Hydroxy-containing Polyimides To Polybenzoxazoles.' *Polymer* **40,** 3463–3468 (1999).

143. Tullos, G. L., Powers, J. M., Jeskey, S. J. & Mathias, L. J. 'Thermal Conversion Of Hydroxy-Containing Imides To Benzoxazoles: Polymer And Model Compound Study.' *Macromolecules* **32,** 3598–3612 (1999).

144. Calle, M., Chan, Y., Jo, H. J. & Lee, Y. M. 'The Relationship Between The Chemical Structure And Thermal Conversion Temperatures Of Thermally Rearranged (TR) Polymers.' *Polymer* **53,** 2783–2791 (2012).

145. Calle, M. & Lee, Y. M. 'Thermally Rearranged (TR) Poly(ether−benzoxazole) Membranes For Gas Separation.' *Macromolecules* **44,** 1156–1165 (2011).

146. Jung, C. H., Lee, J. E., Han, S. H., Park, H. B. & Lee, Y. M. 'Highly Permeable And Selective Poly(benzoxazole-co-imide) Membranes For Gas Separation.' *Journal of Membrane Science* **350,** 301–309 (2010).

147. Han, S. H. *et al.* 'Thermally Rearranged (TR) Polybenzoxazole: Effects Of Diverse Imidization Routes On Physical Properties And Gas Transport Behaviors.' *Macromolecules* **43,** 7657–7667 (2010).

148. Sanders, D. F. *et al.* 'Gas Permeability, Diffusivity, And Free Volume Of Thermally Rearranged Polymers Based On 3,3′-dihydroxy-4,4′-diamino-biphenyl (HAB) And 2,2′-bis-(3,4-dicarboxyphenyl) Hexafluoropropane Dianhydride (6FDA).' *Journal of Membrane Science* **409-410,** 232–241 (2012).

149. Smith, Z. P. *et al.* 'Gas Sorption And Characterization Of Thermally Rearranged Polyimides Based On 3,3′-dihydroxy-4,4′-diamino-biphenyl (HAB) And 2,2′-bis-(3,4-dicarboxyphenyl) Hexafluoropropane Dianhydride (6FDA).' *Journal of Membrane Science* **415-416,** 558–567 (2012).

150. Sanders, D. F. *et al.* 'Influence Of Polyimide Precursor Synthesis Route And Ortho-position Functional Group On Thermally Rearranged (TR) Polymer Properties: Pure Gas Permeability And Selectivity.' *Journal of Membrane Science* **463,** 73–81 (2014).

151. Han, S. H. *et al.* 'Tuning Microcavities In Thermally Rearranged Polymer Membranes For CO2 Capture.' *Physical chemistry chemical physics : PCCP* **14,** 4365–73 (2012).

152. Wang, H. & Chung, T.-S. 'The Evolution Of Physicochemical And Gas Transport Properties Of Thermally Rearranged Polyhydroxyamide (PHA).' *Journal of Membrane Science* **385-386,** 86–95 (2011).

153. Commonwealth Scientific and Industrial Research Organization. 'CSIRO.'

154. Park, C. H. *et al.* 'A Simulation Study On OH-containing Polyimide (HPI) And Thermally Rearranged Polybenzoxazoles (TR-PBO): Relationship Between Gas Transport Properties And Free Volume Morphology.' *Journal of Physical Chemistry B* **118,** 2746–2757 (2014).

155. Park, C. H., Tocci, E., Lee, Y. M. & Drioli, E. 'Thermal Treatment Effect On The Structure And Property Change Between Hydroxy-containing Polyimides (HPIs) And Thermally Rearranged Polybenzoxazole (TR-PBO).' *The journal of physical chemistry. B* **116,** 12864–77 (2012).

156. Thornton, A. W., Hilder, T., Hill, A. J. & Hill, J. M. 'Predicting Gas Diffusion Regime Within Pores Of Different Size, Shape And Composition.' *Journal of Membrane Science* **336,** 101–108 (2009).

157. Thornton, A. W., Nairn, K. M., Hill, A. J., Hill, J. M. & Huang, Y. 'New Relation Between Diffusion And Free Volume: II. Predicting Vacancy Diffusion.' *Journal of Membrane Science* **338,** 38–42 (2009).

158. Guo, R. *et al.* 'Synthesis And Characterization Of Thermally Rearranged (TR) Polymers: Effect Of Glass Transition Temperature Of Aromatic Poly(hydroxyimide) Precursors On TR Process And Gas Permeation Properties.' *Journal of Materials Chemistry A* **1,** 262–272 (2013).

159. Soo, C. Y., Jo, H. J., Lee, Y. M., Quay, J. R. & Murphy, M. K. 'Effect Of The Chemical Structure Of Various Diamines On The Gas Separation Of Thermally Rearranged Poly(benzoxazole-co-imide) (TR-PBO-co-I) Membranes.' *Journal of Membrane Science* **444,** 365–377 (2013).

160. Scholes, C. a., Ribeiro, C. P., Kentish, S. E. & Freeman, B. D. 'Thermal Rearranged Poly(benzoxazole-co-imide) Membranes For CO2 Separation.' *Journal of Membrane Science* **450,** 72–80 (2014).

161. Do, Y. S., Seong, J. G., Kim, S., Lee, J. G. & Lee, Y. M. 'Thermally Rearranged (TR) Poly(benzoxazole-co-amide) Membranes For Hydrogen Separation Derived From 3,3'-dihydroxy-4,4'-diamino-biphenyl (HAB), 4,4'-oxydianiline (ODA) And Isophthaloyl Chloride (IPCl).' *Journal of Membrane Science* **446,** 294–302 (2013).

162. Li, S. *et al.* 'Mechanically Robust Thermally Rearranged (TR) Polymer Membranes With Spirobisindane For Gas Separation.' *Journal of Membrane Science* **434,** 137–147 (2013).

163. Calle, M., Doherty, C. M., Hill, A. J. & Lee, Y. M. 'Cross-linked Thermally Rearranged Poly(benzoxazole-co-imide) Membranes For Gas Separation.' *Macromolecules* **46,** 8179–8189 (2013).

Chapter II

General Methodology

2.1. SYNTHESIS OF AROMATIC POLYIMIDES – PRECURSORS OF TR POLYMERS

As mentioned previously, polybenzoxazoles can be formed by thermal rearrangement of *ortho*-functional polyimides in solid state. In this regard, polyimides for this purpose have been synthesized by reacting bis(aminophenol) derivatives with an aromatic dianhydride. The high number of versatile synthetic methods for the formation of polyimides has facilitated their use in high performance applications. In this work, aromatic polyimides synthesis was performed using the "two-step" method which is clearly the most widely used method in polyimide synthesis. This two-step method, also known as the "classical method", involves the formation of a poly(amic acid) (PAA) precursor, which is subsequently cyclized to form the imide linkage (**Scheme 2.1**) [1,2].

Poly(amic acid) intermediate
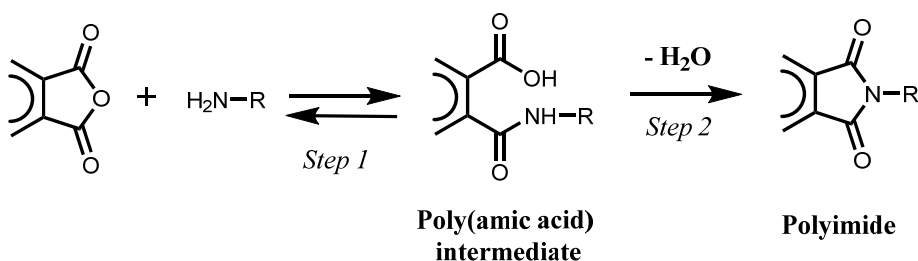
Polyimide

Scheme 2.1. Generalized reaction mechanism of aromatic polyimide formation by "two-step" polycondensation procedure

In order to obtain films with good mechanical properties that can be evaluated as gas separation membranes, it is essential to attain polymers with high molecular weight. For this reason, an optimized polymerization reaction must be taken into account. To achieve this goal, several aspects should be considered:

High purity of monomers, well-chosen solvents and proper catalysts. The presence of impurities in monomers does not allow to reach the optimal conditions of polymer formation, as defined by the Carothers equation, which is used to determine the degree of polymerization in polycondensation reactions:

$$DP = \frac{r+1}{r+1-2pr} \qquad \text{(Eq. 2.1)}$$

where *DP* is the degree of polymerization, *p* is the extent of the reaction (yield conversion) and *r* is the stoichiometric imbalance defined as $r = \frac{Eq_a}{Eq_b}$ ($1 \geq r > 0$), being Eq_a and Eq_b the amount in equivalents of reactive groups of the monomers present in the medium. The maximum theoretical degree of polymerization will be infinite only when $r = 1$ (equivalence of functional groups) and the reaction conversion is complete. Thus, high purity of monomers is crucial to obtain high molecular weight polymers. In addition, undesirable side reactions should be negligible. Thus, for instance, water present in the solvent may react with the dianhydride moiety, resulting in non-reactive acid compounds what leads to stoichiometric disproportion and consequent decrease of the molecular weight. Also, partial oxidation of diamines results in mono-functional or non-functional species. Other plausible side-reactions could include the hydrolysis of the amide solvents, giving aliphatic amines that can compete with the diamine monomer, producing lower molecular weight polymers. In particular, the use of inert atmosphere of very pure anhydrous solvents plays an important role in these polymerizations.

Concentration of monomers. It is well known that high monomer concentrations lead to high molecular weight poly(amic acid)s [3]. In the current work, monomer concentrations from 0.5 to 1M have been used.

Monomer addition order. According to the literature, the addition of the dianhydride on the diamine solution is critical to avoid the side reactions between the electrophilic monomer and water present in the medium [4].

Reaction control. In the case of working with dianhydrides having low reactivity and solubility, the polymerization process can be controlled by diffusion similarly to interfacial polymerization processes [5,6]. These type of reactions, where monomer is partially soluble, can lead to polymers with wider molecular weight distributions than those observed for classical polymerization reaction (DP higher than 2).

Solvent effect. The presence of solvents which provide strong acid-base interactions with the PAA will produce a favourable displacement of the equilibrium to polyimide formation. Generally, aprotic polar solvents as *N,N*-dimethylformamide (DMF), *N,N*-dimethylacetamide (DMAc) and *N*-methyl-2-pyrrolidinone (NMP) are the solvents more used in these reactions. These solvents also help to maintain the growing polymer chains in solution.

Reaction reversibility. In spite of the slow kinetic of the reverse reaction, the storage of PAA can produce a considerable decrease in its molecular weight. This is mainly caused by the effect of residual water, which reacts with the small amount of anhydride present, thus pulling the equilibrium to left [7]. It is well described that preservation of PAA at low temperature minimizes this process. PAA formation stage is an exothermic process at room temperature and, consequently, an increment in reaction temperature produces equilibrium displacements to monomers, lessening the polymerization degree. Thus, the reaction temperature control is crucial to obtain a high molecular weight polymer and, due to this fact, addition of the dianhydride to the diamine solution must be made at low temperatures (0 °C) [8].

- *Step 1: Formation of Poly(amic acid)s*

Usually, the corresponding PAA is formed when a diamine and a dianhydride mutually react in a polar aprotic solvent such as *N,N*-dimethylacetamide (DMAc) or *N*-methyl-2-pyrrolidinone (NMP). This reaction proceeds by a reversible nucleophilic substitution when the nitrogen amine center attacks one of the carbonyl carbons in the anhydride moiety and forms

carboxylate functionality, followed by proton transfer (**Scheme 2.2**). The reactivity and concentration of each of the monomeric units and the nature of the solvent will determine the rate of PAA formation and its stability with regard to other reagents. Hence, the reaction is expected to depend upon the electrophilicity of the carbonyl groups of the dianhydride and the nucleophilicity of the nitrogen atoms of the diamine. Diamine reactivity is controlled by the electronic density on the nitrogen, so that, in diamines with the general structure shown in **Scheme 2.3**, the substituent X will enhance the reactivity of the diamine if it is an electron-donor group (-O-, -S-, -CH$_2$-, -C(CH$_3$)$_2$-, etc.) and the diamine reactivity will be reduced if there is an electron-withdrawing one (-CO-, -SO$_2$-, etc.). The effect is opposite for dianhydrides of the general formula also shown in **Scheme 2.3**. Accordingly, the dianhydride with the greatest electrophilicity, i.e. the lowest LUMO energy (E_{LUMO}), will react first with a diamine having the highest nucleophilicity, i.e. the highest HOMO energy (E_{HOMO}). In conclusion, high E_{HOMO} values of the diamines and low E_{LUMO} of the dianhydrides will help for a higher reaction rate.
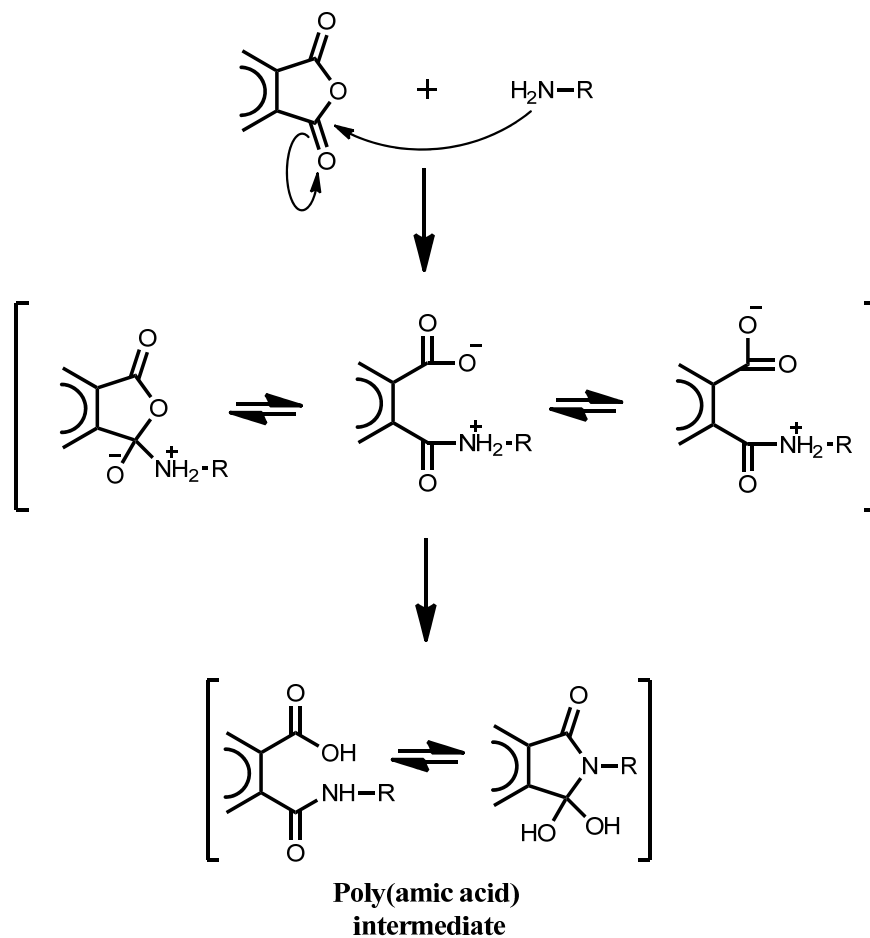
Scheme 2.2. General reaction mechanism of poly(amic acid) intermediate formation
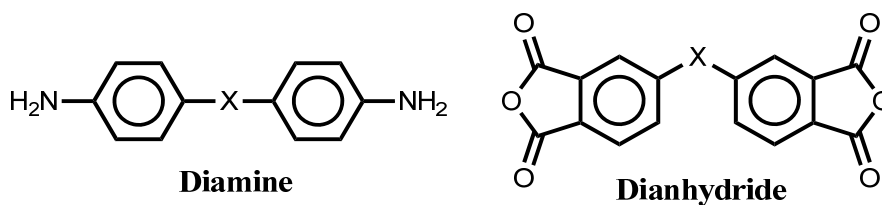
Scheme 2.3. General structure of diamines and dianhydrides employed in this memory

Furthermore, improvement of the reactivity of monomers by known methods should be translated to materials with better properties. In this work, the use of base-assisted silylation [9,10] as an activated polycondensation method was employed throughout the polyimide synthesis. This method is unique in order to increase the reactivity of the diamines, contributing to an increase in the molecular weight far above those obtained by other polyimidization methods. *In situ* silylation is based on the use of chlorotrimethylsilane (CTMS) and a base such as pyridine (Py) and small amounts of a highly-nucleophilic cobase such as *N,N*-dimethylaminopyridine (DMAP) as polycondensation promoters. The function of the base on the *in situ* silylation method consists in favoring the silylation of the diamine. This silylated aromatic diamine is by far more nucleophilic than non-silylated ones and thus the transfer of electronic density of the amine to the dianhydride moiety is highly favored. This activated reaction is also more convenient for low-reactivity diamines; i.e, diamines having electron-withdrawing groups. This transfer opens the anhydride cycle simultaneously with the trimethylsilyl group elimination. The synthesis of poly(amic acid silyl ester) follows the mechanism described in **Scheme 2.4**. As the cobase (higher pKa) interacts more strongly than pyridine with the silicon atom, the trimethylsilyl removal is easier, and hence the global reaction is more favored and polymers with high or very high molecular weights are obtained.
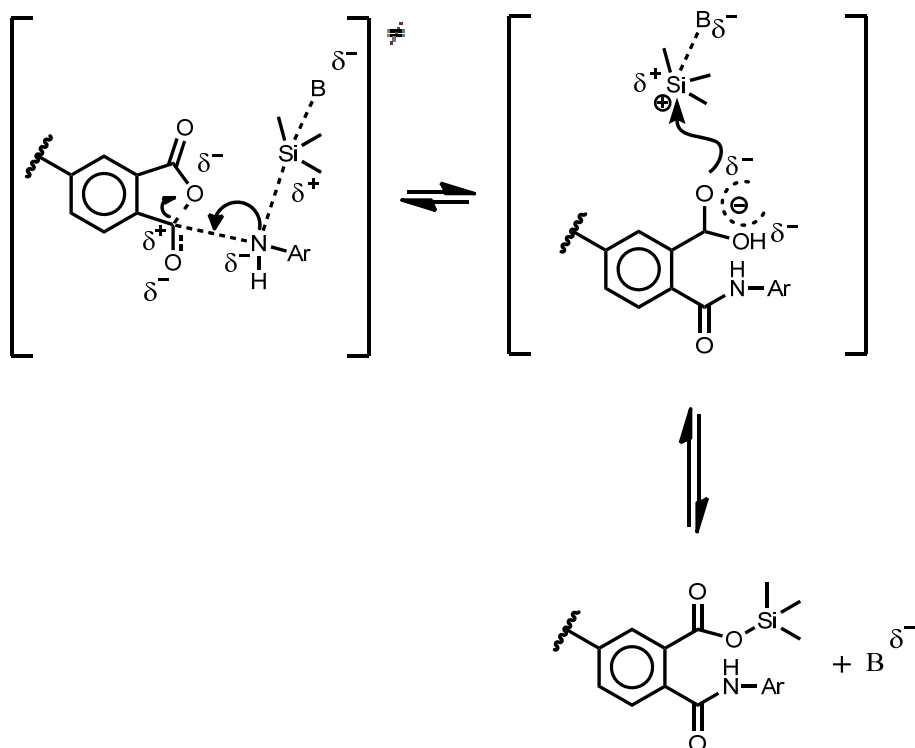
Scheme 2.4. Synthesis of poly(amic acid silyl ester) with CTMS and Py

- *Step 2: Cyclodehydration of Poly(amic acid)s*

Cyclodehydration reaction or cycloimidization of the PAA to its corresponding polyimide (imide ring formation) is produced by the loss of two H_2O molecules per repeat unit. Thermal and chemical imidization methods have been commonly used to synthesize polyimide membranes via the two-step reaction. These imidization routes can affect the formation of polyimides with respect to their chemical structure, solubility, and physical and transport properties [11]. Thus, the formation of thermally rearranged (TR) polymers obtained from polyimides with *ortho*-functional groups and their physical and transport properties are very dependent upon the imidization routes as well [12].

a. *Chemical imidization*

Chemical cyclization is performed by chemical reaction of aliphatic anhydride and a base (trimethylamine, pyridine, quinoline, etc.) with an amic acid moiety [13-17]. The mechanism involves the formation of a mixed anhydride intermediate followed by an iminolactone and consequent formation of the imide linkage, which is the thermodynamically favored product (**Scheme 2.5**). The percentage of imidization achieved thus depends on the solubility of the polyimide in the imidization mixture, with more soluble polyimides attaining higher degrees of imidization [18] and on avoiding undesirable side reactions which lead to insolubility and infusibility [19]. In general, the chemical imidization technique requires a final treatment where the polyimide is heated briefly to high temperatures, depending on the glass transition temperature (T_g) of the polyimide, to complete the imidization and remove traces of any solvent [20].
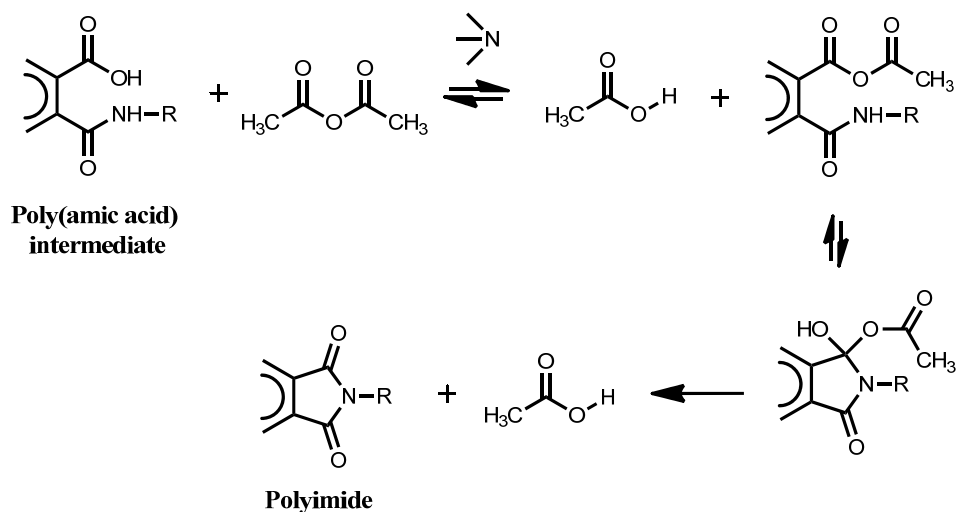
Scheme 2.5. Reaction mechanism of chemical imidization of poly(amic acid) by acetic anhydride

It is worthy of emphasis that, in this method, where chemical reaction of PAA and acetic anhydride was conducted, the highly reactive acetic anhydride attacked the hydroxyl group in the diamine moiety as well as the carboxylic acid in the main chain of the PAA. Thus, by the use of chemical imidization without any protecting group, the hydroxyl groups of *ortho*-hydroxylated polyimides were converted to acetate groups, obtaining *ortho*-acetyl polyimides. This remark is relevant due to this thesis is mainly focused on the synthesis of *ortho*-hydroxylated polyimides, which are precursors of TR polymers.

b. Thermal imidization

Thermal cyclization is a common imidization method, which is performed by heating the PAA intermediate in a several step thermal treatment which involves the loss of H_2O followed by ring closure to imides. This process occurs at high temperatures, above 200 °C. At this temperature, a polar aprotic solvent, such as NMP or DMAc, or a mixture of solvents (aprotic polar solvents plus cresols or other aromatic compounds such as *ortho*-dichlorobenzene and xylenes) is evaporated along with water. This method is generally used when the final polyimide is obtained as a film or coating. Also, this process is usually accompanied by cross-linking reactions that produce insoluble polyimides. In thermal imidization, the PAA solution is casted onto a substrate and, subsequently, subjected to thermal treatment. There has been extensively debated in the literature which is the best thermal cycle for achieving close to 100% imidization of the PAAs. While the types of thermal cycles utilized are many, they can essentially be divided into two different groups:

1) Formation of the polyimide by heating gradually to 250-350 °C, or even higher, depending on the stability and T_g of the polyimide [7,8,21].

2) Formation of the polyimide by subjecting the materials to successive thermal cycles. For instance, heating the PAA mixture to 100 °C and holding for 1 h, heating from 100 °C to 200 °C and holding for 1 h, heating from 200 °C to 300 °C and holding for 1 h and slowly cooling to room temperature from 300 °C [22-25].

However, irrespective of the type of thermal cycle, it is important to recognize that there are complicating factors involved in these seemingly simple thermal imidization processes, which finally determine the degree of imidization and the final features of the polyimide product. It needs to be emphasized that the imidization reactions take place in a very concentrated viscous solution (during initial and intermediate stages) and that the presence of residual solvent plays a very important role at the later stages of the reaction. In this regard, the imidization proceeds faster in the presence of polar amide solvents owing to the specific solvation that allows the PAA group to adopt the most favorable conformation to cyclize [25], the plasticizing effect of the solvent to increase the mobility of the reacting functional groups [7] and the basicity of the amide solvent that allows it to accept protons and hence permits a catalytic effect [8].

The rate of imidization is usually faster during the initial stages due to the presence of solvent and to higher chain mobility. At this respect it is worth remarking that 100% conversion in the ring closure step is virtually impossible to be achieved, particularly for thermal imidation at high temperature (about 300 °C) in the solid state, due to the complexity of the process and to the inherent molecular rigidity of polyimides.

c. *Azeotropic imidization*

Azeotropic imidization is a solution thermal imidization. In other words, while thermal imidization takes place with evaporation of solvents, azeotropic imidization occurs in solution by adding reagents to form azeotropes with water during the reaction. At a mild reaction temperature around 140-180 °C, the azeotropic imidization method may result in a soluble polyimide if the main chain of the polyimides is flexible enough to be dissolved in the organic solvent mixture and remain dissolved until a high molecular weight is attained. In addition, the hydroxyl groups in the main chain remain unmodified when this method is used.

2.2. EFFECT OF SYNTHESIS ROUTE ON POLYIMIDE PROPERTIES

The effect of the polyimide synthesis route on the transport properties of polymers has been previously studied in the literature [26,27]. Thus, Matsumoto *et al*. studied the pure gas permeability of CO_2 and CH_4 in the 6FDA-4,4'-ODA polyimide synthesized via chemical and thermal imidization [26]. The authors found that chemically imidized samples had higher permeability and selectivity than thermally imidized ones. However, the two polymers had drastically different molecular weights, which may explain these differences. Xu *et al*. also showed that permeability and selectivity were very similar for the 6FDA-DAM homopolyimides with similar molecular weights synthesized via each route, but significant differences based on the synthesis route appeared in 6FDA-DAM-DABA copolymers. Thus, the thermally imidized copolymer showed higher permeability but lower selectivity. This result was ascribed to the generation of some isoimide moieties and to the presence of residual poly(amic acid) in the chemically imidized copolymers [27].

These different synthesis routes have also resulted in physical properties differences. Martinez-Richa et al. found that chemically imidized polymers exhibited a less ordered structure and, in this case, showed up to 15% of isoimide groups [28]. Xie et al. showed that chemically imidized samples were generally more soluble and had lower thermal stability than thermally imidized samples [29]. This result was attributed to non-complete imidization.

Han *et al*. also studied the effect of the imidization methods on the physical and transport properties of TR-PBO membranes [12]. The final properties of the TR-PBO membranes depended on the synthetic method used to prepare the polyimide precursors. They demonstrated the effect of these routes on the final properties of the PBOs. Although the structures of the PBOs were similar, the structures of the precursor polyimides were different. Chemical imidization formed acetate-containing polyimides, whereas thermal and azeotropic imidization produced hydroxyl-containing polyimides. During the thermal rearrangement, acetate-polyimides (formed from chemical imidization) underwent deformation of the acetate domain and evolution of larger acetic acid

molecules prior to conversion into PBO via decarboxylation, while hydroxyl-polyimides experienced a structural change directly related to the formation of PBO with decarboxylation. Thus, the intrinsic differences in the precursor polyimides resulted in larger cavities formed during thermal rearrangement for acetate-polyimides. The bulky side chain in acetate-polyimides gave rise to an increment in the fractional free volume as well as in interchain distances of the polymer matrix compared to hydroxyl-polyimides. As a consequence, chemically imidized polymers could achieve much higher permeabilities and lower onset temperature for thermal rearrangement than polymers thermally imidized in solution using an azeotrope [12,30,31]. The work of Han *et al*. also compared samples thermally imidized in the solid state from Park's work [32] with chemically and azeotropically imidized polyimides in solution. Interestingly, the solid state thermal imidization showed similar properties to the chemically imidized sample, and both had much higher permeabilities than the samples azeotropically imidized. However, the work of Han et al. did not decouple the effect of synthesis route from the chemical *ortho*-position change in these polymers.

In the current work, all aromatic polyimides were obtained using the *in situ* silylation base-assisted method in the formation of the PAAs. However, diverse imidization routes were used depending on the desired final polyimide. Azeotropic imidization was used in order to obtain soluble *ortho*-hydroxyl polyimides which, as mentioned above, could not be prepared via chemical imidization without any protecting group due to the conversion of the hydroxyl groups into acetate groups. The synthesis route and the experimental conditions employed for each polyimide is detailed in the corresponding chapter.

2.3. FILM FORMATION

Polymer solutions, 10% (w/v) in NMP or DMAc, were filtered through a 3.1 µm polytetrafluoroethylene (PTFE) syringe filter, degassed at room temperature and cast on a well-leveled glass plate provided with an aluminum frame. Next, the films were dried at 60 °C overnight to remove most of the solvent and, subsequently, gradually heated to 250 °C, being held for 1 h each at 100, 150, 200, and 250 °C under vacuum to evaporate the residual solvent. The films were then removed from the glass plate, washed with deionized water, and dried overnight at 130 °C under vacuum. Film thicknesses were between 40 and 50 µm and, in all cases, suitable film uniformity was verified by measuring the film thickness standard deviation, which was lower than 5 %. Defect-free and clean polyimide membranes were cut into 3 cm x 3 cm pieces and placed between ceramic plates to prevent film deformation at elevated temperatures in a tubular furnace under an inert gas atmosphere. Each sample was then heated to 300 °C at a heating rate of 5 °C min^{-1} under N_2 and held at that temperature for 1, 2 or 3 hours, depending on the polyimide film, to ensure complete solvent removal and full closure of the imide ring structure. The particular thermal treatment for each series of polyimides is specified in the corresponding chapter.

2.4. TR MEMBRANES: THERMAL REARRANGEMENT FROM PI INTO TR-PBO

The precursor polyimide membranes were converted into TR membranes by a further thermal treatment. Thus, the polyimide membranes were heated to different target temperatures (350 ºC, 400 ºC, 425 ºC or 450 ºC) at a rate of 5 ºC min^{-1} in a tubular furnace, and maintained for the desired time length (30 min or 1 h) in a high-purity nitrogen atmosphere. The thermal treatment procedure was chosen following the protocol described in literature, in such way that the samples were exposed to thermal treatments similar to those reported in previous studies related to the formation of TR materials [12,32-36]. The cooling protocol for all samples consisted on allowing the furnace to reach room temperature at a rate not greater than 10 ºC min^{-1}. The specific thermal treatment for each series of membranes is described in the corresponding chapter.

2.5. MATERIALS

4,4´-Dihydroxybiphenyl (97 %), glacial acetic acid, hydrazine monohydrate, palladium 10 wt% on activated carbon, chlorotrimethylsilane (CTMS), pyridine (Py), *N,N*-dimethylaminopyridine (DMAP), acetic anhydride, *o*-xylene, anhydrous *N,N*-dimethylacetamide (DMAc), *N,N*-dimethylformamide (DMF) and *N*-methyl-2-pyrrolidinone (NMP) were all purchased from Aldrich and used as received. 2,2´-Bis(3,4-dicarboxyphenyl) hexafluoropropane dianhydride (6FDA) was provided by Cymit Química (Barcelona) and sublimed just before use. 3,3´-Dihydroxybenzidine (*p*HAB or HAB) (TCI Europe) was dried at 120 °C under vacuum prior to be used. Diamines including 2,4-diaminophenol dihydrochloride (DAP), 4,6-diaminoresorcinol dihydrochloride (DAR), m-phenylenediamine (MPD) and 3,3´-Dimethoxybenzidine (DMAB) were supplied by Aldrich. DAP was dried at 100 °C under vacuum, DAR was recrystallized in a solution of $SnCl_2$ in HCl 3.5 M and diamines MPD and DMAB were sublimed prior to be used.

2.6. Measurements

Structural elucidation of polyimide precursors was carried out by ^{1}H-NMR spectra obtained from a Bruker Advance 300 or from a Varian System 500 nuclear magnetic resonance (NMR) spectrometer operating at 300 and 500 MHz, respectively. ^{13}C-NMR spectra were recorded on the same Bruker Advance 300 spectrometer at 75 MHz. Elemental analyses were performed with a Carlo Erba EA1108 elemental analyzer.

A Perkin Elmer Fourier transform infrared spectrometer (FT-IR) with Universal ATR Sampling Accessory was used to characterize the precursor polyimides and TR-PBO films. In addition, FT-IR was used to prove the conversion of the precursor polyimide films into PBO films. The scan range was from 4000 to 650 cm^{-1}.

Inherent viscosities of polyimide precursors were evaluated at 30 °C with an automated Canon-Ubbelohde suspended level viscometer using NMP as solvent. The polymer concentration was 0.5 g/dL in every case.

Glass transition temperatures (T_g) of polyimide films were determined by differential scanning calorimetry (DSC) on a TA Q-2000 calorimeter (TA Instruments, DE, USA). The temperature calibration was performed by taking the onset of the endothermic melting peak of several calibration standards: octane (T_m = 217.26 K), indium (T_m = 430.61 K) and zinc (T_m = 693.38 K). The organic standard was a high-purity Fluka product, while the metal standards were supplied by TA Instruments Inc. Enthalpy was calibrated using indium (melting enthalpy ΔH_m = 28.71 J g^{-1}). Two heating-cooling cycles, at a heating rate of 20 °C min^{-1}, were accomplished and T_g was obtained from the second heating cycle. Tested films were heated to a temperature below the onset temperature of conversion into PBO for each polyimide in the first heating, then cooled to room temperature and finally, in the second scan, heated up again to 400 °C. In the case of polyimide films with high rigidity or where coupling of different processes avoids a clear T_g observation, modulated temperature differential scanning calorimetry (MDSC) analyses have been conducted. MDSC allows separation of the *reversing* contribution to the average heat flow (attributed to the heat capacity), as well as the *non-reversing* contribution to the

average heat flow (attributed to kinetic effects such as enthalpy recovery or recrystallization). The module of the complex heat capacity was calibrated by measuring with sapphire in the studied temperature range and for the frequencies of modulation used in the experiments. An underlying heating ramp of 5 °C min^{-1} to 450 °C was accomplished with a modulation period of 40 s and with amplitude of the temperature modulation of 1.5 °C. T_gs were attained from the *reversing* heat flow signal.

Thermogravimetric analyses (TGA) were conducted on a TA Q-500 thermobalance (TA Instruments, DE, USA), combined with mass spectrometer (MS) ThermoStar™ GSD 301T (Pfeiffer Vacuum GmbH, Germany). Dynamic ramp scans were run at 5 or 10 °C min^{-1} to find out about thermal stability characteristics as well as the thermal rearrangement, in the temperature range from 60 to 850 °C. Furthermore, isothermal thermogravimetric analyses were carried out in order to adjust the most appropriate thermal treatment settings for TR films preparation and to estimate the percent conversion from the polyimide precursors to the final TR-PBOs. Therefore, polyimide film samples, thermally treated at 300 °C, were heated to the selected rearrangement temperature (350, 400, 425 and 450 °C) at a heating rate of 5 °C min^{-1}, and held isothermally for 3 h. The purge gas was nitrogen (60 mL min^{-1}) and the sample mass was around 5 mg.

Dynamic mechanical analysis was performed using a TA Instruments Q800 DMA configured in tensile geometry. Storage modulus (E´) and tan δ were both measured in temperature sweep mode (1 Hz; 3 °C/min) at temperatures ranging from RT to 450 °C. All measurements were carried out under N$_2$ atmosphere.

Intermolecular distances of PI precursor membranes and TR-PBO membranes were proved by wide angle X-ray diffraction (WAXD) diagrams, which were performed in the reflection mode at room temperature by using a Bruker D8 Advance system fitted with a Goebel mirror and provided with a PSD Vantec detector. Cu *Ka* radiation source of wavelength 1.54 Å was used, operating in a 2θ range of 2-55° with a scan rate of 0.5 s per step.

The average *d*-spacing was obtained from the Bragg's equation:

$$n\lambda = 2d \sin \theta \qquad \text{(Eq. 2.2)}$$

where *d* is the *d*-spacing, θ the scattering angle and *n* is an integer number related to the Bragg order.

Densities were determined from Archimedes' principle using a XS105 Dual Range Mettler Toledo balance coupled with a density kit by weighting the samples, at room temperature, in air and then in a liquid of known density (Isooctane, Sigma Aldrich, > 99%). The density of the sample was estimated from the expression:

$$\rho_{sample} = \rho_{liquid} \frac{W_{air} - W_{liquid}}{W_{air}} \qquad \text{(Eq. 2.3)}$$

The density data were used to evaluate the chain packing through the fractional free volume (FFV), which was calculated using the following relation:

$$FFV = \frac{V_e - 1.3 \, V_W}{V_e} \qquad \text{(Eq. 2.4)}$$

where V_e is the polymer specific volume and V_W is the Van der Waals volume, which was given by molecular modeling applying the semi-empirical method Austin Model 1 (AM1) [37] in the Hyperchem computer program, version 8.0 [38].

Mechanical properties (uniaxial tension tests) were determined on a MTS Synergie 200 apparatus fitted with a 100 N load cell at room temperature. The samples of 5.0 mm width and 3.0 cm length were clamped at both ends with an initial gauge length of 10.0 mm, and the elongation rate was of 5 mm min^{-1}. At least eight samples were tested for each film.

Computer molecular simulation was carried out by first drawing the molecules in the desktop of Hyperchem [38] and optimizing the structures of molecules and intermediates at the AM1 level of theory [37]. Subsequently, electronic energies of the optimized geometries were calculated by Density Functional Theory (DFT) (without any geometrical constraint (use of Opt keyword) for starting molecules and final molecules) by using the Becke's three parameter hybrid functional [39] and the Lee *et al.* [40,41] correlation functional with the 6-31G(d) basis set (B3LYP/6-31G(d)). For intermediate molecules, the molecule obtained by AM1 was subsequently put to calculate by using the Gaussian 03 and Gaussian 03W packages [42] using the energy job type (single point calculation). Molecular depicting of molecules was carried out by using the Arguslab 4.01 freeware program [43].

Positron annihilation lifetime spectroscopy (PALS) was used to evaluate the cavity size distribution and the relative intensity of free volume components inside of the polymer membranes. The main source of positrons in PALS is ^{22}Na, which is tied up as NaCl. Positrons can form two bound states with electrons, known as positronium (Ps): *o*-Ps is their parallel-spin configuration and *p*-Ps is the antiparallel-spin configuration. Self-annihilation of *p*-Ps and free annihilation (positron annihilation with an electron within the sample) occur at 0.125 ns and ~0.4 ns, respectively. Pick-off annihilation of *o*-Ps in a molecular system is affected by the electron density in its surroundings. That is, the o-Ps can survive longer in a system or local domain with low electron density, such as pores, cavities, or free volume elements. Assuming the unoccupied volume has a spherical shape, the measurement of the *o*-Ps lifetime (τ, ns) and its intensity (I, %) not only provide the size and distribution of free volume elements in the polymer, but also shed light on the topologies in which different sized pores exit. PALS is able to distinguish the presence of bimodal porosity such as in highly microporous materials by fitting several *o*-Ps components. The size and distribution of free volume elements in the polymers was determined by PALS using an automated EG&G Ortec (Iak Ridge, TN) fast-fast coincidence spectrometer which had a resolution function of 230 ps fwhm peak when measures with ^{60}Co. The samples were composed of 10 mm X 10 mm size polymer films stacked to 1 mm in thickness with a ~30 μCi ^{22}NaCl sealed Mylar source placed between the polymers. A source correction for the Mylar was

required (1.6 ns, 3.12%). The samples were placed in a cell and subjected to a vacuum of 5×10^{-4} Pa at room temperature. The range of the time-to-amplitude converter (TAC) was extended to 200 ns to measure the long lifetimes, and the coincidence unit was removed to improve the count rates. A minimum of five files were collected with 1×10^6 integrated counts per file. The acquired data were analyzed using either a three- or four-component fit with the LTv9 software. The first lifetime (τ_1) was fixed to 0.125 ns due to *p*-Ps annihilation, and τ_2 was fitted to free annihilation (~0.4 ns). The *ortho*-positronium lifetimes (τ_3 and τ_4) were used to calculate the free volumes within the membranes using the Tao–Eldrup equation:

$$\tau_3^{-1} = 2\left[1 - \frac{r_3}{r_3 + \Delta r} + \frac{1}{2\pi}\sin\left(\frac{2\pi(r_3)}{r_3 + \Delta r}\right)\right] \qquad \text{(Eq. 2.5)}$$

where, τ_3 is lifetime (ns), r_3 is cavity radius (Å), and Δr is determined empirically and is related to the thickness of the electron layer on the pore wall which interacts with positronium (1.66 Å).

Gas permeation properties were determined using the *timelag* method, which was described extensively by Barrer in 1939 [44], using a barometric permeation instrument for single gas feeds at 30 °C. **Figure 2.1** illustrates a scheme of the permeation instrument used in this work. The downstream pressure was maintained below 10^{-2} mbar, while the upstream pressure was kept at 1 or 3 bar for all gases. He (2.6 Å), O_2 (3.46 Å), N_2 (3.64 Å), CH_4 (3.8 Å) and CO_2 (3.3 Å) were used for the permeation experiments. Values in parenthesis represent the kinetic diameters of the different gases. The purities for CH_4 and O_2 were greater than 99.95% and 99.99% for the others gases. Helium permeation tests at three upstream pressures (1, 3 and 5 bar) were carried out to verify the absence of pinholes.
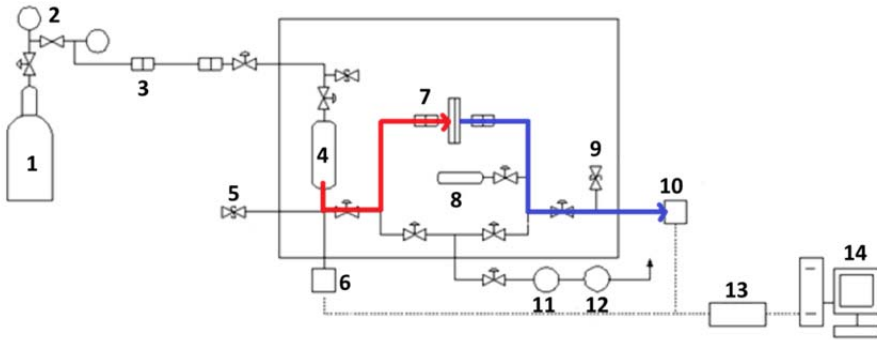
Figure 2.1. Scheme of the permeation device: (1) Gas supply, (2) Pressure regulator, (3) Quick connection, (4) Gas reservoir, (5) Relief valve, (6) High pressure transducer, (7) Permeation cell, (8) Expansion cylinder, (9) Relief valve, (10) Low pressure transducer, (11) Turbo-molecular pump, (12) Rotary pump, (13) Power source and (14) Data acquisition

Gas permeability coefficients (P), which are usually expressed in Barrers [45] [1 Barrer = 10^{-10} (cm³ (STP) cm)/(cm² s cm Hg) = $7.5005 \cdot 10^{-18}$ m² s² Pa⁻¹ (SI units)], were obtained from the slopes and intercepts in a steady state region of pressure increment as a function of time, according to the following expression:

$$P = \frac{273}{76} \frac{Vl}{ATp_0} \frac{dp(t)}{dt} \qquad \text{(Eq. 2.6)}$$

where A, V and l are the effective area, the downstream volume and the thickness of the membrane, respectively. T denotes the temperature of the measurement in Kelvin, p_0 refers to the pressure of the feed gas in the upstream compartment and ($dp(t)/dt$) is the rate of the pressure rise at steady state. The including factors refer the results to standard conditions of pressure and temperature (76 cmHg and 273.15 K).

Determination of the permeability from this way is associated with a relative error of 10%. By extrapolating the steady state permeation curve, the intercept (θ) on the t-axis can be obtained, which is referred to as the *time lag*:

$$\theta = \frac{l^2}{6D} \qquad \text{(Eq. 2.7)}$$

In **Figure 2.2** a typical permeation curve is reported, showing the *time lag* extrapolation for the given steady state. In addition, it was established that 6θ is enough waiting time between different gas measurements to ensure the material has achieved the initial situation. The estimated values allow the diffusion coefficient calculation, hence the determination of the thermodynamic and kinetic contribution to the permeability coefficient from the relation $P = DS$.

The ideal selectivity ($\alpha_{A/B}$) for components A and B was calculated from the ratio of permeability coefficients:

$$\alpha_{A/B} = \frac{P_A}{P_B} \qquad \text{(Eq. 2.8)}$$

where P_A and P_B are the permeability coefficients of pure gases A and B, respectively.
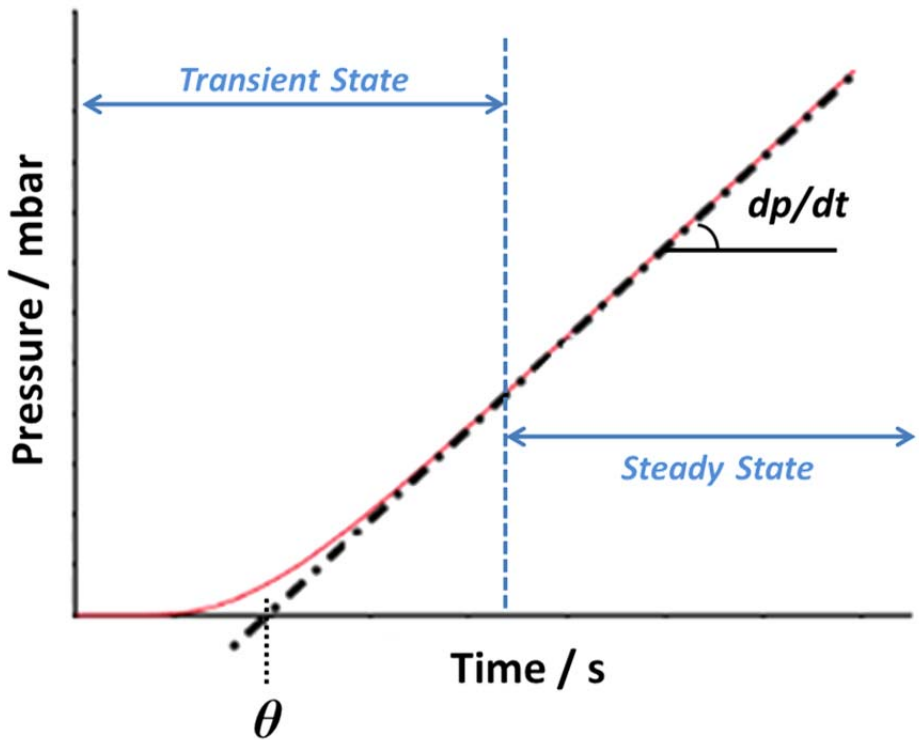
Figure 2.2. Curve describing the permeated gas over time, showing the *time-lag*

2.7. REFERENCES

1. Wallach, M. L. 'Aromatic Poly(amic Acids): Fundamental Structural Studies.' *Journal Polymer Science, Part A-2* **5,** 653–662 (1967).

2. Yang, C. P. & Hsiao, S. H. 'Effects Of Various Factors On The Formation Of High Molecular Weight Polyamic Acid.' *Journal of Applied Polymer Science* **30,** 2883–2905 (1985).

3. Dine-Hart, R. A. & Wright, W. W. 'Preparation And Fabrication Of Aromatic Polyimides.' *Journal of Applied Polymer Science* **11,** 609–627 (1967).

4. Bower, G. M. & Frost, L. W. 'Aromatic Polyimides.' *Journal of Polymer Science Part A: General Papers* **1,** 3135–3150 (1963).

5. Volksen, W. & Cotts, P. M. 'The Synthesis Of Polyamic-acids With Controlled Molecular Weights.' in *Polyimides: Synthesis, Characterization and Properties* (ed. Mittal K.L.) 163–170 (1984). Springer

6. Orwoll, R. A., St. Clair, T. L. & Dobbs, K. D. 'Phase Behavior Of Some Polyamic Acid Plus Ether Systems.' *Journal of Polymer Science: Polymer Physics Edition* **19,** 1385–1393 (1981).

7. Harris, F. W. 'Synthesis Of Aromatic Polyimides From Dianhydrides And Diamines.' in *Polyimides* (ed. Wilson D., Stenzenberger, H.D., Hergenrother, P. M.) 1–37 (1990). Springer Netherlands

8. Takekoshi, T. 'Synthesis Of Polyimides.' in *Polyimides: fundamentals and applications* (ed. Ghosh, M.K. and Mittal, K. L.) 7–48 (1996).

9. Muñoz, D. M., De La Campa, J. G., De Abajo, J. & Lozano, A. E. 'Experimental And Theoretical Study Of An Improved Activated Polycondensation Method For Aromatic Polyimides.' *Macromolecules* **40,** 8225–8232 (2007).

10. Muñoz, D. M., Calle, M., de la Campa, J. G., de Abajo, J. & Lozano, A. E. 'An Improved Method For Preparing Very High Molecular Weight Polyimides.' *Macromolecules* **42,** 5892–5894 (2009).

11. Likhatchev, D., Gutierrez-Wing, C., Kardash, I. & Vera-Graziano, R. 'Soluble Aromatic Polyimides Based On 2,2'bis(3'amino-4'hydroxyphenyl)hexafluoropropane: Synthesis And Properties.' *Journal of Applied Polymer Science* **59,** 725–735 (1996).

12. Han, S. H. *et al.* 'Thermally Rearranged (TR) Polybenzoxazole: Effects Of Diverse Imidization Routes On Physical Properties And Gas Transport Behaviors.' *Macromolecules* **43,** 7657–7667 (2010).

13. Ding, Y., Bikson, B. & Nelson, J. K. 'Polyimide Membranes Derived From Poly(amic Acid) Salt Precursor Polymers. 1. Synthesis And Characterization.' *Macromolecules* **35,** 905–911 (2002).

14. Endrey, A. L. 'Process For Preparing Polyimides By Treating Polyamide-Acids With Lower Fatty Monocarboxylic Acid Anhydrides.' US Patent 3179630 (1965).

15.   Endrey, A. L. 'Aromatic Polyimide Particles From Polycyclic Diamines.' US Patent 3179631 (1965).

16.   Hendrix, W. R. 'Process For Preparing Polyimides Polyamic Acids With Aromatic Monocarboxylic Acid Anhydrides.' US Patent 3179632 (1965).

17.   Endrey, A. L. 'Aromatic Polyimides From Meta-Phenylene Diamine And Para-Phenylene Diamine.' US Patent 3179633 (1965).

18.   Bessonov, M. I., Koton, M. M., Kudryavtsev, V. V & Laius, L. A. 'POLYIMIDES: THERMALLY STABLE POLYMERS.' (1987).

19.   Kim, Y. J., Glass, T. E., Lyle, G. D. & McGrath, J. E. 'Kinetic And Mechanistic Investigations Of The Formation Of Polyimides Under Homogeneous Conditions.' *Macromolecules* **26,** 1344–1358 (1993).

20.   Cotts, P. M. 'Characterization Of Polyimides And Polyamic Acids In Dilute Solution.' in *Polyimides: Synthesis, Characterization and Properties* (ed. Mittal K.L.) 223–226 (1984).

21.   Sroog, C. 'Polyimides.' *Journal of Polymer Science: Macromolecular Reviews* **11,** 161–208 (1976).

22.   Brink, M. H., Brandom, D. K., Wilkes, G. L. & McGrath, J. E. 'Synthesis And Characterization Of A Novel "3F"-based Fluorinated Monomer For Fluorine-containing Polyimides'. *Polymer* **35,** 5018–5023 (1994).

23.   Bell, V. L., Stump, B. L. & Gager, H. 'Polyimide Structure–property Relationships. II. Polymers From Isomeric Diamines.' *Journal of Polymer Science: Polymer Chemistry Edition* **14,** 2275–2291 (1976).

24.   Brandom, D. K. & Wilkes, G. L. 'Study Of The Multiple Melting Behaviour Of The Aromatic Polyimide LaRC CPI-2.' *Polymer* **35,** 5672–5677 (1994).

25.   Woodard, M. H., Rogers, M. E., Brandom, D. K., Wilkes, G. L. & McGrath, J. E. 'Synthetic Investigations Of High-Tg Fluorinated Polyimides.' *Polymer Preprints (American Chemical Society, Division of Polymer Chemistry)* **33,** 333 (1992).

26.   Matsumoto, K. & Xu, P. 'Gas Permeation Properties Of Hexafluoro Aromatic Polyimides.' *Journal of Applied Polymer Science* **47,** 1961–1972 (1993).

27.   Xu, W. Y. 'Synthesized Polyimide Membranes For Pervaporation Separations Of Toluene/iso-octane Mixtures.' *Thesis Dissertation* (2005).

28.   Martínez-Richa, A. & Vera-Graziano, R. 'A Solid-state NMR Study Of Aromatic Polyimides Based On 4,4'-diaminotriphenylmethane.' *Journal of Applied Polymer Science* **70,** 1053–1064 (1998).

29.   Xie, K. *et al.* 'Soluble Fluoro-polyimides Derived From 1,3-bis(4-amino-2-trifluoromethyl- Phenoxy) Benzene And Dianhydrides.' *Polymer* **42,** 7267–7274 (2001).

30.   Guo, R. *et al.* 'Synthesis And Characterization Of Thermally Rearranged (TR) Polymers: Effect Of Glass Transition Temperature Of Aromatic Poly(hydroxyimide) Precursors On TR Process And Gas Permeation Properties.' *Journal of Materials Chemistry A* **1,** 262–272 (2013).

31. Calle, M., Chan, Y., Jo, H. J. & Lee, Y. M. 'The Relationship Between The Chemical Structure And Thermal Conversion Temperatures Of Thermally Rearranged (TR) Polymers.' *Polymer* **53,** 2783–2791 (2012).

32. Park, H. B. *et al.* 'Polymers With Cavities Tuned For Fast Selective Transport Of Small Molecules And Ions.' *Science* **318,** 254–258 (2007).

33. Park, H. B., Han, S. H., Jung, C. H., Lee, Y. M. & Hill, A. J. 'Thermally Rearranged (TR) Polymer Membranes For CO2 Separation.' *Journal of Membrane Science* **359,** 11–24 (2010).

34. Calle, M. & Lee, Y. M. 'Thermally Rearranged (TR) Poly(ether−benzoxazole) Membranes For Gas Separation.' *Macromolecules* **44,** 1156–1165 (2011).

35. Sanders, D. F. *et al.* 'Gas Permeability, Diffusivity, And Free Volume Of Thermally Rearranged Polymers Based On 3,3'-dihydroxy-4,4'-diamino-biphenyl (HAB) And 2,2'-bis-(3,4-dicarboxyphenyl) Hexafluoropropane Dianhydride (6FDA).' *Journal of Membrane Science* **409-410,** 232–241 (2012).

36. Smith, Z. P. *et al.* 'Gas Sorption And Characterization Of Thermally Rearranged Polyimides Based On 3,3'-dihydroxy-4,4'-diamino-biphenyl (HAB) And 2,2'-bis-(3,4-dicarboxyphenyl) Hexafluoropropane Dianhydride (6FDA).' *Journal of Membrane Science* **415-416,** 558–567 (2012).

37. Dewar, M. J. S., Zoebisch, E. G., Healy, E. F. & Stewart, J. J. P. 'Development And Use Of Quantum Mechanical Molecular Models. 76. AM1: A New General Purpose Quantum Mechanical Molecular Model.' *Journal of the American Chemical Society* **107,** 3902–3909 (1985).

38. 'HYPERCHEM(TM), PROFESSIONAL 8.0.3 HYPERCUBE, INC., VERSION 8.0.3, FLORIDA, USA.'

39. Becke, A. D. 'Density-functional Thermochemistry. III. The Role Of Exact Exchange.' *The Journal of Chemical Physics* **98,** 5648 (1993).

40. Lee, C., Yang, W. & Parr, R. G. 'Into A Functional Of The Electron Density F F.' *Physical Review B* **37,** 785–789 (1988).

41. Hehre, W. J. 'Ab Initio Molecular Orbital Theory.' *Accounts of Chemical Research* **9,** 399–406 (1976).

42. M. J. Frisch, G. W. Trucks, H. B. Schlegel, G. E. Scuseria, M. A. Robb, J. R. Cheeseman, J. A. Montgomery Jr., T. Vreven, K. N. Kudin, J. C. Burant, J.M.Millam, S. S. Iyengar, J. Tomasi, V. Barone, B. Mennucci, M. Cossi, G. Scalmani, N. Rega, G. A. Peters, C. G. and J. A. P. 'GAUSSIAN 03 (REVISION C.02).' *Gaussian, Inc., Wallingford CT* (2004).

43. M. A. Thompson. 'ARGUSLAB 4.0.1.' .

44. Barrer, R. M. & Rideal, E. K. 'Permeation, Diffusion And Solution Of Gases In Organic Polymers.' *Transactions of the Faraday Society* **35,** 628 (1939).

45. Stern, S. A. 'The "barrer" Permeability Unit'. *Journal of Polymer Science Part A-2: Polymer Physics* **6,** 1933–1934 (1968).

Chapter III

Thermally rearranged polybenzoxazoles and poly(benzoxazole-co-imide)s from *ortho*-Hydroxyamine Monomers:

Influence of OH Amount

3.1. INTRODUCTION

Within the framework of the continuous research effort on developing polymers with high fractional free volume (FFV) to improve permeability and having high molecular rigidity to attain high selectivity [1,2], this chapter introduces two commercial *ortho*-aminophenols (DAPs) as polycondensation monomers. This class of molecules is sensitive to both air and light, and can easily evolve to oxidized products. These oxidized chemicals are inactive with respect to polycondensation, and that is the reason why DAPs are not traditionally used for the synthesis of aromatic polymers, unless they contain an electron acceptor group such as sulfonyl, trifluoromethyl or hexafluoroisopropylidene [3]. However, it is possible to achieve high molecular weight polyamides and polyimides from the corresponding hydrochloride derivatives using a base as promoter [4,5]. In the present study, we have used this approach wherein the preparation of HPIs from 2,4-diaminophenol dihydrochloride (DAP-Cl) and 4,6-diaminoresorcinol dihydrochloride (DAR-Cl) was optimized to obtain high molecular weight polymers.

Poly(*o*-hydroxyimide)s similar to those described in the previous chapter can be attained from the symmetric diaminodiphenol monomer DAR-Cl and appropriate dianhydrides; however, by using an asymmetric diaminophenol monomer, such as DAP-Cl, *ortho*-hydroxypolyimide-co-polyimide will be attained on reacting with dianhydrides. So, treating them at high temperature, under the conditions applied for TR-polymers, can render TR poly(benzoxazole-co-imide)s.

TR poly(benzoxazole-co-imide) membranes have been previously reported by Jung et al. [6]; however, these authors did not use DAPs as monomers, but rather mixtures of aromatic diamines and aromatic diaminodiphenols (DAP) in combination with dianhydrides to prepare HPIs that were eventually converted into poly(benzoxazole-co-imides) (TR-PBO-PI) by thermal rearrangement.

Diamine hydrochlorides are not actually usual condensation monomers, thereby the reaction conditions to get high molecular weight are not as well established as they are for pristine aromatic diamines, so the polycondensation reaction was optimized by 1) using chlorotrimethylsilane in order to form the in-situ silylated diamine, which is more reactive against dianhydrides than the pure diamine [7], and 2) by thorough purification of DAP-Cl, DAR-Cl, and the dianhydride 6FDA. In this way, high molecular weight HPIs, with good film-forming capability, could be achieved. For comparison purposes, a pristine polyimide was also prepared from 6FDA and *meta*-phenylenediamine (MPD), which allowed for the creation of three chemically related polymers with final compositions corresponding to polyimide (PI), *ortho*-hydroxypolyimide-co-polyimide (HPI-PI) and *ortho*-hydroxypolyimide) (HPI) and their corresponding thermally-formed polyimide, poly(benzoxazole-co-imide) (PBO-PI) and polybenzoxazole (PBO). The goal of this study consisted of exploring the latent capability of these polymers in TR gas separation materials, as well as studying the influence of the amount of OH groups present in the chemical structure of precursor polyimides in the final properties of the TR materials.

3.2. EXPERIMENTAL SECTION

3.2.1. MATERIALS

This chapter focuses on three polyimides: PI-DAR (formed by the reaction of 4,6-diaminoresorcinol dihydrochloride (DAR-Cl, Sigma Aldrich) and 2,2'-bis-(3,4-dicarboxyphenyl) hexafluoropropane dianhydride (6FDA, Cymit Química (Barcelona)), PI-DAP (formed by the reaction of 2,4-diaminophenol dihydrochloride (DAP-Cl, Sigma Aldrich) and 6FDA) and PI-MPD (formed by the reaction of m-phenylenediamine (MPD, Sigma Aldrich) and 6FDA). The chemical structures of these aromatic polyimides and their precursor monomers are shown in **Scheme 3.1**. The 6FDA dianhydride was selected due to its favourable performance in other polymeric gas separation membrane studies, including previous TR research [8–10] and also because this dianhydride increases polyimide solubility. DAR is one of the promising monomers for the synthesis of aromatic polymers having high thermal stability. Thus, PI-DAR (two –OH groups in its repeating unit) was chosen due to its ability, after a convenient thermal treatment, to convert into a rigid-rod PBO, which could offer significant opportunities in membrane science. The PI-DAP (just one –OH group in its repeating unit), gives rise to poly(benzoxazole-co-imide) structure after thermal treatment. This PBO-PI structure could be a suitable candidate for gas separation membranes due to its combined polybenzoxazole and polyimide properties. PI-MPD was also prepared in order to compare with *ortho*-hydroxylated polyimides and also to demonstrate that polyimides without *ortho*-positioned groups can not convert into PBO via thermal treatments in solid state.
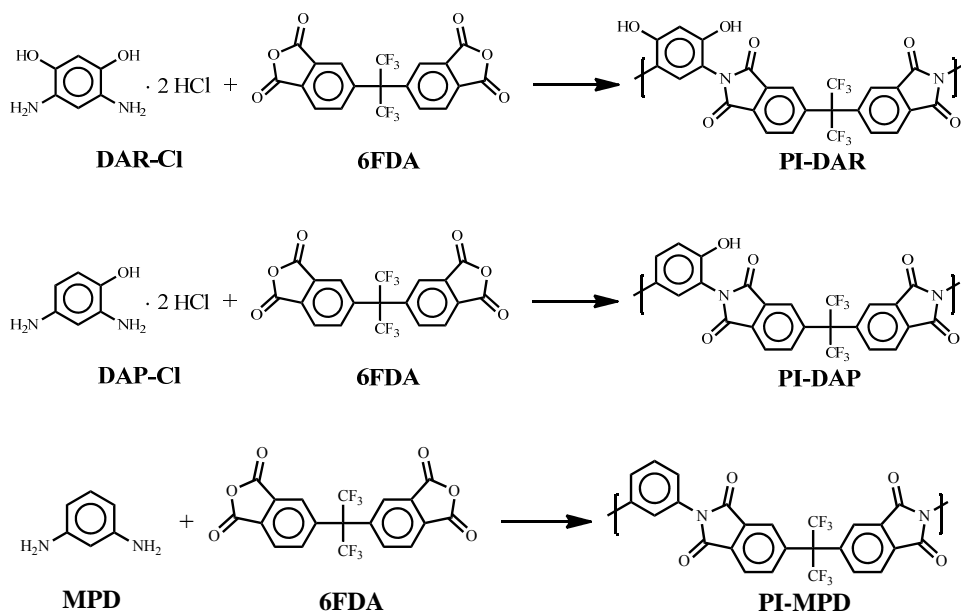
Scheme 3.1. Chemical structure of PI-DAR, PI-DAP and PI-MPD polyimides and their precursor monomers

3.2.2. SYNTHESIS OF POLYIMIDES

3.2.2.1. Polyimide from MPD and 6FDA (PI-MPD)

A total of 10.0 mmol of MPD was dissolved in 10 mL of anhydrous DMAc in a three-necked flask equipped with a mechanical stirrer under a nitrogen atmosphere. The solution was cooled to 0 °C and 20 mmol of CTMS were mixed into the reaction vessel, followed by addition of 20 mmol Py and 2 mmol DMAP. The temperature was raised to room temperature and the solution was stirred for 15 min to ensure formation of the silylated diamine. Next, the solution was cooled to 0 °C and 6FDA (10.0 mmol) was added. The mixture was then stirred for 12 h at room temperature upon which a very viscous clear solution of polyamic acid formed. To this solution a mixture of acetic anhydride (80 mmol) and pyridine (80 mmol) was added followed by stirring for 6 h at room temperature and an additional 45 min at 60 °C. The viscous polyimide solution was poured onto water and the resulting precipitate was washed several times with water and finally dried in a vacuum oven at 130 °C overnight.

PI-MPD.^{1}H-NMR (DMSO-d_6, 300 MHz): 8.18 (d, 2H, J=7.9 Hz), 7.95 (d, 2H, J=7.9 Hz), 7.76 (s, 2H), 7.69 (m, 1H), 6.62 (s, 1H), 7.57 (s, 2H), 7.54 (s, 1H). FT-IR (film): imide ν(C=O) at 1785 and 1716 cm^{-1}, imide ν(C-N) at 1353 cm^{-1}. η_{inh} (dL/g) = 0.56.

3.2.2.2. Ortho-hydroxypolyimides (HPIs)

A three-necked flask equipped with a mechanical stirrer and gas inlet and outlet was charged with 10.0 mmol of diamine dihydrochloride, DAP-Cl, or DAR-Cl and 10 mL of NMP. The mixture was then cooled to 0 °C and the required amount of CTMS (1 mol/mol reactive group) was added, followed by pyridine (1 mol/mol reactive group) and DMAP (0.1 mol/mol pyridine). The hydrochloride protection of the unstable amino groups of DAP-Cl and DAR-Cl was not removed prior to synthesis, and thus an extra amount of pyridine (10 mmol/ mmol of diamine) was required to remove the HCl formed during the deprotection. The solution was allowed to warm to room temperature and then stirred for 15 min to guarantee the formation of the silylated diamine. Subsequently, the solution was again cooled to 0 °C and 6FDA (10.0 mmol) was rapidly added followed by 10 mL of NMP. After stirring for 15 minutes at 0 °C the solution was heated to room temperature and left overnight to form poly(amic acid). Next, *o*-xylene (20 mL) was added to the solution as an azeotropic water remover and vigorously stirred and heated for 6 h at 180 °C to promote the ring-closure reaction. During this stage, water from the imidization reaction was released as a xylene azeotrope along with other by-products. Remaining o-xylene was distilled out from the polymer solution, which was successively cooled to room temperature and poured on distilled water. The obtained polymer was thoroughly washed with water and ethanol, and then dried at 150 °C for 12 h under vacuum. **PI-DAP**: ^{1}H-NMR (DMSO-d$_6$, 300 MHz): 10.31 (s, 1H, OH), 8.15 (d, 2H, J=7.9 Hz), 7.95 (s, 2H), 7.77 (d, 2H, J=7.9 Hz), 7.41 (d, 2H, J=8.0 Hz), 7.41 (s, 2H), 7.13 (d, 2H, J=8.0 Hz). FT-IR (film): ν(-OH) at 3415 cm^{-1}, imide ν(C=O) at 1785 and 1719 cm^{-1}, imide ν(C-N) at 1360 cm^{-1}. η_{inh} (dL/g) = 0.64. **PI-DAR**: ^{1}H-NMR (DMSO-d$_6$, 300 MHz): 10.16 (s, 2H, OH), 8.14 (d, 2H, J=7.6 Hz), 7.95 (d, 2H, J=7.6 Hz), 7.78 (s, 2H), 7.19 (s, 1H), 6.62 (s, 1H). FT-IR (film): ν(-OH) at 3402 cm^{-1}, imide ν(C=O) at 1785 and 1716 cm^{-1}, imide ν(C-N) at 1371 cm^{-1}. η_{inh} (dL/g) = 0.83.

3.2.3. POLYIMIDES FILM FORMATION

Polymer solutions, 10% (w/v) in NMP, were cast on a well-leveled glass plate and dried at 60 °C overnight to remove most of the solvent. Next, the films were stepwise heated, being held for 1 h each at 100, 150, 200, and finally at 250 °C under vacuum to evaporate the residual solvent. The films were then removed from the glass plate, washed with deionized water, and dried overnight at 130 °C under vacuum. Film thicknesses were between 40 and 50 μm and, in all cases, suitable film uniformity was verified by measuring the film thickness standard deviation, which was lower than 5 %. Defect-free and clean polyimide membranes were cut into 3 cm x 3 cm pieces and placed between ceramic plates to prevent film deformation at elevated temperatures in a muffle furnace under an inert gas atmosphere. Each sample was then heated to 300 °C at a heating rate of 5 °C min^{-1} under N_2 and held at that temperature for 3 hours to ensure complete solvent removal and full closure of the imide ring structure.

3.2.4. THERMAL CONVERSION OF HPI MEMBRANES TO PBO

HPIs were heated to the target temperature for conversion into polybenzoxazoles (350, 400 or 450 °C) at a rate of 5 °C min^{-1}, and maintained for the desired time (30 min or 1 h) in a high-purity argon atmosphere. After thermal treatment, the furnace was cooled to room temperature at a rate no greater than 10 °C min^{-1}. This protocol was used to expose the samples to thermal histories similar to those reported in previous studies related to TR polymers [11-13]. The thermally treated membranes, obtained from PI-DAP and PI-DAR, were coded as TR-DAPX and TR-DARX respectively, where X specifies the final rearrangement temperature applied.

The polyimide without hydroxyl groups in the *ortho* position, PI-MPD, which cannot be converted into PBO, was treated to the highest temperature (450 °C) at the same heating rate as PI-DAP and PI-DAR, in order to compare its properties with those of the TR-PBO membranes. This membrane was coded as PI-MDP450.

3.3. RESULTS AND DISCUSSION

3.3.1. SYNTHESIS AND CHARACTERIZATION OF PI-MPD, PI-DAP AND PI-DAR

Polyimide PI-MPD was synthesized by a classical two-step procedure in which diamine MPD was combined with dianhydride 6FDA to polymerize at room temperature in a solution of DMAc. The intermediate poly(amic acid) was attained through a base-assisted *in situ* silylation method [14] which involved the use of chlorotrimethylsilane as the silylating agent and pyridine and 4-dimethylaminopyridine as activating reagents. Next, the intermediate poly(amic acid) was chemically imidized by cyclodehydration with a mixture of acetic anhydride and pyridine.

The *ortho*-hydroxypolyimides PI-DAP and PI-DAR were synthesized using diaminophenol dihydrochloride, DAP-Cl, and diaminoresorcinol dihydrochloride, DAR-Cl, as monomers via the two-step polycondensation method. These monomers were combined with 6FDA dianhydride in an NMP solution to form the desired polymer. The monomers were introduced into the reaction mixture in the form of dihydrochlorides in order to minimize the amount of oxidation of the air-sensitive amino groups. The *in situ* silylation base-assisted method was also employed to prepare these intermediates, increasing the reactivity of the $-NH_2$ groups. In addition, excess of pyridine was added as a proton acceptor agent of the hydrochloride salt giving the poly(amic acid) in high yield, which was then imidized. Unlike PI-MPD, hydroxypolyimides PI-DAP and PI-DAR are prone to thermal conversion to TR-PBO due to the *ortho* positioned hydroxyl groups (**Scheme 3.2**).

To prevent acetylation of these hydroxyl groups, the poly(amic acid) formed during the reaction was imidized by azeotropic cyclization using o-xylene as a water removal agent. During this process, water produced by the ring-closure reaction was removed as a xylene azeotrope, along with silanol and siloxane by-products.

PI-MPD, PI-DAP, and PI-DAR polyimides exhibited values of inherent viscosity of 0.56, 0.64 and 0.83 dL/g, respectively, indicating that they were of sufficiently high molecular weight to be employed in the preparation of dense membranes for gas separation applications. Yield was higher than 98-99 % for all polyimides.

All three polyimides were soluble in polar aprotic solvents such as DMF, DMAc or DMSO, as well as in common organic solvents as THF and acetone. However, insolubility in methanol, ethanol, isopropanol or ethylene glycol was observed, contrarily to what was previously commented for related hydroxyl containing polyimides from 6FDA dianhydride [13].

Polyimide chemical structures were confirmed by ^{1}H-NMR and FT-IR. **Figure 3.1** presents the ^{1}H-NMR spectra of the three polyimides prepared in the current work. All of the observed signals were readily assigned and were in good agreement with expected shifts for individual hydrogen atoms. In particular, it was possible to differentiate between protons corresponding to diamine moieties and those corresponding to the dianhydride. In addition, the OH phenolic protons denoted the electronic features of the aromatic ring. Specifically, the presence of two electron-donating OH groups shifted the OH protons to high field when compared with the monomer which had only one OH group. Likewise, the electronic shielding of the OH groups moved the protons of the aromatic diamine moiety (*b* and *c*) to lower chemical shifts. Finally, the *e*, *f*, and *g* protons (6FDA) exhibited a similar chemical shift for all polymers, which indicated that the influence of the electronic features of the diamine aromatic rings on the dianhydride ones was negligible.

PI-MPD

PI-DAP

PI-DAR

Δ | - CO$_2$

Δ | - CO$_2$

TR-PBO-PI-DAP

TR-PBO-DAR
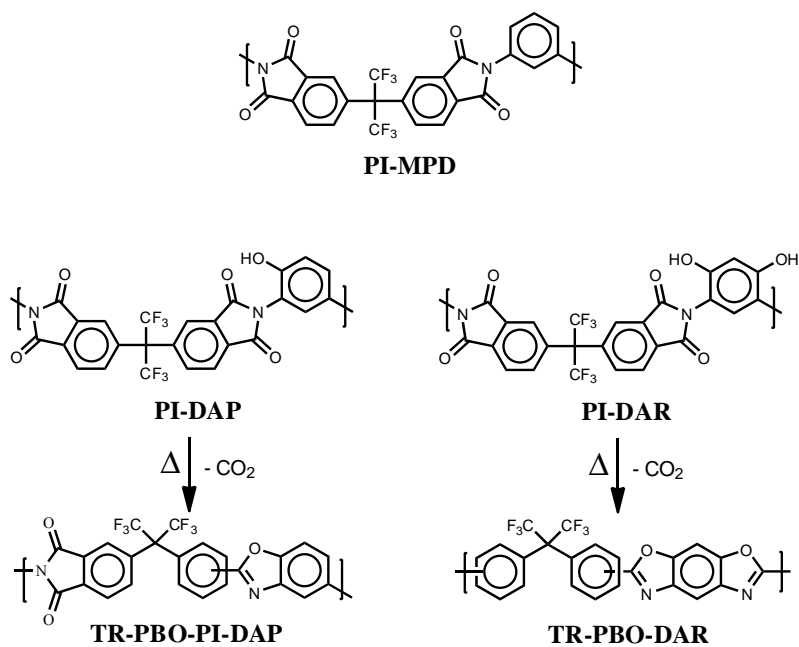
Scheme 3.2. Chemical structure of precursor polyimides and their corresponding TR-PBOs
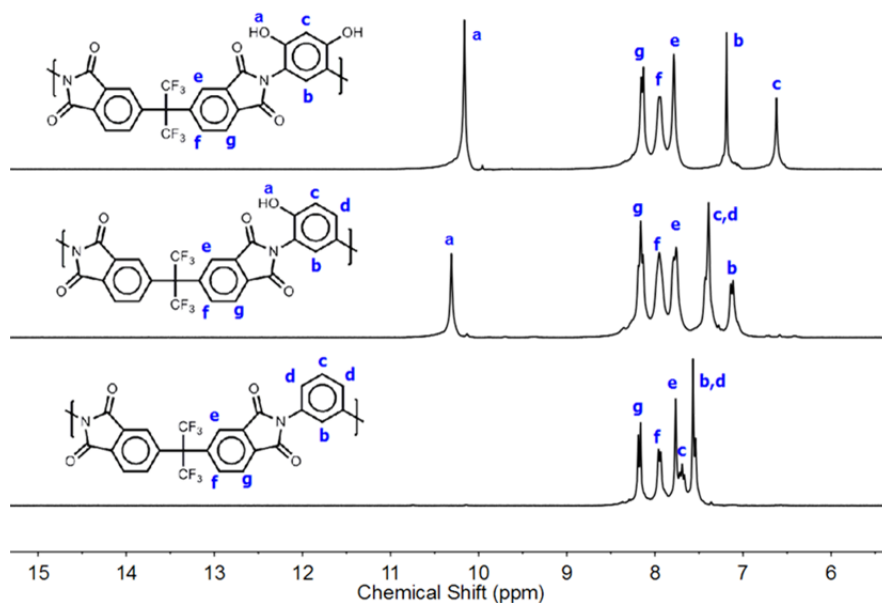
Figure 3.1. ¹H-NMR spectra of PI-DAR, PI-DAP and PI-MPD polyimides (DMSO-d$_6$, 300 MHz)

The IR spectra of the three polyimides are shown in **Figure 3.2**. The spectra of all of them (PI-DAR, PI-DAP and PI-MPD) showed the characteristic absorption bands of polyimides, denoted by stretching vibration bands of C=O, (*b* and *c*) (1786 and 1720 cm⁻¹); asymmetric stretching of C-N, (*d*) (1365 cm⁻¹); stretching of C-N-C groups at 1102 cm⁻¹; and out-of-plane bending of C-N-C groups around 725 cm⁻¹. In addition, absorption peaks at around 1250-1100 cm⁻¹ denoted the C-F stretching of the hexafluoroisopropylidene moiety. Lastly, the broad band in the region of 3200-3600 cm⁻¹ (*a*) observed in the spectra of hydroxypolyimides, PI-DAR and PI-DAP, was ascribed to O-H vibration of the OH groups.
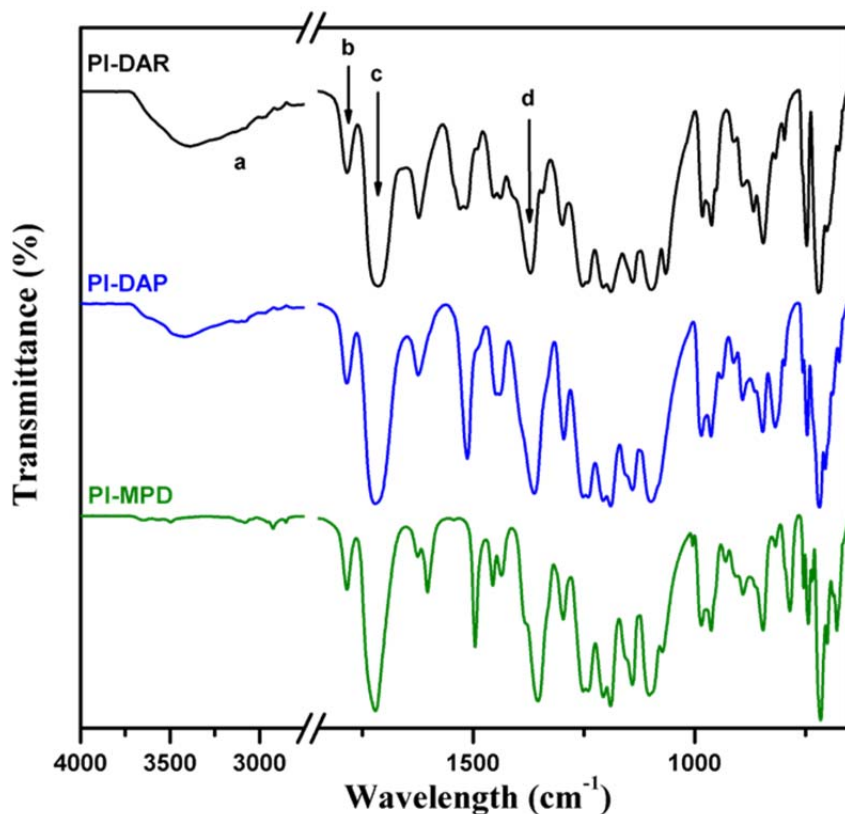
Figure 3.2. ATR-FTIR spectra of PI-DAR, PI-DAP and PI-MPD precursor polyimides

The thermal behavior of PI-MPD and the hydroxy-containing polyimides PI-DAP and PI-DAR was studied using DSC and thermogravimetric analysis coupled with mass spectroscopy (TGA-MS). The polymer made from MPD had a glass transition temperature of 295 °C, whereas polymers made from PI-DAP and PI-DAR exhibited higher T_g values due to the hydrogen bonding provided by the interaction of hydroxyl groups. Accordingly, PI-DAP showed a T_g of 313 °C and PI-DAR exhibited a T_g of 338 °C. The difference between them was attributed to the ability of the latter to create more hydrogen bonds, which in turn produced a more rigid structure and thus a higher T_g. In addition, as mentioned in a previous study [12], it was observed that the gradual conversion to PBO, which starts immediately above T_g, produces a more rigid structure resulting in a higher T_g. This finding also implies that the values of T_g were reliant on the first scan final temperature due to the fact that T_g and the conversion temperatures were very close (see **Table 3.1**).

Table 3.1. Thermal Properties of Precursor Polyimide Membranes

Polymer code	T_g (°C)[a]	T_{AP} (°C)[b,d]	T_{TR} (°C)[c,d]	CO_2 theoretical wt. loss (%)	CO_2 found wt. loss (%)[d]	T_d (°C)[d]
PI-MPD	295	-	-	-	-	585
PI-DAP	313	323	412	8.26	8.1	570
PI-DAR	338	345	438	16.05	11.2	550

[a] Middle point of the endothermic step during the second scan of DSC measurements conducted at a heating rate of 20 °C/min under a nitrogen atmosphere. [b] Apparent starting temperature at which thermal rearrangement begins. [c] Temperature at the maximum point of weight loss or maximum rate of conversion to PBO. [d] Determined by TGA at a heating rate of 10 °C/min under nitrogen atmosphere.

3.3.2. *THERMAL REARRANGEMENT OF HPIS TO POLYBENZOXAZOLES (TR-PBOS)*

As reported previously [9,10,13,15], the thermal rearrangement process of HPIs can be studied by thermogravimetric analysis just by monitoring the evolution of two distinct weight loss steps. In the first step, in the range of 300-500 °C, mass spectroscopy shows CO_2 release, the result of thermal rearrangement to form the PBO structure. The second step, at around 500-600 °C, corresponds to the generalized decomposition of the in-situ formed PBO backbone. TGA curves along with first derivative traces for all precursor polyimide films are shown in **Figure 3.3**. The hydroxypolyimide precursors PI-DAR and PI-DAP exhibited the two weight loss steps described above, while PI-MPD exhibited only the second weight loss as predicted.

Interestingly, the initial weight loss assigned to the thermal rearrangement process, as confirmed by thermogravimetric analysis combined with mass spectroscopy (TGA-MS) (**Figure 3.4**), revealed significant differences between PI-DAR and PI-DAP. As shown in **Figure 3.3** and **Figure 3.4**, the starting temperature of the first weight loss step, which denotes the temperature at which the rearrangement process started, was slightly lower for PI-DAP than for PI-DAR. In addition, the temperature at the maximum of CO_2 release, or maximum conversion rate (T_{TR}), showed a value for PI-DAP of 412 °C, while it was 438 °C for PI-DAR (in both cases T_{TR} was 100 °C above T_g). According to the differential TGA curves (DTG), PI-DAP exhibited a rather higher cyclization rate than PI-DAR. PI-DAP also exhibited a greater conversion into PBO (CO_2 weight loss ~8.1 %; 98 % of the theoretical conversion) when compared to PI-DAR (~11.2 %; 70 % of the theoretical conversion).

A reliable explanation for these differences has not yet been determined, although partial trapping of CO_2 molecules within the emerging PBO structures and deceleration of their evolution out of the PI-DAR film may be responsible for that. Regarding generalized thermal decomposition, the initial degradation temperatures of polymer films were observed at nearly 570 °C for PI-DAP and at 550 °C for PI-DAR, whereas a higher value was found for the non-hydroxylated polyimide PI-MPD (T_d~585 °C).
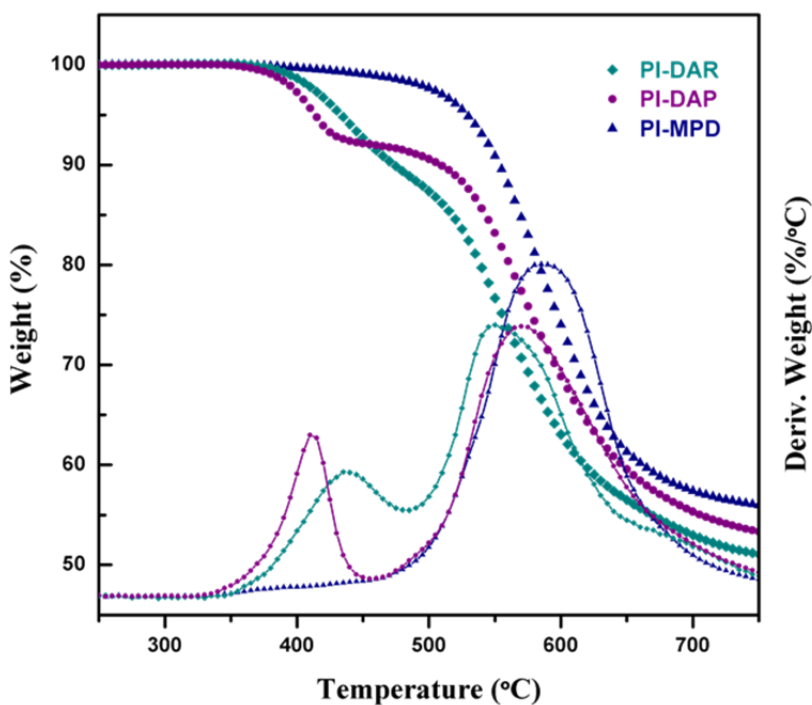
Figure 3.3. TGA and DTG curves of hydroxypolyimide films (PI-DAR and PI-DAP), and also of PI-MPD polyimide film. The TGA heating rate was 10 °C min-1 under a N_2 atmosphere
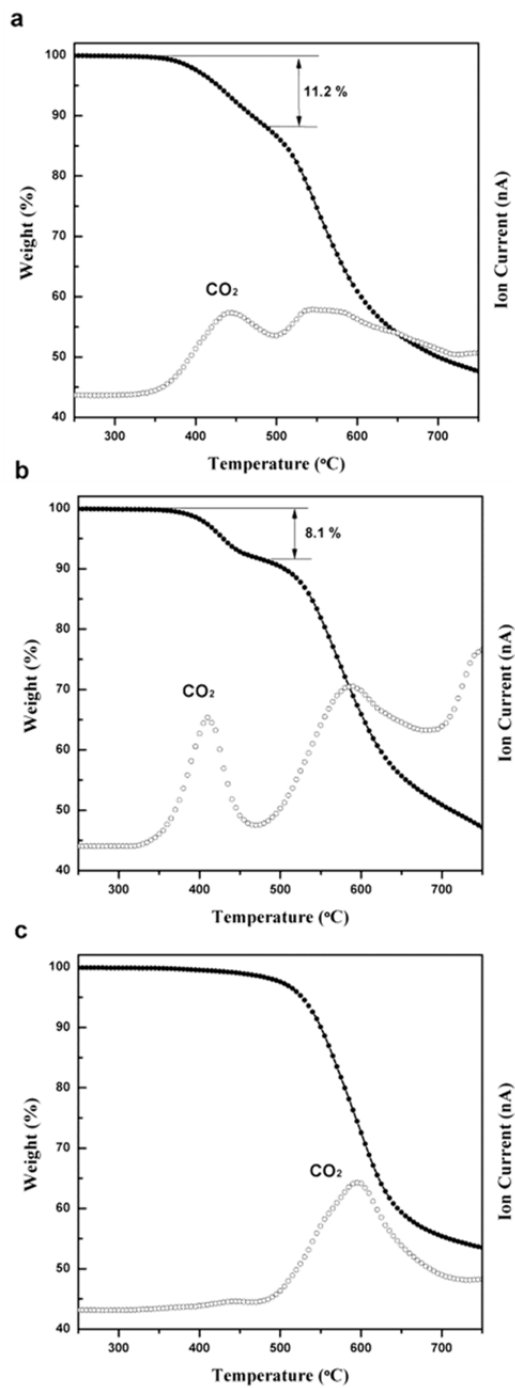
Figure 3.4. Thermogravimetric analysis coupled with mass spectroscopy (TGA-MS) of (a) PI-DAR, (b) PI-DAP, and (c) PI-MPD polyimide

The rearrangement temperature to PBO for the hydroxypolyimides was apparently influenced by the capability to create more hydrogen bonds producing a more rigid structure. In agreement with previous results [12,15], it was noted that the initial temperature of the rearrangement process, and the conversion rate into PBO as well, was controlled by the chain stiffness of HPI, revealing an important dependence on T_g.

Additional TGA isothermal analyses were carried out to optimize the thermal treatment conditions for TR films preparation. In this regard, it is crucial to consider that FFV and cavity size of membranes are considerably affected by the thermal treatment protocol [9,10,12,16]. Therefore, HPI film samples (PI-DAP and PI-DAR) treated at 300 °C were further heated to the desired temperature (350, 400 and 450 °C) at a heating rate of 5 °C min^{-1} and held isothermally at that temperature for 3 h. **Figure 3.5** shows the isothermal thermograms for PI-DAP and PI-DAR membranes, which depict the weight loss as a function of time when the target rearrangement temperature was achieved. The theoretical CO_2 weight loss to complete conversion of both precursors into the final PBO structure was 8.26 % for PI-DAP and 16.05 % for PI-DAR, which was estimated from the weight of one repeating unit of the HPI molecule and shown as a grey dotted line in the figure. **Figure 3.5** also shows the extent of weight loss as a function of temperature and time for both HPI polymers.
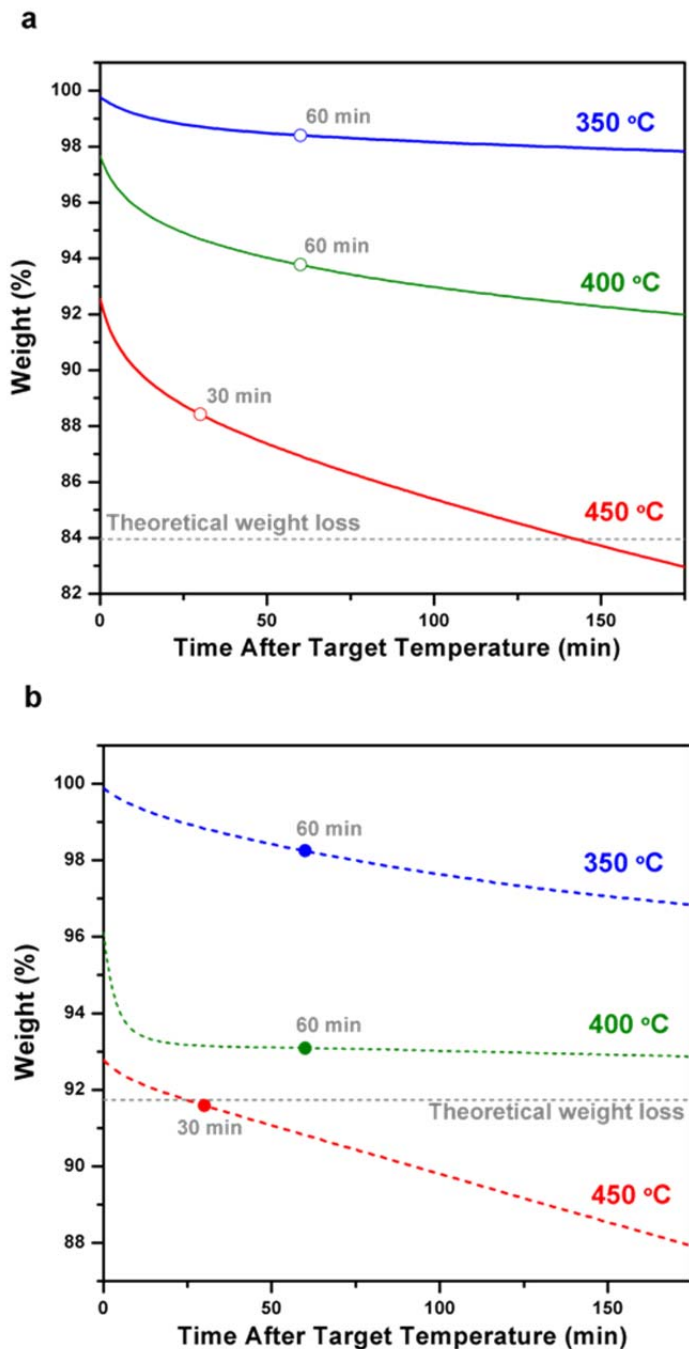
Figure 3.5. Isothermal thermogravimetric analysis, under a N_2 atmosphere, of (a) PI-DAR and (b) PI-DAP precursor OH-polyimide membranes. This graph shows the weight loss of these polyimides as a function of time at the indicated temperatures. Circles represent the conditions used for membranes employed in transport property characterization

The loss was low for any heating time at 350 °C; however, it was notably greater at 450 °C, exceeding the theoretical weight loss value for prolonged treatment times in PI-DAR and even for short treatment times in the case of PI-DAP. On the other hand, lower weight loss was observed for PI-DAR due to its higher rigidity (higher T_g), which led to a lower degree of conversion into PBO at all temperatures.

In order to ensure that samples underwent minimal thermal degradation, and also to reproduce the thermal histories published in previous reports on TR polymers [11-13], we selected times for thermal treatment at the desired rearrangement temperatures of 1 h at 350 and 400 °C and 30 minutes at 450 °C (denoted by circles in **Figure 3.5**).

Based on TGA data, Equation 3.1 was used to quantify the conversion of the precursor HPIs into TR-PBO membranes:

$$\% \ Conversion = \frac{Experimental \ Mass \ Loss}{Theoretical \ Mass \ Loss} \times 100 \hspace{2cm} \text{(Eq. 3.1)}$$

The conversion values are recorded in **Table 3.2**, which shows that the PBO conversions were higher for the PI-DAP polyimide, with percentages of conversion ranging from 21 to 100 % while the conversions observed for PI-DAR ranged from 10 to 72 %. These data indicated that the more flexible PI-DAP was able to easily achieve higher thermal conversion degrees at a faster rate. On the other hand, the thermal rearrangement rate of both polyimides increased with temperature, which correlated with previous TR studies [11,12,16]. Both HPIs exhibited a low degree of conversion at 350 °C, which was increased at 400 °C and reached a maximum at 450 °C.

The thermal rearrangement process of *ortho*-hydroxypolyimides can be readily followed by ATR-FTIR spectroscopy as several chemical or structural changes can be detected. **Figure 3.6** shows the ATR-FTIR spectra for both HPI precursors (upper spectrum) and their TR-PBO analog treated membranes. ATR-FTIR spectra were also included for PI-MPD and its corresponding treated membrane, which was heated to 450 °C and upheld for 30 min in order to ensure that the thermal treatment did not produce any structural change to the PI-MPD membrane.

Table 3.2. Physical Properties of Precursor Polyimides and TR-PBO derived Membranes from OH-precursors

Polymer code	Conv. [a] (%)	Density (g cm^{-3})	Vw (cm^{3}g^{-1})	FFV	Increment in FFV (%)	*d*-spacing (Å)
PI-MPD	-	1.464	0.432	0.178	−	5.68
PI-MPD450	-	1.462	0.432	0.179	~ 0	5.87
HPI-DAP	0	1.484	0.427	0.176	−	5.02
TR-DAP350	21	1.485	0.429	0.171	~ 0	5.36
TR-DAP400	84	1.435	0.437	0.185	5.1	5.77
TR-DAP450	100	1.411	0.439	0.194	10.2	5.88
HPI-DAR	0	1.512	0.422	0.171	−	5.27
TR-DAR350	10	1.509	0.424	0.169	~ 0	5.48
TR-DAR400	39	1.460	0.429	0.185	8.2	5.54
TR-DAR450	72	1.391	0.437	0.210	22.8	5.88

[a] PBO conversion after 60 min at 350 and 400 ˚C and 30 min at 450 ˚C
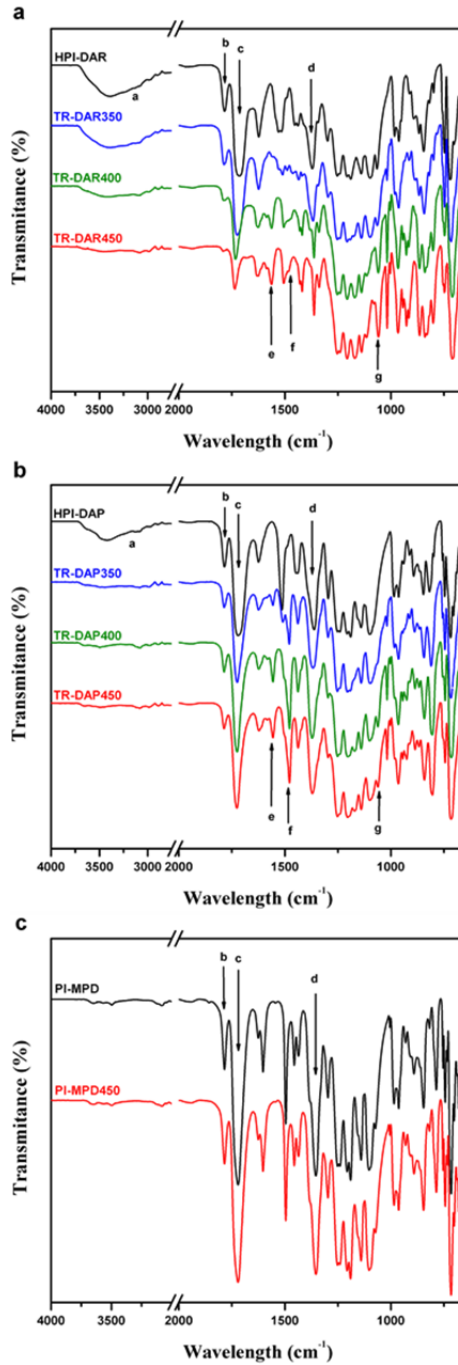
Figure 3.6. ATR-FTIR spectra of (a) PI-DAR and (b) PI-DAP hydroxypolyimides and their corresponding membranes treated at different temperatures, and (c) PI-MPD pristine membrane and film treated at 450 °C

The appearance of new peaks at wavenumbers around 1559, 1479 and 1059 cm^{-1} (*e*, *f* and *g*), which are representative of the polybenzoxazole structure, verified that the thermal rearrangement began at 350 ºC in the case of the PI-DAP membrane. However, PI-DAR did not exhibit any perceivable changes in its FTIR spectrum due to the low degree of conversion at that temperature. By raising the treatment temperature to 400 ºC, PBO bands augmented for both HPIs, becoming more intense when the thermal treatment reached 450 ºC. The intensity of the imide peaks at 1786, 1720, 1365, and 1102 cm^{-1} and the OH band at 3400 cm^{-1}, considerably decreased for PI-DAR at 400 and 450 ºC, whereas they remained as expected for PI-DAP, with the exception of the strong and broad band from hydroxyl group that was entirely absent at that temperature. It should also be noted that the final TR structure of this polymer, PI-DAP, contains imide linkages owing to the presence of only one OH group in the *ortho* position in its polyimide precursor. In addition, it is worth mentioning that the absence of significant degradation or partial carbonization is supported by the well-defined absorption intensities and bandwidths for all of the TR-PBO dense membranes.

Wide-angle X-ray diffraction (WAXD) was used to determine average d-spacing values for precursor polyimides and thermally treated membranes in order to explore the effect of the rearrangement process on the polymer chain packing, which has a large effect on gas transport properties. As shown in **Figure 3.7**, the X-ray patterns of all polyimide precursors and their corresponding thermally treated films indicated that these polymers were in a completely amorphous state, as only the presence of an amorphous halo could be observed.
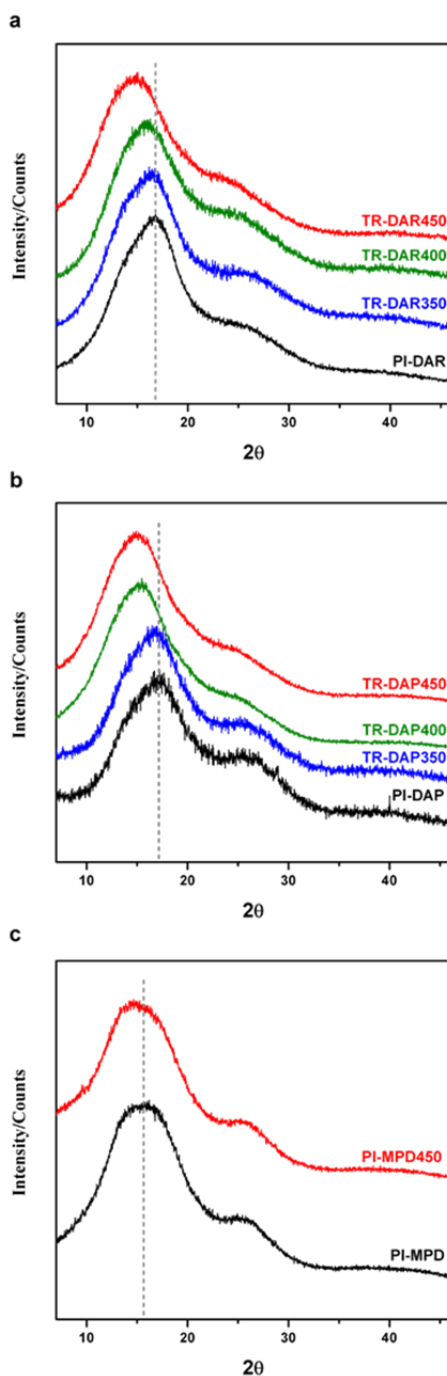
Figure 3.7. Wide angle X-ray diffraction (WAXD) patterns of (a) PI-DAR and (b) PI-DAP OH-polyimides along with the derived TR-PBO membranes at different temperatures. (c) PI-MPD polyimide and its membrane treated at 450 ºC

The most probable intersegmental distance (*d*-spacing) values, calculated according to Bragg's equation, are shown in **Table 3.2**. As observed previously for other TR polymers [10,12], thermal rearrangement to TR-PBO translated into larger *d*-spacing. The original polyimides, PI-DAR, PI-DAP and PI-MPD, exhibited preferential intersegmental distances with values of 5.27, 5.02 and 5.68 Å, respectively, whereas samples treated at 450 °C resulted in larger intersegmental distances (5.88, 5.88 and 5.87 Å, respectively). Accordingly, the higher treatment temperatures resulted in lower chain packing densities, which was in agreement with the higher percentage of PBO conversion. It is necessary to note that, although the membrane TR-DAR450 showed a lower conversion (72 %), it exhibited the same *d*-spacing value of 5.88 Å as its counterpart TR-DAP450. Presumably, applying a longer thermal treatment should result in a higher percentage of conversion and, consequently, higher *d*-spacing values. These results support the gain in fractional free volume (FFV), as *d*-spacing can be considered as an indication of the degree of *openness* of the polymer matrix for this family of TR membranes.

It is well known that FFV increases significantly during conversion from HPIs to TR-PBOs in conjunction with an important decrease in density, resulting in a direct enhancement of permeability [17,18]. Thus, FFV of precursors and thermally treated films were determined using Equation 3.2, where V_o is commonly referred to as the occupied volume of the polymer chain and V_e is the specific volume, which is the inverse of the polymer density. The occupied volume of a polymer is generally determined according to Bondi's group contribution theory [19] using Equation 3.3, where V_W, shown in **Table 3.2**, is the van der Waals volume. In our case, V_W was calculated applying Equation 3.4, which considers the degree of conversion of the polyimide precursor to the final TR-PBO structure:

$$FFV = \frac{V_e - V_o}{V_e} \qquad \text{(Eq. 3.2)}$$

$$V_0 = 1.3 \sum V_W \qquad \text{(Eq. 3.3)}$$

$$V_W = c\, V_{W,PBO} + (1 - c)V_{W,HPI} \qquad \text{(Eq. 3.4)}$$

where c is the fractional mass conversion determined as the quotient of the experimental mass loss measured by TGA and the theoretical mass loss to attain virtual 100 % conversion into PBO (Equation 3.1). $V_{W,PBO}$ and $V_{W,HPI}$ values refer to the Van der Waals volume of polybenzoxazole and polyimide structures, respectively.

The density of films was measured by the buoyancy method in a density balance. In this method, based on Archimedes' principle, the polymer sample is weighed in air and in isooctane, and the density of the polymer is assumed from the difference of the sample weight in both cases. The density of the polyimide film was higher for PI-DAR, which is consistent with its higher amount of hydroxyl groups and its capability of creating more hydrogen bonds, which led to denser packing. In this way, the PI-MPD membrane without any OH group showed the lowest density (1.464 g cm^{-3}), while the PI-DAP sample, which has only one OH group per repeating unit, exhibited a density value of 1.484 g cm^{-3} and the PI-DAR membrane had the highest density of 1.512 g cm^{-3}, owing to the presence of two hydroxyl groups per repeating unit (**Table 3.2**). The smaller density of a polymer usually corresponds to larger free volume elements, accordingly the found fractional free volumes followed the trend: FFV (PI-MPD) = 0.178 > FFV (PI-DAP) = 0.176 > FFV (PI-DAR) = 0.171.

As expected, density decreased as TR conversion was further increased. Thus, thermally treated membranes at 450 °C, excluding PI-MPD450, exhibited lower densities than their precursor polyimides, with a density of 1.411 g cm^{-3} for TR-DAP450 and 1.391 g cm^{-3} for TR-DAR450. PI-MPD450 did not undergo any noticeable change in density after thermal treatment due to its unfeasible conversion into PBO.

As thermal rearrangement proceeded, FFV increased in accordance with the decrease in density. Similar behavior was observed in the previous study of the monomer isomeric effect in TR polymers [12], where it was pointed out that the thermal rearrangement produces not only an increase in FFV, but modifies the polymer free volume distribution as well, usually leading to a more favorable cavity distribution [9,13]. The FFV of samples treated at 350 °C was close to that of the HPI precursors, consistently with the similar densities observed for those membranes. The TR-DAR450 sample exhibited the highest FFV (0.210), indicating an increase of 22.8 % compared to the PI-DAR membrane. In contrast,

a smaller increase in FFV (10.2 %) was observed for TR-DAP450, probably due to compaction of the polymer chains. As a consequence, the initially more packed and denser PI-DAR resulted in a more open TR-PBO structure with higher free volume, and it was so despite its lower degree of conversion as detected by CO_2 loss. Hence, the intermolecular distances observed by WAXD were consistent with densities and FFVs of TR-PBOs. These notable changes in the physical properties of TR-PBO membranes may result in an improvement in gas transport performance [20].

3.3.3. GAS SEPARATION PROPERTIES

The pure gas permeability values (*P*) of precursors and thermally treated membranes for five gases He, O_2, N_2, CH_4 and CO_2, as well as the ideal selectivity (α) for some interesting gas pairs are listed in **Table 3.3**. As previously reported, significant increases in free volume elements translate to improved gas permeation properties [6,9,10,13,18]. Consequently, the HPI precursors had relatively low permeability whereas TR-PBO membranes exhibited much higher permeability values. Specifically, as conversion increased, permeability augmented for both HPI series, which correlated with the tendency in FFV commented above.

In accordance with this observation and as expected from the measured values of *d*-spacing, density and FFV, the incremental changes in permeability were greater when thermal rearrangement was carried out at 450 °C, which provided a higher conversion percentage. On the other hand, when the thermal conversion was performed at 350 °C, the permeability values were barely increased due to the small degree of conversion that was achieved. The TR-DAR series of membranes showed higher permeability improvement with the thermal treatment compared with the TR-DAP series for all gases. This trend can be derived from **Table 3.3**, and this increase is particularly important for membranes treated at 450 °C. Even though the DAR series exhibited a lower relative degree of conversion, the CO_2 permeabilities for the DAR series were significantly greater than those observed for the DAP series irrespective of treatment temperature (approximately 2.5 times greater at 450 °C). As an example of this trend observed in all gases, **Figure 3.8** shows the increase in CO_2 permeability for the three series. The CO_2 permeability of the TR-DAR450

membrane was 354 Barrers, 43-fold higher than the precursor HPI, but it was only 142 Barrers for the TR-DAP450 membrane (13-fold increase with respect to the precursor HPIs). The outstanding improvement of permeability observed for TR-DAR450 was attributed primarily to the higher PBO proportion produced by the thermal treatment, due to the double amount of *ortho* hydroxyl groups available in the precursor structure. In fact, the percentage of CO_2 weight loss for TR-DAR450, determined from the isothermal curves of the **Figure 3.5**, which is referred in **Table 3.2**, was 11.6 % and the percentage of CO_2 weight loss for TR-DAP450 was 8.2 %.

Table 3.3. Gas Permeation Properties of Precursor Polyimides and Thermally Treated Membranes

Polymer code	Permeabilities (Barrers)[a]					Ideal Selectivities[b]	
	PHe	PN_2	PO_2	PCH_4	PCO_2	$\alpha_{O2/N2}$	$\alpha_{CO2/CH4}$
PI-MPD	46	0.29	2.1	0.10	7.6	7.3	76
PI-MPD450	46	0.32	2.3	0.12	9.2	7.3	76
HPI-DAP	62	0.43	2.9	0.11	11	6.8	100
TR-DAP350	78	0.60	4.2	0.17	16	7.0	93
TR-DAP400	157	3.7	18	1.7	78	4.9	46
TR-DAP450	221	7.1	34	3.8	142	4.8	38
HPI-DAR	43	0.29	2.1	0.08	8.2	7.3	102
TR-DAR350	90	0.89	5.1	0.19	18	5.7	93
TR-DAR400	123	4.0	22	1.5	92	5.4	61
TR-DAR450	341	16.4	77	8.9	354	4.7	40

[a] 1 Barrer = 10^{-10} cm^3 (STP) cm / (cm^2 s cm Hg), measured at 3 bar , 30 °C. [b] Ideal selectivities were obtained by the ratio of two gas permeabilities.
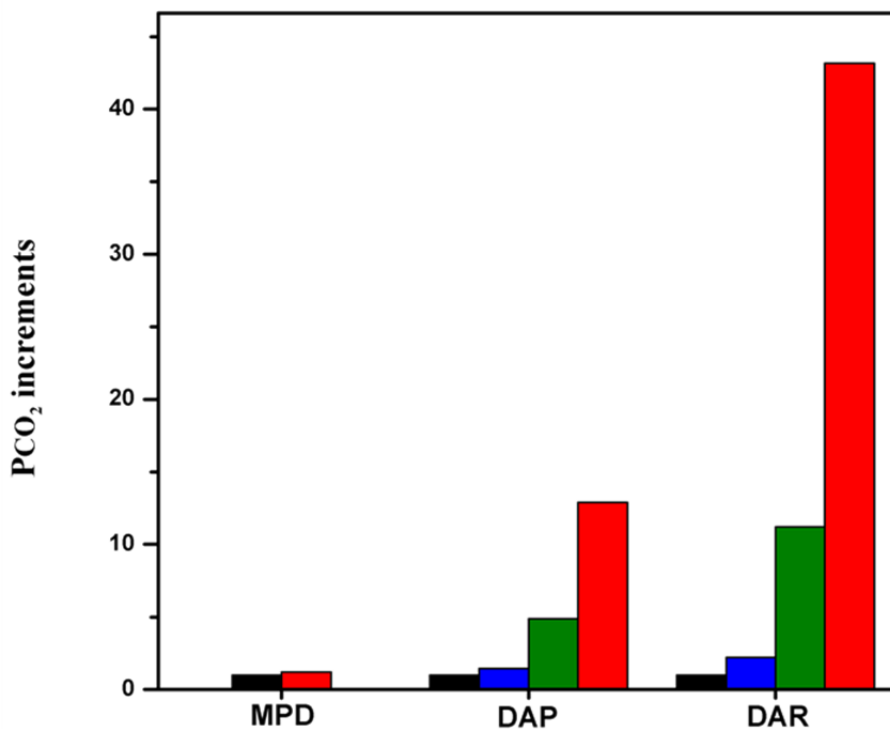
Figure 3.8. CO_2 permeability increase for all polymer membranes; ● Pristine membranes, ● Membranes treated at 350 ℃ for 1h, ● Membranes treated at 400 ℃ for 1h, and ● Membranes treated at 450 ℃ for 30 min. For comparison purposes, the permeability values in this figure for each series were normalized by dividing the permeability values by the lowest value of the series (precursor HPI), PCO_2increment = $P_i/P_{precursor\ HPI}$

Therefore, the percentage of converted PBO units for TR-DAR450 was 72 % of the theoretical value, whilst the percentage of converted PBO units for TR-DAP450 was 100 %. However, each repeat unit in the DAR series has two potential groups capable to form a PBO moiety, indicating a greater amount of thermal rearrangement conversion and consequently a higher increase in FFV and permeability.

Along with the increased FFV, an enlargement in cavity size occurs during thermal treatment, which produces a gradual detriment with respect to gas selectivity [9,13]. As it can be inferred from **Table 3.3**, a progressive selectivity decay was observed as treatment temperature increased, illustrating this general trend on ideal separation factors.

However, the loss in permselectivity was compensated by the huge gain in permeability. Thus, when the selectivity for a certain gas pair is plotted vs. the permeability of the gas having the highest gas flux, it can be clearly observed (**Figure 3.9** and **Figure 3.10**) that the experimental values are close to the empirical 2008 Robeson upper-bound [21,22], in such a way that the value of TR-DAR450 for the CO_2/CH_4 gas pair (**Figure 3.9**) surpasses the corresponding Robeson limit. In addition, and in contrast to common TR membranes, it was noted that some TR membranes developed in the current work showed notable O_2/N_2 separation because the decrease in selectivity was lower than that observed for other TR materials. Again, the TR-DAR450 membrane (**Figure 3.10**) showed the best separation properties due to its high O_2 permeability (77 Barrers) combined with an acceptable permselectivity of 4.7.
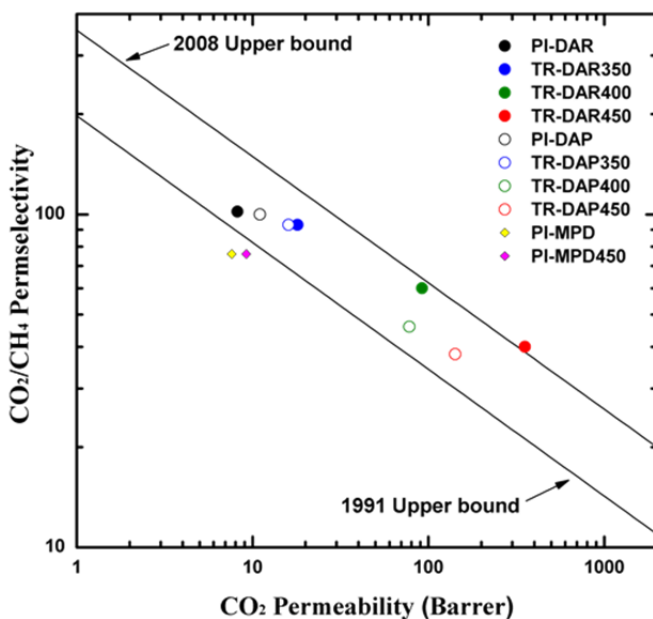
Figure 3.9. Relationship between CO_2 permeability and CO_2/CH_4 selectivity of all membranes tested in this study along with the Robeson upper bounds [21,22]
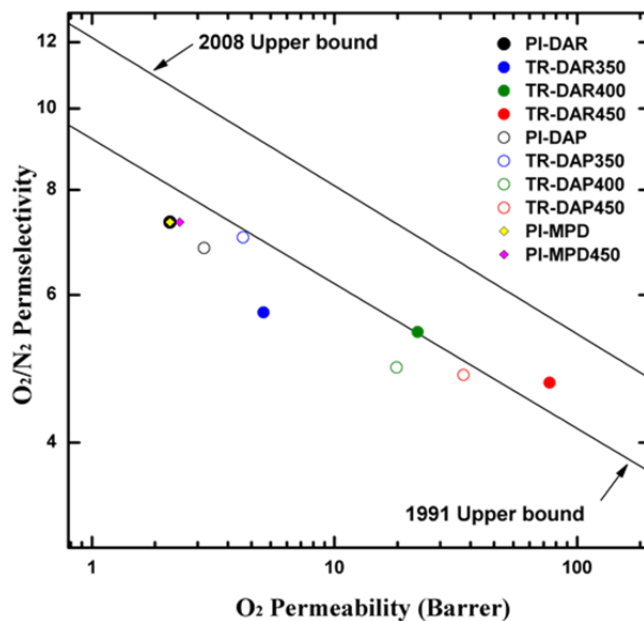
Figure 3.10. Relationship between O_2 permeability and O_2/N_2 selectivity of all membranes tested in this study along with Robeson upper bounds [21,22]

3.4. CONCLUSIONS

Two high molecular weight polyimides (HPIs) having *ortho*-hydroxyl groups to the nitrogen of the imide moiety were attained via the reaction of 2,2'-bis(3,4-dicarboxyphenyl) hexafluoropropane dianhydride (6FDA) and the hydrochloride salts of two inexpensive monomers, 2,4-diaminophenol (DAP) and 4,6-diaminoresorcinol (DAR), using an *in situ* silylation method. Both polyimides were processed in the form of films with good mechanical properties. It should be noted out that although TR materials TR-PBOs do not maintain the global mechanical resistance of the precursor HPIs, they still show the dimensional stability and flexibility to be properly handed for permeation measurements. The glass transition temperatures of these polymers were higher than 295 °C (value corresponding to the reference, non-hydroxylated polyimide), showing a direct dependence between T_g and the amount of OH groups in the polyimide structure. Thus, the polyimide having two hydroxyl groups per repeating unit had a T_g 25 °C larger than that observed for the PI-DAP polyimide.

The *ortho*-hydroxypolyimide films underwent thermal rearrangement in the solid state at temperatures above 350 °C, which led to polybenzoxazoles (TR-PBO). It was observed that the thermal conversion rate and the relative extension of the rearrangement process were much greater for the PI-DAP polyimide than for PI-DAR at all the temperatures tested. However, the total amount of benzoxazole groups formed was higher for PI-DAR due to the double amount of OH groups in its repeat unit.

The gas separation properties of the polymer films were evaluated at different treatment temperatures, where a sharp increment in permeability was detected when the thermal treatment was 400 °C or higher. For example, the enhancement in CO_2 permeability, compared with the polymer film treated at 350 °C, was 5-fold and 9-fold for the polymer TR-DAP at 400 and 450 °C, respectively, while for TR-DAR, the CO_2 permeability increase was 5-fold at 400 °C and 20-fold at 450 °C. Importantly, the balance permeability-selectivity was better than any of the other related TR-PBOs described in the literature, placing these polymers above the 2008 Robeson limit for some gas pairs. Therefore, it

can be concluded that the set of TR membranes derived from inexpensive monomers prepared and evaluated in this chapter, should be considered as excellent materials for gas separation.

3.5. REFERENCES

1. Kim, S. & Lee, Y. M. 'Rigid And Microporous Polymers For Gas Separation Membranes.' *Progress in Polymer Science* **43,** 1–32 (2015).

2. Guiver, M. D. & Lee, Y. M. 'Polymer Rigidity Improves Microporous Membranes.' *Science* **339,** 284–285 (2013).

3. Joseph, W. D., Abed, J. C., Mercier, R. & McGrath, J. E. 'Synthesis And Characterization Of Fluorinated Polybenzoxazoles Via Solution Cyclization Techniques.' *Polymer* **35,** 5046–5050 (1994).

4. Moy, T. M. & McGrath, J. E. 'Synthesis Of Hydroxyl-containing Polyimides Derived From 4,6-diamino-resorcinol Dihydrochloride And Aromatic Tetracarboxylic Dianhydrides.' *Journal of Polymer Science, Part A: Polymer Chemistry* **32,** 1903–1908 (1994).

5. Tanaka, Y., Oishi, Y., Kakimoto, M.-A. & Imai, Y. 'Synthesis And Properties Of Aromatic Polyamide- Diaminophenol And Aromatic Dicarboxylic Acid Chlorides.' *Journal of Polymer Science Part A: Polymer Chemistry* **29,** 1941–1947 (1991).

6. Jung, C. H., Lee, J. E., Han, S. H., Park, H. B. & Lee, Y. M. 'Highly Permeable And Selective Poly(benzoxazole-co-imide) Membranes For Gas Separation.' *Journal of Membrane Science* **350,** 301–309 (2010).

7. Lozano, A. E., de Abajo, J. & de la Campa, J. G. 'Synthesis Of Aromatic Polyisophthalamides By In Situ Silylation Of Aromatic Diamines.' *Macromolecules* **30,** 2507–2508 (1997).

8. Koros, W. J. & Fleming, G. K. 'Membrane-based Gas Separation.' *Journal of Membrane Science* **83,** 1–80 (1993).

9. Park, H. B. *et al.* 'Polymers With Cavities Tuned For Fast Selective Transport Of Small Molecules And Ions.' *Science* **318,** 254–258 (2007).

10. Park, H. B., Han, S. H., Jung, C. H., Lee, Y. M. & Hill, A. J. 'Thermally Rearranged (TR) Polymer Membranes For CO2 Separation.' *Journal of Membrane Science* **359,** 11–24 (2010).

11. Sanders, D. F. *et al.* 'Gas Permeability, Diffusivity, And Free Volume Of Thermally Rearranged Polymers Based On 3,3′-dihydroxy-4,4′-diamino-biphenyl (HAB) And 2,2′-bis-(3,4-dicarboxyphenyl) Hexafluoropropane Dianhydride (6FDA).' *Journal of Membrane Science* **409-410,** 232–241 (2012).

12. Comesaña-Gándara, B. *et al.* 'Thermally Rearranged Polybenzoxazoles Membranes With Biphenyl Moieties: Monomer Isomeric Effect.' *Journal of Membrane Science* **450,** 369–379 (2014).

13. Han, S. H. *et al.* 'Thermally Rearranged (TR) Polybenzoxazole: Effects Of Diverse Imidization Routes On Physical Properties And Gas Transport Behaviors.' *Macromolecules* **43,** 7657–7667 (2010).

14. Muñoz, D. M., Calle, M., de la Campa, J. G., de Abajo, J. & Lozano, A. E. 'An Improved Method For Preparing Very High Molecular Weight Polyimides.' *Macromolecules* **42,** 5892–5894 (2009).

15. Calle, M., Chan, Y., Jo, H. J. & Lee, Y. M. 'The Relationship Between The Chemical Structure And Thermal Conversion Temperatures Of Thermally Rearranged (TR) Polymers.' *Polymer* **53,** 2783–2791 (2012).

16. Calle, M. & Lee, Y. M. 'Thermally Rearranged (TR) Poly(ether−benzoxazole) Membranes For Gas Separation.' *Macromolecules* **44,** 1156–1165 (2011).

17. Jiang, Y. *et al.* 'Cavity Size, Sorption And Transport Characteristics Of Thermally Rearranged (TR) Polymers.' *Polymer* **52,** 2244–2254 (2011).

18. Han, S. H., Lee, J. E., Lee, K.-J., Park, H. B. & Lee, Y. M. 'Highly Gas Permeable And Microporous Polybenzimidazole Membrane By Thermal Rearrangement.' *Journal of Membrane Science* **357,** 143–151 (2010).

19. Bondi, A. 'Van Der Waals Volumes And Radii.' *The Journal of Physical Chemistry* **68,** 441–451 (1964).

20. Fukumaru, T., Fujigaya, T. & Nakashima, N. 'Extremely High Thermal Resistive Poly(p -phenylene Benzobisoxazole) With Desired Shape And Form From A Newly Synthesized Soluble Precursor.' *Macromolecules* **45,** 4247–4253 (2012).

21. Robeson, L. M. 'Correlation Of Separation Factor Versus Permeability For Polymeric Membranes.' *Journal of Membrane Science* **62,** 165–185 (1991).

22. Robeson, L. M. 'The Upper Bound Revisited.' *Journal of Membrane Science* **320,** 390–400 (2008).

Chapter IV

Thermally Rearranged Polybenzoxazol Membranes with Biphenyl Moieties:

Monomer Isomeric Effect

4.1. INTRODUCTION

Polyimides based on isomeric diamines have attracted increasing attention due to characteristic properties that are of special importance in the search for relationships between structure and properties in order to find out new materials with improved properties for specific applications. Previous studies [1-4] of a series of polyimides have shown that systematic variations of intrasegmental mobility and intersegmental chain packing can be used to achieve increases in permeability without decreases in permselectivity. Thus, the effect of changing the bond location on the diamine, i.e. from *para* to *meta* should affect the gas separation behavior of the material.

Monomers with amino groups oriented in *para* and *meta*-oriented hydroxyl groups have been preferably used as monomers for preparation of TR-PBO precursor hydroxypolyimides. In the present chapter, a nucleophilic compound, 3,3´-diamino-4,4´-dihydroxybiphenyl (*m*HAB), has been prepared as a novel condensation monomer that will be put to react with 2,2'-bis-(3,4-dicarboxyphenyl) hexafluoropropane dianhydride (6FDA) in order to obtain a precursor polymer (PI-*m*HAB) of TR gas separation membranes. This monomer, relatively easy to be made, is isomer of the commercial HAB monomer. Both diamines have been employed for the preparation of OH-polyimides by an optimized polycondensation with the dianhydride 6FDA, combining the *in situ* silylation of the aromatic diamines [5,6] with azeotropic cycloimidization, in order to obtain high molecular weight polymers with good film-forming properties. PI-HAB structure was chosen due to the relatively high reactivity of HAB compared to other commercially available diamines and also because this monomer is isomer of *m*HAB. The 6FDA dianhydride was selected due to its favourable performance in other polymeric gas separation membrane studies, including previous TR research [7-9] and also because this dianhydride increases polyimide solubility. The synthesized *ortho*-hydroxypolyimides were used as precursors of polybenzoxazoles (PBO) obtained after thermal treatment in solid state.

The aim of this chapter consisted of exploring the potential of this polymer (PI-*m*HAB) in gas separation applications, as well as to study the effect of the isomeric substitution of the functional groups in the diamine moiety of the precursor polymers (comparing PI-*m*HAB with the polymer made from 6FDA and 3,3'-dihydroxy-4,4'-diamino-biphenyl (HAB) (polyimide PI-HAB)) on the physical (T_g, thermal resistance, temperature of conversion into PBO, etc.) and on gas separation properties of polyimide precursors and their corresponding TR-PBO membranes.

4.2. EXPERIMENTAL SECTION

4.2.1. MATERIALS

This chapter focuses on two isomeric polyimides: PI-HAB (formed by the reaction of 3,3'-dihydroxy-4,4'-diamino-biphenyl (HAB, TCI Europe) and 2,2'-bis-(3,4-dicarboxyphenyl) hexafluoropropane dianhydride (6FDA, Cymit Química (Barcelona)) and PI-*m*HAB (formed by the reaction of 4,4'-dihydroxy-3,3'-diamino-biphenyl (*m*HAB, non-commercial) and 6FDA). The chemical structures of the *ortho*-hydroxypolyimides and their precursor monomers are shown in **Scheme 4.1**. The non-commercial isomeric diamine, *m*HAB, could be synthesized in good yield and high purity by a two-step synthesis, which involves the nitration of 4,4´-dihydroxybiphenyl (97%, Aldrich) followed by a reduction reaction. This synthetic process is very efficient and it permits to obtain *m*HAB as a relatively low-cost monomer.
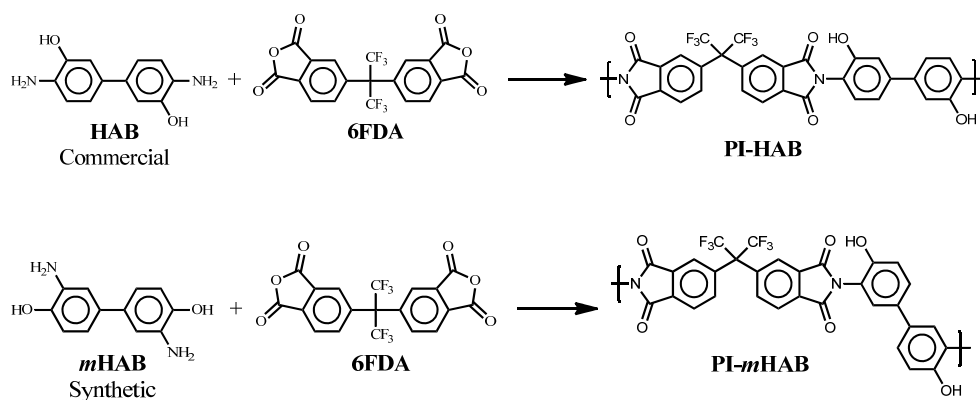
Scheme 4.1. Chemical structure of isomeric PI-HAB and PI-*m*HAB polyimides and their precursor monomers

117

4.2.2. MONOMER SYNTHESIS

4.2.2.1. Synthesis of 3,3´-dinitro-4,4´-dihydroxybiphenyl

Concentrated nitric acid (12.2 mL) was added dropwise over 1 h to a stirred solution of 4,4´-dihydroxybiphenyl (10.0 g, 0.0537 mol) in toluene (60 mL), and glacial acetic acid (40 mL) maintained at 0-5 ºC. After stirring for an additional 1 h, the mixture was allowed to warm up to room temperature. The dinitro compound was then separated as a solid by filtration, which was thoroughly washed with cold water, methanol and diethyl ether. The collected solid was finally recrystallized from toluene/DMF to give a yellow product. Yield: 95%. mp 284 ºC (DSC). *E.A.* for $C_{12}H_8N_2O_6$: C, 52.18; H, 2.92; N, 10.14%. *Found:* C, 52.95; H, 3.04; N, 10.68%. ^{1}H-NMR (DMSO-d_6, 300 MHz): 11.13 (s, 2H, OH), 8.14 (d, 2H, *J* = 2.4 Hz), 7.86 (dd, 2H, *J* = 8.6 Hz, *J* = 2.4 Hz), 7.20 (d, 2H, *J* = 8.6 Hz). ^{13}C-NMR (DMSO-d_6, 75 MHz): δ 151.38, 137.37, 132.80, 129.16, 122.49, 119.71.

4.2.2.2. Synthesis of 3,3´-diamino-4,4´-dihydroxybiphenyl (mHAB)

A three-necked flask was charged with 3,3´-dinitro-4,4´-dihydroxybiphenyl (3.000 g, 0.0138 mol), 100 ml of ethanol and 0.300 g of 10% palladium on carbon (Pd/C). Hydrazine monohydrate (12 mL) was added dropwise at 85 °C to the mixture over a period of 30 min. When the addition was complete, the solution was heated and maintained at reflux for 24 h. DMAc was then slowly added to the reaction suspension until the precipitate was completely dissolved. The final hot solution was filtered through Celite® to remove the Pd/C catalyst, and partially evaporated in a rotary evaporator before pouring into cold distilled water. The crude product precipitated as a white solid, which was filtered, washed carefully with water, dried and purified by sublimation at 270 ºC under reduced pressure. Yield: 92%. mp 329 ºC (DSC). *E.A.* for $C_{12}H_{12}N_2O_2$: C, 66.65; H, 5.59; N, 12.96%. *Found:* C, 66.73; H, 5.48; N, 13.11%. ^{1}H-NMR (DMSO-d_6, 300 MHz): 8.92 (s, 2H, OH), 6.75 (d, 2H, *J* = 2.2 Hz), 6.63 (d, 2H, *J* = 8.1 Hz), 6.53 (dd, 2H, *J* = 8.1 Hz, J = 2.2 Hz), 4.51 (s, 4H, NH₂). ^{13}C-NMR (DMSO-d_6, 75 MHz): δ 144.26, 134.92, 129.83, 116.81, 114.78, 111.89.

4.2.3. S*YNTHESIS OF* P*OLY(O-HYDROXYIMIDE)S* (HPI*S*)

A three-necked flask, equipped with a mechanical stirrer and gas inlet and outlet, was charged with 10.0 mmol of diamine (*p*HAB or *m*HAB), and 10.0 mL of NMP. The mixture was stirred at room temperature under nitrogen atmosphere until the solid was entirely dissolved. Then, the solution was cooled to 0 °C and the required amount of CTMS (1 mol/mol reactive group) was added, followed by pyridine (1 mol/mol reactive group) and a small amount of DMAP (0.1 mol/mol pyridine). The temperature was raised to room temperature, and the solution was stirred for 15 min to ensure the formation of the silylated diamine. After this time, the solution was cooled to 0 °C and 6FDA (10.0 mmol) was rapidly added followed by 10 mL of NMP. The reaction mixture was stirred for 15 min at 0 °C and then the temperature was raised up to room temperature and left overnight to form the poly(amic acid) solution. The viscosity of the solution greatly increased during this period. *o*-Xylene (20 mL) as an azeotropic agent was then added to the solution, which was stirred vigorously and heated for 6 h at 180 °C to promote imidization. During this step, the water side-product formed during the cycloimidization was separated as a xylene azeotrope, along with silanol and other siloxane by-products. Excess of *o*-xylene was distilled out from the polymer solution, which was subsequently cooled to room temperature and precipitated in distilled water. The polymer thus obtained was repeatedly washed with water and ethanol, and dried in an oven at 170 °C for 24 h under vacuum. **PI-HAB**: ^{1}H NMR (DMSO-d_6, 300 MHz): 10.09 (s, 2 H, OH), 8.21 (d, 2 H, *J*=8.0 Hz), 8.02 (d, 2H, *J*=8.0 Hz), 7.81 (s, 2 H), 7.40 (d, 2H, *J*=8.1 Hz), 7.21 (s, 2H), 7.21 (d, 2H, *J*=8.1 Hz). FT-IR (film): ν(-OH) at 3401 cm^{-1}, imide ν(C=O) at 1785 and 1715 cm^{-1}, imide ν(C-N) at 1378cm^{-1}, imide ν(C-N-C) at 1100 and 720 cm^{-1}. η$_{inh}$ (dL/g) = 1.51. **PI-*m*HAB**: ^{1}H NMR (DMSO-d_6, 300 MHz): 9.92 (s, 2 H, OH), 8.15 (d, 2 H, *J*=8.0 Hz), 7.96 (d, 2H, *J*=8.0 Hz), 7.74 (s, 2 H), 7.55 (d, 2H, *J*=8.1 Hz), 7.55 (s, 2H), 7.03 (d, 2H, *J*=8.1 Hz). FT-IR (film): ν(-OH) at 3415 cm^{-1}, imide ν(C=O) at 1784 and 1713 cm^{-1}, imide ν(C-N) at 1370 cm^{-1}, imide ν(C-N-C) at 1100 and 720 cm^{-1}. η$_{inh}$ (dL/g) = 0.54

4.2.4. POLYIMIDES FILM FORMATION AND THERMAL CONVERSION TO POLYBENZOXAZOLES

The casting of the polyimides was done from a 10% (w/v) filtered solution in NMP onto a clean glass plate. Cast film was placed in a vacuum oven and heated slowly to 250 °C, with holds for 1 h at 100, 150 and 200 °C under vacuum to evaporate most of the solvent. The solid film was taken off from the glass plate, rinsed with deionized water, and dried at 120 °C overnight. The defect-free and clean membrane was cut into 3 cm x 3 cm size strips and sandwiched between ceramic plates to prevent film deformation at elevated temperature in a tubular furnace under an inert gas. Each sample was heated to 300 °C at a heating rate of 5 °C/min, upheld for 2 or 3 h for complete solvent removal, and heated further to the target temperature (350, 400, 425 or 450 °C) at a rate of 5 °C/min, and maintained for the desired amount of time (30 min or 1 h) in a high-purity argon atmosphere. After thermal treatment, the furnace was cooled to room temperature at a rate no greater than 10 °C/min. This protocol was used to expose the samples to thermal histories similar to those reported in previous studies of TR polymers [8-11]. The thermally rearranged membranes, obtained from PI-HAB and PI-*m*HAB, were designated as TR-HABX and TR-*m*HABX, respectively, where X indicates the final rearrangement temperature applied. Both series of thermally treated membranes can be observed in **Figure 4.1**.
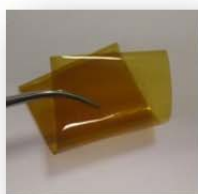
PI-HAB

PI-*m*HAB
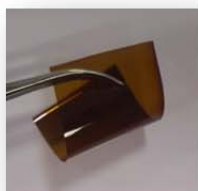
TR-HAB350
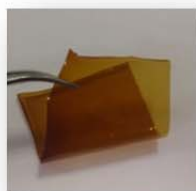
TR-*m*HAB350
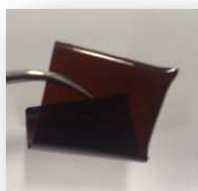
TR-HAB400
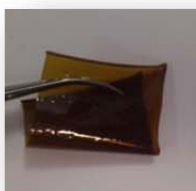
TR-*m*HAB400

TR-HAB425

TR-*m*HAB425

TR-HAB450

TR-*m*HAB450

Figure 4.1. *PI-HAB* and *PI-mHAB* polyimide precursors and their corresponding thermally treated membranes

121

4.3. RESULTS AND DISCUSSION

4.3.1. MONOMER SYNTHESIS

The non-commercially available *meta* diamine monomer 3,3′-diamino-4,4′-dihydroxybiphenyl (*m*HAB), was synthesized using an efficient two-steps method, by direct nitration of 4,4′-dihydroxybiphenyl with nitric acid in glacial acetic acid, followed by reduction with hydrazine monohydrate and 10% Pd/C as catalyst, what rendered, by an additional sublimation at high vacuum, a high purity monomer with good yield. Elemental analysis and ^{1}H-NMR and ^{13}C-NMR spectroscopic techniques were used to elucidate the structures of the intermediate dinitro compound and the final dihydroxy diamine, which were in good agreement with previous literature data [12].

4.3.2. SYNTHESIS AND CHARACTERIZATION OF ISOMERIC ORTHO-HYDROXYPOLYIMIDES (HPIS) PI-HAB AND PI-mHAB

Two isomeric *o*-hydroxypolyimides having a biphenyl moiety were synthesized from 2,2′-bis(3,4-dicarboxyphenyl)hexafluoropropane dianhydride (6FDA) and *o*-hydroxy diamine isomers; 3,3'-dihydroxy-4,4'-diamino-biphenyl (HAB) and 3,3′-diamino-4,4′-dihydroxybiphenyl (*m*HAB), by a two-step polyimidization method (**Scheme 4.1**). The formation of the high molecular weight poly(amic acid)s was carried out through an *in situ* silylation base-assisted method [5,6], involving the use of chlorotrimethyl silane (CTMS) as the silylating reagent, and a mixture of pyridine (Py) and *N,N*-dimethylaminopyridine (DMAP) as activating agents. In a second stage, *o*-xylene, used as an azeotropic agent to produce the cycloimidization of the polyamic acid to polyimide, was added to the solution of polyamic acid, which was stirred and heated for 6 h at 180 °C. During this step, water released by the ring-closure was separated as a xylene azeotrope, along with other by-products. The PI-HAB and PI-*m*HAB polyimides showed values of inherent viscosity of 1.51 and 0.54 dL/g, respectively. These values of inherent viscosity along with the good mechanical properties showed by the polymer films indicated that these polymers had high enough molecular weight to be employed in gas

separation membranes at high pressures.

In order to figure out the reactivity and kinetic of the monomers, the energy of the highest occupied molecular orbital (E_{HOMO}), which is an indicative of the reactivity of nucleophiles, was determined for both monomers by using the semi-empirical quantum-mechanical AM1 method [13]. The found E_{HOMO} was 8.13 eV and 8.21 eV for HAB and *m*HAB, respectively. Thus, the reactivity of these monomers is high enough comparable to other nucleophilic monomers and by far larger than the APAF diamine, and the E_{HOMO} differences cannot justify the different inherent viscosity values experimentally found. It is plausible, therefore, to consider that the inherent viscosity value differences observed for these polymers could denote not so large differences in molecular weight. This is because conformation of the macromolecular chains and polymer-solvent interaction could be quite diverse and in this way the exponents in the Mark-Houwink-Sakurada equation for these two macromolecules could be different.

The solubility of these two polymers was studied in different solvents. Both polyimides were soluble in polar aprotic solvents such as DMF, DMAc or DMSO, and even in common organic solvents as THF and acetone. However, they showed insolubility in methanol, ethanol, isopropanol or ethylenglycol in contrast to what was previously observed for related hydroxyl containing polyimides from 6FDA dianhydride and 2,2-bis(3-amino-4-hydroxyphenyl)hexafluoropropane (APAF) diamine, which included another solubilizing hexafluoroisopropylidene linkage (-CF$_3$)$_2$ in the diamine monomer [11]. On the other hand, polyimides derived from *para*-diamines usually present strong interactions between the chains, promoting a better chain packing, which leads to lower solubility than those exhibited for other polymers having isomeric *meta*-diamine moieties [4]. Nonetheless, *PI*-HAB and PI-*m*HAB isomers showed similar solubility characteristics in all solvent tested.

Chemical structure for these polymers was confirmed by ^{1}H-NMR and FT-IR. FT-IR spectra showed characteristic absorption bands of polyimides (**Figure 4.2**): the stretching vibration bands of C=O (1785 and 1715 cm^{-1}), the asymmetric stretching of C-N (1370 cm^{-1}), the streching of C-N-C groups at 1100 cm^{-1} and out-of-plane bending of C-N-C groups at 720 cm^{-1}. In addition, the C-F stretching of hexafluoroisopropylidene moiety was denoted by absorption peaks at around 1250-1100 cm^{-1}, whereas the broad band in the region of 3600-3200 cm^{-1} was attributed to the O-H vibration of the hydroxyl groups. Only minor differences in the stretching and bending modes in aromatic regions, 1600-1550 cm^{-1} and 900-700 cm^{-1} respectively, were observed between PI-HAB and PI-*m*HAB polyimides.
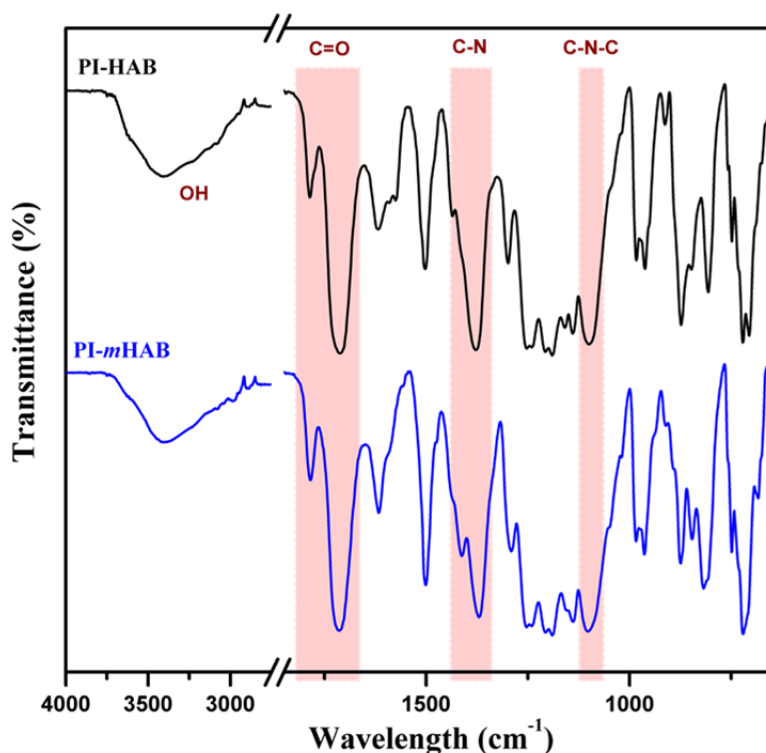
Figure 4.2. ATR-FTIR spectra of PI-HAB and PI-*m*HAB precursor polyimides

Indeed, the influence of *meta-* or *para-* substitution on the polyimide chemical structure was more evident by ^{1}H-NMR spectroscopy. Different ^{1}H-NMR spectral assignments for both polymers in terms of the *meta-* or *para-* connected diamine moieties could be established (**Figure 4.3**). The comparison of both spectra unambiguously reveals the position of the aromatic protons for the isomeric biphenyl moieties. Thus, in PI-HAB the resonance of the *ortho-* proton to the phenol group H_b is shifted downfield at 7.21 ppm, as compared to 7.03 ppm for PI-*m*HAB counterpart. In addition, the protons *meta-* to the hydroxyl group (H_c and H_d) in PI-*m*HAB have a chemical shift of 7.55 ppm in contrast to 7.40 ppm for the *meta-* proton H_d in PI-HAB. This characteristic electronic effect is actually due to the slight electron-withdrawing nature of the phenyl ring, as it was already observed in the synthesis of analogous non-hydroxylated 3,3′-diaminobiphenyl polyimide [14].
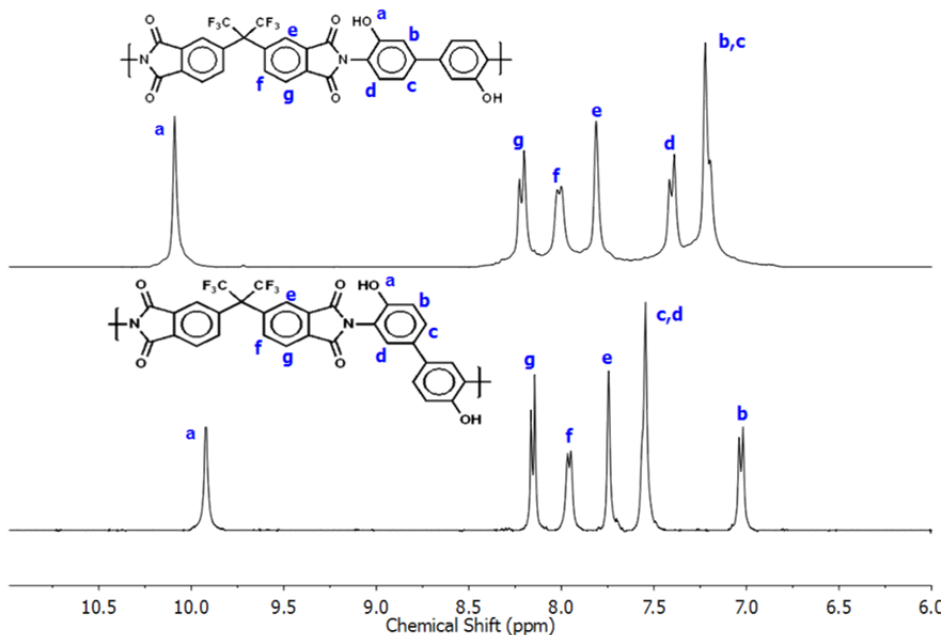
Figure 4.3. ^{1}H-NMR spectra of PI-HAB and PI-*m*HAB precursor polyimides (DMSO-*d₆*, 300 MHz)

Glass transition temperatures (T_g) were determined by DSC and also by DMA. DSC showed that the polymer made from HAB had a glass transition temperature of 356 °C, whereas PI-*m*HAB showed a lower T_g of 330 °C. These results are in agreement with those data observed for isomeric diamines [14]. However, it was seen in our work that the values of T_g were dependent on final temperature employed in the first DSC scan, because T_g and thermal rearrangement temperatures are very close and they overlapped. Therefore, the progressive conversion to PBO, which starts at temperatures immediately right above T_g, produced a more rigid structure with higher T_g.

DMA results of these polymers were quite different. Thus, the T_gs obtained by this technique (**Figure 4.4**) gave a value of 410 °C for PI-HAB and of 370 °C for PI-*m*HAB. These values are much higher than those obtained by DSC, and here again a notable T_g difference between isomeric HPIs was observed (ΔT_g of 40 °C by DMA, and ΔT_g of 26 °C by DSC).
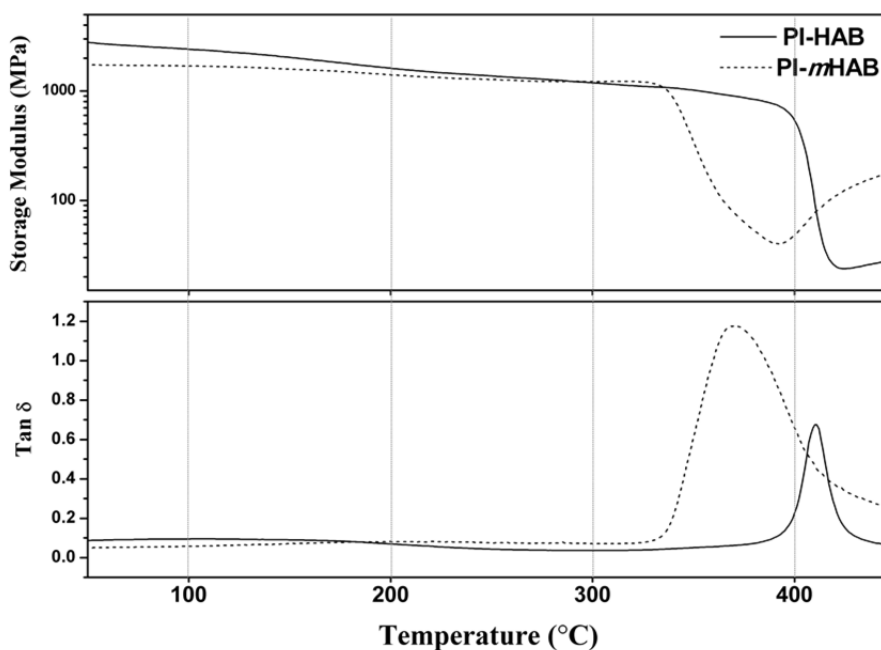
Figure 4.4. Dynamic mechanical results (storage modulus and tan δ vs. temperature) for PI-HAB and PI-*m*HAB precursor polyimides

4.3.3. THERMAL REARRANGEMENT OF HPIS TO POLYBENZOXAZOLES (TR-PBOS)

The intramolecular thermal rearrangement process for PI-HAB and PI-*m*HAB polyimides to their polybenzoxazole analogs was monitored by dynamic mechanical analysis (DMA) [15] and thermogravimetric analysis coupled with mass spectroscopy (TGA-MS).

Scheme 4.2 illustrates the corresponding change in both composition and functional group location for these isomeric HPIs after thermal conversion.

Solvent-cast films of PI-HAB and PI-*m*HAB were prepared from NMP by heating slowly to 250 °C with final ramp to 300 °C maintaining at this temperature for 2 or 3 h of treatment (until complete removal of the solvent). **Figure 4.4** shows dynamic mechanical scans for both isomers, performed at temperatures ranging from 30 to 450 °C at a heating rate of 3 °C min^{-1}. As it can be observed, the isomeric structure of biphenyl HPI precursors has a significant influence on overall chain mobility characteristics. For both polyimides, two relaxation processes were observed with increasing temperature, designated as β and α, respectively. The β-relaxation process, detected at temperatures below 300 °C for both polymers, may be associated to localized sub-glass motions of limited range. Nonetheless, it should be noted that an exhaustive study of these sub T_g relaxations fell beyond the scope of this study.

The strong drop in storage modulus (E´) corresponds to the glass-rubber transition process. The PI-*m*HAB polymer displayed a glass transition peak temperature based on tan δ of 370 °C/ (1Hz), whereas for PI-HAB the tan δ peak was shifted upward to 410 °C/ (1Hz). Generally, it is usual finding significant differences of T_g for polyimides based on isomeric diamines with a given dianhydride. So, the *para*- connected isomer generally shows higher T_g values; 3,3´- or *meta*- oriented diamines provide more conformational freedom to the macromolecular chains than *para*-connected diamines, resulting in less ordered and less packed structures with lower T_g [3,4]. As an example, by changing the diamine moiety from a *para* to a *meta* connection in polyimides derived from 6FDA dianhydride and non-hydroxylated biphenyl diamine analogs, a decrease in the T_g from 359 to 282 °C (as measured by DSC) has been observed [14,16].
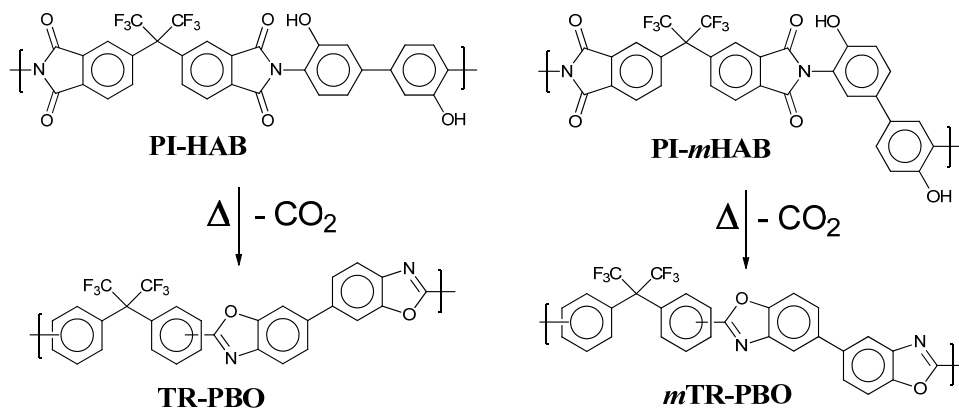
Scheme 4.2. Chemical structure of isomeric PI-HAB and PI-*m*HAB precursor polyimides and their corresponding polybenzoxazoles after thermal rearrangement

Besides, a recovery in modulus above T_g was noticed for both *ortho*-hydroxypolyimide isomers. These recoveries ranged from temperatures around 390 °C for PI-*m*HAB to 425 °C for the PI-HAB. This recovery has been observed for some polyimides having benzoxazoles moieties in the macromolecular chain, and it was ascribed to the use of high temperatures that produces an intensification of interchain interactions such as charge transfer complexes (CTC) along with the formation of ordered structures [17]. Other authors, studying the synthesis of polyimides via chemical and thermal imidization from HAB and their conversion to PBO, found a much lower decrease of the modulus value than that observed for our HPI structures synthesized by azeotropic imidization [15,18]. The authors assumed that the increase of molecular rigidity going from HPI to PBO is the main cause of the low storage modulus decrease. Therefore, it could be thought that the formation of rigid PBO structure along with the plausible formation of crosslinking points can justify the observed storage modulus recovery for the structures studied in this chapter.

It has been widely reported that thermogravimetric analysis is a suitable technique to make clear the thermal rearrangement characteristics of *ortho*-hydroxypolyimides as TGA traces of *ortho*-hydroxypolyimides show two well defined weight loss steps. In the first weight loss, in the range of 300-500 °C, the polybenzoxazole structure is formed (by thermal rearrangement) with releasing of CO_2. The second one is associated to the generalized decomposition of the *in-situ* formed polybenzoxazole backbone at around 500-600 °C [11,19,20]. **Figure 4.5** shows TGA and DTG curves as well as mass spectroscopic analysis of CO_2 (TGA-MS) for PI-HAB and PI-*m*HAB precursor polyimides, at a heating rate of 5 °C/min under N_2 atmosphere. As it can be seen, the initial mass loss ascribed to the thermal rearrangement process took place in a slightly lower temperature range for PI-*m*HAB isomer, where the temperature at the maximum of CO_2 release or maximum conversion rate (T_{TR}) showed a value of T_{TR}(PI-*m*HAB)= 414 °C, while T_{TR}(PI-HAB)= 427 °C (see **Table 4.1**).
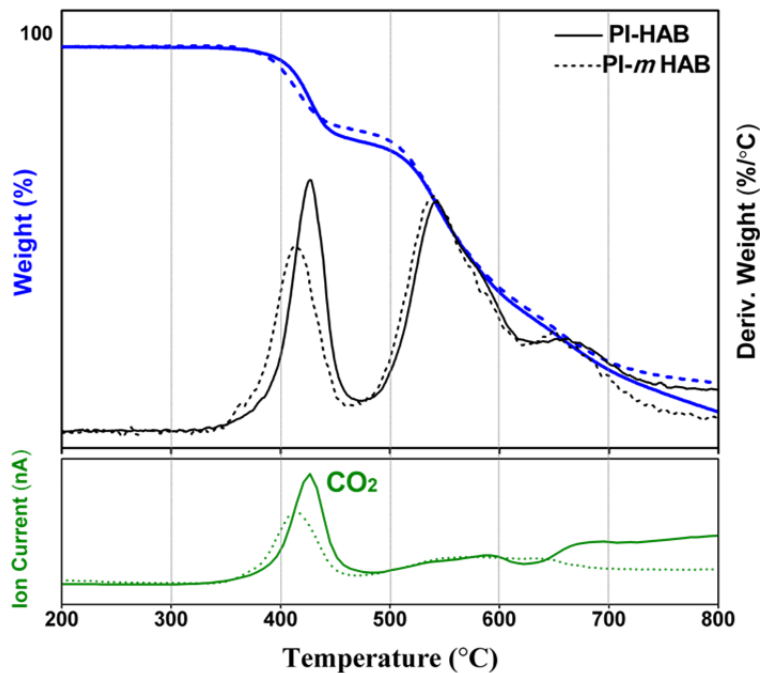
Figure 4.5. Thermogravimetric analysis combined with mass spectroscopy (TGA-MS) of PI-HAB and PI-*m*HAB precursor polyimide membranes (heating rate of 5 °C/min under N_2 atmosphere)

Table 4.1. Thermal Properties of Precursor Polyimide Membranes

Polymer code	T_g $(^oC)^a$	T_{TR} $(^oC)^{b,d}$	CO_2 theoretical wt. loss (%)^c	CO_2 found wt. loss (%)^{c,d}	T_d $(^oC)^d$
PI-HAB	356	427	14.09	12.6	540
PI-*m*HAB	330	414	14.09	11.0	540

^{a} Middle point of the endothermic step during the second scan of DSC measurements conducted at a heating rate of 20 ^oC/min under a nitrogen atmosphere. ^{b} Temperature at the maximum point of weight loss or maximum rate of conversion to PBO. ^{c} In %. ^{d} Determined by TGA at a heating rate of 5 ^oC/min under nitrogen atmosphere.

Interestingly, significant differences between these two biphenyl polyimides were observed in the rearrangement rate as a function of temperature. Thus, according to the differential TGA curves (DTG), the *meta*-connected isomer displayed rather higher cyclization rates at temperatures below or about 400 ^oC relative to its *para*- counterpart. However, at temperatures above 400 ^oC PI-HAB exhibited conversion values higher than PI-*m*HAB, which means that PI-HAB rearrangement takes place in a smaller temperature range. This seems to indicate that the lower mobility of the *para*-isomer makes difficult the start of the rearrangement, but after this starting it proceeds at a higher rate. In this way, as a reference, maximum conversion or PBO rearrangement rate (r_{TR}) for PI-HAB membrane, analyzed from the differential TGA curve, was r_{TR}= 0.30 %/^oC, whereas a lower value of r_{TR}= 0.22 %/^oC was found for the isomeric PI-*m*HAB polymer. Furthermore, PI-HAB isomer exhibited the highest CO_2 weight loss (~12.6 %) when compared to PI-*m*HAB (~11.0 %), although in both cases these values are below the theoretical value of full conversion to the final PBO structure (14.09 %). Additionally, the *in-situ* formed polybenzoxazoles degraded at nearly the same temperature for both precursors (Td~540 ^oC). Therefore, rearrangement temperature to PBO for this pair of rigid biphenyl HPI isomers is clearly affected by the 3,3´- or 4,4´- orientation of the diamine unit, and it is also proved that chain rigidity of HPI directly governs the thermal conversion temperature to PBO that consequently shows a high dependence with T_g [20]. In addition, the effect of functional group location was also evidenced on the amount of cyclization reaction and the conversion rate to PBO.

Supplementary isothermal TGA analyses were performed in order to optimize the thermal treatment conditions for TR sample preparation in the tubular furnace. Thus, HPI films thermally treated at 300 °C were further heated to the desired temperature (350, 400, 425 and 450 °C) at a heating rate of 5 °C/min, and held isothermally at that temperature for 3 h. **Figure 4.6** exhibits the isothermal thermograms for both isomers, showing weight loss as a function of time when the desired rearrangement temperature was reached. The theoretical CO_2 weight loss to complete conversion of both precursors to the final PBO structure (14.09 %) is sketched in the figures as a dashed line.

As can be seen, the amount of weight loss increases as a function of rearrangement temperature and time for both polymers. At 350 °C the value of weight loss was very low for any time, whereas it notably increased at 450 °C, exceeding the rearrangement theoretical weight loss value for long treatment times. Indeed, at high temperatures and prolonged heating times, thermal degradation is prone to occur as well, alongside thermal rearrangement, as recently suggested for other related TR polymers based on *ortho*-acetylated PI-HAB precursor polyimide [21]. On the other hand, higher levels of weight loss were observed for PI-HAB membranes, except at the low treatment temperature of 350 °C and at the high one, where both series experienced the same weight loss. At the low temperature the *meta*- isomer displayed slightly higher values of weight loss than the *para*- isomer, probably because the rearrangement is restricted by the high T_g of PI-HAB. Based on this TGA study, thermal treatment protocols were established for TR membrane preparation to ensure that samples experienced minimal thermal degradation, but also to have thermal histories similar to those reported in previous studies [11,21].
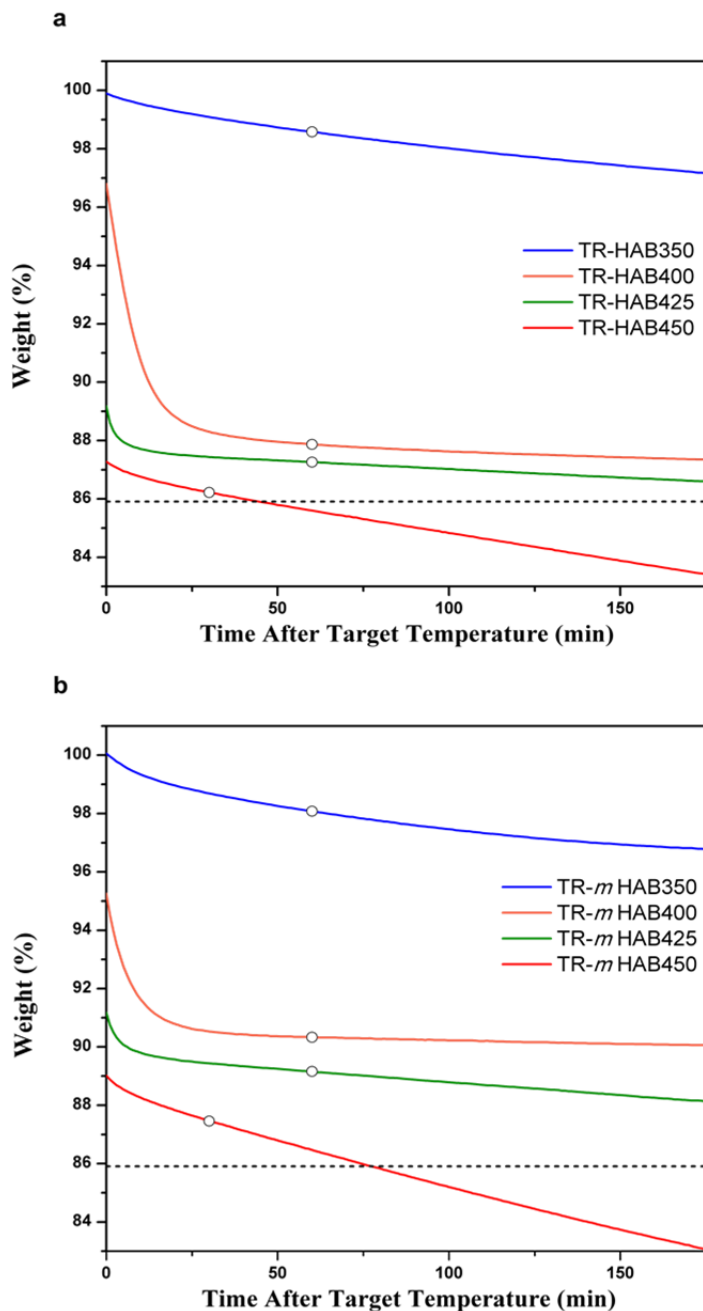
Figure 4.6. Isothermal thermogravimetric analysis of (a) PI-HAB and (b) PI-*m*HAB precursor polyimide membranes, under N_2 atmosphere, showing the weight loss as a function of time at a certain treatment temperature. Empty circles represent the conditions used for the membranes employed in gas transport characterization. The dashed line corresponds to the theoretical full conversion

The empty circles in **Figure 4.6** represent the times chosen for thermal treatment of the membranes at the desired rearrangement temperature, that is 350 (1 h), 400 (1 h), 425 (1 h) and 450 °C (30 min). The percent conversion of the polyimide precursors to the final TR-PBO membranes was estimated based on TGA data using Equation 4.1:

$$\% \: Conversion = \frac{Experimental \: Mass \: Loss}{Theoretical \: Mass \: Loss} \times 100 \qquad (Eq. \: 4.1)$$

Conversion values for PI-HAB and PI-*m*HAB polyimides, after the treatment commented in previous paragraph, are collected in **Table 4.2**. As mentioned above, the thermal cyclization reaction to PBO was very sensitive to the applied temperature. At 350 °C, very low conversion degrees were attained for both isomers (around 11-16%), whereas the percent conversion significantly increased at 400 °C, reaching the highest values of conversion at 450 °C. These results are consistent with previous TR studies, which showed a sudden acceleration in the thermal rearrangement kinetics to PBO by increasing temperature [10,21]. On the other hand, PBO conversions were generally higher for the *para*- connected isomer, with values ranging from 86 % to 96 %, as compared to the *m*eta- counterpart that displayed percentages of conversion between 70 % and 88 %.

Table 4.2. Physical Properties of Precursor Polyimide and TR-PBO derived Membranes

Polymer code	Conv. [a] (%)	Density (g cm^{-3})	Vw (cm^{3}g^{-1})	FFV	Increment in FFV (%)	d-spacing (Å)
PI-HAB	0	1.458	0.443	0.160	−	5.6
TR-HAB350	11	1.453	0.444	0.159	~ 0	5.7
TR-HAB400	86	1.373	0.461	0.176	10	6.0
TR-HAB425	90	1.361	0.462	0.182	14	6.0
TR-HAB450	96	1.337	0.464	0.194	21	6.1
PI-*m*HAB	0	1.438	0.444	0.170	−	5.6
TR-*m*HAB350	16	1.431	0.446	0.170	~ 0	5.9
TR-*m*HAB400	70	1.364	0.458	0.188	11	6.1
TR-*m*HAB425	77	1.351	0.459	0.193	14	6.1
TR-*m*HAB450	88	1.329	0.462	0.202	19	6.3

[a] PBO conversion after 60 min at 350, 400 and 425 ˚C and 30 min at 450 ˚C

4.3.4. CHARACTERIZATION OF THERMALLY REARRANGED POLYBENZOXAZOLE (TR-PBO) MEMBRANES

The chemical or structural changes occurring in the precursor polyimides after thermal treatment in the tubular furnace were monitored using ATR-FTIR analysis. **Figure 4.7** shows the ATR-FTIR spectral results for all the thermally treated samples as well as for the HPI precursors. As can be seen, PI-HAB sample thermally treated at 350 °C did not show any noticeable change in the FTIR spectrum. Nevertheless, the emergence of new peaks at wave numbers around 1557 and 1470 cm^{-1}, which are characteristics of the PBO structure [22], was evidenced for the PI-*m*HAB isomer at this temperature. This fact correlates well with the incipient conversion observed by TGA for this sample at 350 °C. When the rearrangement temperature increased up to 400 °C, PBO bands were very intense for both isomers, including the distinctive aromatic -O-C stretching of the benzoxazole ring at 1058 cm^{-1}, which was not observed before.
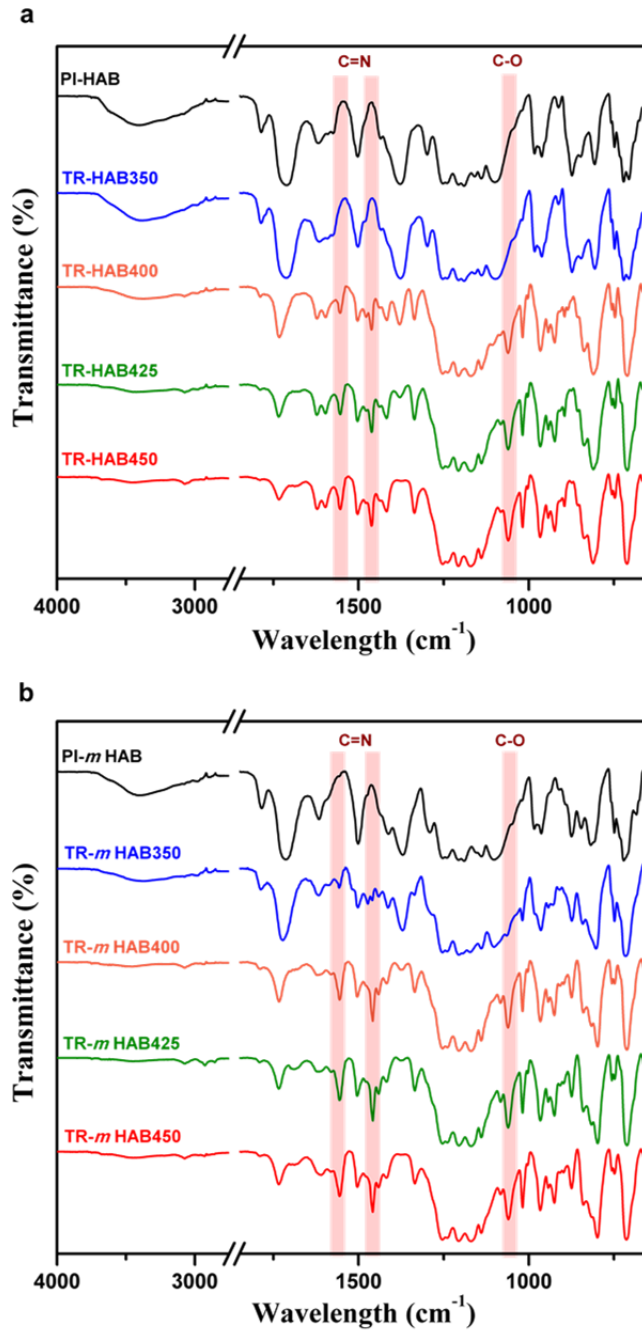
Figure 4.7. ATR-FTIR spectra of (a) PI-HAB and (b) PI-*m*HAB precursor polyimides and TR-PBO analog membranes, treated at different temperatures and heating times

Furthermore, the imide peaks at 1785, 1715, 1370, and 1102 cm^{-1} substantially decreased, whereas the strong and broad absorption band from hydroxyl group around 3400 cm^{-1} totally disappeared. Further heat treatment at 425 and 450 °C led to further decrease in the imide peaks intensity, which correlates with the higher ratio of PBO structure found for those TR samples. It is worth mentioning the well-defined absorption intensities and band wideness for all of these TR-PBO membranes, irrespective of the thermal protocol, supporting the absence of significant degradation for all these thermally treated membranes.

The effect of the thermal treatment (TR process) on the polymer chain packing, which has a substantial influence on the gas transport properties, was analyzed by wide-angle X-ray diffraction (WAXD). In **Figure 4.8**, the X-ray patterns, measured at room temperature, of thermally treated and polyimide precursor films are compared. All samples showed a broad amorphous halo, proving the amorphous nature for all of these membranes. Also, *d*-spacing values were calculated according to Bragg's equation, and data are collected in **Table 4.2**. The original polyimides exhibited similar preferential intersegmental distances, with values around 0.56 nm. As it has been observed before for other TR polymers, thermal rearrangement to PBO turned out in larger d-spacing. Thus, thermal treatment at 350 °C led to minor increments in d-spacing, 0.57 and 0.59 nm for TR-HAB350 and TR-*m*HAB350 respectively, whereas samples treated above this temperature (400-450 °C) presented slightly larger intersegmental distances (0.61-0.63 nm).
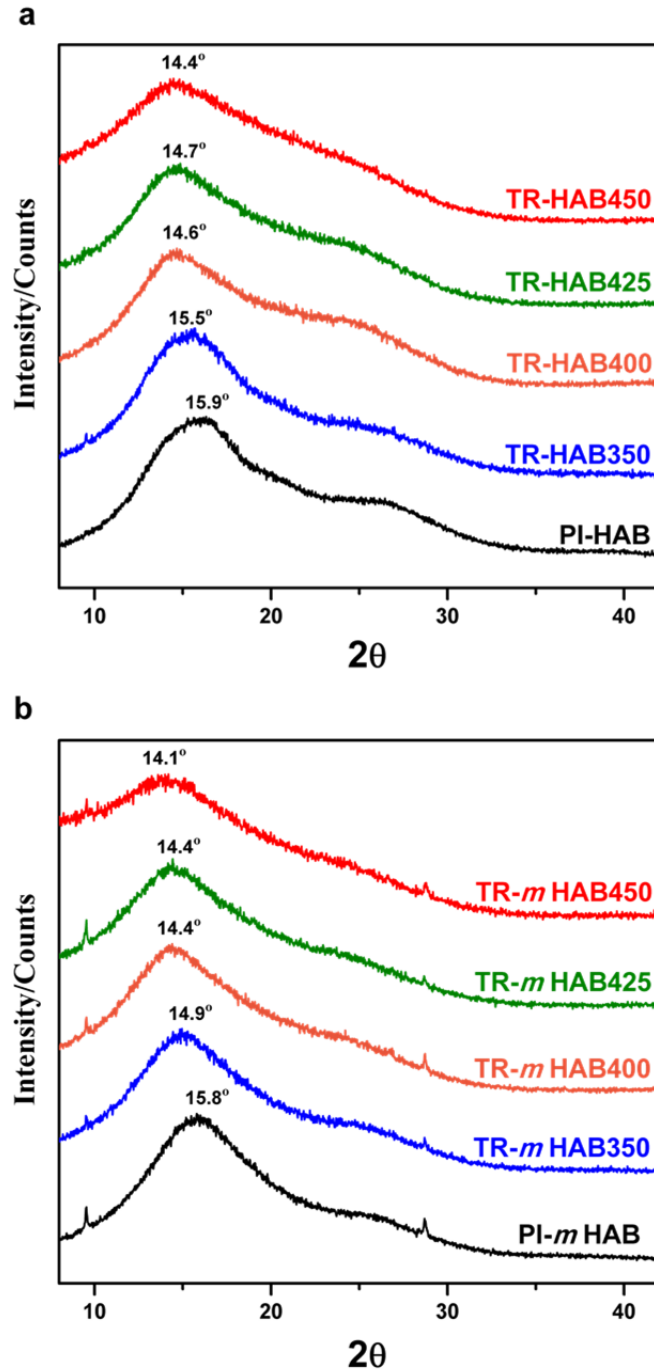
Figure 4.8. Wide angle X-ray diffraction (WAXD) patterns of (a) PI-HAB and (b) PI-*m*HAB precursor polyimides along with the TR-PBO derived membranes, treated at different temperatures and heating times

To better evaluate the effect of packing in the x-ray diffraction, the shape of the curve and not only the maximum should be considered. In this way, as seen in **Figure 4.8**, there is a shoulder at around $2\theta = 27°$ that also shifts to lower values with the rearrangement. Moreover, the contribution to the halo of the angles below the maximum (higher distances) also increases with the thermal treatment. Therefore these two contributions, together with the observed maximum shift, should account for the density decrease and the corresponding fractional free volume increase that will be commented below.

Along with *d*-spacing, fractional free volume (FFV) was also considered as an index of the degree of *openness* of the polymer matrix for this new family of TR membranes. In this way, FFV of TR-PBO and precursor membranes was estimated using Equation 4.2, where V_o is the so-called occupied volume of the polymer chains, and V_e is the specific volume, which is the inverse of the density of the polymer. The occupied volume of a polymer is normally estimated as $V_o = 1.3 \ V_W$, where V_W is the van der Waals volume, determined by molecular modeling or by using Bondi's group contribution theory [23]. In this particular case, V_W was calculated according to Equation 4.3 which takes into account the degree of conversion of the precursor polyimide to the final PBO structure:

$$FFV = \frac{V_e - V_o}{V_e} \qquad \text{(Eq. 4.2)}$$

$$V_W = c \ V_{W,PBO} + (1 - c)V_{W,HPI} \qquad \text{(Eq. 4.3)}$$

where *c* is the fractional mass conversion, calculated as the experimental mass loss measured by TGA analysis divided by the theoretical mass loss to reach virtual 100% conversion to PBO (Equation 4.1). $V_{W,PBO}$ and $V_{W,HPI}$ refer to the Van der Waals volume of polybenzoxazole and hydroxypolyimide structures, respectively. The estimated V_W values are presented in **Table 4.2**. The density of the films was measured by a buoyancy method in a density balance. It was observed that the density of the precursor membranes was higher for the *para*-HPI (1.458 g cm^{-3}) than for the *meta*-HPI (1.438 g cm^{-3}) (**Table 4.2**). The more linear 4,4´-orientation in the diamine moiety probably favored the existence of stronger polymer interchain interactions, giving rise to a more packed and dense

polyimide structure [14]. Besides, the density values for TR-PBO membranes were lower than those of HPI precursors for all membranes (see **Table 4.2**). As a rule, it was observed that the greater the TR conversion the lower the film density. It was also seen that ρ(*meta*-TR-PBO) < ρ(*para*-TR-PBO) for all membranes. However, the decrease was the same in both cases (9% when comparing TR450 with the reference hydroxy-polyimide precursor).

The smaller density of a polymer usually corresponds to larger free volume elements. Accordingly, FFV (PI-*m*HAB) = 0.170 > FFV (PI-HAB) = 0.160, proving the more open and less packed morphology for the 3,3´-oriented precursor membrane. As thermal rearrangement proceeded, FFV raised accordingly with the drop in the density values. Only the FFV of TR350 samples showed values close to that of HPI precursors, in spite of the lower densities observed for those membranes. It should be noted out that a similar behavior was found by Sanders *et al*. on the study of analogous TR polymers based on *ortho*-acetylated PI-HAB precursor [21]. As pointed out by these authors, apart from increasing the fractional free volume, the thermal rearrangement also brings about a change of the polymer free volume distribution, usually resulting in a more favorable cavity distribution [8,11]. In the present work, the increments in FFV as a function of the rearrangement temperature were quite similar for both isomers, as corresponded to the same change in density, ranging from 10 to 21 % (**Table 4.2**). As a consequence, the initially less packed *meta*- precursor polyimide resulted in more open TR-PBO structures, with higher free volume, in spite of the lower conversion degrees observed for this *meta*- series of TR polymers. Thus, FFV (*meta*-) > FFV (*para*-) in all cases (i.e. FFV (TR-*m*HAB450) = 0.202 as compared to FFV (TR-HAB450) = 0.194). These significant changes in the physical properties of TR-PBO membranes should result in improved gas transport behavior.

4.3.5. CAVITY SIZE DISTRIBUTION

As mentioned before, the free volume elements in amorphous glassy polymers are of crucial importance for elucidating gas transport through the membranes. Certainly, experimental density measurements allowed for the estimation of the fractional free volume from the estimated occupied volume of the polymer chains by Bondi's method [23]. However, Positron Annihilation Lifetime Spectroscopy (PALS) was considered to analyze quantitatively and precisely the mean size and concentration of the free volume elements occurred during the thermal rearrangement. In PALS, the free volume cavities are investigated by lifetime of *ortho*-positronium (*o*-Ps) before annihilation in the free volume regions of the materials [24]. Thus, the lifetime (τ) is directly correlated with cavity size in the material, while the intensity of the annihilation (I) is often indicative of the concentration of the cavities. The PALS data for precursor polyimides (PI-HAB and PI-*m*HAB) and their corresponding thermally treated membranes are collected in **Table 4.3**.

Table 4.3. Pore Size Characterization by Positron Annihilation Lifetime Spectroscopy (PALS)

Polymer code	τ_3 (ns)	I_3 (%)	τ_4 (ns)	I_4 (%)	Cavity diameter d_3 (Å)	Cavity diameter d_4 (Å)
PI-HAB	2.652 ± 0.04	3.537 ± 0.14			6.78 ± 0.07	
TR-HAB350	2.617 ± 0.04	4.842 ± 0.14			6.72 ± 0.07	
TR-HAB400	0.840 ± 0.04	10.849 ± 1.27	3.151 ± 0.03	14.766 ± 0.62	2.74 ± 0.18	7.48 ± 0.48
TR-HAB425	0.978 ± 0.05	9.346 ± 0.88	3.244 ± 0.02	14.443 ± 0.36	3.24 ± 0.2	7.60 ± 0.02
TR-HAB450	0.913 ± 0.05	9.740 ± 0.84	3.265 ± 0.02	13.299 ± 0.23	3.02 ± 0.12	7.62 ± 0.04
PI-*m*HAB	2.367 ± 0.09	1.537 ± 0.04			6.34 ± 0.16	
TR-*m*HAB350	2.323 ± 0.06	2.878 ± 0.12			6.28 ± 0.16	
TR-*m*HAB400	0.914 ± 0.06	9.080 ± 0.96	3.346 ± 0.05	9.486 ± 0.28	3.02 ± 0.24	7.72 ± 0.06
TR-*m*HAB425	0.980 ± 0.07	8.961 ± 0.83	3.48 ± 0.05	13.207 ± 0.43	3.26 ± 0.25	7.90 ± 0.06
TR-*m*HAB450	0.973 ± 0.07	8.821 ± 1.33	3.629 ± 0.05	11.528 ± 0.34	3.23 ± 0.26	8.06 ± 0.06

According to the literature for this type of materials [9,11], analysis of the PALS data for the PIs and TR-PBOs showed that there was one o-Ps component (τ_3) fitted for the PIs and two components (τ_3 and τ_4) for the TR-PBOs. As can be seen in **Table 4.3**, thermal rearrangement of the polyimide membranes changes the 6.28 –6.78 Å pores into a bimodal pore distribution for TR-PBO membranes, signifying that two kinds of pores are present: ultrafine micropores, $\tau_3 \sim 0.9$ ns that corresponds to a mean cavity diameter of $d_3 \sim 3 - 3.3$ Å, and micropores where $\tau_4 \sim 3.4$ ns and cavity size of $d_3 \sim 7.5 - 8$ Å. The PIs unimodal pore distribution and the TR-PBOs bimodal pore distribution can be seen in **Figure 4.9**. The absence of the smaller cavities in the precursor materials suggests that the PIs may have very low gas permeability because the small pores are not providing interconnections between the larger 6.28 –6.78 Å pores. The 3 – 4 Å cavities in the TR-PBO membranes are an optimal size for selective transport of gas molecules, in particular for CO_2 separations.
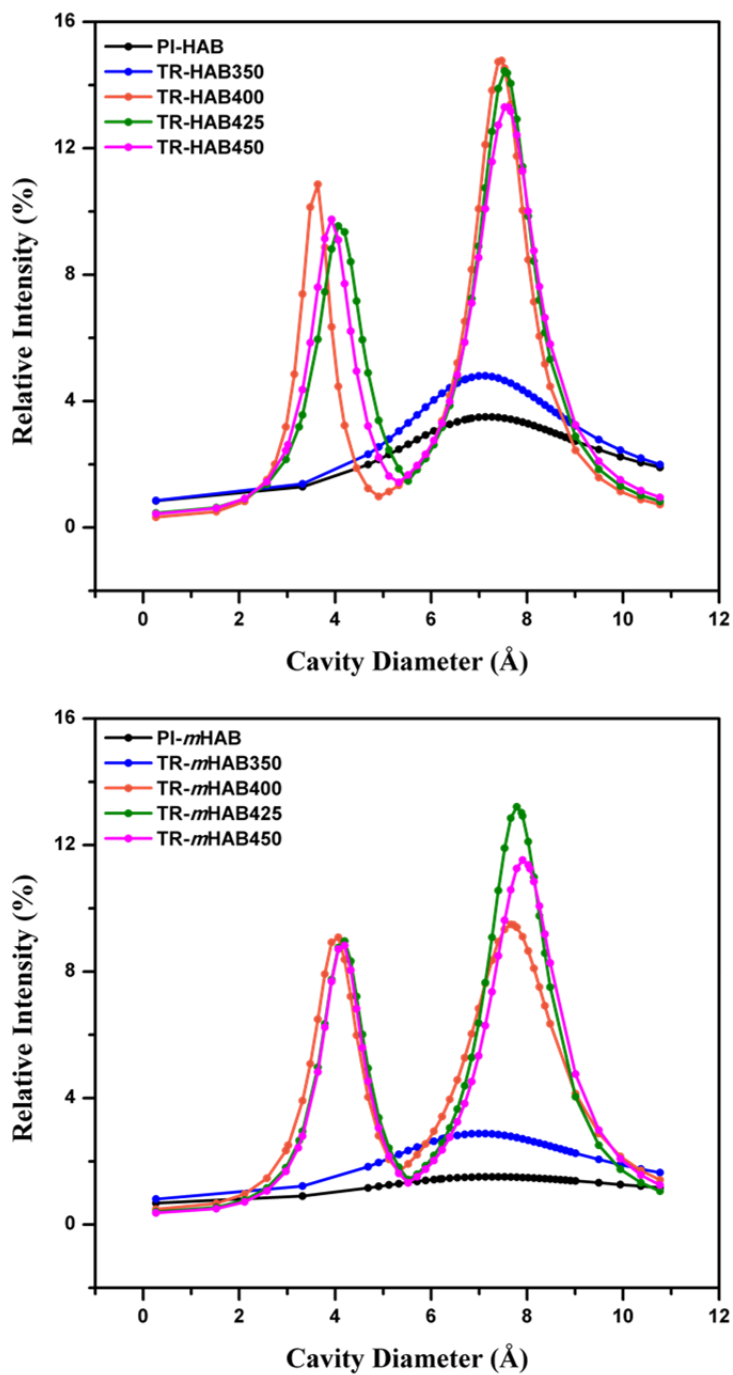
Figure 4.9. Cavity size analysis of (a) HAB isomer series and (b) *m*HAB isomer series by positron annihilation lifetime spectroscopy (PALS)

4.3.6. GAS TRANSPORT BEHAVIORS OF TR-PBO MEMBRANES

The effect of isomerism on the gas separation properties for this set of TR-PBO membranes was investigated. The pure gas permeabilities (P) of thermally rearranged and precursor membranes for the gases He, H_2, CO_2, O_2, N_2 and CH_4, as well as the ideal separation factors (α) for some gas pairs are listed in **Table 4.4**. Precursors HPI had only moderate permeability, the *meta*-connected isomer showing higher permeability values than its *para*- counterpart. Solid-state thermal rearrangement resulted in improved gas permeation properties [8,9], in such a way that as conversion augmented permeability increased for both series of isomers, in agreement with the trend observed in FFV.

Except for CO_2, the most condensable gas tested, permeability showed a strong dependence with kinetic diameters of the gases: the larger the gas molecule, the more the permeability increases with increasing conversion percentage. As it has been already established for TR-polymers, the penetrant diffusivity should be more strongly affected than the gas solubility by PBO conversion, being diffusivity the dominant contribution to the observed increase in gas permeability [21,25]. Most remarkable, the increments in permeability with conversion were much greater for the *meta*- series of TR membranes. Thus, **Figure 4.10** clearly demonstrates this trend of CO_2 permeability for TR-PBO membranes and precursor ones for both series of isomers as a function of conversion degree. As an example, the CO_2 permeability of TR-*m*HAB450 is 720 Barrers as compared to the permeability of 240 Barrers for the TR-HAB450 analog, which gives an increment of 65-fold against 24-fold when they are compared with the values of the precursor polyimides. A similar trend was found for the rest of gases tested. This fact might be mainly attributed to the formation of a much less densely packed structure for the *meta*-TR-PBO set of polymers, as proved by their higher FFV values.

Table 4.4. Gas Permeation Properties of Precursor Polyimides and TR-PBO Membranes measured at 1 bar and 30 °C

Polymer code	Permeabilities (Barrers)[a]					
	PHe	PH_2	PO_2	PN_2	PCH_4	PCO_2
PI-HAB	46	35	2.3	0.35	0.16	10
TR-HAB350	70	54	3.8	0.59	0.29	16
TR-HAB400	94	97	12	2.3	1.5	57
TR-HAB425	100	110	14	2.9	1.9	66
TR-HAB450	200	260	45	10	7.7	240
PI-*m*HAB	57	46	2.8	0.41	0.18	12
TR-*m*HAB350	61	52	4.1	0.62	0.30	18
TR-*m*HAB400	190	220	30	6.4	4.2	150
TR-*m*HAB425	210	240	32	7.3	5.3	160
TR-*m*HAB450	350	570	130	34	31	720

Polymer code	Ideal Selectivities[b]					
	$\alpha O_2/N_2$	$\alpha CO_2/N_2$	$\alpha H_2/N_2$	$\alpha H_2/CO_2$	$\alpha N_2/CH_4$	$\alpha CO_2/CH_4$
PI-HAB	6.6	29	100	3.5	2.2	63
TR-HAB350	6.4	27	92	3.4	2.0	55
TR-HAB400	5.2	25	42	1.7	1.5	38
TR-HAB425	4.8	23	38	1.7	1.5	35
TR-HAB450	4.5	24	26	1.1	1.3	31
PI-*m*HAB	6.8	29	112	3.8	2.3	67
TR-*m*HAB350	6.6	29	84	2.9	2.1	60
TR-*m*HAB400	4.7	23	34	1.5	1.5	36
TR-*m*HAB425	4.4	22	33	1.5	1.4	30
TR-*m*HAB450	3.8	21	17	0.80	1.1	23

[a] 1 Barrer = 10^{-10} cm³ (STP) cm / (cm² s cm Hg). [b] Ideal selectivities were obtained by the ratio of two gas permeabilities.

A difference of about 6-7 % in FFV among isomer membranes was found, irrespective of the treating temperature. Nevertheless, for TR-*m*HAB450 and TR-HAB450 samples only a 4 % difference in FFV was obtained.

As already mentioned above, TR process increases FFV, but also alters the polymer free volume distribution. Most likely, the marked difference in permeability among both isomeric series of TR-PBO membranes should also be due to a difference in size distribution of free volume elements.

Besides, a noteworthy observation is that TR-*m*HAB450 exhibited a higher value of P for CO_2 than for H_2, signifying that, when the FFV increases beyond a certain limit, the size sieving effect, and therefore the diffusivity selectivity, does not play a role so significant, and consequently, the solubility contribution to permeability becomes more important and, because of that, the more soluble gas (CO_2) turns to be the more permeable in spite of its slightly lower diffusivity. Consequently, this behavior must be mainly ascribed to the large free volume of the TR-*m*HAB450 membrane (FFV= 0.202), as it has been observed before for other high free volume polymer membranes [26-29].

It has been widely demonstrated for TR polymers that the increase in free volume during the thermal rearrangement to PBO is usually accompanied by an increase in mean cavity size [8,11]. This fact would account for the general trend observed in the ideal separation factors, where progressive dropping was observed when the TR conversion increased (**Table 4.4** and **Figure 4.11**). Moreover, the higher FFV of *meta*-TR-PBO causes a greater selectivity decrease in this series.
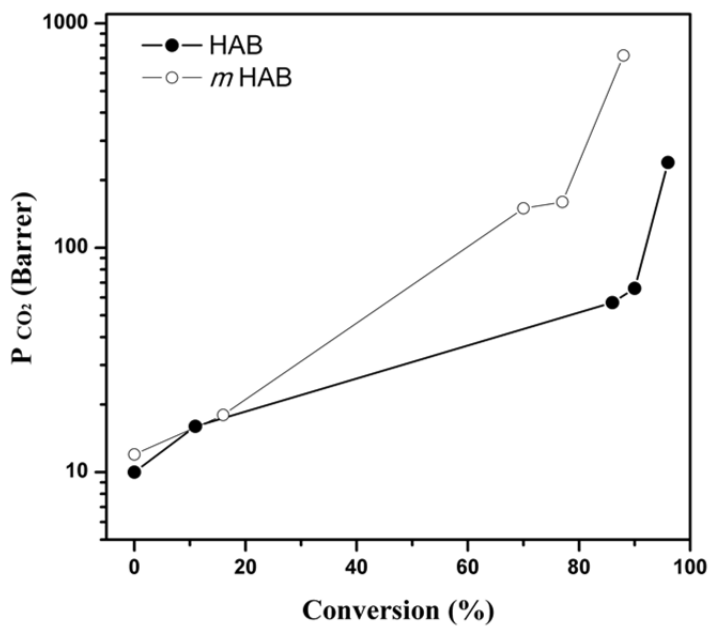
Figure 4.10. CO_2 permeability of PI-HAB and PI-*m*HAB precursor polyimides and TR-PBO analog membranes, as a function of TR conversion percentage
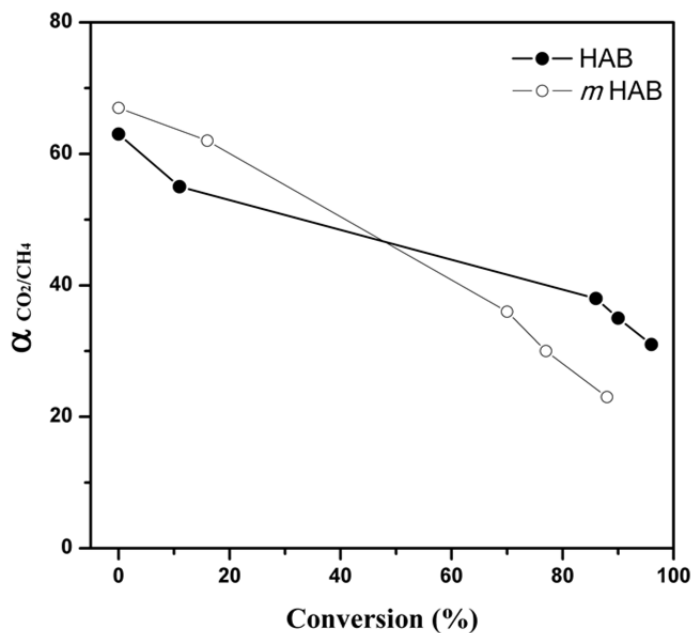
Figure 4.11. CO_2/CH_4 pure gas selectivity of PI-HAB and PI-*m*HAB precursor polyimides and TR-PBO derived membranes, as a function of TR conversion percentage

The productivity of these membranes for gas separations applications is excellent for separations where CO_2 is involved. Thus, when the permeability of CO_2 vs CO_2/CH_4 selectivity is depicted, it can be seen that pristine HPIs and also HPIs treated at the lowest temperatures are clearly well below the 1991 Robeson limit [30] (**Figure 4.12**). However, when the extension of PBO conversion is the highest (membranes treated at 450 ºC) both polymer series overpass the 1991 Robeson limit. With regards to the differences between the isomeric polymers, it has been found that the polymer from *m*HAB showed much better separation properties than that from HAB.

Thus, all the polymer membranes from the latter did not overpass, except the membrane wholly converted into PBO, the 1991 Robeson limit whilst for the *m*HAB series, even the polymers with PBO conversion as low as 70 % (treatment temperature of 400 ºC) could cross this upper bound and got close to 2008 Robeson limit [31]. For other non-condensable gas pairs, the productivity of these membranes was inferior, which is typical for TR polymers. Thus, for the O_2/N_2 separation, all of the tested membranes were below the 1991 Robeson limit [30] (**Figure 4.13**).
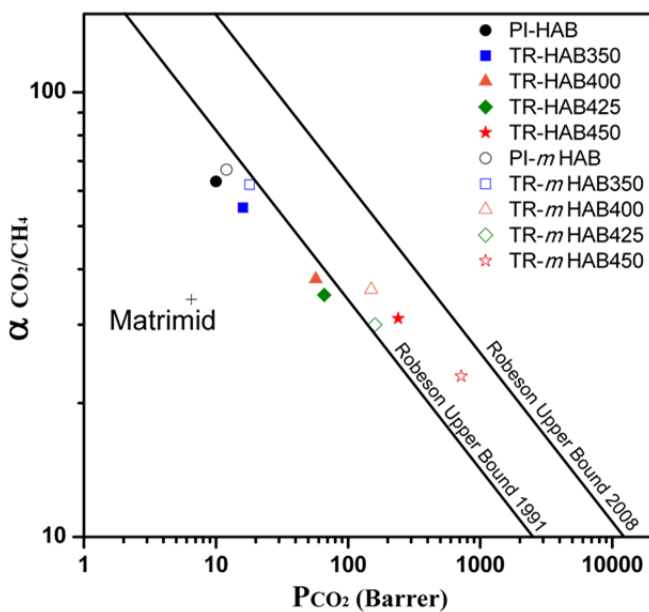
Figure 4.12. Relationship between CO_2 permeability and CO_2/CH_4 selectivity of PI-HAB and PI-*m*HAB precursor polyimides and TR-PBO derived membranes depicted along with the upper bounds [30,31]
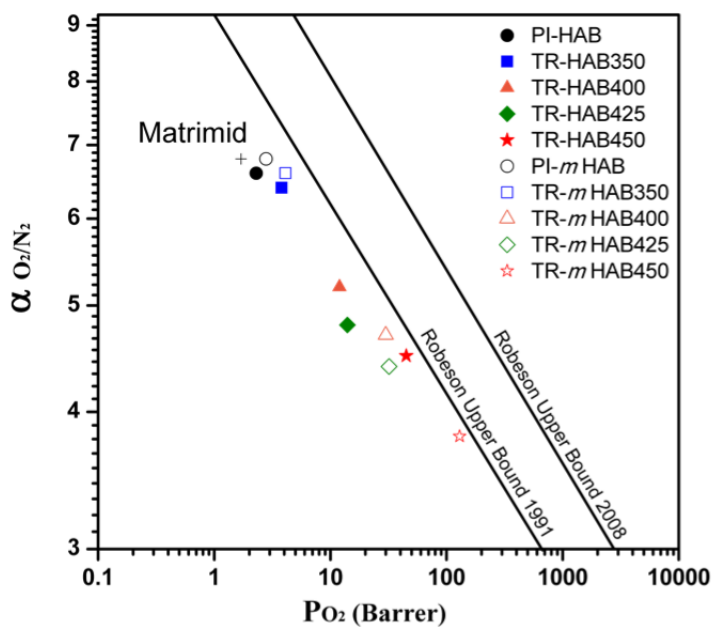
Figure 4.13. Relationship between O_2 permeability and O_2/N_2 selectivity of PI-HAB and PI-*m*HAB precursor polyimides and TR-PBO derived membranes depicted along with the upper bounds [30,31]

4.4. CONCLUSIONS

A diamine monomer with *ortho*-hydroxy groups (3,3´-diamino-4,4´-dihydroxybiphenyl, *m*HAB) has been obtained by a short, low-cost and highly efficient synthetic methodology. This monomer is isomer of the commercial 3,3´-dihydroxybenzidine (HAB). Both monomers were polymerized with 6FDA by using the *in situ* silylation of the diamine in a first stage (formation of the polyamic acid) and consequent azeotropic cycloimidization in a second stage to form two *o*-hydroxypolyimides (HPIs) having high molecular weights. These polyimides were able to undergo, at temperatures above 350 °C, a thermal rearrangement in solid state to polybenzoxazoles (TR process). Extensive characterization and physical properties measurements were carried out for HPIs and for thermally obtained polybenzoxazoles of both (PI-HAB and PI-*m*HAB) polymers. The HPI from *m*HAB showed high solubility in organic solvents and high T_g (330 °C). By means of a thermal study, it was found that PI-*m*HAB had a lower onset TR temperature than its isomeric counterpart PI-HAB, although the PBO conversion, achieved by treating the polymeric films at high temperature and elevated residence times, was higher for PI-HAB. However, the FFV of PI-*m*HAB was higher than that of PI-HAB irrespective of the considered temperature. From this fact, TR-PBO from PI-*m*HAB showed higher permeability for several gases (around 3-fold) than those derived from *p*HAB. In particular, the permeability to CO_2 (720 Barrers) is higher than those exhibited for most of the TR materials described in the bibliography, which, along with the affordable cost of making this monomer, could motivate the use of PI-*m*HAB in industrial carbon capture applications.

4.5. REFERENCES

1. Changlu Gao, Xuee Wu, Guanghua Lv, Mengxian Ding & and Lianxun Gao. 'Syntheses And Properties Of Soluble Biphenyl-Based Polyimides From Asymmetric Bis(chlorophthalimide)s.' *Macromolecules* **37**, 2754–2761 (2004).

2. Rozhanskii, I., Okuyama, K. & Goto, K. 'Synthesis And Properties Of Polyimides Derived From Isomeric Biphenyltetracarboxylic Dianhydrides.' *Polymer* **41**, 7057–7065 (2000).

3. Coleman, M. R. & Koros, W. J. 'Isomeric Polyimides Based On Fluorinated Dianhydrides And Diamines For Gas Separation Applications.' *Journal of Membrane Science* **50**, 285–297 (1990).

4. Ding, M. 'Isomeric Polyimides.' *Progress in Polymer Science* **32**, 623–668 (2007).

5. Muñoz, D. M., De La Campa, J. G., De Abajo, J. & Lozano, A. E. 'Experimental And Theoretical Study Of An Improved Activated Polycondensation Method For Aromatic Polyimides.' *Macromolecules* **40**, 8225–8232 (2007).

6. Muñoz, D. M., Calle, M., de la Campa, J. G., de Abajo, J. & Lozano, A. E. 'An Improved Method For Preparing Very High Molecular Weight Polyimides.' *Macromolecules* **42**, 5892–5894 (2009).

7. Koros, W. J. & Fleming, G. K. 'Membrane-based Gas Separation.' *Journal of Membrane Science* **83**, 1–80 (1993).

8. Park, H. B. *et al.* 'Polymers With Cavities Tuned For Fast Selective Transport Of Small Molecules And Ions.' *Science* **318**, 254–258 (2007).

9. Park, H. B., Han, S. H., Jung, C. H., Lee, Y. M. & Hill, A. J. 'Thermally Rearranged (TR) Polymer Membranes For CO2 Separation.' *Journal of Membrane Science* **359**, 11–24 (2010).

10. Calle, M. & Lee, Y. M. 'Thermally Rearranged (TR) Poly(ether−benzoxazole) Membranes For Gas Separation.' *Macromolecules* **44**, 1156–1165 (2011).

11. Han, S. H. *et al.* 'Thermally Rearranged (TR) Polybenzoxazole: Effects Of Diverse Imidization Routes On Physical Properties And Gas Transport Behaviors.' *Macromolecules* **43**, 7657–7667 (2010).

12. Xu, Y., Fei, F., Zhao, J. & Yu, X. 'Preparation And Characterization Of Novel Polyimides With Hydroxyl Groups.' *Journal of Macromolecular Science, Part B* **50**, 2090–2102 (2011).

13. Dewar, M. J. S., Zoebisch, E. G., Healy, E. F. & Stewart, J. J. P. 'Development And Use Of Quantum Mechanical Molecular Models. 76. AM1: A New General Purpose Quantum Mechanical Molecular Model.' *Journal of the American Chemical Society* **107**, 3902–3909 (1985).

14. Lozano, A. E., De La Campa, J. G. & De Abajo, J. 'Aromatic Polyamides And Polyimides Derived From 3,3'-diaminobiphenyl: Synthesis, Characterization, And Molecular Simulation Study.' *Journal of Polymer Science Part A: Polymer Chemistry* **37**, 4646–4655 (1999).

15.   Comer, A. C., Ribeiro, C. P., Freeman, B. D., Kalakkunnath, S. & Kalika, D. S. 'Dynamic Relaxation Characteristics Of Thermally Rearranged Aromatic Polyimides.' *Polymer* **54,** 891–900 (2013).

16.   Han, K., You, K., Jang, W.-H. & Rhee, T. H. 'Synthesis And Properties Of Chlorinated Polyimides.' *Macromolecular Chemistry and Physics* **201,** 747–751 (2000).

17.   Song, G. *et al.* 'Synthesis And Properties Of Polyimides-containing Benzoxazole Units In The Main Chain.' *High Performance Polymers* (2012).

18.   Okabe, T. & Morikawa, A. 'Synthesis of polyimides from 3,3'-dihydroxybenzidine and conversion to polybenzoxazoles.' *High Performance Polymers* **20,** 53–66 (2007).

19.   Tullos, G. L., Powers, J. M., Jeskey, S. J. & Mathias, L. J. 'Thermal Conversion Of Hydroxy-Containing Imides To Benzoxazoles: Polymer And Model Compound Study.' *Macromolecules* **32,** 3598–3612 (1999).

20.   Calle, M., Chan, Y., Jo, H. J. & Lee, Y. M. 'The Relationship Between The Chemical Structure And Thermal Conversion Temperatures Of Thermally Rearranged (TR) Polymers.' *Polymer* **53,** 2783–2791 (2012).

21.   Sanders, D. F. *et al.* 'Gas Permeability, Diffusivity, And Free Volume Of Thermally Rearranged Polymers Based On 3,3'-dihydroxy-4,4'-diamino-biphenyl (HAB) And 2,2'-bis-(3,4-dicarboxyphenyl) Hexafluoropropane Dianhydride (6FDA).' *Journal of Membrane Science* **409-410,** 232–241 (2012).

22.   Calle, M., Lozano, A. E. & Lee, Y. M. 'Formation Of Thermally Rearranged (TR) Polybenzoxazoles: Effect Of Synthesis Routes And Polymer Form.' *European Polymer Journal* **48,** 1313–1322 (2012).

23.   Bondi, A. 'Van Der Waals Volumes And Radii.' *The Journal of Physical Chemistry* **68,** 441–451 (1964).

24.   Eldrup, M., Lightbody, D. & Sherwood, J. N. 'The Temperature Dependence Of Positron Lifetimes In Solid Pivalic Acid.' *Chemical Physics* **63,** 51–58 (1981).

25.   Kim, S., Jo, H. J. & Lee, Y. M. 'Sorption And Transport Of Small Gas Molecules In Thermally Rearranged (TR) Polybenzoxazole Membranes Based On 2,2-bis(3-amino-4-hydroxyphenyl)-hexafluoropropane (bisAPAF) And 4,4'-hexafluoroisopropylidene Diphthalic Anhydride (6FDA).' *Journal of Membrane Science* **441,** 1–8 (2013).

26.   De Abajo, J., de la Campa, J. G. & Lozano, A. E. 'Designing Aromatic Polyamides And Polyimides For Gas Separation Membranes.' *Macromolecular Symposia* **199,** 293–306 (2003).

27.   Budd, P. M. *et al.* 'Gas Permeation Parameters And Other Physicochemical Properties Of A Polymer Of Intrinsic Microporosity: Polybenzodioxane PIM-1.' *Journal of Membrane Science* **325,** 851–860 (2008).

28.   Budd, P. M. *et al.* 'Gas Separation Membranes From Polymers Of Intrinsic Microporosity.' *Journal of Membrane Science* **251,** 263–269 (2005).

29.   Reijerkerk, S. R., Knoef, M. H., Nijmeijer, K. & Wessling, M. 'Poly(ethylene Glycol) And Poly(dimethyl Siloxane): Combining Their Advantages Into Efficient CO2 Gas Separation Membranes.' *Journal of Membrane Science* **352,** 126–135 (2010).

30.   Robeson, L. M. 'Correlation Of Separation Factor Versus Permeability For Polymeric Membranes.' *Journal of Membrane Science* **62,** 165–185 (1991).

31.   Robeson, L. M. 'The Upper Bound Revisited.' *Journal of Membrane Science* **320,** 390–400 (2008).

Chapter V

Gas Separation Membranes Made through Thermal Rearrangement:

Influence of the *ortho*-Substituent

5.1. INTRODUCTION

The generally accepted mechanism for the imide-to-polybenzoxazole in solid state thermal rearrangement involves the decarboxylation of *ortho*-hydroxypolyimide at high temperatures (well over 350 °C) through the formation of a carboxy-benzoxazole, which is finally converted to the sought polybenzoxazole (PBO) by the elimination of a CO_2 molecule [1–3]. Additionally, other functionalized polyimides have been studied as precursors, particularly polyimides containing *ortho*-ester groups [4]. The use of esters instead of hydroxyl-free groups seems to eventually render PBOs that show slightly higher permeation performance than those prepared from *ortho*-hydroxypolyimides. In addition *ortho*-ester polyimides simultaneously offer better solubility and a lower glass transition temperature. However, it should emphasize that the weight loss associated to the *ortho*-ester process is higher than that from *ortho*-hydroxy polyimides and consequently it is observed a large shrinkage during the whole process. Guo *et al*. have recently reported about the effects of different *ortho*-functional groups on the transformation of polyimide precursors into polybenzoxazoles and on their permeation properties [4]. These authors observed that using *ortho*-esterpolyimides significantly affected the rearrangement process, and that by changing the –OH groups into RCOO- groups enhances permeability due to the increased free volume provided by the larger leaving ester group (when compared to the hydroxyl group).

Based on these precedents, and looking for new routes towards TR-PBO polymers, a study was performed on the preparation and evaluation of TR-PBO materials obtained from *ortho*-methoxy containing polyimides. The thermal rearrangement of *ortho*-methoxy-polyimides to TR-PBOs was recently reported [5]; however, a detailed study of the mechanism was not done at that time, nor any investigation on the gas permeation properties was carried out. Additionally, polybenzoxazoles have been attained from *ortho*-methoxy aromatic polyamides, mainly by looking for a substantial thermal resistance increase of the precursor polyamides [6]. Other authors used this approach to prepare PBOs with various end-goals [7,8]. However, these precursors with side methoxy groups have not

been studied for TR-PBOs in gas separation applications. Also, the weight loss associated to the methoxy group is much lower than that of the acetate moiety, and consequently the shrinkage should be much lower.

In this study, we report on the preparation of soluble *ortho*-methoxy polyimides made from 6FDA dianhydride and 3,3'-dimethoxybenzidine, which is a comparatively low-priced monomer. The conversion of this precursor into TR-PBO at high temperatures was the objective of this chapter and our focus was on the search of relationships between time-temperature schedule and the final properties of films fabricated from the precursor. Special attention was given to the possible reactions that occurred alongside the thermal treatment. Results were compared with *ortho*-hydroxy and *ortho*-acetylpolyimides of similar structure comparing the permeation properties of the final films with those of earlier reported TR-PBOs [4,9–17].

5.2. EXPERIMENTAL SECTION

5.2.1. MATERIALS

This chapter focuses on three different polyimides: *PI-HAB* and *PI-AcAB* (both formed by the reaction of 3,3'-dihydroxybenzidine (HAB, TCI Europe) and 2,2'-bis-(3,4-dicarboxyphenyl) hexafluoropropane dianhydride (6FDA, Cymit Química), but cyclized by different imidization methods; azeotropic and chemical imidization, respectively) and *PI-MeAB* (formed by the reaction of 3,3'-dimethoxybenzidine (DMAB, TCI-Europe) and 6FDA). The chemical structures of the *ortho*-substituted polyimides and their precursor monomers are shown in **Scheme 5.1**. As can be seen, the backbone structure is similar in the three polyimides, just differing in the *ortho*-substituted group. *PI-HAB* structure was chosen due to the relatively high reactivity of HAB compared to other commercially available diamines. The 6FDA dianhydride was selected due to its favourable performance in other polymeric gas separation membrane studies, including previous TR research [18,1,2] and also because this dianhydride increases polyimide solubility. Azeotropic and chemical imidizations were accomplished in order to convert the poly(amic acid) precursor to this polyimide, attaining *PI-HAB* and *PI-AcAB*, respectively. The low-cost DMAB monomer was chosen to synthesize the polyimide with the *ortho*-methoxy group in its structure, *PI-MeAB*.
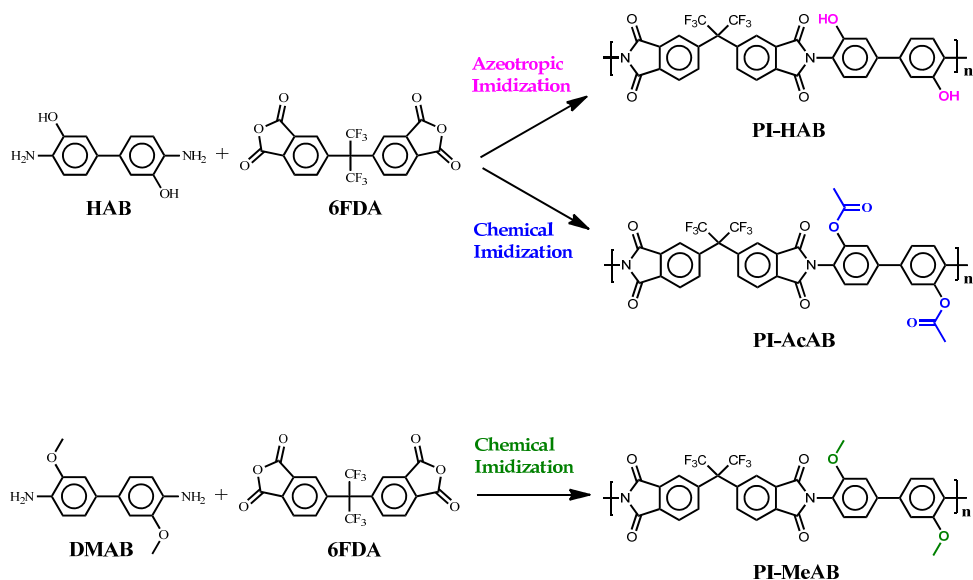
Scheme 5.1. Chemical structure of *PI-HAB*, *PI-AcAB* and *PI-MeAB* polyimides and their precursor monomers

5.2.2. SYNTHESIS OF POLYIMIDES DERIVED FROM 6FDA AND HAB

The formation of the hydroxy-containing poly(amic acid) intermediates (*OH-PAA*) is common during the synthesis of both *PI-HAB* and *PI-AcAB*, with the exception that the solvent employed in the reactions are different. For the chemical imidization process, DMAc was used as a solvent, while NMP was chosen for azeotropic imidization to facilitate water removal. *Ortho*-hydroxy polyamic acid (*OH-PAA*) intermediates were prepared using the following general route: 10.0 mmol of HAB diamine and 10 mL of the chosen solvent were added to a round bottomed three-necked flask and stirred at room temperature under a dry nitrogen atmosphere. When the solid had entirely dissolved, the solution was cooled to 0 °C and the required amount of CTMS (20 mmol, 1 mol/mol reactive group) was added to the solution, followed by Py (20 mmol, 1 mol/mol reactive group) and DMAP (0.1 mol/mol Py). The temperature was subsequently raised to room temperature and maintained for 15 min to ensure the formation of the silylated diamine. After this time, the solution was cooled once again to 0 °C, and a stoichiometric amount of 6FDA (10.0 mmol) was

carefully added followed by 10 mL of solvent to rinse the inner flask walls. The reaction mixture was stirred for 15 min and then the temperature was raised to room temperature where it was left overnight to form the *OH-PAA* intermediates.

To attain the final polyimide with the -OH groups in the *ortho*-position, polyimide designated as *PI-HAB*, *o*-xylene (20 mL), as an azeotropic agent, was added to the *OH-PAA* solution, which was then vigorously stirred and heated for 6 h at 180 °C to promote cycloimidization. During this step, the water released from the ring-closure reaction was separated out as a xylene azeotrope, along with silanol and other siloxane by-products derived from the use of the silylating agent. Additional *o*-xylene was stripped out from the polymer solution, which was then cooled to room temperature and precipitated in distilled water. The polymer obtained was washed several times with water, then a mixture of water/ethanol (1/1), then pure ethanol, and finally dried in a vacuum oven at 150 °C for 12 h. **PI-HAB**: η_{inh} (dL/g) = 1.51. ^{1}H-NMR (DMSO-d_6, 500 MHz): 10.23 (s, 2H, OH), 8.27 (d, 2H), 8.08 (d, 2H), 7.87 (s, 2H), 7.46 (d, 2H), 7.29 (s, 2H), 7.27 (s, 2H). FT-IR (film): ν(-OH) at 3401 cm^{-1}, imide ν(C=O) at 1785 and 1715 cm^{-1}, imide ν(C-N) at 1378 cm^{-1}, imide ν(C-N-C) at 1099 cm^{-1}.

In order to obtain -OAc groups in the final polyimide structure, polyimide designated as *PI-AcAB* was obtained from the *OH-PAA* intermediate that was chemically imidized by adding to the solution a mixture of acetic anhydride (80 mmol, 4 mol/mol reactive group) and Py (80 mmol, 4 mol/mol reactive group). The solution was stirred for 6 h at room temperature and 1 h more at 60 °C to promote complete imidization. The viscous polyimide solution was cooled at room temperature and poured into water where a fiber precipitate formed that was then repeatedly washed with water and a mixture of water/ethanol (1/1). The precipitate was finally dried in a vacuum oven at 150 °C overnight. **PI-AcAB**: η_{inh} (dL/g) = 0.62. ^{1}H-NMR (DMSO-d_6, 500 MHz): 8.22 (d, 2H), 8.00 (d, 2H), 7.86 (s, 2H), 7.80 (m, 2H), 7.68 (d, 2H), 2.16 (s, 6H, CH$_3$). FT-IR (film): imide ν(C=O) at 1778 and 1724 cm^{-1}, imide ν(C-N) at 1370 cm^{-1}, imide ν(C-N-C) at 1096 cm^{-1}.

5.2.3. SYNTHESIS OF POLYIMIDES DERIVED FROM 6FDA AND DMAB VIA CHEMICAL IMIDIZATION (PI-MeAB)

A three-necked flask was charged with 10.0 mmol of diamine DMAB and 10 mL of DMAc as a solvent. The mixture was cooled to 0 °C and the required amount of CTMS (20 mmol, 1 mol/mol reactive group) was incorporated, followed by Py (20 mmol, 1mol/mol reactive group) and DMAP (2 mmol, 0.1 mol/mol Py). The solution was allowed to come to room temperature and was then stirred for 15 min to ensure the formation of the silylated diamine. After this, the solution was cooled once again to 0 °C and 6FDA (10.0 mmol) was added followed by 10 mL of DMAc. After 15 minutes of stirring at 0 °C, the solution was allowed to come to room temperature where it was left overnight to form the methoxy-containing poly(amic acid) intermediate designated as *OMe-PAA*. Subsequently, the *OMe-PAA* intermediate was cyclized into its corresponding polyimide via a chemical imidization process by adding a mixture of acetic anhydride (80 mmol, 4 mol/mol reactive group) and Py (80 mmol, 4 mol/mol reactive group) to the solution. In order to promote complete imidization, the solution was stirred for 6 h at room temperature and 1 h more at 60 °C. The polyimide solution was cooled to room temperature and then poured into water. The precipitate obtained was thoroughly washed with water and ethanol, and then dried at 150 °C for 12 h under vacuum. **PI-MeAB**: η_{inh} (dL/g) = 0.59. ^{1}H-NMR (DMSO-d_6, 500 MHz): 8.19 (d, 2H), 8.00 (d, 2H), 7.86 (s, 2H), 7.53 (s, 2H), 7.52 (d, 2H), 7.46 (d, 2H), 3.88 (s, 6H, CH$_3$), FT-IR (film): imide ν(C=O) at 1787 and 1724 cm^{-1}, imide ν(C-N) at 1373 cm^{-1}, imide ν(C-N-C) at 1099 cm^{-1}.

5.2.4. *FORMATION OF POLYIMIDE FILMS AND SUBSEQUENT THERMAL TREATMENT*

To prepare polyimide films, 10 wt. % polyimide solutions in NMP or DMAc (the same solvents used for both polyimide synthesis routes) were filtered through a 3.1 µm glass-fiber syringe filter and cast onto well-leveled glass plates. The films were dried at 60 °C overnight to remove the majority of the solvent and then placed in a vacuum oven. The polyimide films were progressively heated to 250 °C, holding for 1 h at 100 °C, 150 °C, 200 °C and 250 °C under vacuum to remove any residual solvent. Self-supported films were stripped off their glass plates, washed with distilled water, and dried at 130 °C, under vacuum, overnight. Film thicknesses were between 40 and 50 µm and suitable film uniformity was verified by measuring the film thickness standard deviation, which was lower than 5 % in all cases. All polyimide samples were cut into 3 cm x 3 cm defect-free pieces and placed between ceramic plates to avoid film rolling at elevated temperatures. These were placed in a quartz tube furnace under an inert gas. In order to completely remove solvent and to ensure full imide ring closure, all polyimide films were heated at a rate of 5 °C/min to 300 °C and held for 2h for the *PI-HAB* film and 1h for the *PI-AcAB* and *PI-MeAB* films, under 0.3 L min⁻¹ nitrogen flow. The precursor polyimide membranes were converted into TR membranes by a further thermal treatment. To do this, the polyimide membranes were heated to 350 °C, 400 °C and 450 °C at a rate of 5 °C min⁻¹, and maintained there for a desired amount of time (30 min or 1 h) in a high-purity nitrogen atmosphere. This procedure follows a protocol described in literature [19], and in performing such a treatment, all samples were exposed to thermal treatments similar to those previously reported. The cooling protocol consisted of allowing the furnace to reach room temperature at a rate no greater than 10 °C min⁻¹. The thermally treated membranes, obtained from the *PI-HAB*, *PI-AcAB* and *PI-MeAB* precursor polyimides, were designated as *TR-HABX*, TR-AcABX and *TR-MeABX*, respectively, where X indicates the final temperature applied to those samples.

5.3. RESULTS AND DISCUSSION

5.3.1. SYNTHESIS AND CHARACTERIZATION OF THE PRECURSOR POLYIMIDES

Precursor polyimides were synthesized using a classical and quantitative two-step low-temperature polycondensation method in which the diamine, HAB or DMAB, was reacted with dianhydride 6FDA at room temperature in a polar aprotic solvent (NMP or DMAc). DMAc was selected for the chemical cyclodehydration reactions since it can be easily removed during the membrane formation step. However, for the azeotropic cycloimidization, NMP was used since the boiling temperature of DMAc is similar to that of *o*-xylene, which can hinder water release. High-viscosity poly(amic acid) intermediates, *OH-PAA* and *OMe-PAA*, were obtained through a base-assisted *in situ* silylation method [20,21] that requires the use of a silylating agent (CMTS), Py and DMAP as activating reagents to increase the reactivity of the $-NH_2$ groups. In the second stage of the process, the poly(amic acid)s *OH-PAA* and *OMe-PAA* were cyclized by different imidization methods depending on the desired final polyimide structure.

Azeotropic imidization was carried out adding *o*-xylene to form an azeotrope with the water produced during the ring-closure reaction. Accordingly, *OH-PAA* was azeotropically imidized to obtain *PI-HAB* precursors. Chemical imidizations were accomplished by the addition of a mixture of acetic anhydride and Py to the *OH-PAA* and *OMe-PAA* solutions. Without the use of a protecting group, the hydroxyl groups of the HAB moiety are converted to acetate groups during the imidization process and thus the acetate-containing polyimide, *PI-AcAB*, was obtained.

PI-HAB, *PI-AcAB* and *PI-MeAB* polyimides showed values of inherent viscosity of 1.51, 0.62 and 0.59 dL/g respectively, offering high enough molecular weights to be employed in the preparation of dense membranes with good mechanical properties. The yield of the polycondensation reactions was higher than 98 - 99 % for all polyimides produced.

The chemical structure of the precursor polyimides was confirmed by ^{1}H-NMR. **Figure 5.1** shows the NMR spectra for the three polyimides where the peak allocations have been included. As can be seen in the aromatic region, the hydrogens that correspond to the phenyl moieties of the diamine (b, c and d) are upshifted relative to the hydrogen peaks ascribed to the phenyl groups of the dianhydride (e, f and g). There was a similar chemical shift seen for all polymers, indicating that the influence of the electronic features of the diamine aromatic rings on the dianhydride ones was negligible. The protons of the hydroxyl group (a_1) were observed at 10.23 ppm on the *PI-HAB* spectrum while, for the *PI-AcAB* and *PI-MeAB* spectra, the peaks in the aliphatic region at 2.16 and 3.88 ppm corresponded to the methyl protons in the acetate group (a_2) and in the methoxide group (a_3), respectively. In addition, the absence of the OH peak at 10.23 ppm in the *PI-AcAB* spectrum indicated that complete acetylation was achieved.

The IR spectra of polyimide films are shown in **Figure 5.2**. All polyimides showed absorption bands at around 1780 cm^{-1} (symmetric C=O stretching), 1720 cm^{-1} (asymmetric C=O stretching) and at approximately 1375 cm^{-1} (C-N stretching), verifying the existence of imide moieties. In addition, absorption peaks at 1250 – 1100 cm^{-1} were denoted as the C-F stretching band of the hexafluoroisopropylidene moiety. In the case of *PI-HAB* pattern, the broad band in the region from 3200 – 3600 cm^{-1} was attributed to O-H vibrations on the phenolic groups.
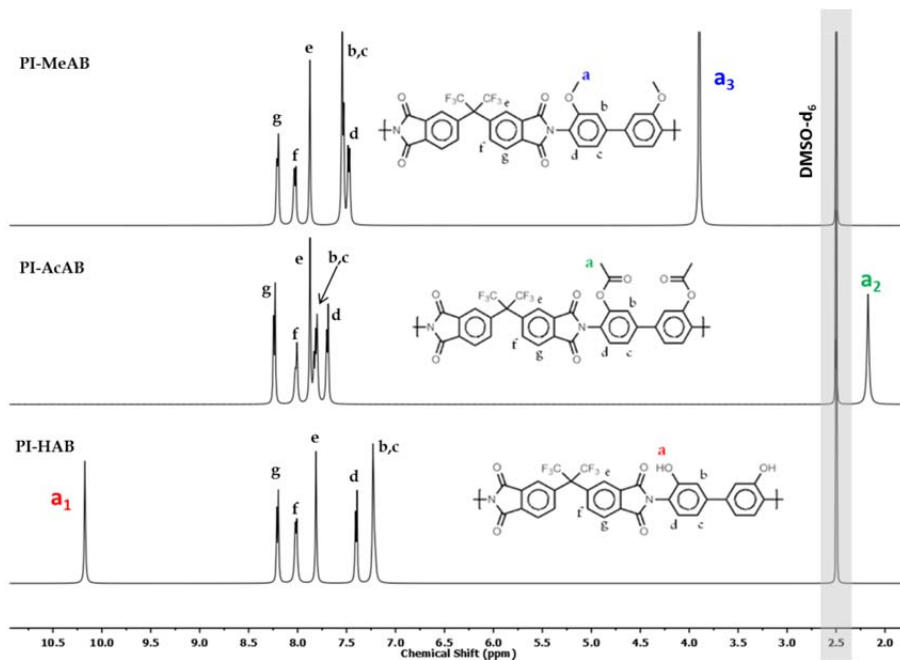
Figure 5.1. ^{1}H-NMR spectra of the precursor polyimides (DMSO-d_6, 500 MHz)
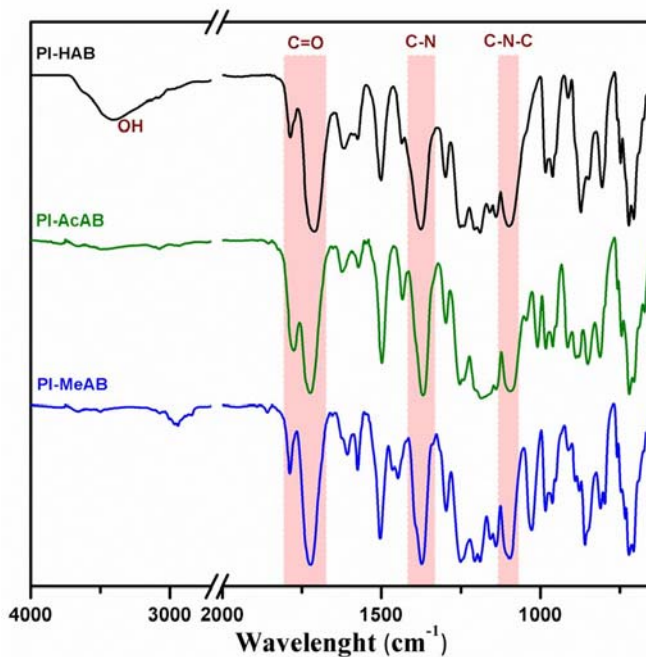
Figure 5.2. ATR-FTIR spectra of precursor polyimide films

164

5.3.2. *THERMAL PROPERTIES OF PRECURSOR POLYIMIDES*

The thermal characteristics of these three polyimides were evaluated using modulated DSC (MDSC) and TGA-MS techniques. As observed in MDSC (**Figure 5.3**), the glass transition temperature, T_g, was clearly affected by the *ortho*-positioned substituent. Thus, the *PI-HAB* exhibited the highest T_g at 356 °C, whereas the non-hydroxylated polyimides showed a lower T_g of 278 °C and 311 °C for *PI-AcAB* and *PI-MeAB*, respectively (see **Table 5.1**). This displacement of the T_g to lower values for the non-hydroxylated polyimides can be attributed to the reduced ability to produce hydrogen bonds, and the higher free volume imparted by the presence of acetate and methoxy groups. The combination of both factors reduces the cohesive energy and consequently the glass transition temperature.
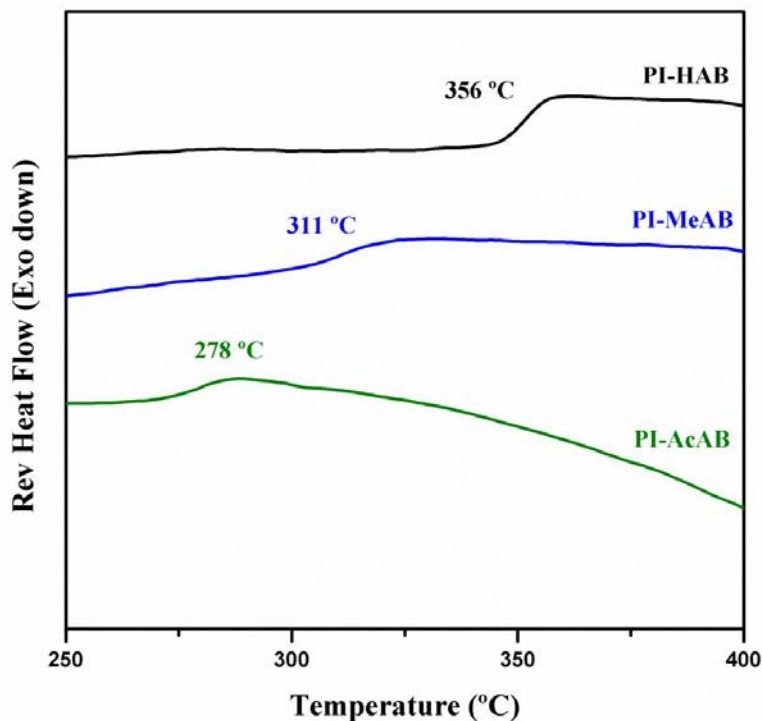
Figure 5.3. Glass transition temperatures of precursor polyimides determined by MDSC

Table 5.1. Thermal Properties of Precursor Polyimide Films

Polymer code	T_g (°C)[a]	T_{AP} (°C)[b,d]	T_{max} (°C)[c,d]	theoretical wt. loss (%)	measured wt. loss (%)[d]	T_d (°C)[d]
PI-HAB	356	345	425	14.1	12.6	550
PI-AcAB	278	282	397	24.3	13.0	546
PI-MeAB	311	380	493	17.8	13.8	546

[a] Middle point of the endothermic step of the "reversing" contribution to the average heat flow during the first scan of MDSC measurements conducted at a heating rate of 5 °C/min, modulation period of 40 s and a temperature modulation amplitude of 1.5 °C, under a nitrogen atmosphere. [b] Apparent starting temperature at which first weight loss begins. [c] Temperature at the maximum point of the first weight loss. [d] Determined by TGA at a heating rate of 10 °C/min under nitrogen atmosphere.

A comparison of TGA and the first derivative traces for all precursor polyimide films at 10 °C min^{-1} under a N_2 atmosphere can be seen in **Figure 5.4**. *PI-HAB* clearly shows two distinct weight loss steps, in agreement with previously reported data [19,22]. The first weight loss step, in the range of 300-500 °C, can be associated with the thermal rearrangement of *PI-HAB* to the TR-PBO structure and the release of CO_2, as confirmed by TGA-MS analyses (**Figure 5.5**). The second step is ascribed to the generalized decomposition of the *in situ* formed TR-PBO backbone at around 500-600 °C [19,22-24]. *PI-AcAB* shows a TGA profile with two steps similar to *PI-HAB*, suggesting that the thermal rearrangement to TR-PBO also took place in this polyimide. However, the apparent starting temperature of the first weight loss of *PI-AcAB* was around 60 °C lower than that of *PI-HAB* (see **Table 5.1).** In addition, the maximum weight loss rate (r_{max}) for the *PI-HAB* film, analyzed from the differential TGA curve (DTG), was r_{max}=0.30%/°C, whereas a lower value of r_{max}=0.13%/°C was found for the *PI-AcAB* film. It was difficult to discern the two-step weight loss for *PI-MeAB* film (they can be observed however in the different curve), possibly due to the improved thermal stability given by the methoxy group or because of the existence of a different rearrangement mechanism. In this case, the apparent starting temperature for the first weight loss was observed at 380 °C, and the maximum weight loss rate (at 495 °C) was 0.22%/°C.

Additionally, the measured weight losses for the *PI-HAB*, *PI-AcAB* and *PI-MeAB* films were 12.6, 13.0 and 13.8 %, respectively. These values are lower than the theoretical ones for full conversion to PBO (which would be 14.1, 24.3 and 17.8 %, respectively), assuming that the TR mechanism from *ortho*-substituted PI into PBO occurs in all cases. TGA-MS was used to identify the composition of the evolved gasses from the film sample during the scan.
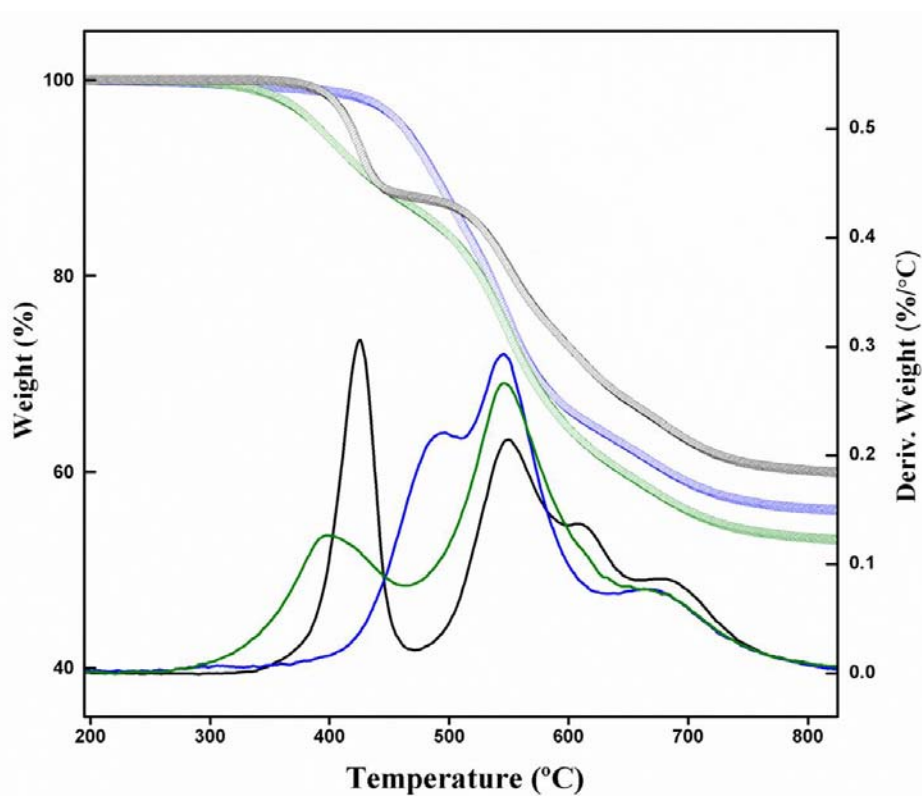
Figure 5.4. Thermogravimetric analysis of precursor polyimide films at a heating rate of 10 °C min^{-1} under N$_2$ atmosphere; ● *PI-HAB*, ● *PI-AcAB* and ● *PI-MeAB*

Figure 5.5 shows that the molecular weight of the produced volatiles was between 10 and 70 amu, using the same experimental settings than those employed in the TGA experiment illustrated in **Figure 5.4**. In the *PI-HAB* film (a), mass components having molecular weights of 17, 18, 19, 20, 44, 51 and 69 amu were evolved during the full scan. As mentioned above, the first mass loss is attributed to the decarboxylation of the polyimide during thermal rearrangement; thus, as previous studies reported [2,9,25], only the peak associated with the molecular weight of 44 was observed below 450 °C. In the second stage, which is associated with polymer degradation, all of the other species were detected. Evolved MS products with 19, 20 and 69 amu, indicate the cleavage of groups containing fluorine atoms (trifluoromethyl) on the polymer backbone. These losses correspond to fragments of F, HF and CF_3, respectively [26]. The peaks associated with molecular weights of 17 and 18 amu indicate loss of water within the polyimide structure. Finally, the molecular weights of 44 and 51 can be attributed to the general degradation of the polyimide. However, for the *PI-AcAB* film, in addition to these molecular losses, other peaks can be observed in the thermal rearrangement region. The mass losses for molecular weights of 41 and 42 were attributed to the acetate groups in the form of a ketene moiety [27]. Moreover, molecular weights of 17 and 18, corresponding to H_2O, were also detected in the first step, which could plausibly indicate that chemical imidization was not complete for this case [28]. In the *PI-MeAB*, in the first weight loss region, along with the peak associated with CO_2, the appearance of species having a molecular weight of 15 was observed, which could be associated to methyl groups loss resulting from the methoxy group breakage [29,30].
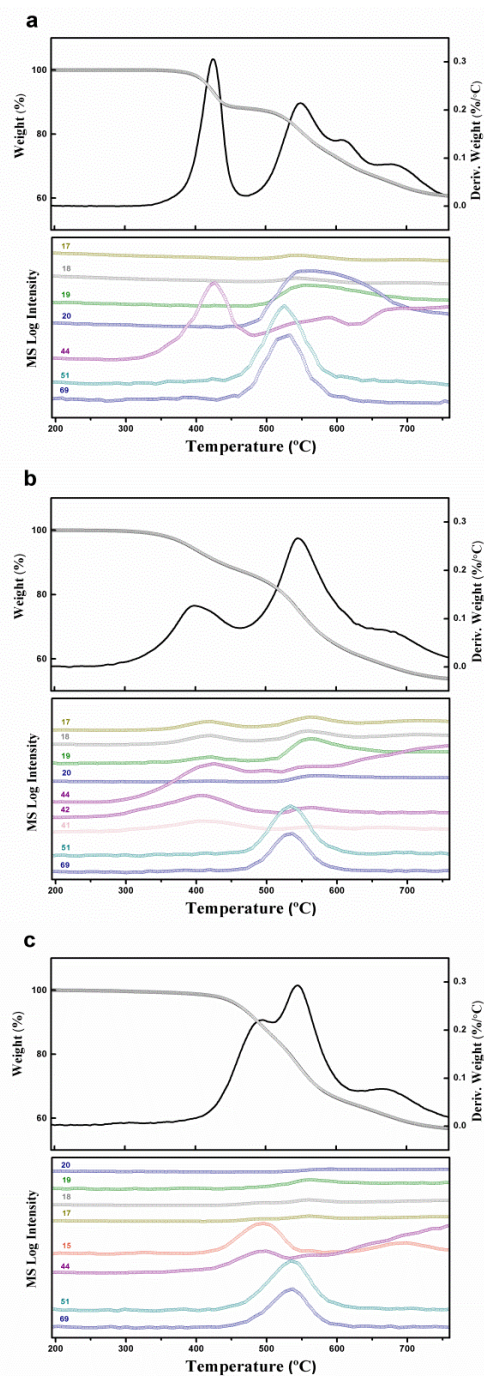
Figure 5.5. Thermogravimetric analysis combined with mass spectroscopy (TGA-MS) of (a) *PI-HAB*, (b) *PI-AcAB* and (c) *PI-MeAB* precursor polyimide membranes (heating rate of 10 °C min^{-1} under N_2 atmosphere)

5.3.3. THERMAL TREATMENT OF PRECURSOR POLYIMIDES

Supplementary TGA analyses were performed to adjust the thermal treatment settings for TR sample preparation in the tubular furnace. To do this, the PI films treated at 300 °C were further heated to the desired temperature (350 °C, 400 °C and 450 °C) using a heating rate of 5 °C min^{-1}, and then held isothermally at the target temperature for 3h. **Figure 5.6** depicts the isothermal thermograms for all precursor films, showing weight loss as a function of time after reaching the rearrangement temperature. The conversion percentage of the precursor polyimide films into the final TR membranes was evaluated based on data obtained from isothermal thermograms using Equation 5.1:

$$\% \; \boldsymbol{Conversion} = \frac{\boldsymbol{Experimental \; Mass \; Loss}}{\boldsymbol{Theoretical \; Mass \; Loss}} \times \boldsymbol{100} \qquad \text{(Eq. 5.1)}$$

This theoretical CO_2 loss, which is 14.1 % for *PI-HAB*, 24.3 % for *PI-AcAB* and 17.8 % for *PI-MeAB*, is shown as a dashed line in the figure.
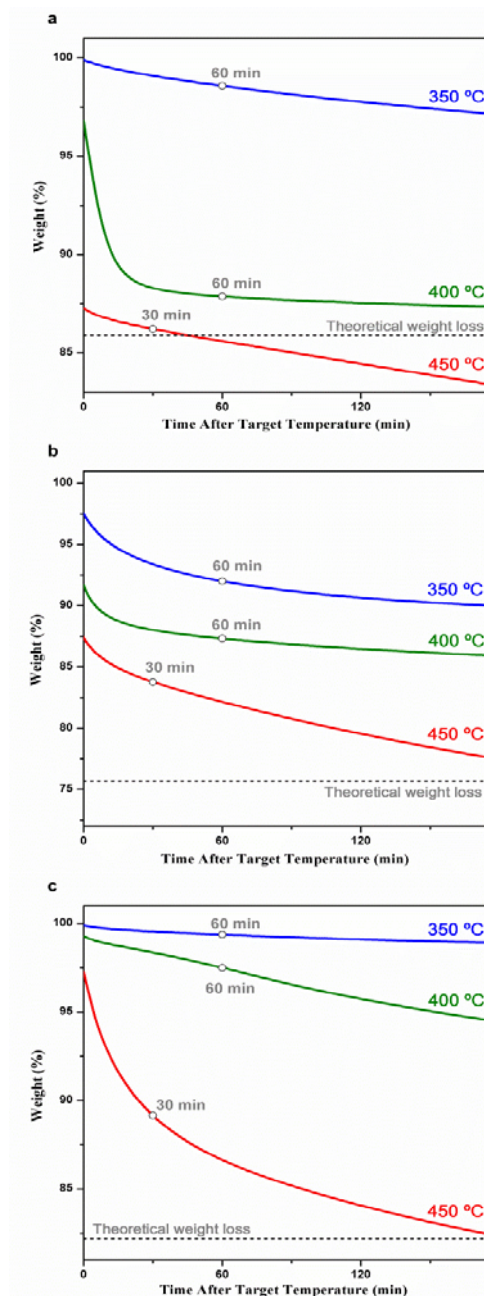
Figure 5.6. Isothermal thermogravimetric analysis, under N_2 atmosphere, of (a) *PI-HAB*, (b) *PI-AcAB* and (c) *PI-MeAB* precursors. The graphs show weight loss of the polyimides as a function of time at the indicated temperatures. Empty circles represent the conditions used for membranes employed in transport property characterization

Conversion values for the precursors polyimides are shown in **Table 5.2**. According to previous studies [19,23,31], the thermal cyclization reaction is very sensitive to the applied temperature, showing an acceleration in the thermal rearrangement kinetics with increasing temperature. For the *PI-HAB* film, at 350 ºC, the weight loss was low at all heating times (11 % in 1 h), whereas it notably increased at 400 ºC reaching its maximum value (100 % in less than 1 h) at 450 ºC, exceeding the theoretical weight loss for longer treatment times. However, the *PI-AcAB* film achieved higher weight losses than *PI-HAB*, (33 % in 1 h at 350 ºC) presumably due to its lower T_g that favors the start of rearrangement at lower temperatures, as can be seen in **Figure 5.4**. At 400 ºC and 450 ºC, the weight loss gradually increased, potentially reaching the theoretical value for treatments longer than 3 h at 450 ºC. For *PI-MeAB*, the weight loss was quite low for all heating times both at 350 ºC (4 % in 1 h) and at 400 ºC (14 % in 1 h). As the T_g of this polymer is also significantly lower than that of *PI-HAB*, the lower reactivity of this PI should be related with the different behavior of the OMe group, as has been indicated previously in the dynamic TGA curves. At 450 ºC, the weight loss notably increased, but the value did not surpass the theoretical weight loss for the first 3 h, reaching a value of 61 % in 30 min. Presumably, using a longer thermal treatment would result in a higher percentage of conversion and, consequently, in higher *d*-spacing values, which would translate into a higher degree of *openness* within the polymer matrix.

Table 5.2. Physical Properties of Precursor Polyimides and their Corresponding TR Membranes

Polymer code	Conv. [a] (%)	Density (g cm^{-3})	FFV	Increment in FFV (%)	d-spacing (Å)
PI-HAB	0	1.458	0.160	–	5.57
TR-HAB350	11	1.453	0.159	–	5.71
TR-HAB400	86	1.373	0.176	10	6.06
TR-HAB450	96	1.337	0.194	21	6.14
PI-AcAB	0	1.413	0.170	–	6.11
TR-AcAB350	33	1.429	0.154		6.05
TR-AcAB400	52	1.139	0.172	1	6.30
TR-AcAB450	67	1.345	0.196	15	6.51
PI-MeAB	0	1.388	0.174	–	5.99
TR-MeAB350	4	1.376	0.181	4	6.16
TR-MeAB400	14	1.360	0.191	10	6.20
TR-MeAB450	61	1.322	0.214	23	6.36

[a] PI transformation for the different series after 60 min at 350 and 400 ˚C and 30 min at 450 ˚C

In order to have thermal histories similar to those reported in other studies related to TR materials, the residence times chosen for thermal treatment were 1 h for both 350 ºC and 400 ºC, and 30 minutes for 450 ºC (represented by empty circles in **Figure 5.6**). Thus, the polyimide precursors, *PI-HAB*, *PI-AcAB* and *PI-MeAB*, were thermally treated in a tubular furnace following the chosen protocols.

The effect of the thermal treatment on polymer chain packing, which has a considerable influence on the gas separation properties, was explored by wide-angle X-ray diffraction (WAXD). In **Figure 5.7,** the X-ray patterns, measured at room temperature, of thermally treated membranes and polyimide precursor films are compared. All of the membranes were in a completely amorphous state, proved by the presence of an amorphous halo. The most probable intersegmental distance (*d*-spacing) values were estimated according to Bragg's equation, and data are shown in **Table 5.2**.
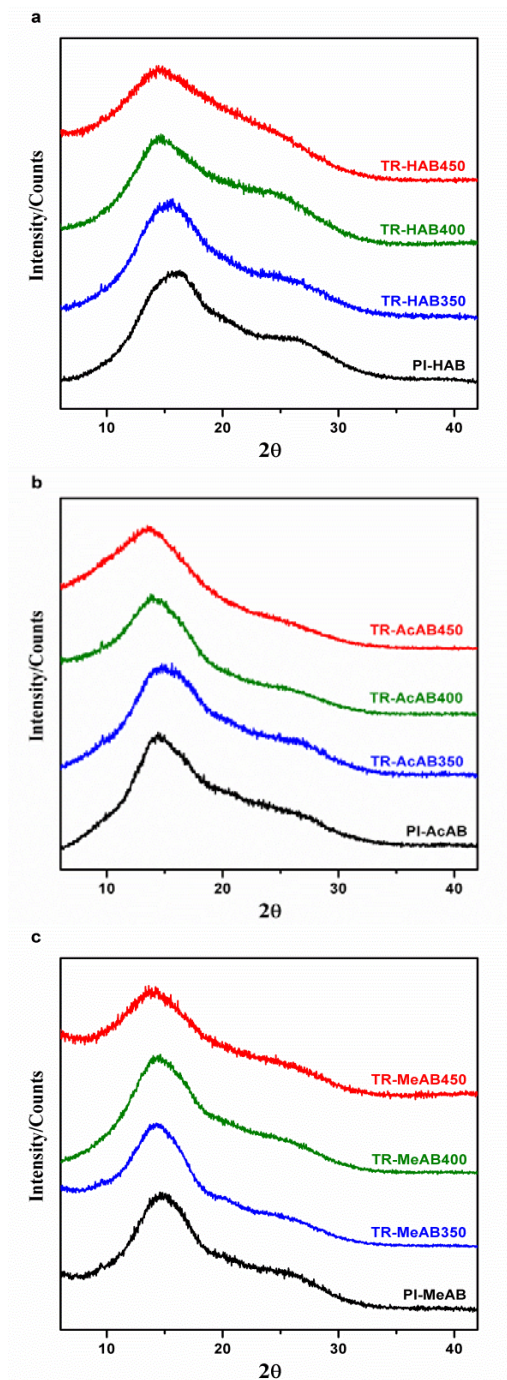
Figure 5.7. Wide angle X-ray diffraction (WAXD) patterns of (a) *PI-HAB*, (b) *PI-AcAB* and (c) *PI-MeAB* precursor polyimides along with the TR derived membranes, treated at different temperatures and heating times

The precursor polyimides, *PI-HAB*, *PI-AcAB* and *PI-MeAB*, showed preferential intersegmental distances with values of 5.57, 6.11 and 5.99 Å, respectively, whereas films treated at 450 °C resulted in larger intersegmental distances, with values of 6.14, 6.51 and 6.36 Å, respectively. For the other treatments, an intermediate change was observed. Accordingly, the use of thermal treatments led to higher intersegmental distances, which was in agreement with other TR polymers previously studied [2,19,23].

Density data are also compiled in **Table 5.2**. It was observed that the density of the polyimide precursor films was higher for *PI-HAB* due to its ability to create hydrogen bonds; these give rise to a more densely packed polyimide structure. As expected, thermally treated membranes showed lower densities as thermal treatment temperature increased, excluding the *TR-AcAB350* membrane, which showed a slightly higher density than its precursor membrane, *PI-AcAB*.

The Van der Waals volumes, V_W, for partially converted samples, were calculated using Equation 5.2, which considers the degree of conversion of the polyimide precursor into the final TR structure, where the value *c* is the fractional mass conversion determined as the quotient of the experimental mass loss measured by TGA and the theoretical mass loss required to achieve 100 % conversion. $V_{W,TR}$ and $V_{W,PI}$ values refer to the Van der Waals volume of TR and PI structures, respectively. These Van der Waals volumes were introduced in Equation 5.3 in order to achieve the FFV values of the partially converted structures.

$$V_W = c\,V_{W,TR} + (1-c)V_{W,PI} \qquad \text{(Eq. 5.2)}$$

$$FFV = \frac{V_e - 1.3V_W}{V_e} \qquad \text{(Eq. 5.3)}$$

The changes that occurred to the structure of the precursor polyimides after thermal treatment in the tube furnace were analyzed using ATR-FTIR. Complete details of these structural changes can be seen in **Figure 5.8**, where the ATR-FTIR spectra for all thermally treated samples as well as for polyimide precursors are shown. **Figure 5.9** shows the spectra of the films thermally treated at the highest temperature (450 °C) for 30 minutes. As can be seen, in the *TR-HAB450* sample spectrum, the appearance of intense peaks at wavenumbers around 1557, 1465 and 1060 cm^{-1}, which are characteristic of the PBO structure, confirmed that the *PI-HAB* film undergoes a thermal rearrangement into PBO. In addition, the intensity of the imide peaks at 1780, 1720, 1375 and 1102 cm^{-1}, and the strong and broad absorption band from the hydroxyl group around 3400 cm^{-1}, were found to substantially decrease. In the *TR-AcAB450* spectrum, the representative peaks for PBO could also be observed, even though they were less intense when compared with the *TR-HAB450* sample, suggesting the existence of PBO in the final structure. In this case, the imide peaks partially decreased, and the emergence of a new strong band around 3400 cm^{-1}, which did not appear on the spectrum of the *PI-AcAB* precursor, proved the presence of new OH phenolic groups. For the *TR-MeAB450*, the characteristic OH phenolic group peak also appeared together with a low decrease of the imide peaks. However, as mentioned above, the polymer density decreased also for this polymer going from the starting material to the final one. This suggests that a structural change took also place, similar to the type underwent by *ortho*-hydroxypolyimides. It is well documented that the pyrolysis of methoxy aromatic compounds proceeds via the homolytic scission of the (H$_3$C)-O linkage, with the subsequent loss of CH$_3$ groups in the form of methane or ethane followed by the recombination of the phenoxy radical to phenol [32]. If this mechanism is accepted as a first step in the transformation, *ortho*-methoxypolyimides would then render TR-PBOs in the same way as *ortho*-hydroxypolyimides do.
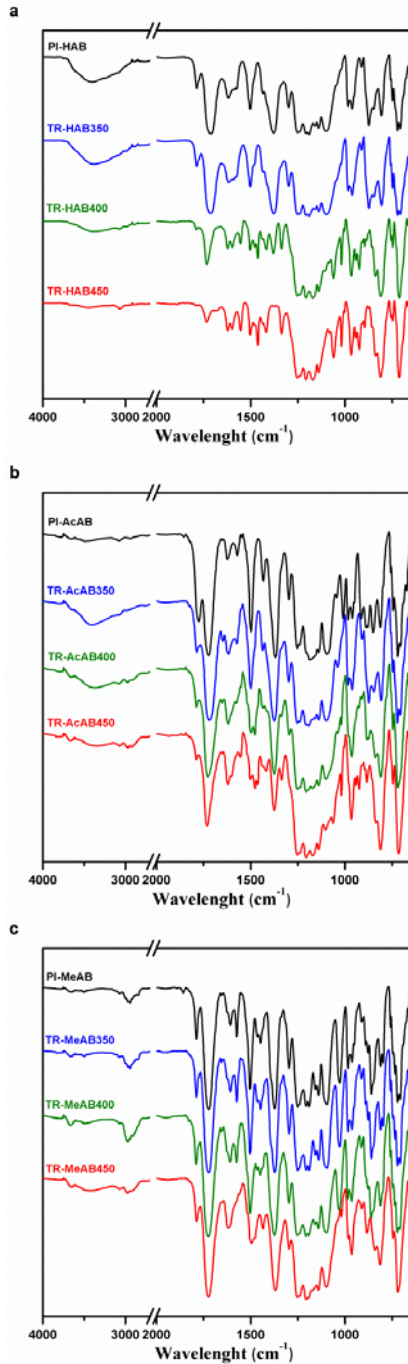
Figure 5.8. ATR-FTIR spectra of (a) *PI-HAB*, (b) *PI-AcAB* and (c) *PI-MeAB* precursor polyimides and thermally rearranged analog membranes, treated at different temperatures

However, the identification of the final material, *TR-MeAB450*, by FT-IR did not entirely agree with this assumption, as a clear transformation into PBO was not confirmed from spectral analysis. As discussed above, the strong carbonyl bands of imide C=O stretching at around 1715 and 1785 cm^{-1} persisted in a great extent after heating at 450 °C for 30 minutes, contrarily to what happens on heating *ortho*-hydroxypolyimides. This seems contradictory with the suggestion that the most probable first step of the thermal treatment is the loss of methyl groups and the subsequent formation of phenols or phenol radicals, with almost simultaneous formation of *ortho*-hydroxypolyimide. Thus, the persistence of the intense imide peaks and the non-appearance of the characteristic PBO bands seem to indicate that thermal rearrangement did not occur via the accepted *TR-PBO* process.
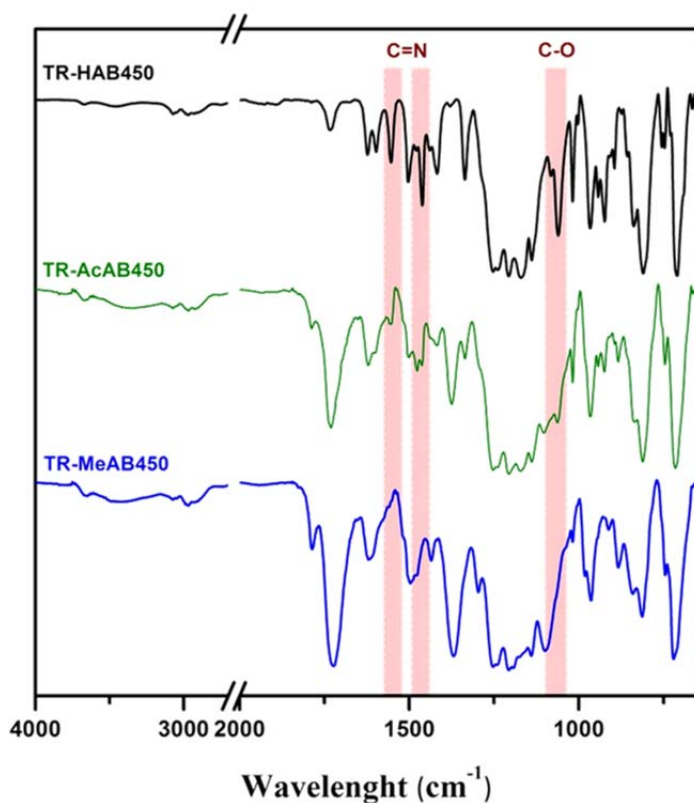
Figure 5.9. ATR-FTIR spectra of films thermally treated at 450 °C for 30 minutes

This spectroscopic evidence moved us to search for a plausible route and make clear the mechanism governing the thermal rearrangement undergone by *ortho*-methoxypolyimides. Upon reviewing the spectral data reported for TR-PBOs in the last years, two points appear most significant: 1) there is general agreement of the mechanism proposed by Tullos *et al.* for the thermal rearrangement of *ortho*-hydroxypolyimides to TR-PBOs [3,22,33–36], although there is not full agreement about the effect of the precursor synthesis route (chemical imidization, azeotropical imidization or direct thermal imidization) on the composition of the final TR-PBO [2,37,14,12], and 2) when starting from *ortho*-esterpolyimides the composition of the final material is far from a neat PBO as strong spectral evidence speaks to the prevalence of polyimides in great extension [34,15]. In fact, if one reviews the attempts made to use *ortho*-esterpolyimides (mainly *ortho*-acetylpolyimides) instead of *ortho*-hydroxypolyimides as precursors for TR-PBOs, it can be seen that the possibility of an alternative mechanism was obviated and authors focused their research effort mainly on studying the advantages of using *ortho*-esters for better solubility, improved *FFV* (splitting off of aliphatic rests should help to increase the amount of regular microcavities) or lower T_g, which could favor a drop in the rearrangement temperature. As a rule, the final heated films of the supposed TR-PBOs exhibited strong IR bands corresponding to aromatic imides, and the authors did not pay attention to this experimental evidence. Thus, another mechanism, or a parallel one, could be responsible for the final chemical composition shown by IR spectra in those cases where *ortho*-hydroxypolyimide is not the precursor.

Kostina *et al.* recently reported a thorough study clearly addressing the mechanisms that govern the molecular transformations undergone by *ortho*-hydroxypolyimides at temperatures over 400 °C [5,38]. They postulated that the formation of rigid aromatic lactams, not only polybenzoxazoles, is responsible for the series of conformational changes that lead to the observed strong effects on physical properties, particularly the dramatic increase in fractional free volume and hence gas diffusivity. In those papers, and based on spectroscopic signals, the observed loss of CO_2 was ascribed to the formation of lactams (phenanthridin-6(5H)-one moieties) through thermal decomposition of an intermediate lactam-lactone (6H-dibenzo[b,f][1,4]oxazocine-6,11(12H)-dione

units). This assumption is supported by quantum chemical calculations that suggest that the formation of lactams is energetically more favorable than the formation of benzoxazoles. Nonetheless, it can be presumed that by applying the very high temperatures used to force intramolecular rearrangement, both lactams and benzoxazoles can be formed, and that the final composition is greatly affected by the final temperature and the heating protocol. It must be remarked that there is spectroscopic indication of the persistence of polyimide, apart from the merging of the bands attributable to lactams, as the characteristic IR bands of imide at about 1778, 1720, 1550 and 725 cm^{-1} remain in the IR spectra reported by Kostina *et al.*, and this is the case for most TR-PBOs prepared from *ortho*-esterpolyimides reported up till now [5,38].

Thus, it seems that, although *ortho*-hydroxypolyimides do lead mostly to TR-PBOs by thermal rearrangement, the thermal treatment of other related precursors, like *ortho*-esterpolyimides or *ortho*-methoxypolyimides, do not follow the same rearrangement paths and therefore the resulting material after heating to 450 °C is far from a neat polybenzoxazole. The presence of lactam, lactone-lactam and benzoxazole can be detected in various proportions depending on: 1) the nature of the precursor, 2) the synthetic method applied to prepare the precursor and 3) the schedule followed in the final heating step. Furthermore, in the particular case of TR polymers attained from *ortho*-methoxypolyimide, benzoxazole units should be present in a small amount as spectral data does not support their presence in significant amounts. So, a mechanistic path is proposed in this work detailing the process of thermal treatment at high temperatures in solid-state *ortho*-methoxypolyimides. This mechanistic explanation is far from thoroughly justified and additional work in this topic will be carried out using other techniques like solid-NMR, XPS and FTIR-MS in models obtained in a regioselective way. Based on our work in TR materials, the mechanistic path we propose will be similar to the one described in **Scheme 5.2**.
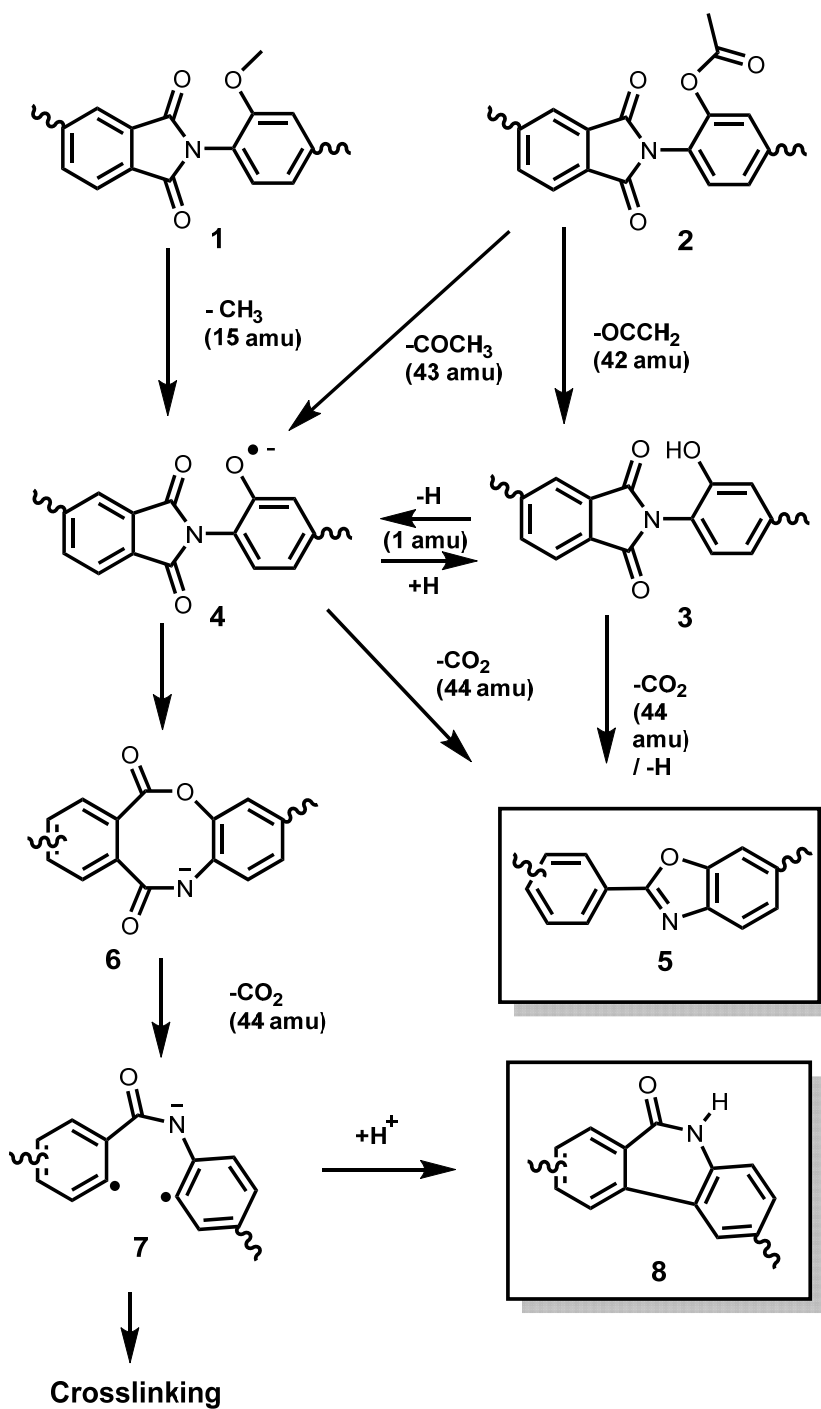
Scheme 5.2. Possible rearrangement mechanisms and final reaction products obtained by thermal treatment of *ortho*-hydroxy, *ortho*-methoxy and *ortho*-acetyl polyimides

Herein, we postulate that the final molecular moieties arising from thermal treatment depends on the group attached to the *ortho* position of the amino group. When the group is OH (3), the high temperature results in conversion to TR-PBO (5) or in the formation of (4) by homolytic breakage of the O-H bond. When the acetyl group (2) is considered, a predominant loss of ethenone (ketene, $CH_2=C=O$) is observed, as evidenced by TGA-MS, with formation of 3 or 4. This ethenone group (m+=42 amu) is formed by the decomposition of the –(OCO) bond with the formation of the acyl group and breakage of this group to ethenone and a proton. However, when the methoxy group is considered (1), TGA-MS indicates the loss of methyl groups (m+=15 amu), which results in the formation of (4). Evidently, 3 can be converted to 4 and 4 to 3 by losing or gaining an H, respectively. The published works and the results of this paper clearly point to the formation of the benzoxazole moiety being most favored by the OH precursor, slightly favored for the $OCOCH_3$ precursor, and less favored by the OCH_3 precursor. Therefore, the reaction from 4 to 5 is not favored and consequently it could be assumed that the presence of H (H+ or H·) in the medium should influence the rearrangement process. Thus, when the amount of H is high (OH polyimide), the classical TR rearrangement is the most favored and benzoxazole moiety formation is evident. However, the production of H groups is very small when the methoxy group is considered and PBO formation is scarcer. For the acetyl polyimide, mixed formation of both (3) and (4) intermediates could explain the observed FTIR results. Two questions arise from this assumption: Q1) What is the role of H in PBO formation? Q2) Why does the formation of non-PBO moieties produce materials with high *FFV* and high gas diffusivities?

Q1) The role of the proton could be ascribed to the protonation of some nucleophilic groups, which could produce an intermediate state that permits the preferential formation of some of the molecular moieties described in the **Scheme 5.2**. It seems to be accepted in the literature that the intermediate moiety formed during the conversion from *ortho*-hydroxypolyimide to polybenzoxazole is the B molecule described in **Scheme 5.3**.
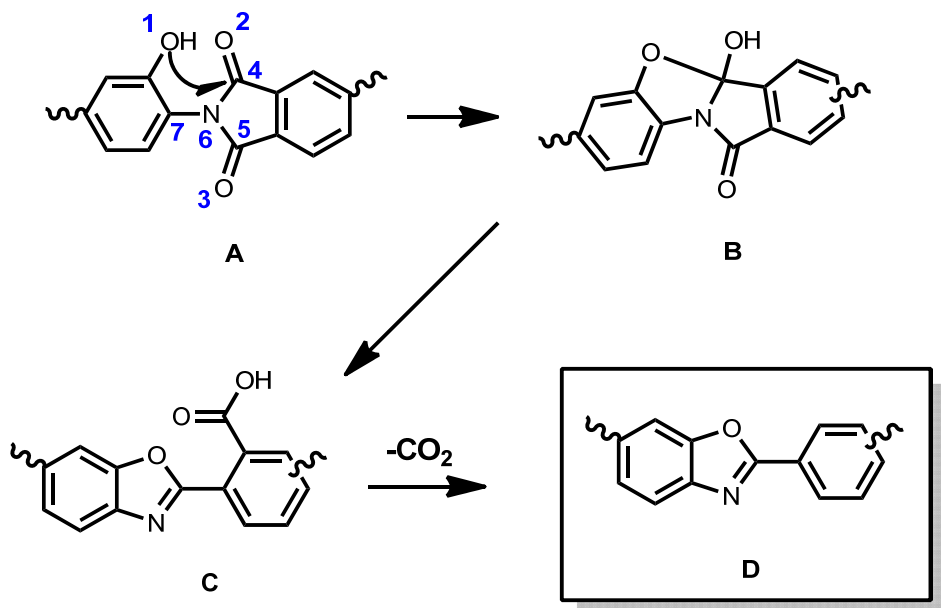
Scheme 5.3. Reaction mechanism proposed for the thermal rearrangement mechanism of PI-HAB to TR-PBO

The formation of intermediate B seems to be evident, and hence many authors consider this moiety to be essential for achieving the final benzoxazole. However, molecular simulations denote that the distance from the nucleophilic center (O1 of the OH moiety after the breakage of the O-H bond) to the carbonylic centers of the imide (C4 or C5) in molecule A is large and a strong conformational change has to take place to permit this attack. However, it is plausible to consider that, at high temperature, a proton is able to jump from the OH to some of the nucleophilic centers of the imide (see **Scheme 5.4**).
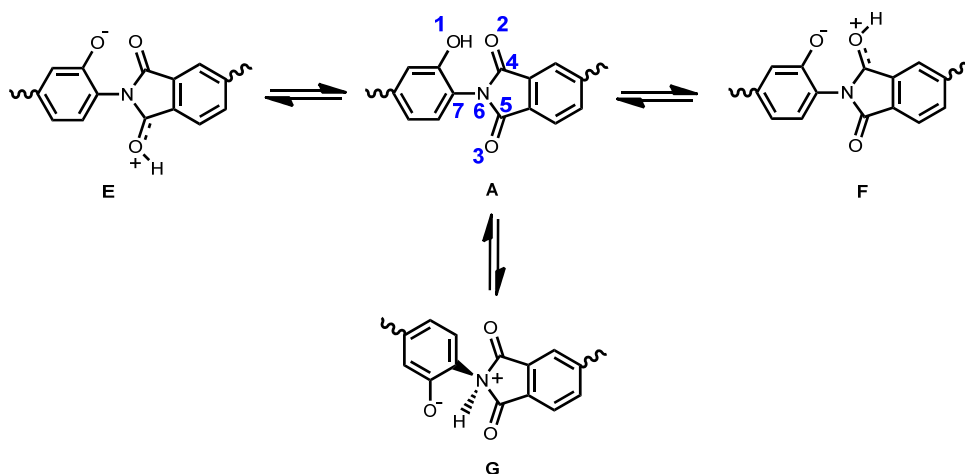
Scheme 5.4. Proton jumping between PI-HAB and the different nucleophilic centers of the imide moiety

When one of the two oxygen atoms of the imide group is protonated by the transfer of a proton from O1 to O2 or O3 (structures E and F) an increase in the molecular energy is observed. No changes are observed, however, in the distance between the O1 and the carbonylic atoms C4 or C5 (the possible value for an eclipsed conformation is higher than 2.8 Å) and consequently the geometry of the protonated molecule does not favor the attack on the carbonylic centers. Nevertheless, when the proton is transferred from O1 to the nitrogen of the imide group (N6) (structure G), an important conformational change takes place and the nitrogen adopts a pyramidal (sp³) conformation. As a consequence of the new nitrogen conformation, the distance from O1 to C4 or C5 is significantly shortened (distance close to 2.00 Å) in such a way that the nucleophilic attack is plausible. **Figure 5.10** depicts the structure of protonated intermediate G showing the short distance between O1 and C4 or C5 that can be attained. Afterwards, the system evolves to a benzoxazole group through the jumping of the hydrogen placed on N6 to the O2, thus forming bi-intermediate state B (**Figure 5.11**). Evolution of this intermediate state gives the 2-carboxy benzoxazole, C (**Scheme 5.3)**, which, after losing a CO_2 molecule, is converted to the final benzoxazole D.
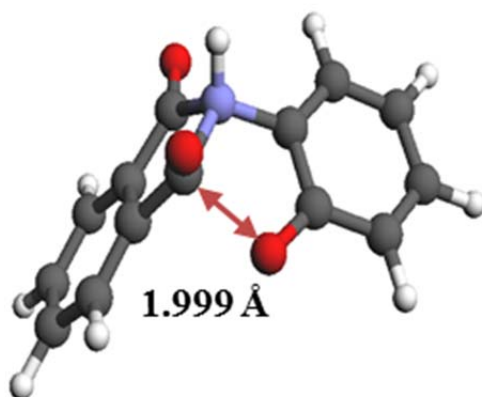
Figure 5.10. Structure of the *ortho*-hydroxypolyimide after the transfer of one proton from the OH group to the nitrogen imide moiety (intermediate G in **Scheme 5.4**), showing the significant shortening of the distance between O1 and C4 or C5
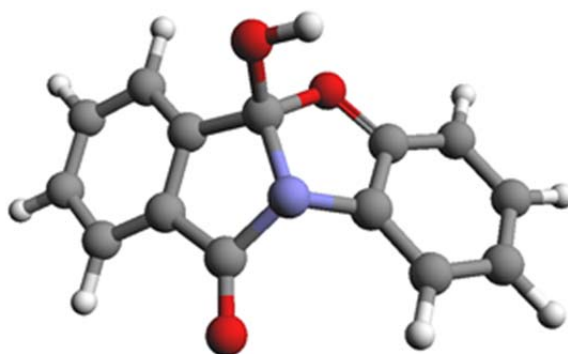
Figure 5.11. Intermediate molecule B formed from intermediate G (**Scheme 5.3**)

When no hydrogens (protons (H+) or hydrogen radicals (H·) are involved in the reaction path, several steps of the proposed mechanism are not possible; the reaction could progress by thermal activation of 4 (**Scheme 5.2**). Thus, the eclipsed conformation of 4 can be achieved by rotating the N6-C7 bond, which is favored at high temperatures. This conformation permits the attack of O1 to C4, allowing the system to spontaneously form the lactone-lactam moiety. This spontaneous reaction has been seen in computer simulations. In fact, if the structure in **Figure 5.10** is minimized by AM1, it spontaneously gives way to the lactone-lactam unit, as shown in **Figure 5.12**. The ulterior decarboxylation of the lactone-lactam forms the proposed lactam. However this decarboxylation also produces a high amount of radical centers, which lead to a massive amount of crosslinking.
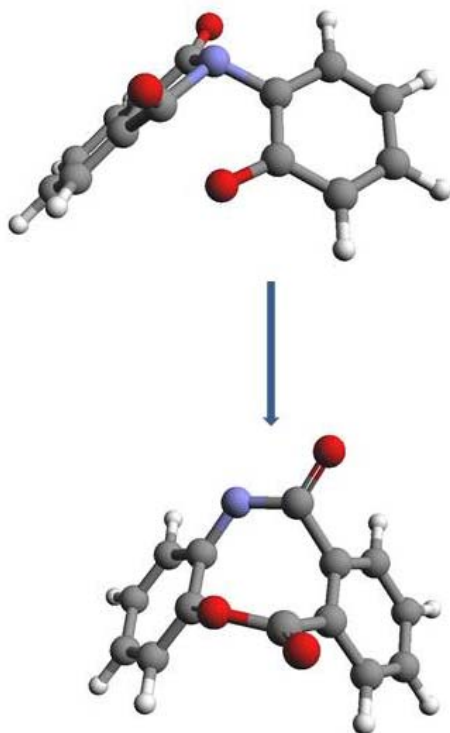
Figure 5.12. Initial and final steps of the reaction of evolving intermediate G (**Scheme 5.4**) to (lactone-lactam) when there is no protonation of the O2 atom

Q2) The high *FFV* of materials made from *ortho*-methoxypolyimides can be explained by the eclipsed and bent conformation associated with the transitory molecule G required to produce the attack. Also, the lactone-lactam has a contorted conformation, which produces an excess of free volume.

5.3.4. MECHANICAL PROPERTIES

Mechanical properties were determined for all polymeric films studied in this work (precursor and thermally treated materials) and are shown in **Table 5.3**. Mechanical properties of the precursors were excellent with elastic moduli above 2.5 GPa, tensile strength higher than 150 MPa and good values for elongation at break. The mechanical properties of the membranes thermally treated at 350 °C did not appreciable change, except for the *PI-AcAB* membranes, probably due to the premature thermal rearrangement that was observed by thermogravimetric analysis. The thermal treatment at 400 °C led to a slight decrease in mechanical properties, which was greater for the membrane derived from *PI-AcAB*. However, the membranes from *PI-MeAB* and *PI-HAB* showed good mechanical properties when compared with other aromatic polymers.

Table 5.3. Mechanical Properties of Precursor Polyimide Films and Their Corresponding Thermally Treated Membranes

Polymer code	Tensile strength (MPa)	Elongation at break (%)	Modulus (GPa)
PI-HAB	166	19.5	2.5
TR-HAB350	167	15.9	2.7
TR-HAB400	127	14.4	1.8
TR-HAB450	27	1.7	1.8
PI-AcAB	169	9.8	2.9
TR-AcAB350	126	5.3	3.0
TR-AcAB400	64	2.8	2.8
TR-AcAB450	33	1.9	2.1
PI-MeAB	176	7.5	3.0
TR-MeAB350	179	8.8	2.7
TR-MeAB400	146	8.7	2.3
TR-MeAB450	56	3.6	1.8

It should be noted that a detailed study of mechanical properties for TR materials has not been carried out and only a few papers have dealt with this issue. Calle *et al*. [31] obtained TR derived from ether-benzoxazole units that showed mechanical properties lower than these obtained in this work for samples thermally treated at 400 °C. Li *et al*. [39] developed a class of TR with excellent mechanical properties, but the precursor had a high *FFV* and the conformational changes associated with thermal rearrangement were favored and it was found that elongation values were clearly higher than for any TR materials obtained so far. The mechanical properties for the samples treated at 450 °C dropped in all cases, and consequently, a decrease between 25-40 % was observed for all mechanic moduli. However, the reduction in tensile strength was significantly higher, with decreases between 70 and 80 % when compared with reference polyimides. Again, and common for TR materials, the elongation values were lower than 5 %. The best balance in mechanical properties for these materials was found with the *TR-MeAB450* sample. In conclusion, it could be stated that the thermal treatment of TR membranes from *PI-MeAB* gave materials with mechanical properties able to withstand the high pressures employed in industrial gas separation applications.

5.3.5. PERMEATION PROPERTIES

Gas transport properties of the produced *ortho*-substituted polyimides and their corresponding TR-polymers were investigated for He, O_2, N_2, CO_2 and CH_4 gases and the results are presented in **Table 5.4**. The gas transport values measured for the thermally untreated precursors were permeability, which were typical values, considering the linearity of the polymers and their chemical composition. Moreover, the substituent seems to play a role on the permeability of the *ortho*-substituted polyimides, which can be related to the effect of the substituent on the *FFV*. Thus, the permeability is higher for *PI-MeAB*, which has the higher *FFV* (0.174), followed by *PI-AcAB*, with *FFV*: 0.170 and finally, *PI-HAB* (0.160). Consequently, the *PI-MeAB* material seems to give TR polymers with higher permeability.

Table 5.4. Gas Permeation Properties of Precursor Polyimides and Thermally Treated Membranes

Polymer code	Permeabilities (Barrers)[a]					Ideal Selectivities[b]	
	PHe	PN_2	PO_2	PCH_4	PCO_2	$\alpha_{O2/N2}$	$\alpha_{CO2/CH4}$
PI-HAB	46	0.35	2.3	0.16	10	6.6	63
TR-HAB350	70	0.59	3.8	0.29	16	6.4	55
TR-HAB400	94	2.3	12	1.5	57	5.2	38
TR-HAB450	200	10	45	7.7	240	4.5	31
PI-AcAB	43	0.44	2.5	0.2	12	5.7	60
TR-AcAB350	75	1.1	6.1	0.48	27	5.5	57
TR-AcAB400	178	5.9	29	3.2	159	4.9	50
TR-AcAB450	348	28	114	21	632	4.1	31
PI-MeAB	56	0.68	4.1	0.31	20	6.0	65
TR-MeAB350	75	1.1	6.1	0.48	28	5.5	58
TR-MeAB400	118	3.0	14	1.6	78	4.7	49
TR-MeAB450	328	23	93	18	540	4.0	30

As mentioned previously above, the TR process for the different *ortho*-substituted polyimides does not take place at the same temperature and, moreover, the conversion, at the intermediate steps and at the final one, is also different in the three cases. **Figure 5.13** shows, at different treatment temperatures, the oxygen permeability increase versus conversion during the transition from the polyimide structure to PBO (the observed behavior is analogous for the other gases). As can be seen, different performances values are observed depending on the structure of the polyimide precursor. When the precursor is *PI-HAB*, it is clear that the thermal process leads to the conversion of the polyimide to polybenzoxazole where the weight loss corresponds to the release of fragments with 44 amu (CO_2). Therefore, the permeability increase can be accurately correlated with weight loss, with the PBO conversion and with the *FFV* change. In this case, the permeability increase seems to be somewhat low, mainly in the first steps of the process, when correlated with the PBO conversion.
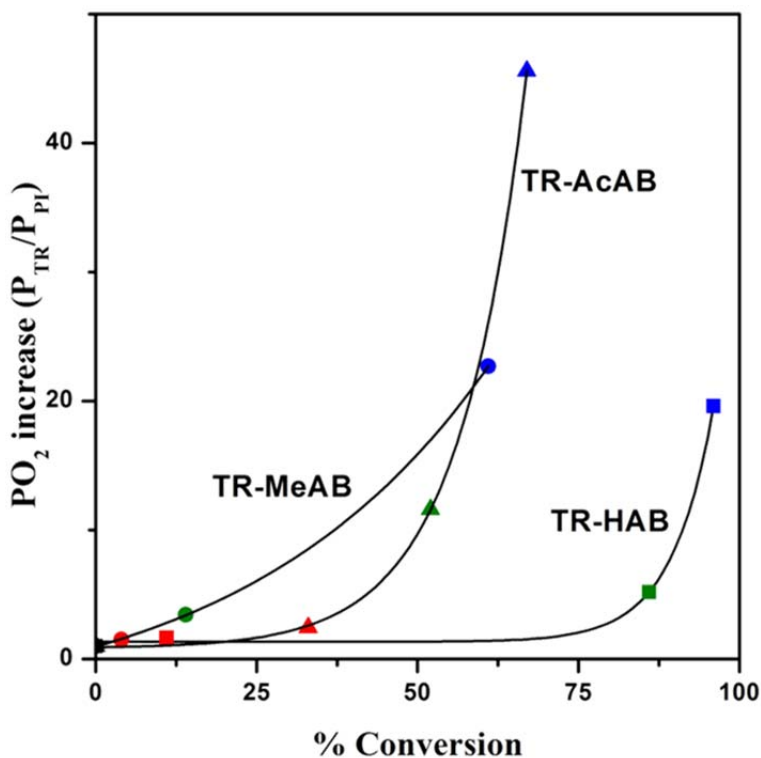
Figure 5.13. Plot of oxygen permeability increase (P(O$_2$)TR/P(O$_2$)PI) vs % conversion, based on a full rearrangement of PI to PBO or to poly(lactam). Red: 350 °C, Green: 400 °C, Blue: 450 °C

A large increase in permeability is achieved when the PBO conversion reaches values greater than 80% (5-fold increase in permeability when the PBO conversion goes from 0% to 86%) reaching a 20 times increase when the PBO conversion is near complete (96%). For the *PI-AcAB* precursor, there is a sudden increase in permeability that starts at approximately 40 % conversion, reaching a 12-times increase at 52% conversion, while the highest permeability increase (46-fold) is achieved when PBO conversion is only 67%. However, the formation of PBO from *PI-AcAB* is not the only way to explain the effects of the thermal treatment. The TGA experiments demonstrate that there is a previous release of ketene and/or acetyl moieties (42 and 43 amu, respectively) that causes an increase in *FFV* due to the elimination of side groups, even if no TR process

takes place at this temperature. After this loss, the resultant macromolecular structure can undergo thermal rearrangement to PBO (on releasing CO_2, 44 amu), form lactam (also on releasing CO_2, 44 amu) and form (lactone-lactam) moieties (with negligible weight loss; H, 1 amu). In this last case, the conversion to lactone-lactam cannot be evidenced by TGA measurements even though the formation of this structure could produce changes in *FFV*. Also, molecular simulation calculations determined that the structural unit of PBO has a molecular volume of 415.8 A^3 whilst the molecular volume of the lactam unit is slightly lower (408.7 A^3) and thus the increase in *FFV* for the last structure should be slightly higher. As was summarized in **Table 5.2**, the conversion of *TR-MeAB350* and *TR-MeAB400* is significantly lower than those corresponding to *TR-HAB* and *TR-AcAB* polymers. This fact could be based on two complementary processes: 1) By TGA measurements it is clearly seen (**Figure 5.4**) that the initial temperature during weight loss, and consequently of conversion from one structure to another one, is considerably higher in *TR-MeAB*, and 2) the initial weight loss in *TR-MeAB* corresponds to the elimination of a moiety smaller than in the other two cases, as it can be observed in **Figure 5.5c**. This shows that in the first steps of thermal weight loss there is simultaneous release of CO_2 (44 amu) and CH_3 (only 15 amu). The 15 amu moiety obviously corresponds to the release of a methyl group derived from the methoxy moiety. Again, after this ether breakage, the resultant chain can follow the mechanism proposed for *PI-AcAB*, and the formation of PBO, lactam, and lactone-lactam can proceed.

In conclusion, related to the thermal treatment that gives the highest gas permeability values, at 450 °C, both *TR-AcAB450* and *TR-HAB450* membranes suffer a significant amount of thermal rearrangement and both experience a significant increase in permeability. However, the permeability increase in *TR-AcAB450* is much higher, despite the much lower conversion. This lower conversion is probably caused by the superposition of the two mechanisms presented in **Scheme 5.2**; that is, the simultaneous formation of PBO and of poly(lactam)s or poly(lactone-lactam)s. The existence of the second mechanism, for the formation of polymers having lactams or lactone-lactam moieties, seems to justify the behavior of *TR-MeAB450* having the lowest conversion and also the lowest increase in permeability, since it did not suffer the sudden improvement

observed in either of the other two cases. Therefore, the permeability behavior also seems to confirm the existence of a different rearrangement mechanism. Finally, the lowest increase in permeability is partially counteracted by the highest permeability of *PI-MeAB*, when compared with the other two precursors, and thus *TR-MeAB450* presents an excellent permeability-selectivity balance.

In order to determine the gas permeability of membranes made in this work and also to figure out the effect of the thermal treatments, Robeson plots of permeability versus selectivity for some selected gas pairs were generated. For the O_2/N_2 gas pair, it was clearly observed that all membranes, pristine and thermally treated ones, placed below the 1991 Robeson limit. For the CO_2/CH_4 gas pair, results were more interesting (see **Figure 5.14**). The thermal treatment at 350 °C produced an improvement for all the membranes that depended on the precursor. Thus, it was observed that the best gas separation properties corresponded to *TR-MeAB350* and *TR-AcAB350*, which slightly overpassed the Robeson limit whilst the other one, *TR-HAB350*, was below. The additional treatment at 400 °C resulted in an important increase in gas productivity in such a way that *TR-AcAB400* was placed near the 2008 Robeson limit. *TR-MeAB400* underwent an enhancement in gas separation properties although the plot was located between both limits. *TR-HAB400* kept well below the 1991 upper-bound. For this case, it should be noted that both substituted polyimides reached excellent values of gas productivity despite their low thermal rearrangement conversion.

After the thermal treatment at 450 °C, all membranes were located clearly above the 1991 Robeson limit. However, *TR-MeAB450* was found to have experienced a significant improvement since this membrane was placed close to the 2008 upper-bound, placing it in the attractive zone for gas separation properties (high permeability while maintaining a good selectivity). After the thermal treatment *TR-AcAB450* showed the best permeability and selectivity.
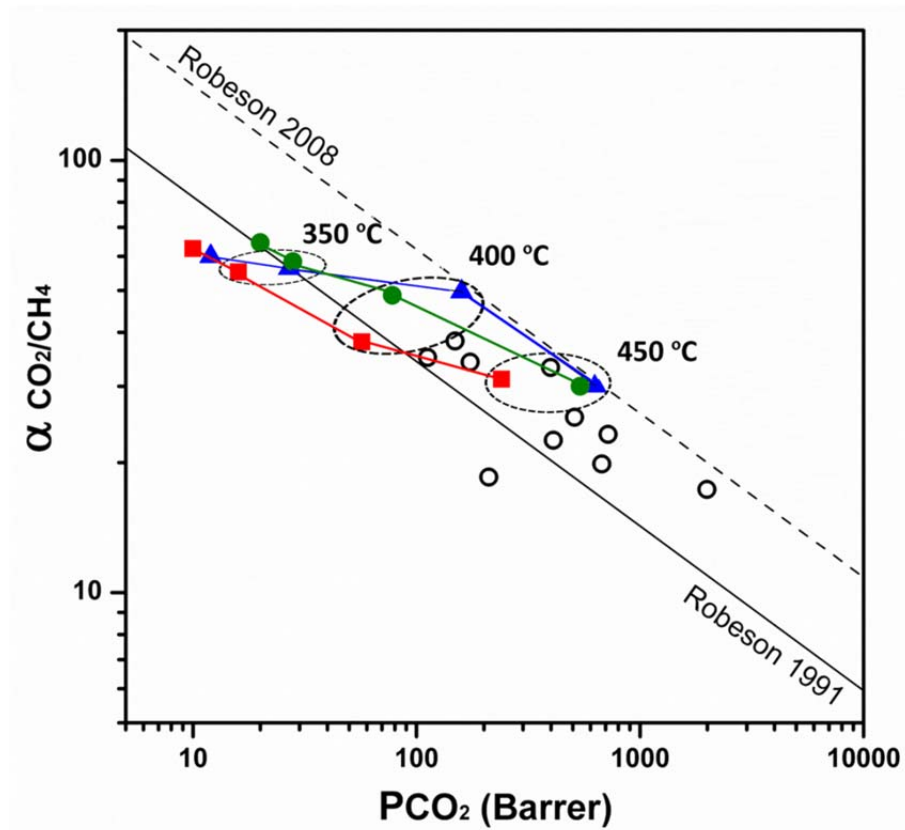
Figure 5.14. Robeson plot for the three series of polymers: ■ *TR-HAB*, ▲ *TR-AcAB*, ● *TR-MeAB*, ○ Literature data for TR. The temperatures of thermal treatment are shown in the plot

5.4. CONCLUSIONS

Ortho-methoxypolyimides were successfully synthesized from 2,2´-dimethoxybenzidine and dianhydride 6FDA. Their treatment at high temperature, up to 450 °C, led to insoluble materials, whose IR spectra indicated a change in chemical composition. Significant changes in physical properties, particularly a dramatic change in permeation properties were also observed. FTIR and TGA combined with mass spectrometry confirmed that methoxy groups were lost in a first weight loss step that started above 350 °C, and that a thermal rearrangement took place at higher temperature. Unlike *ortho*-hydroxypolyimides, *ortho*-methoxypolyimides did not seem to be converted into PBOs, the starting polyimide remained in a great proportion along even after the formation of benzoxazole and lactam units. Benzoxazoles and lactams appeared as a result of intramolecular recombination that occurred simultaneously at high temperature. This was unable to be quantitatively evaluated by FT-IR. Thus, there is still a lack of knowledge about the actual mechanism that governs the path from *PI-MeAB* to TR polymers. In this work, based on the accepted mechanistic paths and also on recent literature, a plausible molecular simulation justification is proposed. In this explanation, the presence of protons or radical hydrogen atoms plays a critical role in benzoxazole formation. Also, the formation of (lactone-lactam) or lactam moieties was justified. Then, it is reasonable to presume that, at the high temperatures used during conversion, more than one rearrangement or recombination is possible. This leads to a final material that contains polyimide and moieties of both lactam and benzoxazole.

Gas permeation of the TR polymers reported here are attractive and compare fairly well with other TR-PBOs previously reported, exhibiting $P(CO_2)$ up to 540 Barrers and selectivities of 30 for the CO_2/CH_4 gas pair. Additionally, the permeability behavior seems to confirm the rearrangement mechanism proposed above, which yields mostly PBO structures in the case of *TR-HAB* and a combination of PBO with poly(lactam) and poly(lactone-lactam) structures in the other two cases. The amount of poly(lactam) and poly(lactone-lactam) structures being higher in the thermally treated materials derived from *PI-MeAB*.

5.5. REFERENCES

1. Park, H. B. *et al.* 'Polymers With Cavities Tuned For Fast Selective Transport Of Small Molecules And Ions.' *Science* **318,** 254–258 (2007).

2. Park, H. B., Han, S. H., Jung, C. H., Lee, Y. M. & Hill, A. J. 'Thermally Rearranged (TR) Polymer Membranes For CO2 Separation.' *Journal of Membrane Science* **359,** 11–24 (2010).

3. Tullos, G. L., Powers, J. M., Jeskey, S. J. & Mathias, L. J. 'Thermal Conversion Of Hydroxy-Containing Imides To Benzoxazoles: Polymer And Model Compound Study.' *Macromolecules* **32,** 3598–3612 (1999).

4. Guo, R. *et al.* 'Synthesis And Characterization Of Thermally Rearranged (TR) Polymers: Effect Of Glass Transition Temperature Of Aromatic Poly(hydroxyimide) Precursors On TR Process And Gas Permeation Properties.' *Journal of Materials Chemistry A* **1,** 262–272 (2013).

5. Kostina, J. *et al.* 'Thermal Rearrangement Of Functionalized Polyimides: IR-Spectral, Quantum Chemical Studies, And Gas Permeability Of TR Polymers.' *Industrial & Engineering Chemistry Research* **52,** 10476–10483 (2013).

6. Yoo, E.-S., Gavrin, A. J., Farris, R. J. & Coughlin, E. B. 'Synthesis And Characterization Of The Polyhydroxyamide/Polymethoxyamide Family Of Polymers.' *High Performance Polymers* **15,** 519–535 (2003).

7. Kim, S. I., Shin, T. J., Pyo, S. M., Moon, J. M. & Ree, M. 'Structure And Properties Of Rodlike Poly(p-phenylene Pyromellitimide)s Containing Short Side Groups.' *Polymer* **40,** 1603–1610 (1999).

8. Al-Masri, M., Fritsch, D. & Kricheldorf, H. R. 'New Polyimides For Gas Separation. 2. Polyimides Derived From Substituted Catechol Bis(etherphthalic Anhydride)s.' *Macromolecules* **33,** 7127–7135 (2000).

9. Han, S. H. *et al.* 'Thermally Rearranged (TR) Polybenzoxazole: Effects Of Diverse Imidization Routes On Physical Properties And Gas Transport Behaviors.' *Macromolecules* **43,** 7657–7667 (2010).

10. Park, C. H., Tocci, E., Lee, Y. M. & Drioli, E. 'Thermal Treatment Effect On The Structure And Property Change Between Hydroxy-containing Polyimides (HPIs) And Thermally Rearranged Polybenzoxazole (TR-PBO).' *The journal of physical chemistry. B* **116,** 12864–77 (2012).

11. Park, C. H. *et al.* 'A Simulation Study On OH-containing Polyimide (HPI) And Thermally Rearranged Polybenzoxazoles (TR-PBO): Relationship Between Gas Transport Properties And Free Volume Morphology.' *Journal of Physical Chemistry B* **118,** 2746–2757 (2014).

12. Calle, M., Lozano, A. E. & Lee, Y. M. 'Formation Of Thermally Rearranged (TR) Polybenzoxazoles: Effect Of Synthesis Routes And Polymer Form.' *European Polymer Journal* **48,** 1313–1322 (2012).

13. Wang, H. *et al.* 'The Evolution Of Poly(hydroxyamide Amic Acid) To Poly(benzoxazole) Via Stepwise Thermal Cyclization: Structural Changes And Gas Transport Properties.' *Polymer* **52,** 5127–5138 (2011).

14. Smith, Z. P. *et al.* 'Gas Sorption And Characterization Of Thermally Rearranged Polyimides Based On 3,3'-dihydroxy-4,4'-diamino-biphenyl (HAB) And 2,2'-bis-(3,4-dicarboxyphenyl) Hexafluoropropane Dianhydride (6FDA).' *Journal of Membrane Science* **415-416,** 558–567 (2012).

15. Smith, Z. P. *et al.* 'Effect Of Polymer Structure On Gas Transport Properties Of Selected Aromatic Polyimides, Polyamides And TR Polymers.' *Journal of Membrane Science* **493,** 766–781 (2015).

16. Jiang, Y. *et al.* 'Cavity Size, Sorption And Transport Characteristics Of Thermally Rearranged (TR) Polymers.' *Polymer* **52,** 2244–2254 (2011).

17. Liu, W. & Xie, W. 'Acetate-Functional Thermally Rearranged Polyimides Based On 2,2-Bis(3-amino-4-hydroxyphenyl)hexafluoropropane And Various Dianhydrides For Gas Separations.' *Industrial & Engineering Chemistry Research* **53,** 871–879 (2014).

18. Koros, W. J. & Fleming, G. K. 'Membrane-based Gas Separation.' *Journal of Membrane Science* **83,** 1–80 (1993).

19. Comesaña-Gándara, B. *et al.* 'Thermally Rearranged Polybenzoxazoles Membranes With Biphenyl Moieties: Monomer Isomeric Effect.' *Journal of Membrane Science* **450,** 369–379 (2014).

20. Muñoz, D. M., De La Campa, J. G., De Abajo, J. & Lozano, A. E. 'Experimental And Theoretical Study Of An Improved Activated Polycondensation Method For Aromatic Polyimides.' *Macromolecules* **40,** 8225–8232 (2007).

21. Muñoz, D. M., Calle, M., de la Campa, J. G., de Abajo, J. & Lozano, A. E. 'An Improved Method For Preparing Very High Molecular Weight Polyimides.' *Macromolecules* **42,** 5892–5894 (2009).

22. Calle, M., Chan, Y., Jo, H. J. & Lee, Y. M. 'The Relationship Between The Chemical Structure And Thermal Conversion Temperatures Of Thermally Rearranged (TR) Polymers.' *Polymer* **53,** 2783–2791 (2012).

23. Comesaña-Gándara, B. *et al.* 'Thermally Rearranged Polybenzoxazoles And Poly(benzoxazole-co-imide)s From Ortho-hydroxyamine Monomers For High Performance Gas Separation Membranes.' *Journal of Membrane Science* **493,** 329–339 (2015).

24. Sanders, D. F. *et al.* 'Gas Permeability, Diffusivity, And Free Volume Of Thermally Rearranged Polymers Based On 3,3'-dihydroxy-4,4'-diamino-biphenyl (HAB) And 2,2'-bis-(3,4-dicarboxyphenyl) Hexafluoropropane Dianhydride (6FDA).' *Journal of Membrane Science* **409-410,** 232–241 (2012).

25. Sanders, D. F. 'The Effect Of Synthesis Route And Ortho-position Functional Group On Thermally Rearranged Polymer Thermal And Transport Properties.' (2013).

26.   Wieneke, J. U. & Staudt, C. 'Thermal Stability Of 6FDA-(co-)polyimides Containing Carboxylic Acid Groups.' *Polymer Degradation and Stability* **95,** 684–693 (2010).

27.   Waters, T., O'Hair, R. A. J. & Wedd, A. G. 'Catalytic Gas Phase Dehydration Of Acetic Acid To Ketene.' *International Journal of Mass Spectrometry* **228,** 599–611 (2003).

28.   Farr, I. V. *et al.* 'Synthesis And Characterization Of Polyimide Homopolymers Based On 5(6)-amino-1-(4-aminophenyl)-1,3,3-trimethylindane.' *Journal of Polymer Science, Part A: Polymer Chemistry* **38,** 2840–2854 (2000).

29.   Xie, W. *et al.* 'Study Of Stability Of High-temperature Polyimides Using TG/MS Technique.' *Journal of Applied Polymer Science* **83,** 1219–1227 (2002).

30.   Xie, W., Heltsley, R., Li, H.-X., Lee, C. & Pan, W.-P. 'Study Of The Processing Chemistry Of Polyimides With Thermogravimetry/Fourier Transform Infrared/mass Spectrometry Techniques.' *Journal of Applied Polymer Science* **83,** 2213–2224 (2002).

31.   Calle, M. & Lee, Y. M. 'Thermally Rearranged (TR) Poly(ether−benzoxazole) Membranes For Gas Separation.' *Macromolecules* **44,** 1156–1165 (2011).

32.   Pecullan, M., Brezinsky, K. & Glassman, I. 'Pyrolysis And Oxidation Of Anisole Near 1000 K.' *The Journal of Physical Chemistry A* **101,** 3305–3316 (1997).

33.   Tullos, G. & Mathias, L. 'Unexpected Thermal Conversion Of Hydroxy-containing Polyimides To Polybenzoxazoles.' *Polymer* **40,** 3463–3468 (1999).

34.   Guzmán-Lucero, D. & Likhatchev, D. 'Imide-to-benzoxazole Rearrangement In Ortho Substituted Poly(4-4'-diphenylene Pyromellitimide)s.' *Polymer Bulletin* **48,** 261–269 (2002).

35.   Hodgkin, J. H., Liu, M. S., Dao, B. N., Mardel, J. & Hill, A. J. 'Reaction Mechanism And Products Of The Thermal Conversion Of Hydroxy-containing Polyimides.' *European Polymer Journal* **47,** 394–400 (2011).

36.   Hodgkin, J. H. & Dao, B. N. 'Thermal Conversion Of Hydroxy-containing Polyimides To Polybenzoxazoles. Does This Reaction Really Occur?' *European Polymer Journal* **45,** 3081–3092 (2009).

37.   Scholes, C. a., Ribeiro, C. P., Kentish, S. E. & Freeman, B. D. 'Thermal Rearranged Poly(benzoxazole-co-imide) Membranes For CO2 Separation.' *Journal of Membrane Science* **450,** 72–80 (2014).

38.   Rusakova, O. Y. *et al.* 'Study Of The Mechanism Of The Thermochemical Reaction Of Polyimides With Hydroxyl Groups Via Vibrational-spectroscopy And Quantum-chemistry Methods.' *Polymer Science Series A* **53,** 791–799 (2011).

39.   Li, S. *et al.* 'Mechanically Robust Thermally Rearranged (TR) Polymer Membranes With Spirobisindane For Gas Separation.' *Journal of Membrane Science* **434,** 137–147 (2013).

Chapter VI

Conclusions

CONCLUSIONS

The general conclusions that can be drawn from the results attained in this work are summarized in the following:

Among the efforts that are being made to improve the gas permeation properties of TR-polymers, the search for novel polymers is a specially important tool as the chemical composition of polymer precursors still can be conveniently modified to achieve a more favourable balance permeability-selectivity, particularly for gas mixtures including CO_2, which has been proved to be one of the major responsible gases of the greenhouse effect.

Results accomplished in this work have proved that using new monomers, specially designed for this goal, can be a suitable way to face this global concern as polymer precursors can be prepared following classical methods of polyimides synthesis, which lead to TR polymers that show permeation properties matching the performances of the best materials previously reported in this field.

An important conclusion of this work is that the conscientious design and synthesis of new monomers and the improvement of monomers preparation and purification methods are still powerful tools to go farther with research efforts to rely on polymer materials, particularly novel polyimides, with better and better properties for gas separation. In agreement with this, the special attention paid in this work to the optimization of monomers synthesis, and the scrupulous methodology applied to monomers purification and polycondensation, which involves an *in-situ* silylation procedure, have led in most instances to polymeric species of high molecular weight. In fact, tough polymer films have been fabricated in every case by casting of polyimide precursors. This improvement of mechanical properties in precursors has permitted to attain TR membranes able to withstand high pressures in gas separation applications.

New poly-*o*-hydroxyimides similar to those reported in the numerous references on TR-polymers can be attained from commercial monomers, which are available and not expensive. As it has been described in the third chapter of this work, poly-*o*-hydroxyimides can be synthesized from dianhydrides and the hydrochloride salts of inexpensive monomers such as the asymmetric diaminophenol (DAP-Cl) and the symmetric dihydroxydiamine 4,6-diaminoresorcinol (DAR-Cl). Additionally, it can be concluded that the purification methods developed in this work for the monomers DAP-dihydrochloride and DAR-dihydrochloride are very convenient as both monomers yielded poly-*o*-hydroxyimides on combining them with the aromatic dianhydride 6FDA using an in situ silylation method, which exhibited the highest molecular weight ever reported for these polymers.

Poly-*o*-hydroxyimides attained from DAR-Cl render TR-PBOs on heating them at the temperatures needed to promote the conversion HO-PI to PBO; however, by using a monohydroxy asymmetric diamine monomer, such as DAP-Cl, poly(imide-co-hydroxyimide)s are attained on reacting with dianhydrides. So, treating them, under the conditions applied for TR-polymers, TR poly(benzoxazole-co-imide)s are attained. In this way, the incorporation of polyimide segments investigated in this work resulted in distinctly different gas permselectivity properties. The conversion goes to higher extension for the poly-*o*-hydroxyimide made from DAP-Cl than for that from DAR-Cl, due to the lower T_g and lower molecular stiffness of the former. However, it was observed that, due to the double amount of OH groups in HPI-DAR, the total amount of benzoxazole groups formed was higher for TR-DAR. Importantly, the balance permeability-selectivity was better than any of the other related TR-PBOs described in the literature, placing these polymers above the 2008 Robeson limit for some gas pairs such as CO_2/N_2 and CO_2/CH_4. Therefore, TR membranes can be attained, derived from inexpensive monomers, with excellent gas separation performance, and the possibility of incorporating imide moieties among the TR-PBO ones allows the gas separation properties of the TR membranes to be tailored through the addition of non-TR segments.

The search for new polymer compositions, which can be attained by using isomeric monomers, opens a door to significant advances in the chemistry of these materials. In this regard, positive results have been achieved using the monomer 3,3´-diamine-4,4´-dihydroxybiphenyl (*m*HAB) instead of its commercial isomer 3,3´-dihydroxybenzidine (HAB). An optimized method of conversion from poly-*o*-hydroxypolimide to TR-PBO led to polymer films, which exhibit permeation properties that surpass the empirical Robeson limit for CO_2/N_2 and CO_2/CH_4 gas pairs. Additionally, using the isomeric monomer present clear advantages respect to the commercial one as the conversion to TR-PBO can be performed at lower temperature, and the FFV of the final TR-PBO prepared from the isomeric monomer is greater than that attained from the commercial monomer. In fact, the TR-PBO from *m*HAB shows higher permeability for several gases, such as O_2, N_2 and CO_2 (720 Barrers), than that derived from HAB, which can help for the use of *m*HBA-6FDA in technical carbon capture applications.

Other inexpensive monomers derived from the biphenyl moiety can be used for the preparation of TR polymer precursors. For instance, diamine monomers with reactive functions *ortho* to the amine group others than hydroxyl, such as methoxy or acetyloxy groups, can be used with this purpose, as it has been confirmed in this work. Thus, poly-*o*-methoxyimides can be successfully synthesized from 3,3´-dimethoxybenzidine and dianhydride 6FDA, and their treatment at high temperature, up to 450 °C, leads to insoluble materials that exhibit significant changes in physical properties respect to the poly-*o*-methoxyimide precursor, particularly a dramatic change in permeation properties. In the same way, poly-*o*-acetylimides, which can be prepared by chemical ring-closing of poly-*o*-hydroxypolyamic acids using acetic anhydride, render TR-polymers upon thermal treatment at temperatures around 450 ºC.

Spectroscopic and thermal analytical methods have confirmed that, unlike poly-*o*-hydroxyimides and poly-*o*-acetylimides, poly-*o*-methoxyimides do not seem to be mostly converted into PBOs after the thermal treatment. Instead, the starting polyimide remains in a great proportion, even after the extreme conditions at which the precursors are treated in order to be converted into TR-polymers, and there are spectroscopic evidences which support the presence of benzoxazole and

lactam units, although the exact proportion of imide, benzoxazole and lactam could not be quantitatively evaluated by FT-IR.

Thus, to cover somehow the lack of knowledge about the actual mechanism that governs the path from *ortho*-substituted polyimides to TR polymers at very high temperature, a plausible justification has been proposed in this work using some molecular simulation methods. In this explanation, it has been proved that the presence of protons or radical hydrogen atoms plays a critical role in benzoxazole formation, and the formation of (lactone-lactam) or lactam moieties has been also justified. The results lead to the conclusion that, at the very high temperatures used during the rearrangement process of *ortho*-substituted polyimides, more than one recombination is possible, what leads to a final material that contains polyimide and moieties of both lactam and benzoxazole, and their proportion depends on the nature of the *ortho*-substituent.

The gas permeation properties of TR polymers attained from poly-*o*-methoxyimides are very attractive and compare fairly well with TR-PBOs previously reported, exhibiting $P(CO_2)$ up to 540 Barrers and selectivities of 30 for the CO_2/CH_4 gas pair. Additionally, the permeability behaviour seems to confirm the rearrangement mechanism proposed by us in this work, which yields mostly benzoxazole repeating units in the case of PI-HAB and a combination of imide, benzoxazole and lactone/lactam in the case of PI-MeAB and PI-AcAB, the amount of imide and lactone-lactam structures being higher in the thermally treated materials derived from poly-*o*-methoxyimides.

As a resume, it can be concluded that TR-PBOs and TR-PI-PBOs with excellent permeation properties for the separation of CO_2 from gas mixtures, can be attained by a convenient thermal treatment of novel poly-*o*-hydroxypolyimides based in original hydroxydiamines. TR-polymers with a varied proportion of imide, benzoxazole and lactone/lactam moieties can be also prepared from poly-*o*-acetyloxyimides and poly-*o*-methoxyimides by thermal treatment up to 450 °C. Their permeation properties, and particularly their separation capabilities for CO_2, compare fairly well with those of previously reported TR-PBOs and greatly exceed

the permeation properties of most polyimides and other technical polymers tested with this purposes so far.

Finally, it should be stated that the targets proposed in the research project have been accomplished. Thus, new generations of gas separation membranes with excellent gas separation properties have been obtained by using low-cost monomers. The optimization of the polycondensation reaction has permitted to obtain high molecular weight *ortho*-substituted polyimides that can undergo a thermal rearrangement process to polybenzoxazoles in solid state. The combination in a monomer of TR-able and non TR-able functionalities has permitted to obtain relationships between the structures of the final TR-PBO materials and their physical and gas separation properties. These materials can be processed as membranes with adequate mechanical properties, which can be employed in industrial gas purification applications. Also, a new approach to TR-materials has been developed by using *ortho*-methoxy polyimides. This latter approach can be expanded to a new generation of membranes by affordable modification of the *ortho*-hydroxy groups to other functionalities, which should lead to materials with improved properties: lower thermal rearrangement temperature, better mechanical properties and enhanced gas separation properties.

Appendix 1

List of Figures, Schemes and Tables

LIST OF FIGURES, SCHEMES AND TABLES

CHAPTER I: *General Introduction*

CHAPTER II: *General Methodology*

CHAPTER III: *Thermally Rearranged Polybenzoxazoles and Poly(benzoxazole-co-imide)s from ortho-Hydroxyamine Monomers: Influence of OH Amount*

CHAPTER IV: Thermally Rearranged Polybenzoxazole Membranes with Biphenyl Moieties: Monomer Isomeric Effect

CHAPTER V: Gas Separation Membranes Made Through Thermal Rearrangement: Influence of the ortho-Substituent

Appendix 2

Abbreviations

ABBREVIATIONS

AM1	Austin Model 1
APAF	2,2′-bis(3-amino-4-hydroxyphenyl)-hexafluoropropane
ATR-FTIR	Attenuated Total Reflectance Fourier Transform Infrared Spectroscopy
CTMS	Chlorotrimethylsilane
DAP	2,4-diaminophenol
DAP-Cl	2,4-diaminophenol dihydrochloride
DAR	4,6-diaminoresorcinol
DAR-Cl	4,6-diaminoresorcinol dihydrochloride
DMA	Dynamic Mechanical Analysis
DMAB	3,3′-dimethoxybenzidine
DMAc	*N,N*-dimethylacetamide
DMAP	4-dimethylaminopyridine
DSC	Differential Scanning Calorimetry
EA	Elemental Analysis
FT-IR	Fourier Transform Infrared Spectroscopy
FFV	Fractional Free Volume
HAB	3,3′-dihydroxybenzidine (3,3'-dihydroxy-4,4'-diamino-biphenyl)
HPAA	hydroxyl-containing poly(amic acid)
HPI	*ortho*-hydroxypolyimide
MDSC	Modulated Temperature Differential Scanning Calorimetry
***m*HAB**	4,4′-dihydroxy-3,3′-diamino-biphenyl
MeOPAA	methoxy-containing poly(amic acid)

MPD	*m*-phenylenediamine
NMP	*N*-methyl-2-pyrrolidinone
NMR	Nuclear Magnetic Resonance
PAA	Poly(amic acid)
PALS	Positron Annihilation Lifetime Spectroscopy
PBO	Polybenzoxazole
PI	Aromatic Polyimide
PIM	Polymer of Intrinsic Microporosity
Py	Pyridine
T_g	Glass Transition Temperature
TR	Thermally Rearranged
TR-PBO	Thermally Rearranged Polybenzoxazole
WAXD	Wide Angle X-Ray Diffraction
6FDA	2,2'-bis(3,4-dicarboxyphenyl)hexafluoropropane dianhydride